Vibratory Micro-dispensing Technology of Bulk Solids and its Application in Pharmaceuticals and Biomaterials

Zongqi Li

Supervised by: Dr. Shoufeng Yang

UNIVERSITY OF Southampton

Thesis submitted for the degree of Doctor of Philosophy

Engineering Materials & Surface Engineering, the Faculty of Engineering and the Environment, University of Southampton

October 2014

Declaration

The work in this thesis is based on research carried out at Engineering Materials, the Faculty of Engineering and the Environment, University of Southampton, UK. No part of this thesis has been submitted elsewhere for any other degree or qualification and it is all my own work unless referenced to the contrary in the text.

Zongqi Li, Candidate	Shoufeng Yang, Supervisor

Acknowledgements

This research work could not have completed without the help and support of numerous people.

Firstly, I owe my thanks to my supervisor, Dr. Shoufeng Yang, for his guidance and advice through this project. I also would like to thank him for opening to me the door to the exciting world of bulk solids handling. And the outputs and goals of this project would not have been achieved without his assistance.

The technical staffs in our school deserve my thanks for their patience and help during my experimental work, in particular, David Beckett in Materials and Bioengineering Group, FEE for lab's daily routine and safety issues, Przemyslaw Tryc in School of Chemistry's Glassblowing Workshop for fabulous glass works and Andy Westerman in ISVR's Electronics Workshop for the ultrasound amplifier's assembly.

My group colleagues, Lin Pan, Srisit Chianrabutra and Mohammad Vaezi, contributed with discussions, valuable ideas, theoretical and technical supports and physical helps all through my research. I also received help from Wanhu Yang in technical support on 3D printing and machining, Su Hu in Reprap assembly and Yang Hu in Reprap programming. The helps of other postdocs, postgraduates and undergraduates are also appreciated.

I sincerely thank the University of Southampton for financial support on my tuition fees and the China Scholarship Council for my living stipends allowing me to advance my research career. In addition, I would like to thank EPSRC (Engineering and Physical Sciences Research Council) instrument pool for the loan of valuable equipment to assist my research.

Last but not least, without the continuous encouragement and loving care of my partner Guanghong Liu, my parents and my friends, it would have been much harder for me to finish this research project and I feel that the completion of this work has justified their support and sacrifices.

Abstract

Bulk solids technology plays a key part in manufacturing process when handled material is an assembly of solid particles in large quantities. Micro-dispensing technology for bulk solids can improve operation efficiency in dispensing relatively small amount of material. The demand for the technology covers a wide range of areas where materials have diverse flow behaviours and flow problems due to different physical properties. This Ph.D. project aims to investigate bulk solids flow behaviour and fluidizing mechanism in a hopper under the influence of vibration, and to develop a bulk solids micro-dispensing technique to demonstrate the dispensing process of active pharmaceutical ingredients (API), excipients and biomaterials.

Experiment work in this project includes design of vibratory dispenser hopper and dispensing test with vibratory dispensers where mechanical vibration and ultrasonic vibration is utilized as the driving force to fluidize coarse granules and fine powders, respectively. The results suggest that the vibratory dispenser is capable of accurately and fast dispensing "dropwise" bulk solid in a small amount per drop. A doming controlled flow mechanism is identified in the vibratory dispenser. Bulk solids dome formed in the dispenser hopper plays as a "valve" of flow under the influence of vibration. The dispensing test results show that the design parameters of dispenser hopper, i.e. orifice size, hopper angle and hopper diameter, and vibration signal parameters, i.e. frequency and amplitude, affect the flow rate and dosage conformity in the vibratory bulk solids micro-dispensing technique. Additionally, a triboelectric charging phenomenon is investigated in the ultrasonic vibration dispenser and a solution to the charging issue is proposed with modifying surfaces of dispenser hopper by using platinum plating method. Pt-coated surface reduces the triboelectric charge generated in the dispensing process and improves the flowability of powders.

The correlation between discharge rate and design parameters of ultrasonic vibration dispenser is derived. The derived equations are used to predict dosing results in the application of producing solid form oral drugs and biomaterial dry powder libraries for high-throughput screening (HTS) experiment.

Abbreviations

AoR	angle of repose
API	active pharmaceutical ingredient
D/A	digital to analog
DC	direct current
DEM	discrete element method
DPI	dry powder inhaler
ERM	eccentric rotating mass
HA	hydroxyapatite
HTS	high throughput screening
IYL	internal yield limit
CT	computerized tomography
PM	personalized medicine
PSD	particle size distribution
PLS	partial least squares
RH	relative humidity
RSD	relative standard deviation
SEM	scanning electron microscope
WYL	wall yield limit
TCP	tricalcium phosphate

Nomenclature

A	constant in Walker's equation (eq. 2.4)	pp. 18
A_o	area of hopper orifice	pp. 34, 35
A_s	surface area of particle	pp. 13
A_γ	area of close-packed particles layer	pp. 12
C	Carr's index;	pp. 16
	relative volume decrease in Kawakita's equation (eq. 2.6);	pp. 19
	constant in Beverloo's equation (eq. 2.21)	pp. 36
C_1	constant in Suzuki's equation (eq. 2.25)	pp. 37, 38
C_2	constant in Suzuki's equation (eq. 2.26)	pp. 38
C^*	constant in equation (7.11)	pp. 129
D	diameter of vertical section of a silo	pp. 54, 55, 56
D_c	critical diameter of hopper orifice for gravity flow	pp. 28, 29, 30 and etc.
D_d	dome width	pp. 91
D_h	hydraulic diameter of hopper orifice	pp. 34, 35, 37 and etc.
D_i	diameter of i^{th} particle	pp. 11
D_o	orifice size	pp. 30, 35, 36 and etc.
$D_{o,vibr}$	orifice size of vibratory dispenser hopper	pp. 68, 69
D_s	equivalent spherical diameter	pp. 9, 13
$D10$	maximum particle size for 10% of the sample	pp. 11
$D50$	maximum particle size for 50% of the sample	pp. 11
$D90$	maximum particle size for 90% of the sample	pp. 11
$D[p,q]$	generalized form of the mean particle size	pp. 11
F_C	cohesive force	pp. 127
F_H	adhesive force	pp. 12, 13

G	intensity of vibration	pp. 38
H	Hausner's ratio	pp. 16, 52
K	constant in Heckel's equation (eq. 2.5)	pp. 18
L	length	pp. 122
M	mass	pp. 17, 92, 93, and etc.
P	pressure	pp. 18, 19, 26
P_i	isotropic pressure	pp. 16
P_o	perimeter of hopper orifice	pp. 34
Q	specific charge	pp. 109
T	time	pp. 122
T_d	duration of vibration	pp. 61, 103, 121
T_i	interval between dispensing cycle	pp. 61
ΔT	duration of the impact between particle and wall of vibrating hopper	pp. 37, 38
U	contact potential	pp. 13
V	volume of particle;	pp. 9
	compacted volume of bulk solid in Walker's equation (eq. 2.4)	pp. 18
V_B	volume of bulk solid before tapping	pp. 16
V_c	cup volume in density measurement	pp. 17
V_T	volume of bulk solid after tapping	pp. 16
V_{rms}	root mean square voltage	pp. 61
V_0	unsettled apparent volume of bulk solid	pp. 17
W	discharge rate	pp. 34, 35, 36 and etc.
W_0	discharge rate predicted by equation (7.3)	pp. 127
W_1	flow rate when particles are in flight in Suzuki's equation (2.27)	pp. 37, 38

W_2	flow rate when particles impact the wall of hopper in Suzuki's equation (2.27)	pp. 37, 38
W_3	flow rate when particles remain on the wall of hopper in Suzuki's equation (2.27)	pp. 37, 38
a	distance between particle and wall;	pp. 13
	constant in Kawakita's equation (eq. 2.6);	pp. 19
	amplitude of vibration	pp. 68
b	constant in Kawakita's equation (eq. 2.6)	pp. 19
c	cohesion	pp. 24
c_w	adhesion between particles and wall	pp. 25
d	particle size	pp. 12, 36, 37 and etc.
d_1	opening diameter of a larger sieve	pp. 35
d_2	opening diameter of a smaller sieve	pp. 35
$\bar{d}$	average diameter of granules	pp. 35
e	porosity of powder	pp. 18
e_0	initial porosity of powder	pp. 18
f	frequency of vibration	pp. 38, 68
ff_c	flow factor	pp. 23
g	gravitational acceleration	pp. 28, 34, 35 and etc.
g_{eff}	effective gravity acceleration of particles in vibrating hopper	pp. 38, 68, 122 and etc.
H	height of dome to the apex of hopper;	pp. 30, 91
	filling height of bulk solid	pp. 26, 93
$\hbar\bar{\omega}$	Lifschitz-van der Waals constant	pp.13
K	constant in Beverloo's equation (eq. 2.21)	pp. 36, 37, 123 and etc.
M	mass of dose	pp. 109
$\bar{m}$	mean dose mass	pp. 121

q	charge	pp. 109
s	side length of square silo	pp. 26
t	time;	pp. 38, 68
	flow rate in minutes per 100 grams	pp. 35
v_{max}	maximum vibration velocity	pp. 33
Δv	relative velocity of free fall particle and the wall of hopper at impact	pp. 37, 38
w	Walker's compressibility coefficient;	pp. 18
	discharging velocity of bulk solid through an outlet	pp. 34
ϕ_d	angle between the stagnant zone boundary and the horizontal	pp. 28, 36, 37
ϕ_w	angle of wall friction	pp. 25, 30, 31 and etc.
α	liquid bridge angle;	pp. 13
	half conical angle of hopper;	pp. 28, 29, 30 and etc.
	constant in equation (7.12)	pp. 129
α_M	angle of repose	pp. 20
α_{max}	critical half conical angle of hopper for bulk solid flow	pp. 30
α'_{max}	critical half conical angle of hopper for mass flow	pp. 31
β	maximum possible shear stress reduction	pp. 33
	constant in equation (7.4)	pp. 125
	constant in equation (7.12)	pp. 129
γ	surface tension of liquid;	pp. 13
	characteristic vibration velocity;	pp. 33
	vibration coefficient in equation (7.14)	pp. 131, 133
δ	contact angle of liquid bridge;	pp. 13
	angle of internal friction	pp. 24, 30, 88
δ_e	effective angle of internal friction	pp. 31

ρ_B	bulk density	pp. 16, 28, 35 and etc.
ρ_T	tapped density	pp. 16, 52
σ	electric charge density;	pp. 13
	normal stress	pp. 21, 24
σ_c	unconfined yield stress	pp. 23, 28, 29 and etc.
$\sigma_{c,\,vibr}$	unconfined yield stress under vibration	pp. 68, 98
σ_h	horizontal compressive stress	pp. 22
σ_v	vertical compressive stress	pp. 12, 22, 26, 27
σ_w	normal stress on the wall	pp. 25, 27, 90
σ_γ	compressive stress	pp. 12
σ_1	major principal consolidation stress	pp. 22, 23, 26 and etc.
σ_2	minor principal consolidation stress	pp. 22
σ_1'	bearing stress of dome	pp. 29, 98
λ	constant in Verghese equation (eq. 2.23)	pp. 37
λ_s	sphericity	pp. 13, 35, 122 and etc.
μ	friction coefficient;	pp. 24, 35
	constant in equation (7.5)	pp. 125, 131, 132 and etc.
τ	shear stress	pp. 21, 24, 33
τ_{vibr}	shear stress in the presence of vibration	pp. 33
τ_w	shear stress on the wall	pp. 25, 90, 98

Contents

Figures

Tables

Chapter 1

Introduction

This chapter introduces the background of establishing this Ph.D. project and an overview of how our work contributes to this area. The objectives of project are presented along with a full preview of project contents and thesis structure. Author's research thoughts and strategy to fulfil the established objectives are framed.

1.1. Project Background

Worldwide materials industries dedicate to improve the quality of human life with continuous development and introducing of new products to meet customer's demand. In the process, bulk solid materials are known as raw materials, intermediates and final products involved in many industries. It is estimated that roughly one-half of the products and at least three-quarters of the raw materials are in the form of bulk solid in the chemical industry [1] (p. 1).

Bulk solid is an assembly of solid particles that is large enough for the statistical mean of any property to be independent of the number of particles [2]. As the handling of bulk solid is always a challenge especially when it comes to the dispensing process, knowledge of the distinct mechanism of collective behaviour of particles is necessary. It was only over the last century that scientists and engineers had endeavoured to find out the science behind the fluidizing mechanism of bulk solids, although it was highly attractive for many people seeking mass control of dispensing bulk solids long time ago [3-12]. Though the bulk solids dispensing process does not directly create the value for industry as particulate materials do in unit operations, e.g. grinding, agglomeration, mixing, and separation, the research on dispensing of bulk solids helps to reduce or solve the problems caused in storing and transforming process and provide effective solution, which is a key cost saving advantage for industry [13] (p. 1-4).

Conventional dispensing technologies, such as gravimetric or volumetric techniques, are either less accurate in continuous dosing (gravimetric) or time consuming (volumetric) in large scale production-line processes [14]. These techniques are also very susceptible to bulk solids flow obstructions caused by poorly designed dispensing unit, e.g. silos, hoppers and bins [6] (p.218-240). Neither method is capable of providing accurate dose-to-dose consistency for dispensing amounts below 1 milligram [14]. Due to the limitations of conventional dispensing technologies, the industry is looking for a more accurate and effective dispensing solution which is also able to handle very small amount of solids.

A great deal of works has been done on the study of bulk solids flow in dispensing units, in most of which solids flow under the influence of gravity [4-6, 15-17]. The fluidization of bulk solids with small particle size, however, is still a challenge due to the high level of cohesion in small particles [18]. Blockage of dispenser along with rat-holing and arching of particles are well-known issues in the dispensing of fine and cohesive powders [13]

(p. 1-4). Despite various practical solutions to these issues have been attempted to overcome the hindrance for the free flowing of fine powders, few is proven versatile in all kinds of situations [14]. Mechanical compaction, pneumatic and vibration are most commonly adopted techniques in powder dispensing [19-23].

S. Yang and his co-workers have been studying on micro-dispensing bulk solids in an acoustic vibration agitated capillary since ten years ago [24-31]. The feasibility of acoustic vibration micro-dispensing technique has been demonstrated with dispensing metal and ceramic powder materials [25, 29, 30]. However, the technology is yet mature to meet all the requirements of bulk solids dispensing, especially in pharmaceuticals and biomaterials as the powders are more cohesive and with worse flowability. This Ph.D. project is therefore established to deal with new issues in dispensing pharmaceutical fine powders and biomaterial solids. It is also promising to be applied to dry powder libraries fabrication for high throughput screening in laboratory trials, solid form oral drugs producing on industrial production line, and customization of personalized medicine for individual patients.

1.2. Project Objectives

The primary objective of this project is to investigate bulk solids fluidizing process under the influence of applied vibration and develop a bulk solids micro-dispensing device taking account of flow properties of materials, device design and processing parameters; to demonstrate the dispensing process with commercial active pharmaceutical ingredients (API), excipients and biomaterials, record and analyse dispensing results with industrial standard; to understand the influence of critical factors such as design and processing parameters on the dispensing results.

The second objective of this project is to develop a robust mathematical model by studying on the correlations between dispensing results, i.e. discharge rate, dosages consistency, device design, vibration signal parameters and materials properties. The derived equation can be used to predict dispensing results to supervise practical applications.

The final objective of this project is to integrate micro-dispensing device with 3D printing technology to achieve practical applications including: the production of solid

dosage forms of pharmaceutics, e.g. capsules and blisters, the fabrication of dry powder libraries for high throughput screening and solid form personalised drugs.

1.3. Project Preview

The thesis contains a total of 9 chapters including this **Chapter 1** as the Ph.D. research project introduction.

Chapter 2 provides the background review of bulk solids fluidization and dispensing. The physical properties of individual particle are primarily introduced as they dominate the collective behaviour of bulk solid. Researches on fluidizing mechanism and flow properties of bulk solid are reviewed mainly in the case that flow and discharge occur in hopper. The methodology and key factors in the design of dispensing hopper are discussed. In addition, important works on correlations between flow rate and design parameters of bulk solid feeding vessel are reviewed. At last, current dispensing techniques are categorized into indirect and direct dispensing methods and their principles and applications are reviewed. The vibratory dispensing technique is mainly introduced as it has proved effective in dispensing fine powders and has not yet been rigorously explored.

Chapter 3 introduces materials and experimental methods in this project. All bulk solid materials are categorized in two classes according to mean particle size and bulk solids properties are probed and measured by general bulk solid characterization processes. The experimental methods of dispensing hopper and vibratory dispenser design are described. A computer controlled auto dispensing and weighing system are set up for the dispensing tests with two mechanical vibration dispensers and an ultrasonic vibration dispenser. The weighing and data evaluation method of dispensing test is described. The mass of dose and relative standard deviation (RSD) of dropwise dispensed samples will be used to evaluate dispensing test results in following chapters.

Chapter 4 presents experimental study investigating the dispensing of hydroxyapatite (HA) granule with mechanical vibration devices. The basic principle of how the vibration works on fluidizing bulk solids in the hopper is presented. The experimental results show that the vibration leads to a reduction of the bridge strength of particles in the hopper. The two types of horizontal vibration provided by electromagnet solenoid and vibration motor were proved effective in dispensing irregular shaped coarse granules

such as HA. The effect of dispensing hopper size, device settings and vibration characteristics on the dispensing was discussed.

Chapter 5 presents experimental study on the ultrasonic vibration dispensing of pharmaceutical and biomaterial fine powders. The inhalation grade lactose powders exhibit a good flowability in the hopper with consistent flow rate, whereas the non-free flowing powders exhibit an "extrusion" mechanism. The experimental results show the dispensing with ultrasonic vibration device is subjected to a dome-controlled flow mechanism. The flow rate of free flowing powder is consistent so that the dosage is mainly determined by the duration of vibration. The flow rate of non-free flowing powder subjected to extrusion mechanism normally is low and less consistent under the influence of ultrasonic vibration. The dosage is found not proportional to the vibration duration due to the strong cohesions and poor flowability of non-free flowing powders. The effect of hopper geometries on the dispensing is assessed with different powder materials.

Chapter 6 describes a triboelectric charging phenomenon investigated in ultrasonic vibration dispensing of pharmaceutical powders. The charge of powder influences the accuracy and consistency of powder dispensing. A solution to the charging issue is proposed by modifying the contact surfaces in the hopper with platinum coating. Glass dispensing hopper and platinum coated hopper was tested respectively to investigate the flow and discharge behaviour of pharmaceutical excipient powders. With comparing the dispensing results from both hoppers, the Pt-coated surface favourably changed the powder charging and flow in the dispensing hopper. The hopper surface modification provides a possible solution to the charging issue in ultrasonic vibration powder dispensing in order to improve dispensing results of pharmaceutical powders.

Chapter 7 presents the derivation of a correlation between ultrasonic vibration dispensing results and device design parameters taking account of different properties of material particles. The correlation aims to predict the flow rate in dispensing with the information of device specification and material properties. Compared with the experimental results, the predicted results suggest the correlation is able to predict the discharge rate for inhalation grade lactose in ultrasonic vibration dispensing when the flow of powder is steady and controllable in the vibrating hopper.

Chapter 8 presents an application by integrating ultrasonic vibration dispensing device with 3D printing technology. The aim is to build a powder dispensing platform to demonstrate the feasibility of producing solid form oral drugs and

pharmaceutical/biomaterial dry powder libraries for high-throughput screening (HTS) of new products.

Chapter 9 This chapter concludes the thesis and summarises the work completed. The scope for future work is also discussed.

The research strategy for this project is shown in Figure 1-1.

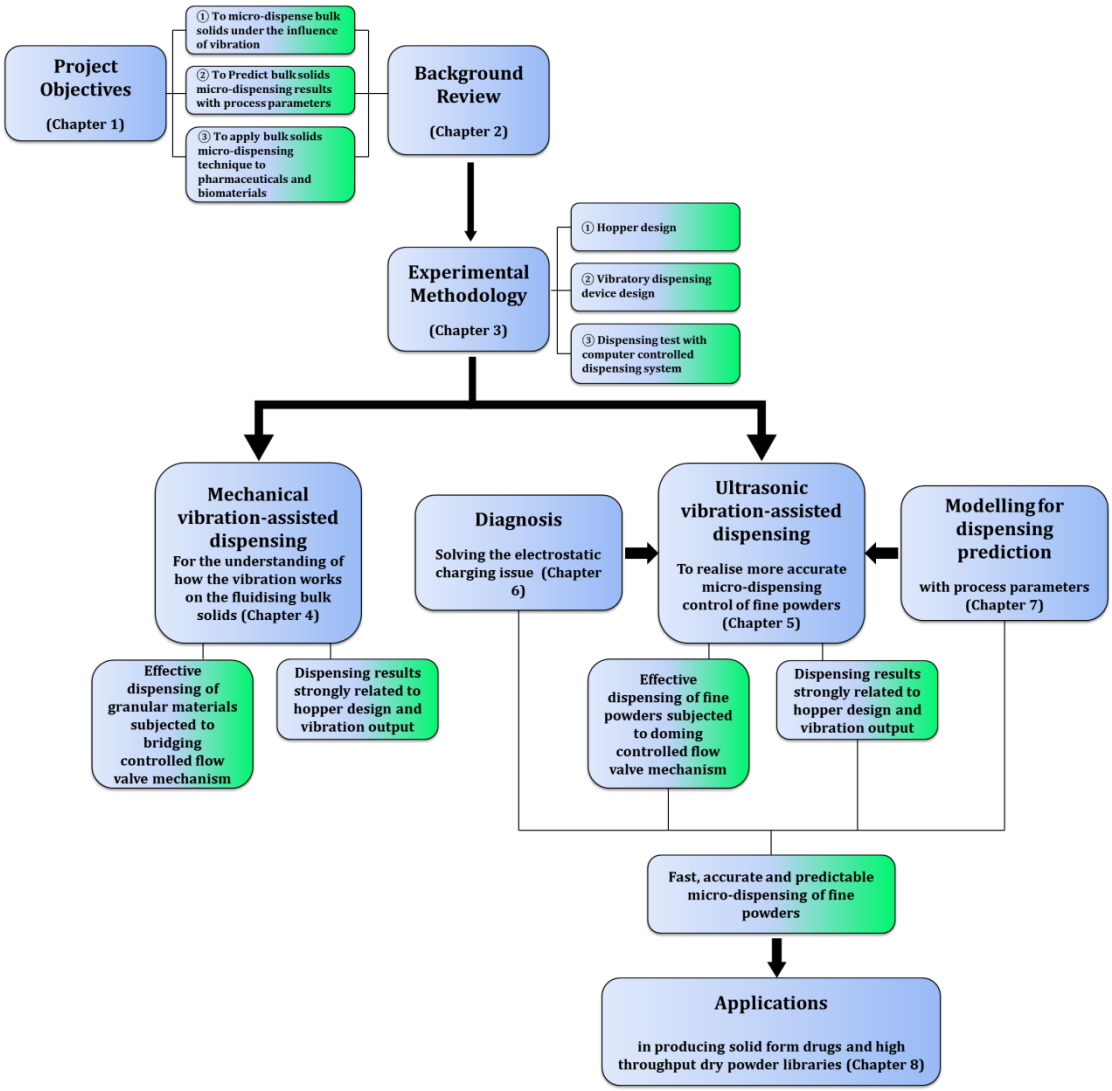

Figure 1- 1 The research strategy for this Ph.D. project

Chapter 2

Background of Bulk Solids Fluidization and Dispensing

This chapter provides the background review of bulk solids fluidization and dispensing. The physical properties of individual particle are primarily introduced as they dominate the collective behaviour of bulk solid. Researches on fluidizing mechanism and flow properties of bulk solid are reviewed mainly in the case that flow and discharge occur in hopper. The methodology and key factors in the design of dispensing hopper are discussed. In addition, important works on correlations between flow rate and design parameters of bulk solid feeding vessel are reviewed. At last, current dispensing techniques are categorized into indirect and direct dispensing methods and their principles and applications are reviewed. The vibratory dispensing technique is mainly introduced as it has proved effective in dispensing fine powders and has not yet been rigorously explored.

2.1. Bulk Solid and Its Properties

2.1.1. Fundamentals

The general term of “bulk solid” is applied to solid material with an assembly of solid particles that is large enough for the statistical mean of any property to be independent of the number of particles [2], such as ores, coal, cement, flour, cocoa, soil and etc. Gravity is usually relied upon to cause these solids to flow where the volume of the solids is substantial. In some of the literatures, the word “powder” is mentioned, e.g., in pharmaceutical industry “powder” is common, whereas materials like cement, sand, and coal are known as bulk solids. To define certain terms for bulk solids with different properties of their individual particle and collective behaviour, many authors have tried to classify solid materials according to their mean particle size. Richards [10] proposes the classification given in Table 2-1.

Table 2- 1 Richards’s classification for bulk solid materials [10]

Particle Size Range	Name of Material	Name of Individual Component
0.1 μm – 1.0 μm	Ultra-fine powder	Ultra-fine particle
1.0 μm – 10 μm	Superfine powder	Superfine particle
10 μm – 100 μm	Granular powder	Granular particle
100 μm – 3.0 mm	Granular solid	Granule
3.0 mm – 10 mm	Broken solid	Grain

For reason of simplifications, the particles of sample materials involved in this work are categorized into two classes, coarse particles (>100μm) and fine particles (≤100μm), according to the individual particle size. And when it refers to materials’ collective behaviour in process of handling, the term “powder” is used to represent active pharmaceutical ingredients (API), excipients and biomaterials with mean particle size smaller than 100μm, while “granule” refers to materials with mean particle size larger than 1mm. The term “bulk solid” is used as a general speaking of all materials consisting of large quantities of particles.

2.1.2. Physical Properties of Bulk Solid

As the definition of “bulk solid” describes, it consists of a large number of individual particles. In theoretical model, there are 10^9 particles of a diameter of 10μm are contained in one cm^3 [13] (p. 9). In principle, the behaviour of bulk solid is able to be described by the properties of its particles or regarding the bulk solid as a continuum. The former is thought to be difficult in many occasions taking account of distinct

physical properties of each particle in bulk solids, such as particle size and shape. Also, the particle-particle interactions can hardly be accurately calculated due to the large quantities of particles. Regarding bulk solid as a continuum, stresses in the bulk solid can be studied on supposed volume elements boundary areas which are similar to the ones in fluid mechanics. The volume elements are large enough with respect to the particle size so that local interactions between individual particles are inconsiderable. Schulze [13] provided a comprehensive treatise on behaviour, characterization, storage and flow of bulk solids, which remains the most complete body of work on the subject to date. In this section, the physical properties relevant to the flow behaviour of bulk solid will be discussed. The analysis of stress state and flow properties of bulk solid in a defined volume of vessel will be presented in section 2.1.3.

2.1.2.1. Particle size

Particle size is one of the most important properties which dominate the collective behaviour of bulk solids. Understanding of the relationship between particle size and flowability of bulk solids will help in the design of dispensing vessel in this project (discussed in Chapter 4 and Chapter 5).

Obviously, the particle size of a spherical particle can be unambiguously and quantitatively defined by its diameter. The simple measurement of a single spherical particle is using micrometer and if the particle is small, a travelling microscope can be used [1] (p. 134). However, a typical material particle is likely to be irregular in shape and non-spherical. In this case, the regular measure of size is to replace the given particle with an imaginary sphere that has one of the properties identical with the particle [32]. The *equivalent spherical diameter* D_s can be defined by

$$D_s = \left(\frac{6V}{\pi}\right)^{1/3} \tag{2.1}$$

where V is the volume of the particle. This is the diameter of the sphere having same volume as the measured non-spherical particle.

Another common measure of non-spherical particle size is *feret diameter* [33]. It is the extent of the particle measured between the two extreme tangents parallel to an arbitrary direction as illustrated in Figure 2-1. The variation of feret diameter with angular position can give a great deal of insight into the shape of particle. The feret diameter is a common method used to measure the particle size in the microscope and the scanning electron microscope (SEM) images analysis. Also, the particle size is able to

be determined by sieving and a current widely used laser diffraction particle sizing technique. The principles of laser diffraction technique will be discussed in next section.

However, the equivalent sphere concept was found not suitable for measuring the size of special shaped particles with low sphericity [32], such as rods, needles or plates. The size in at least one dimension can differ significantly from that of the other dimensions, and thus this featured size can be used to represent the particle size. Several researchers have investigated online particle characterization techniques to measure non-spherical particles [34-38].

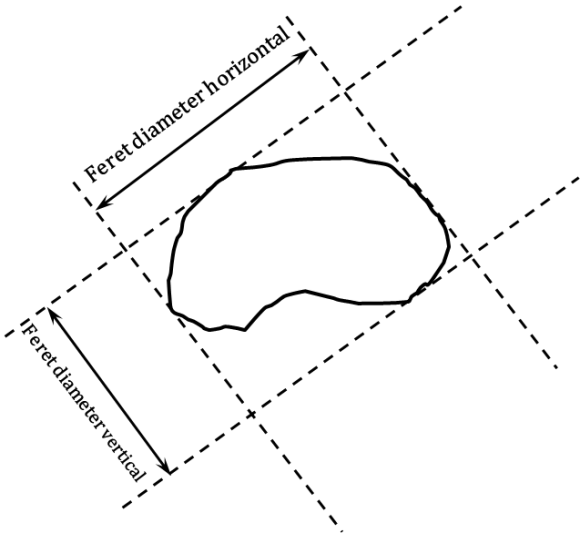

Figure 2- 1 Definition of the feret diameter

2.1.2.2. Particle size distribution (PSD) and mean particle size

Although the measuring of single particle size has little difficulty, it is most unlikely all the particles in bulks have same particle size. Thus, particle size distribution and mean particle size are two important properties when the bulk solid is treated as continuum.

Particle size distribution (PSD) of bulk solids can be defined by number which means a certain number of particles having sizes in a size range [39]. Counting technique such as microscope images analysis can be used to determine a number weighted distribution that each particle is given equal importance [40]. For this method, knowing the absolute number of particles is important. PSD is also able to be weighed by mass which refers to a certain mass of particles having sizes in that range [40]. The traditional method of PSD determination is sieve analysis, where powder is separated by sieves of different sizes so that the PSD is defined in terms of discrete size ranges by mass.

In this project, volume weighted distributions and intensity weighted distributions are measured by laser diffraction particle sizing technique (Malvern® Mastersizer 2000, U.K.) [40]. The measurement method is described in Appendix I. The laser diffraction technique measures particle size distributions by measuring the angular variation in intensity of light scattered as a laser beam passes through a dispersed particulate sample. Large particles scatter light at small angles relative to the laser beam and small particles scatter light at large angles. The angular scattering intensity data is then analysed to calculate the size of the particles responsible for creating the scattering pattern, using the Mie theory of light scattering. The particle size is reported as a volume equivalent sphere diameter. In one of recent researches, Adi et. al [41] have applied laser diffraction technique to determine particle size distributions of cohesive lactose powders.

With particle size distribution measurements, mean particle size can be determined. It has various definitions because the mean value is associated with the basis of the distribution calculation [40]. The generalized form of the mean particle size can be given by $D[p,q] = \frac{\sum_1^n D_i^p}{\sum_1^n D_i^q}$, where D_i is the diameter of the ith particle and n is the number of particles [42]. As bulk solid materials used in this project have distinct particle size distribution, a statistic value D (D10, D50 and D90) is used to represent the volume weighted particle size distributions. The D value is the maximum particle size for a given percentage volume of the sample, e.g. the D50 is the maximum particle size below which there is 50% of the sample volume exists.

In pharmaceutical manufacturing industry, different particle size and particle size distribution can be achieved by dry milling approach such as pin milling [43] and jet milling [44], and wet milling approach such as high shear rotor-stator [45], ultrasound [46] and etc. Another way to generate fine particles is through crystallization i.e., nucleation, under high supersaturation [47]. The particle size D50 of materials in this project is provided in Chapter 3.

2.1.2.3. Adhesive and cohesive forces

Empirically, the flow of bulk solid improves with an increasing particle size. In essence, adhesive forces between particle and wall of vessel and cohesive forces between individual particles are main interparticle forces affect the flow of bulk solid [48]. The intensity of cohesive and adhesive forces depends on particle size, the distance between particles and the interacting surfaces [13] (p. 23-31). Rumpf [49] has studied the

interparticle forces in bulk solid. It has been indicated that the adhesive forces between a sphere and a wall are proportional to the particle size (Figure 2-2(a)). The spherical particle and wall are assumed to have ideally smooth surface and the distance between them is a constant. When particle size is small (less than 100μm), liquid bridge is the major adhesive force between particle and a wall if the particles are moist, while in dry powder van der Waals force is dominant followed by electrostatic force [49]. Regarding to the influence of distance between spherical particle and smooth surface, liquid bridge plays an important part in moist powder yet only within a small range of distance. It vanishes when the distance is larger than around 1 μm [49]. In dry bulk solid, the van der Waals force has most influence when the distance between surfaces is very small as shown in Figure 2-2(b). The van der Waals and electrostatic forces also decreases significantly with increasing distance [49]. Thus, the van der Waals force is dominant in dry bulk solid (particle-particle/particle-wall) when the surfaces are in contact; the cohesive and adhesive forces decrease with increasing distance between surfaces.

As it also shown in Figure 2-2(a), the function curve of particle weight against particle size has the largest slope. When it reaches to a sufficiently large particle size, the weight force becomes the dominant one in adhesive forces. This can explains that in a bulk solid material with certain particle size distribution, the fine particles tend to adhere to a vertical wall of container whereas the large ones cannot.

According to Rumpf's results, one would expect smaller particles has smaller adhesive forces between particles and the wall of vessel. Nevertheless, in the case that bulk solid flows in a vertical vessel, bulk solid is consolidated under the gravity and thus the distance between particles decreases. Consequently, cohesive forces between individual particles increase. When bulk solid is subjected to a compressive stress, the compressive stress σ_γ is inversely proportional to particle size [13](p. 32-34), which can be given by

$$\sigma_\gamma \propto \frac{F_H}{A_\gamma} \propto \frac{d}{d^2} = \frac{1}{d} \tag{2.2}$$

where A_γ is area of particles where compressive stress acts. Therefore, with smaller particle size the bulk solid is more compressed and the strength of bulk solid becomes greater. The flowability of bulk solids depends on both interparticle forces and other forces acting on the bulk solid. It can be concluded that the influence of interparticle forces on the flowability increases with reduced particle size. More about stress state and flowability of bulk solids in the static vessel will be discussed in section 2.1.3.

In reality, the adhesive and cohesive forces are found more complex in the bulk solid composed of particles with different particle size. Even if particles have identical size, they also exhibit a wide range of interparticle forces due to different shape and/or surface structure which affects the distance between surfaces.

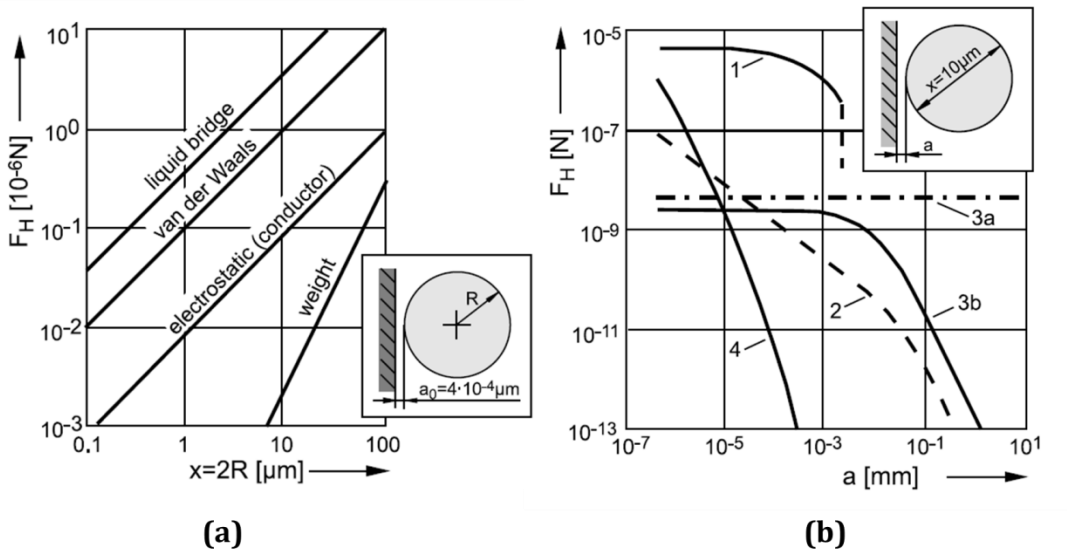

Figure 2- 2 Influence of (a) particle size, x, and (b) distance, a, on the adhesive force F_H between a spherical particle and a wall in ideal conditions (ideally smooth surfaces of sphere and wall): *liquid bridge* (curve 1 in (b): bridge angle α = 20°, surface tension of the liquid γ = 7.2·10^{-2} N/m, contact angle δ= 0°); *electrostatic force for a conductor* (curve 2 in (b): contact potential U = 0.5 V); *electrostatic force for an insulator* (3a. sphere semispace; 3b. sphere-point charge in (b): electric charge density σ = 10^2 e/µm^2 = 1.6·10^{-17} As/µm^2); *van der Waals force* (curve 4 in (b): Lifschitz-van der Waals constant $\hbar\bar{\omega}$ = 8·10^{-19} J). Re-printed from [13] (p.25-26) which is originally from [49] (p. 114-120)

2.1.2.4. Particle shape and surface roughness

The influence of particle size on cohesive and adhesive forces discussed in section 2.1.2.3 is based on ideal conditions, i.e. spherical particle; smooth surfaces of particle and wall. However, it is most likely that particles in bulk solids have different shapes in reality. The overall shape of a particle can be characterized using relatively simple parameters such as aspect ratio. For a non-spherical particle, parameter λ_s known as the shape factor, can be defined by [50],

$$\lambda_s = \frac{A_s}{\pi D_s^2} \tag{2.3}$$

where D_s is the equivalent spherical diameter defined in eq. (2.1) and A_s is the surface area of the particle. Thus, the shape factor λ_s is also called the sphericity. For particulate material, one often finds that smooth, spherical particles exhibit a better flowability under the gravity than rough, sharp-edged, non-spherical particles. Particle shape and surface roughness affects flow properties through interparticle forces as less sphericity of particles result in higher static and dynamic friction forces [51]. Sandler et al. [52] and Yu et al. [53] established a partial least squares (PLS) modelling approach to predict powder flowability of pharmaceutical materials from their particle size and shape distributions. The results revealed that both particle size and shape play an important role in determining the powder flow behaviour.

Surface roughness of particles is a component of surface texture of particle. It can be quantified by the deviations between a real surface and its ideal smooth surface. The adhesive force and cohesive force can be greatly affected by surface roughness of particles and the effect is complex in different particulate system. Burnett et al. [54] indicates the rank order of drug-carrier adhesion in roughness of the larger carrier particle is “rough surface > smooth surface > micro-rough surface” when other particle properties has no change. The rough particles with higher dispersive surface energy and specific surface area would form strong agglomerates [55].

To change the adhesion between particles, bulk solid are also mixed with a small portion of particles as a flow agent [56-58]. The influence of flow agent particles is similar to increase the surface roughness of bulk solid particles. As result, the adhesive forces are reduced due to the increased distance between bulk solid particles [56]. A number of works have been reported on changing flowability of bulk solid by mixing differernt particles.

Irwin et al. [59] investigated the relationship between flow rate of different blends of clomacran phosphate and fill weight uniformity. Different blends were prepared by mixing API (active pharmaceutical ingredient) with different lubricants at different grades. Data suggested that the differences in particle size were responsible in part for the observed weight variation; large particle size showed less variation and small particle sizes presented greater variation. Apart from the particle size, other factors were found to affect the dose fill weight such as batch-to-batch variability and concentration of API.

Podczeck & Miah [60] studied the influence of particle size and shape on the angle of internal friction and the flow factor (see section 2.1.3) of unlubricated and lubricated

powders in an annular shear cell. The tests were undertaken for powders with different particle sizes and shapes and blends with a range of lubricants concentrations. For unlubricated powders, it was found that the flowability depended on the particle shape whereas the angle of internal friction depended on the shape and particle size. When the lubricant was added to the blends, the optimal lubricant content, flowability and angle of internal friction were dependant only on the particle shape.

Liu et al. [61] studied the flowability of a needle shaped ibuprofen size fractions using two flow measurement methods. The experimental results showed that powder flowability is significantly affected by both the particle size and size distribution. The finest size fraction that is separated from the bulk ibuprofen powder flows better than the bulk. For powders with narrow size distributions, the flowability increases significantly with the increase in particle size. In addition, admixing magnesium stearate to ibuprofen not only increases the flowability of the powder, but also reduces the internal friction angle.

2.1.2.5. Density and compressibility

The density and compressibility are two physical properties of bulk solids and also indications of flowability. The discussions on density is similar to that on particle size as the density of single particle and density of bulk solid are two distinct properties to the material.

The actual density of the particle is also called solid density. Even if the particles themselves may be compressible, the change in solid density over the range of stresses normally encountered is small, so that solid density is effectively a constant for a given material [1] (p. 5-6). Generally, it can be measured by the standard techniques of liquid displacement [62] following Archimedes' principle and gas displacement with a gas pycnometer usually using air as the medium.

Bulk density is defined by the ratio of the mass of an amount of bulk solid to its volume. It is always less than solid density, since voids exist between the individual particles of a bulk solid [63]. The bulk density is always found to vary significantly with applied stress, mainly as a result of rearrangement of the particles [64]. In another word, it depends on the state of consolidation of the bulk solid. It was studied by Nedderman [1] (p. 128-134) that the bulk solid material does not necessarily expand to former state when the compressive stress is reduced or removed. As described in Nedderman's work, the variation in the bulk density of an initially loose bulk solid is shown in Figure 2-3. An

isotropic pressure acts on the solid. The bulk solid is compressed with increasing the isotropic pressure along the section AB due to rearrangement of particles. However, with reducing the pressure, little expansion can be observed along BC. It has proved an irreversible change of bulk density which is similar for CD section. To keep increasing the pressure along DEF, the bulk solid is finally crushed and irreversible changes in the nature of material take place.

However, the isotropic stress state discussed above is an ideal state. In practice, the variable bulk density is usually measured in a shear tester. The bulk density obtained after consolidation of a bulk solid specimen depends not only on the consideration stress (see section 2.1.3), but also on the consolidation procedure (e.g. uniaxial, isotropic) [65]. A considerable part, about 60%, of stored bulk solids continue to gain strength if stored at rest under compressive stress for a long time period [66]. This effect is called time consolidation, and also known as caking. The reasons for time consolidation are also to be found in the effects of adhesive forces, which increase through approach of particles and enlargement of contact areas. [67]. If particles are moved against each other, these adhesive forces diminish and can build up again during further storage at rest.

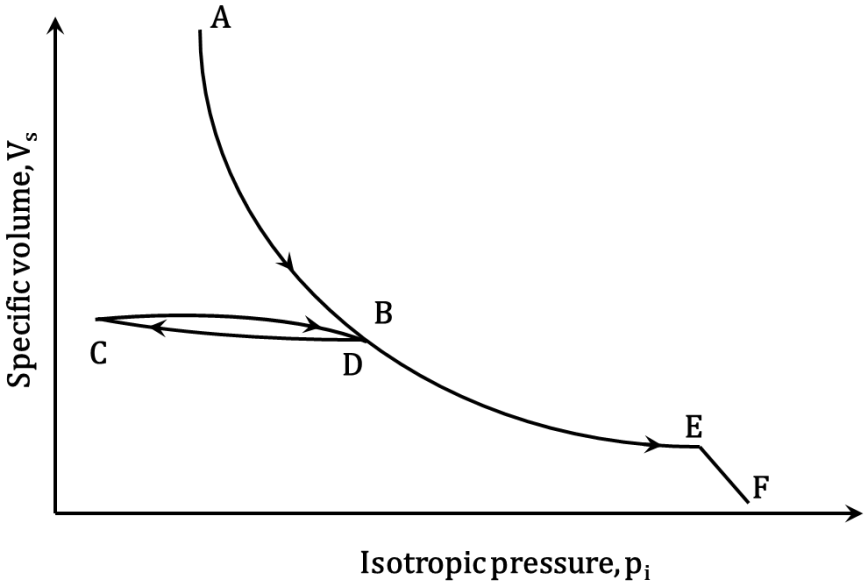

Figure 2- 3 Dependence of the specific volume on isotropic pressure. The sample is measured in isotropic stress state when three principle stresses are equal to isotropic pressure. The test is processed from A to B, B to C, C to D and then D to E,F. Reprinted from [1] (p.129)

When bulk solids initially occupied a certain volume in a container such as a measuring cylinder, the volume would be reduced by particles re-arranging if the cylinder

continues to be tapped by mechanical action. The bulk density ρ_B is increased and this increased density is called tapped density ρ_T. The bulk density and tapped density are used to calculate the flowability of bulk solids by using compressibility index, $C = 100\frac{V_T - V_B}{V_B}$ (V_T, V_B are volumes of bulk solid after and before tapping), which firstly described by Carr [7], or closely related Hausner's ratio, $H = \frac{\rho_T}{\rho_B}$, [8]. To calculate these parameters, which are not intrinsic properties and can be influenced by particle size and shape, surface area, moisture content, and cohesiveness of the material, it is necessary to determine the unsettled apparent volume and final tapped volume or the corresponding bulk and tapped density. Therefore, the European Pharmacopeia (Ph. Eur.) 8.0 has issued standardized methods [68, 69] to determine bulk density and tapped density of a powder. The bulk density of powder is measured by passing a known mass of powder through a sieve into a 250 mL graduated cylinder without compacting. The apertures of sieve are greater than or equal to 1.0 mm. The unsettled apparent volume (V_0) is read and the bulk density is calculated by equation M/V_0. A similar method is introduced by passing the powder through a volumeter into a cup or vessel of minimum 25 cm^3 (Figure 2-4) until the powder overflows from cup. The mass of powder fully filled in the cup is weighed by carefully removing the residual powder from the side of cup and the bulk density is calculated by equation M/V_c, where V_c is the cup volume.

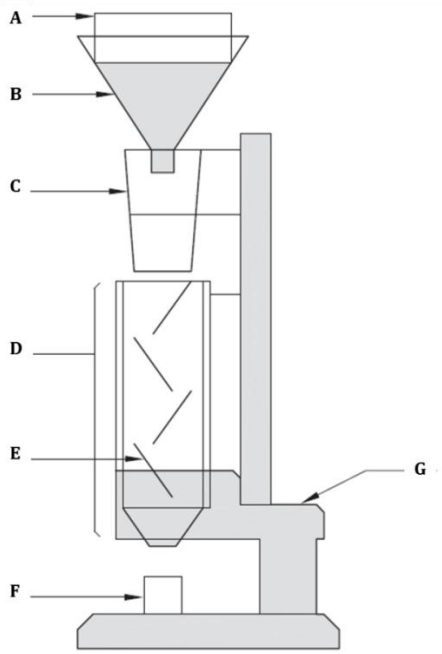

Figure 2- 4 Volumeter for measuring the bulk density of powders: A. 1.0 mm sieve; B. powder funnel; C. loading funnel; D. baffle box; E. glass baffle; F. cup; G. stand. Reprinted from [68] (p. 344)

The tapped density is obtained by mechanically tapping the graduated cylinder or vessel mentioned above until little further volume or mass change is observed. The tapping is completed by raising the cylinder or vessel and allowing it to drop under gravity. The method described in European Pharmacopoeia 8.0 introduced a settling apparatus capable of producing 250±15 taps per minute from 3±0.2 mm height or 300±15 taps per minute from 14±2 mm height [68].

In a free flowing powder, the bulk density and tapped density would be close in value. Thus the Carr's index would be small or Hausner's ratio would be small. For a non-free flowing powder where there are greater interparticle interactions, the difference between the bulk and tapped density observed would be greater, therefore, the Carr's index would be bigger or Hausner's ratio would be larger. For the Carr's index and Hausner's ratio, the generally accepted scale of flowability of solid particles is given by Carr [7] in Table 2-2.

Table 2- 2 Flowability Scale of Solid Particles Given by Carr [7]

Carr's Index (%)	Flow Character	Hausner Ratio
≤10	Excellent	1.00-1.11
11-15	Good	1.12-1.18
16-20	Fair	1.19-1.25
21-25	Passable	1.26-1.34
26-31	Poor	1.35-1.45
32-37	Very poor	1.46-1.59
>38	Very, very poor	>1.60

The density and compressibility of bulk solids have caught more attentions in industry as they are always related to the other properties of bulk solids as well as flowability. Since the 1920's the compaction of powders has been studied with a view to predict the bulk solids density in industrial process. Walker [3] proposed the first compaction equation for predicting volumes V as a function of the axial pressure P applied,

$$V = -w \cdot logP + A \tag{2.4}$$

where w is Walker compressibility coefficient and A is a constant. This equation was developed empirically where w values were found different for materials with different plasticity.

Denny's [70] has reviewed and compared the most commonly used compaction equations in pharmaceutical industry: Heckel's equation and Kawakita's equation. Each

industry tends to use different equations for reasons linked to the research priorities or the kind of powder used to develop the equation.

Heckel's equation:

$$ln\frac{1}{e} = ln\frac{1}{e_0} + KP \tag{2.5}$$

where e and e_0 are porosity and initial porosity of powder being compacted. K is a constant related to plasticity of material; P is pressure applied.

Kawakita's equation:

$$\frac{P}{C} = \frac{1}{ab} + \frac{P}{a} \tag{2.6}$$

where P is pressure applied; C is relative volume decrease, $C = \frac{V_0 - V}{V_0}$; a and b are compatibility constant.

Equation 2.5 and 2.6 have been reported only available for a limited range of materials as they are less successful in relating densification behaviour to the physical and mechanical properties of the materials being compacted [70]. Mendez et al. [71] developed an experimental methodology for the characterization of density in a powder bed utilizing X-ray micro-computerized tomography (micro-CT). The density changes of three common pharmaceutical powders were studied in his work. It was found that the three powders exhibited different packing rates and final states. It was also found that the density increased in the powder bed as a function of the number of taps, frequency, and amplitude. Additionally, a more uniform density profile was achieved by employing higher amplitudes. It was found that changes in density were more significant in less cohesive powders when tapped with lower amplitude and frequency, while the density changed enormously in cohesive powders when tapped with higher frequency. As powders increase in cohesion, it was found that more mechanical energy was required to alter the agglomerated powder bed. Additionally, the density at the top of the powder bed was significantly more dense than that at the bottom for free-flowing microcrystalline cellulose, however, the results were directly opposite for the other more cohesive powders. Traina et al. [72] introduced an additional porous volume added to the optimal granular packing to represent the difference between the volume of the powder bed and that of the same powder but when ideally packed. It was found

that the volume of additional air trapped/stored between the particles when the powder passes from a dynamical state to a static state. If the powder bed traps air, it is then able to restore air partially or completely or not at all, depending on the interparticle cohesion level. The data showed if the powder is non-cohesive or free flowing, it traps a small amount of air in its static state. Conversely, if the powder is cohesive, it traps more air.

2.1.2.6. Angle of repose

When bulk solid is piled on a plate, the top surface of the pile is not necessarily horizontal. The maximum angle between the slope, where the particles are on the verge of sliding, and the plate is called Angle of Repose (AoR). It can be measured with a conical pile made from bulk solids (Figure 2-5(a)). The pile is usually formed by pouring the bulk solid through a funnel which is located above a bottom plate. The funnel can be either fixed or moved upwards while the pile is formed in order to keep the distance between the tip of the pile and the funnel constant [73, 74]. Different measurements are drained angle of repose (Figure 2-5(b)) and dynamic angle of repose (Figure 2-5(c)) [74] (p. 25-27). Angle of repose is not intrinsic property of bulk solid material as it is very dependent on the test procedure, e.g. the way pile is formed.

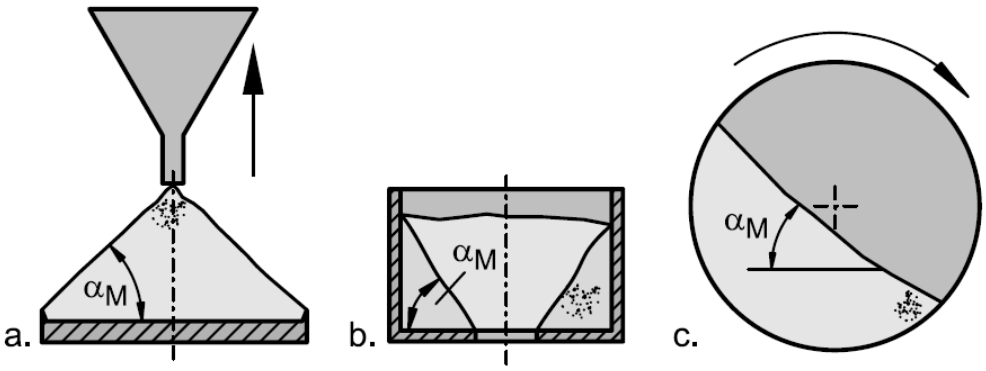

Figure 2- 5 Measurement of angle of repose, α_M: (a) poured angle of repose; (b) drained angle of repose; (c) dynamic angle of repose, re-printed from [13] (p.172)

Angle of repose is a bulk solid property related to the internal friction so that measuring angle of repose can compare the flowability of bulk solids [75, 76]. In general, the material with good flowability has a smaller angle of repose [77, 78]. Due to poor flowability, cohesive powders is often piled with a peaked tip and varying angle from top to the bottom so that the angle of repose of cohesive material is unlikely to be measured

[13, 79, 80]. Carr [7] classified flowability according to angle of repose measured with solid particles poured from bins, hoppers, and feeders, shown in Table 2-3.

Angle of repose can be used in the design of vessel, such as hopper or silo, for feeding particulate solids [81]. AoR related to the angle of internal friction of bulk solid material (see section 2.1.3) determines the angle of the hopper (angle between the slope of hopper and the horizontal), which needs to assure a mass flow of bulk solids [6] (p. 219-228) (discussed in section 2.2.2). The influence of angle of repose of materials on powder dispensing will be discussed in Chapter 5 section 5.2.2.

Table 2- 3 Flowability and corresponding angle of repose classified by Carr [7] with solid particles poured from bins, hoppers, and feeders.

Flow Character	Angle of Repose (°)
Excellent	25-30
Good	31-35
Fair—aid not needed	36-40
Passable—may hang up	41-45
Poor—must agitate, vibrate	46-55
Very poor	56-65
Very, very poor	>66

Gold et al. [82] compared the results from the angle of repose and powder flowmeter, for range of powders previously classified empirically as glidants. It was found that some glidants did not necessarily increase flow rate and many of them that lowered the angle of repose but did not necessarily improve the flow behaviour. It was also stated that from the comparison between two methods used, the angle of repose was not a reliable method for evaluating flow behaviour for the reason of strong cohesion in finer particles.

2.1.3. Flow Properties of Bulk Solids

2.1.3.1. Stress state

In bulk solids dispensing, the flow properties of bulk solids in defined feeding vessels is the main objective of study including initiation and suspension of flow, steady-state mass flow in the vessel, and solids discharging through the outlet of vessel. Bulk solids flow refers to the deformation of particulate solids bed under stresses, and it is a reflection of the mechanical behaviour of bulk solids under the certain state of stresses in the vessel [83]. One of the most important contributions in understanding the bulk solids mechanics was made by Jenike in 1960s. The state of stresses in all possible

cutting planes within a bulk solid element can be represented by a normal stress - shear stress diagram, which is also known as Mohr's stress circle [6] (p. 5-10).

The Figure 2-6 shows the Mohr's circles of shear stress, τ, and normal stress, σ, measured in different stages of unconfined failure test undertaken by Schulze [13] (p. 35-41). As the assumption in Schulze's tests, the gravity and friction between wall and bulk solids were neglected. In the first part of test, the bulk solid specimen was compacted under the vertical compressive stress $\sigma_v = \sigma_1$ and the horizontal compressive stress $\sigma_h = \sigma_2$. The circle A represents the consolidation stage in the test. In this stage, a vertical failure stress was applied to the specimen and the failure did not take place under the stress. In the stage represented by circle C, a vertical stress caused the failure of bulk solid when compressive stress in the horizontal direction, σ_2, was constant. The vertical failure stress σ_v was equal to principal consolidation stress σ_1 in the horizontally confined condition.

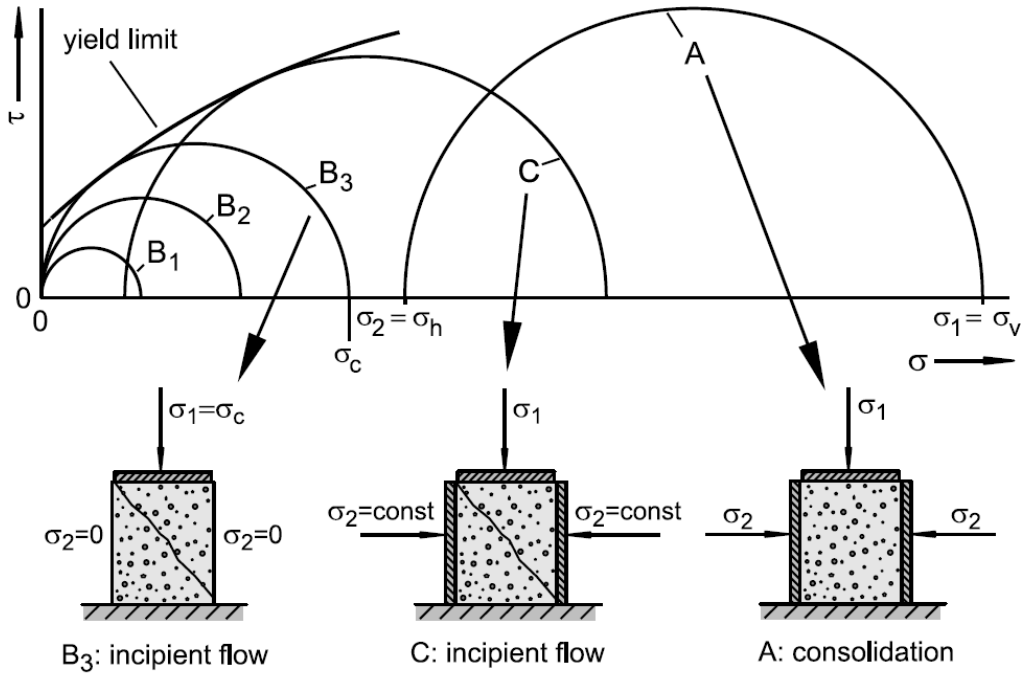

Figure 2- 6 Mohr's circles plotted by bulk solid unconfined failure test in diagram of shear stress against normal stress. Re-printed from [13] (p. 40). For full explanation refer to the text

In the second part of unconfined failure test, the bulk solid specimen was pre-compacted under the principal stress, σ_1 and the horizontal constrain was removed. Circle B_1 and B_2 represent vertical stresses applied to the bulk solid specimen only cause a deformation of the bulk solid specimen but no failure. When the vertical stress increased until the bulk solid specimen failed represented by circle B_3, the critical stress causing failure is

defined as unconfined yield stress σ_c, which equals to the principal consolidation stress σ_1 in unconfined condition.

As seen in Figure 2-6, both Mohr's stress circles B_3 and C representing the failure stage reached to a yield limit, whereas the circles could not reach to it in consolidation stage. Thus, the yield limit of the bulk solid must have been attained in one cutting plane of the specimen when the stress causes the incipient flow of bulk solid. Schwedes [84] studied the relationship between the unconfined yield stress and the principal consolidation stress at steady state flow by using shear tester. A series of yield limit locus can be obtained with shearing bulk solid specimen under different principal consolidation stress σ_1. Each yield locus gives one pair of values of the unconfined yield stress σ_c and the principal consolidation stress σ_1 which can be used to determine the flow function of bulk solid (see 2.1.3.2).

2.1.3.2. Flow function

The level of stress causing the incipient flow of bulk solids can be used to measure the flowability with a flow function introduced by Jenike [6] (p. 26-28). Jenike's flow function is described as that the unconfined yield stress σ_c is a function of the principal consolidation stress σ_1. Flow function A of unconfined yield stress σ_c against principal stress σ_1 is shown in Figure 2-7. A ratio ff_c of principal consolidation stress to unconfined yield stress is defined as flow factor to characterize flowability,

$$ff_c = \frac{\sigma_1}{\sigma_c} \tag{2.7}$$

The flow factors are represented by straight lines in Figure 2-7 which can be tested by ring shear tester (Appendix II). Jenike [6] (p. 215) classified the flowability according to flow factor ff_c listed in Table 2-4. It shows that larger ff_c indicates better flowability of bulk solid.

Table 2- 4 Flowability and corresponding flow factor ff_c classified by Jenike [6] (p. 215)

Flow Factor ff_c	**Flow Character**
$ff_c<1$	Not flowing
$1<ff_c<2$	Very cohesive
$2<ff_c<4$	Cohesive
$4< ff_c<10$	Easy-flowing
$10< ff_c$	Free-flowing

As shown in Figure 2-7, the flow factor becomes greater with increasing consolidation stress for bulk solids. It's because the voids between particles get filled when the specimen is consolidated with larger principal. Consequently, there is an increase in the flowing density of bulk solid and hence the flowability. Because of the dependence of flowability on consolidation stress, it is not possible to describe the flowability of a bulk solid without taking account of the consolidation stress history [13, 84].

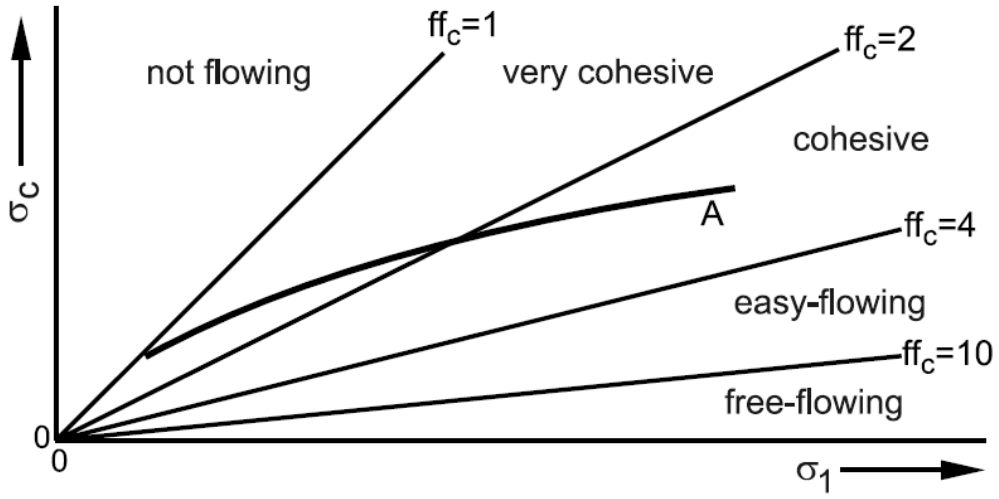

Figure 2- 7 Lines of constant flowability and flow function A of unconfined yield stress σ_c against the principal consolidation stress σ_1. Re-printed from [13] (p.42)

2.1.3.3. Angle of internal friction and angle of wall friction

According to the Coulomb criterion [85], when a bulk solid fails under a stress, it may divide itself into two parts which slide past each other. If internal sliding occurs in the bulk solid, the shear stress on the slip plane is dependent on the normal stress, σ, acting on the plane, which takes the form,

$$\tau = \mu\sigma + c \tag{2.8}$$

where μ and c are coefficient of friction and the cohesion. When the friction coefficient, μ, is constant, a linear internal yield limit locus (IYL) (shown in Figure 2-8) can be obtained from equation 2.8. The particles slip on an internal plane of bulk solid under the failure stress when the Mohr's circle is tangential to the IYL. The angle of internal friction, δ, is defined by [85]

$$\tan\delta = \mu \tag{2.9}$$

Angle of internal friction is determined by the properties of particle, i.e. particle size and particle shape [60]. It has a range from about 20° for smooth spheres to about 50° for angular particles [1] (p. 25). Attention is needed to distinguish the angle of friction and angle of repose discussed in section 2.1.2.6. The angle of repose can be considered as a critical state friction angle. Critical state is the state of failure when normal stress and shear stress do not change any more during shearing and the volume is constant. In this circumstance, the angle of repose can be used to represent the angle of internal friction. In this project, the angle of repose is assumed to be equivalent to the angle of internal friction as bulk solids flow in dispensing hoppers is considered as the failure in the critical state for simplification.

Besides internal sliding, the bulk solid can also slip along the wall of the container. Similar to internal angle of friction, the angle of wall friction ϕ_w is defined by [1] (p. 40-46)

$$\tau_w = \sigma_w \cdot \tan \phi_w + c_w \tag{2.10}$$

where c_w is adhesion between particles and wall. In Figure 2-8, it also shows a wall yield limit locus (WYL), by reaching to which the bulk solid can form a slide along the wall.

Both angle of internal friction and angle of wall friction play important roles in powder flow on the slopes in a hopper. It will be further discussed in section 2.2.2.

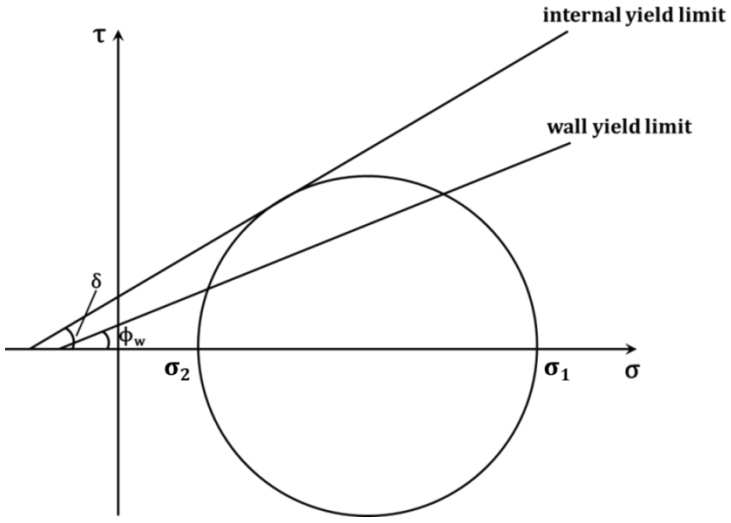

Figure 2- 8 Mohr's circle with internal yield limit locus and wall yield limit locus. δ is angle of solid friction; ϕ_w is angle of wall friction

2.1.3.4. Flow properties of bulk solids in silo

An actual case of bulk solid flow in a silo is reviewed by Schulze [13] (p. 249-257). When bulk solid is discharged from an outlet at the bottom of silo, the bed of particulate solids in the silo moves downward from the vertical section to the hopper section. In the vertical section, the bulk solid is compressed vertically by gravity, but strain in the horizontal direction is prevented. The principal consolidation stress, σ_1, is identical to the resultant of vertical stress σ_v and wall normal stress σ_w and this state of stress is called "active state of stress" [86]. The orientations of the principal consolidation stress can be represented by solid lines in the silo in Figure 2-9. Thus, the deformation in the vertical section is comparable to the consolidation stage shown in Figure 2-6 A in section 2.1.3.1. As seen in Figure 2-9, both vertical stress σ_v and wall normal stress σ_w increase but the increasing is less and less in downwards direction in the vertical section of hopper. It is assumed due to the shear stress exerted from the bulk solid onto the wall carries part of the bulk solids weight. Janssen's tests in 1895 (translated by Sperl [11]) found the pressure at the flat bottom of a square bin does not increase linearly with filling height of the solid but becomes constant from a certain height. A simplified Janssen's equation derived to calculate the total pressure of the solid on the bottom of silo,

$$P = s^3(1 - e^{-0.8\frac{h}{s}}) \tag{2.11}$$

where P is total pressure of the solid on the bottom of silo; s is the side length of the square silo; h is filling height of solid in the silo. The results of his tests also indicate that the change of pressure gets smaller with filling height increases when the ratio of filling height and the side length of bottom, h/s, is larger than 2. When the ratio, h/s, is larger than 6, the pressure on the bottom can be considered as a constant.

In Figure 2-9, in the transition region from vertical section to the hopper section a peak wall normal stress is developed. In the hopper section, the bulk solid is compressed horizontally due to the convergent flow zone in the hopper, while it dilates in the vertical direction due the downwards flow [87]. As result, the wall normal stress, σ_w, is larger than the vertical stress σ_v, and thus the orientations of principal consolidation stress in the hopper can be represented by the arches shown in Figure 2-9 [87]. When bulk solid is discharged from a hopper, a stress field in the hopper was reported to cause solid particles to be "arched" or form a "dome" subjected to the consolidation stress [88,

89]. This state of stress is called “passive state of stress” or “radial stress field” where the local stress decreases in downwards direction approaching the hopper apex [86].

Schulze [13] (p. 252-257) indicated that in the discharging state the stresses close to the outlet are independent of the stresses in the upper part of the hopper and, therefore, also independent of the silo’s dimensions or level of filling. The deformation of the bulk solid while flowing in the hopper approximately corresponds to steady-state flow in which stresses and bulk density are constant. However, with local stress decreasing in downwards direction in the hopper, the flowability of bulk solid becomes worse when it gets closer to the outlet of hopper (or the radius of hopper is decreased) (see section 2.1.3.2). Dome of particles may be formed in the hopper to prevent the steady-state flow. The hopper design regarding to the formation of dome and the steady state flow will be discussed in next section.

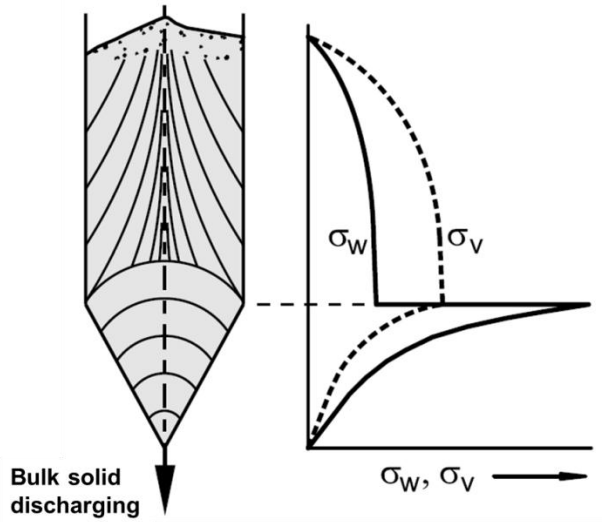

Figure 2- 9 Schematic diagram of bulk solid discharging from a silo and qualitative distributions of wall normal stress, σ_w, and vertical stress, σ_v, vs. the vertical coordinate. Re-printed from [13] (p.253). For full explanation refer to the text

2.2. Hopper Design for Flow of Bulk Solids

Symmetric conical hopper is often used as the storing and transporting vessel for bulk solids [6, 87, 90]. Dispensing bulk solids with a hopper has advantages as follows: The shape of hopper is regular and easy to be processed and modified; the wall of hopper requires no lateral reinforcement in bulk solid dispensing, because they do not transfer

any bending stresses from applied external forces; the well-designed hopper can assure a steady-state flow of bulk solid with relatively small outlet [1, 6, 13]. Generally, flow in the hopper with a vertical angle α shown in Figure 2-10 can form two flow patterns: mass flow and core flow. The mass flow, which can be described as the whole bulk solid is in motion (Figure 2-10(a)), occurs when the retaining wall of dispensing hopper is sufficiently steep and smooth, and the hopper does not have any sharp corners, abrupt transitions, or discontinuities in the frictional properties of the wall [6] (p. 28-34). Otherwise, a core flow pattern is developed with a stagnant zone formed at the transition region in the hopper, though mass flow may prevail in the vertical section. The angle between the stagnant zone boundary and the horizontal is ϕ_d shown in Figure 2-10(b). Hopper design, such as dimension and shape, has been studied on assuring a steady-state flow of bulk solids with different flow properties [91, 92]. The use of computer simulations, specifically the discrete element method (DEM) was attempted to identify the internal mechanism of bulks solids flow in the hopper [93, 94]. The DEM results suggest possible practical solutions using information which may be difficult or impossible to obtain in practice using traditional observation and experimental techniques. A poorly designed hopper may cause flow problems of bulk solids such as rat-holing (piping), plugging, strong arching (blocking) and flooding (overflow) in dispensing [1, 6, 10, 13, 17, 74].

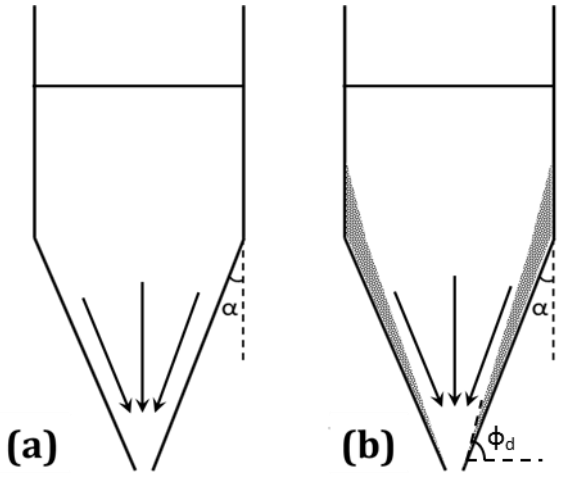

Figure 2- 10 Flow patterns in hoppers (a) mass flow; (b) core flow

2.2.1. Orifice Size of Hopper

In a standing hopper, bulk solids stay put when the hopper has a closed end. With opening an orifice at the bottom of hopper and increasing the size, bulk solids start to

flow through the orifice under the influence of gravity when the size exceeds a critical value [87, 95]. Jenike [6] (p. 231) and McLean [96] provided a method to calculate the minimum diameter of the orifice which assures a spontaneous gravity flow of bulk solid. For the circular orifice of conical hopper, the critical diameter is obtained from the equation,

$$D_c = \frac{H(\alpha)\sigma_c}{\rho_B g} \tag{2.12}$$

where function H(α) takes into account the hopper angle, α (shown in Figure 2-10). The value of H(α) is given in Figure 2-11 by Schulze [13] (p. 305). σ_c is unconfined yield stress and ρ_B is the bulk density.

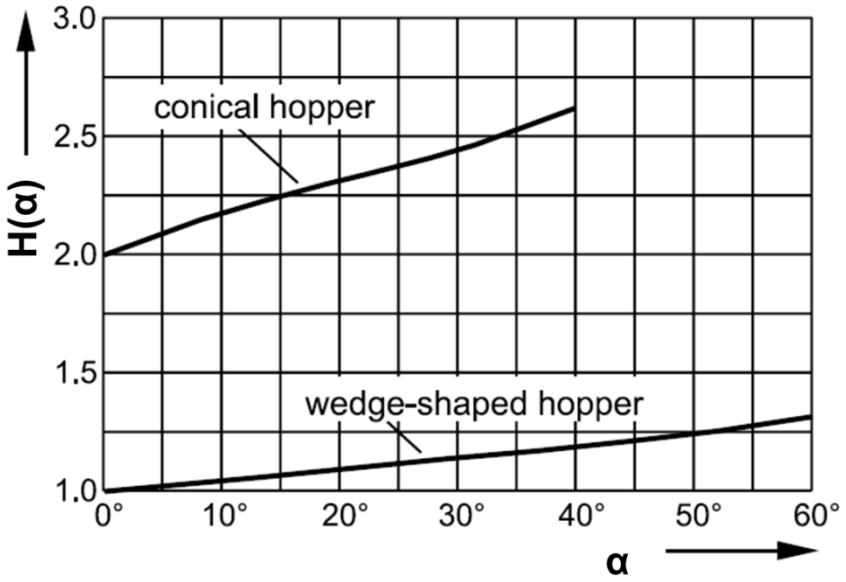

Figure 2- 11 Function H(α) [13] (p. 305). α is the hopper angle defined in Figure 2-10

When an empty hopper is filled with a bulk solid, the orifice size determines whether the bulk solid is preserved in the hopper or discharged. When the orifice size is larger than the critical value D_c given in equation 2.12, the flow is unlikely to be stopped in the convergent flow zone in the hopper and, therefore, the bulk solid flows out while the hopper is filled. When the orifice size is smaller than D_c, the bulk solid can form a dome across a channel of width D_c in the hopper to prevent flowing (Figure 2-12) and meanwhile, the radial stress field is developed in the process (see section 2.1.3.4). In the dome, the principal stress, σ_1, resulting from the weight of the bulk solid is transferred to the hopper wall as a bearing stress, σ_1', to support a stable bulk solid dome. Jenike [6] (p. 156) developed a flow criterion by assuming that the bulk solid dome has a smooth

shape with a constant thickness in vertical direction, and that the dome must carry only its own weight. Jenike's flow criterion can be described as the failure of dome only occurs when

$$\sigma_1' \geq \sigma_c \tag{2.13}$$

The above discussion is based on the case of spontaneous bulk solid flow under the gravity. In the hopper with an orifice smaller than the critical value D_c, the dome is formed at a height of h from the outlet and stable when the flow criterion is not met. External forces can be applied as the driving force of dome failure to initiate the flow of bulk solid in the domed hopper [6, 13]. The use of vibration as the driving force for the flow of bulk solids in the hopper will be discussed in section 2.2.3.

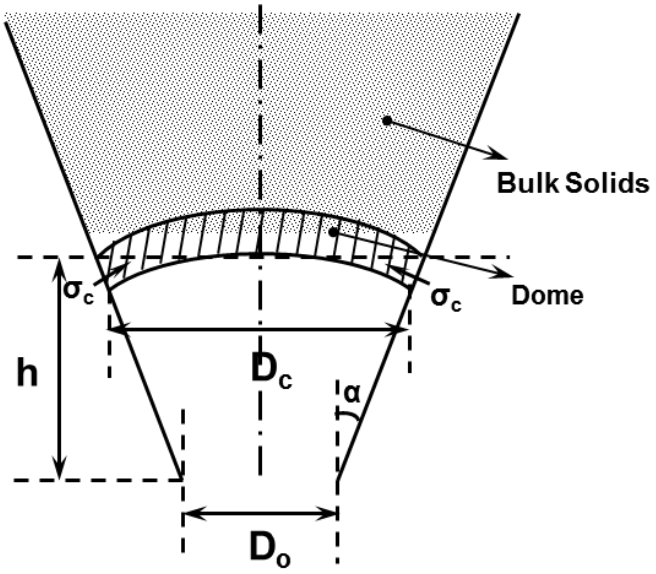

Figure 2- 12 Schematic diagram of dome formed in the hopper with orifice size D_o. The dome formed at a height of h from the outlet. The span of dome is D_c in horizontal direction.

2.2.2. Angle of Hopper

As the conical hopper with circular orifice is symmetric, the half conical angle, α, (the angle between the slope and the vertical, represented in Figure 2-10 and Figure 2-12, respectively) is important for the hopper design. Jenike [6] (p. 220-228) and Arnold et al. [17] discussed the selection of the hopper slopes for mass flow based on the angle of internal friction, δ, and the angle of wall friction, ϕ_w. Jenike [6] (p. 226) suggested the half angle of hopper, α, should not exceed a critical value as a function of the angle of internal friction, δ (Figure 2-13), which can be described as

$$\alpha_{max} = -0.5\delta + 55 \quad (2.14)$$

Thus, bulk solid can flow in a hopper with angle less than α_{max}, which is dependent on the material flow properties. As discussed in section 2.1.3.3, the angle of internal friction of materials is normally between 20° and 50°. According to equation 2.14, it can be concluded that the bulk solid with poor flowability requires a small angle of hopper, whereas the angle of hopper for the material with good flowability is not that circumscribed.

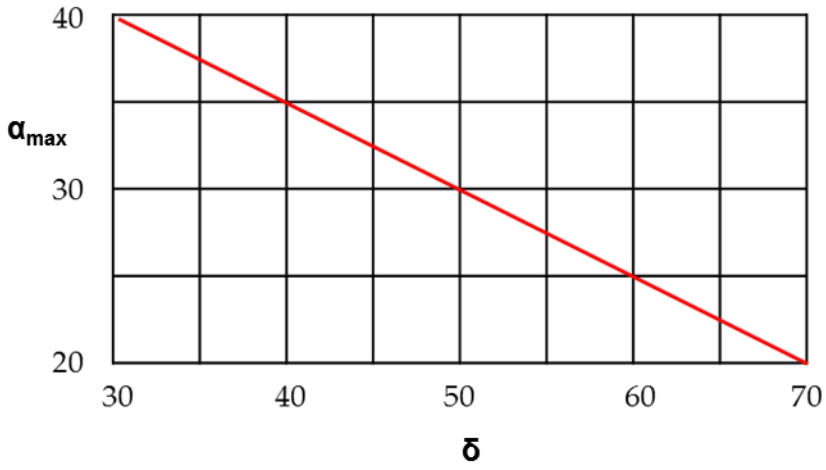

Figure 2- 13 Critical value of half conical angle of hopper, α_{max}, as a function of the angle of internal friction, δ, represented by the red line. Re-printed from [6] (p.227)

However, when the angle α is large, the bulk solid may flow in a core flow pattern [97, 98]. The presence of stagnant zone was found in the experiment affecting the discharge consistency of the bulk solid as the stagnant zone varied in its size and shape in different experimental conditions [97]. Jenike [6] (p. 220-228) also reported that the maximum angle α_{max}' of the hopper for mass flow to occur can be determined by the angle of wall friction, ϕ_w, and the effective angle of internal friction, δ_e. The boundary lines are plotted in Figure 2-14 indicating that the maximum hopper slope for mass flow is steeper when the angle of wall friction, ϕ_w, is larger.

Lu et al. [29] used a glass capillary (Figure 2-15) to dispense fine powders under ultrasonic vibration. Same glass capillary was tested in the early stage of this project and proved to have three main disadvantages. Firstly, the diameter of both the vertical section and nozzle section shown in Figure 2-15 is too small for some cohesive powders. Also, the designed 75mm and 90mm nozzles are too long to be applied with effective vibration in the whole range so that the dome forms easily in this section. Secondly, the

dispensing capillary has a convergent section with an abruptly reduced diameter in transition zone where the unconfined yield stress is very large (see section 2.1.3.4) and therefore, the powder can be strongly arched in the convergent section to cause the blockage of hopper. Thirdly, the overall dimension of this capillary is too small which lacks of capacity for dispensing larger particles and running for long hours.

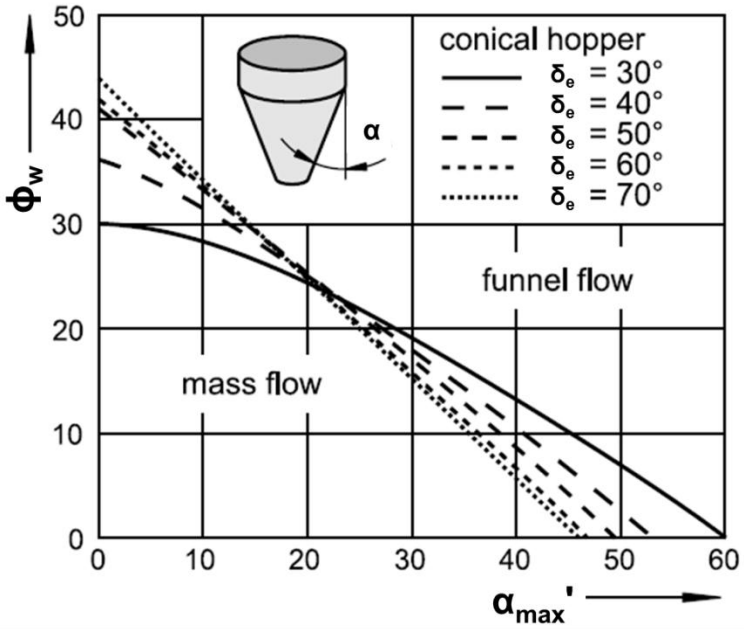

Figure 2- 14 Critical value of half conical angle of hopper, α_{max}', for mass flow determined by the angle of wall friction, ϕ_w, and the effective angle of internal friction, δ_e [13] (p. 298)

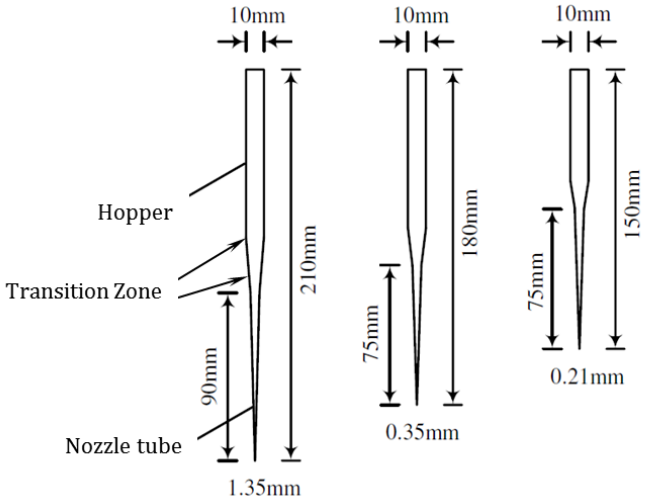

Figure 2- 15 Dispensing capillaries used in the work of Lu et al. Re-printed from [29]

2.2.3. Vibration induced bulk solid flow in hopper

As discussed in previous sections, when the gravitational force is the only driving force to discharge particles from hopper, the flow of bulk solid may be hindered in hoppers with smaller outlet diameters and shallower wall slope angles. Vibration has been used as a means of promoting flow in hoppers [99-102].

A number of works have been done on the study of bulk solids fluidization under the influence of vibration. Takahashi et al. [19] reported the appearance of convection cells near the inclined wall boundaries of the hopper. The particulate solids assume a circulatory motion in a two-dimensional hopper-shaped vessel when the vessel is subjected to vertical sinusoidal vibration.

Matchett [103] studied the effects of vibration on promoting flow of bulk solid in the hopper with considering two extremes of vibration: the push mode and the pull mode. In the push mode, the vibrated section of the hopper wall moves inwards towards the hopper axis, so that the bulk solid in the hopper is in plastic compression, and therefore at yield. In the pull mode, the vibrated section moves away from the hopper axis and hence the enclosed bulk solid, thus relaxing the hoop stress which is over the wall in contact with the contained bulk solid. The pull mode is assumed to induce a switch in consolidation stress orientation from a passive to an active stress state (see section 2.1.3.4).

Yang et al. [26] and Jiang et al. [104] reported when the hopper is vibrated, a small clearance is formed between particles and the wall. As a result, the adhesive and cohesive forces are reduced, and then particles move down through the hopper. As particles flow out of the hopper, the void fraction in the bulk solid increases and thus the distance between particles are enlarged, therefore, the particles can easily move in the hopper [104].

Roberts [100] developed a failure criterion for the vibrational bulk solid flow. The shear stress in the presence of vibrations τ_{vibr} depends on the maximum vibration velocity v_{max}. It can be represented by

$$\frac{\tau_{vibr}}{\tau} = 1 - \frac{\beta}{\tau}\left[1 - exp\left(-\frac{v_{max}}{\gamma}\right)\right] \tag{2.15}$$

where τ_{vibr} is shear stress in the presence of vibrations and τ is shear stress without vibration. v_{max} is the maximum vibration velocity. The parameter β indicates the maximum possible shear stress reduction. The parameter γ represents a characteristic vibration velocity.

Janda et al. [105] in their extensive study on understanding the jamming behaviour of powder particles in a vibrated hopper found that an increase in vibrations could lead to a gradual decrease in the hopper orifice diameter and in the absence of vibrations the flow could be continuous for a certain period followed by a complete blockage. It was also reported that flow rate increases at higher vibrational amplitudes until a certain time of vibration is reached where the mean flow rate is similar.

The fluidization of bulk solid under the influence of vibration can be described as the vibration inducing a boundary layer interaction between bulk solids and the wall of vessel. The mechanism is different from conventional solids flow based on particle saltation [106]. As a result of vibration, the friction between the powder and the wall surface is decreased due to dilation of bulks [107]. It causes the failure of dome along a vertical plane through the solid, after which the solid slides down along the inclined wall. Dumbaugh [108] proposed the term “vibration induced gravity flow”, an appropriate description for such applications. The current bulk solids dispensing techniques applying the vibration as the driving force will be introduced in section 2.3.2.2.

Based on previous works, the effect of vibration on bulk solid flow in the hopper can be concluded as:

(1) Vibration can be very effective in promoting bulk solid flow in hoppers and can generate flows at shallower wall-slope angles and much smaller outlet diameters than gravitational method [103-105].
(2) The most effective strategy is to induce vibration over the complete height of the hopper. When vibration is applied to a section of the cone, the location of the vibration source is a critical design parameter [103].
(3) Vibration leads to a significant reduction of the shear stress to initiate the flow [26, 104, 109].
(4) Vibration may also cause problems for bulk solid flow, e.g., irregular flow due to collapsing arches and ratholes, consolidation of the bulk solid due to inappropriate operation [13] (p. 353).

2.2.4. Correlations between Bulk Solid Flow Rate and Design Parameters

The knowledge of correlations between bulk solid flow rate and hopper design parameters can be used to predict dispensing results in practical applications. However, it is limited as the mechanism of bulk solids flow and discharge is complex and not well understood. Early researchers discovered mass flow equations of bulk solids based on an analogy to the outflow of liquids following the Torricelli's law [13] (p. 341). The velocity of bulk solid flow under the gravity, w, can be expressed by

$$w \propto \sqrt{gD_h} \tag{2.16}$$

The hydraulic diameter of outlet opening, D_h, is defined by $D_h = \frac{4A_o}{P_o}$, where A_o is the area of the orifice and P_o is the perimeter of the orifice. When the bulk solid flowing through the outlet with a cross section area, A_o, the mass flow rate, W, can be presented by

$$W \propto A_o \rho_B \sqrt{gD_h} \propto \rho_B \sqrt{g} D_h^{2.5} \tag{2.17}$$

where ρ_B is the bulk density.

Deming and Mehring [4] examined the flow of granular solids in conical bins and derived an equation to predict the flow rate. There were seven physical quantities and four dimensions involved in the investigation of the motion of bulk solid. With dimensional analysis, a function was found in the form of,

$$t{D_o}^{2.5}\rho_B g^{1/2} = f\left(\frac{d}{D_o}, \mu, \alpha\right) \tag{2.18}$$

where t is the flow rate in minutes per 100 grams; D_o is orifice size in millimetres; ρ_B is the bulk density of bulk solids; g is gravitational acceleration; d is the diameter of granule; μ is the tangent of angle of repose; α is the half angle of conical bin. According to the experimental results, linear regression between $t{D_o}^{2.5}\rho_B$ and $\frac{d}{D_o}$ obtained the correlation between flow rate, t, and other physical quantities in the form of

$$t = \frac{\mu}{{D_o}^{5/2}\rho_B}\left[34.6 + (67.4 + 444\sin\alpha)\left(\frac{\bar{d}}{D_o} + 0.130 - 0.161\mu\right)\right] \tag{2.19}$$

where $\bar{d}$ is the average diameter of granules. The granules tested in the experiment were not perfectly spherical and with exactly same diameter. $\frac{1}{2}(d_1 + d_2)$ was used for $\bar{d}$ in his

work as an approximation, where d_1 and d_2 referred to the opening of a larger and a smaller sieve passed by the granules, respectively. The equation was claimed to be applicable to granules with any density and shape free flowing in the conical bin with 10 to 55 degrees half angle [4]. However, in their work relatively large deviation was found in the case of less free flowing when the value of $\frac{\bar{d}}{D_o}$ was larger than its limit of 0.15 to 0.25 [4].

Fowler and Glastonbury [5] studied the flow of granular materials with different particle shape from flat-bottomed hoppers. They proposed an equation to predict the discharge rate of spherical and non-spherical materials.

$$W = 0.236\rho_B A_o \sqrt{2gD_h}\left(\frac{D_h}{\lambda_s d}\right)^{0.185} \tag{2.20}$$

where g is the gravity acceleration. The particle shape factor λ_s is sphericity defined in equation (2.3). The equation conforms the basic structure of mass flow rate equation provided by equation (2.17) with free-flowing granular materials, such as wheat, rice, rape seed, sugar and sand, which particle size is in a range of 0.2-2 mm. They suggested the discharge rate is a function of the ratio of orifice size to particle size taking account of the shape of particle [5].

Beverloo et al. [110] found the gravity flow of granules in a flat bottom cylinder with circular orifice was developed through an effective area in the cross-section of orifice. The margin of the orifice was useless for granules flow. The extent of the margin is proportional to the particle size, d. Thus, the flow rate, W, in equation 2.17 can be presented by

$$W = C\rho_B \sqrt{g}(D_o - kd)^{2.5} \tag{2.21}$$

where the constant k is related to the surface properties of solid materials [110]. The orifice size D_o was replaced by an effective flow diameter $D_o - kd$. Brown and Richards [74] (p. 193-195) suggested there is an annulus with width d/2 adjacent to the orifice edge where no flow takes place and thus, all particles pass through an orifice of reduced diameter equal to (D-d). However, the reason for k being greater than 1 was failed to be explained by the authors. The constant C was introduced as the coefficient of various orifice shapes, such as circle, square, rectangle and triangle. Beverloo's equation is simpler than Deming's equation in the form, and it introduced an effective flow diameter $D_o - kd$ to represent the influence of the particle size on the flow. Beverloo's equation is

applicable for the gravity flow of free-flowing granules through the orifice with various shapes in flat bottom cylinders. Additionally, it was indicated that head of granules in the range investigated (10-30 cm) has no influence on the flow-rate, and the diameter of the cylinder does not have an influence on the flow-rate [110].

Rose and Tanaka [15] studied the gravity flow of bulk solids in a conical hopper. It was reported in their work that the flow rate, *W*, is a function of the half conical angle of hopper, α, and the angle between the stagnant zone boundary and the horizontal, ϕ_d, (see in Figure 2-10(b)),

$$W \propto D_o^{2.5}\left(\frac{D_o}{d}-3\right)^{0.3} F(\alpha,\phi_d) \tag{2.22}$$

Function F is given by,

$$F(\alpha,\phi_d) = (\tan\alpha\tan\phi_d)^{-0.35}, \qquad for\ \alpha < 90-\phi_d$$

$$F = 1, \qquad for\ \alpha > 90-\phi_d \tag{2.23}$$

As he angle ϕ_d is hard to be determined in experiment, a value of 45° can be used for simplification [111].

The discovery of all above flow equations is based on the flow of coarse-grained, cohesionless bulk solids. Verghese and Nedderman [112] investigated the flow of fine particles sized between 100 and 600 μm in conical hoppers and derived a flow rate equation conformed to the equations of Beverloo et al. [110] and Rose and Tanaka [15]. It was reported in Verghese's work that the gravity flow of bulk solid was retarded by interstitial pressure gradients resulting from the dilation of bulk solid approaching the outlet in conical hopper. The interstitial pressure gradients were independent of orifice diameter and inversely proportional to the square of the particle diameter, d^2. Thus, the flow rate is given by:

$$W = 0.5\tan^{-0.35}\alpha\sqrt{1+\frac{\lambda}{d^2}}\rho_B\sqrt{g}(D_o-kd)^{5/2} \tag{2.24}$$

λ is a parameter related to the compressibility and density of material and was found to be a negative value in the correlation. Thus, the flow rate is reduced when the particle size is smaller.

As discussed in section 2.2.3, vibration can play as an extra driving force to promote bulk solids flow in hopper. Suzuki et al. [113] proposed an equation for the flow rate of bulk solids from a vibrating hopper. They suggested that the discharge of bulk solid from a vibrating hopper can be divided into three steps:

(1) Particles are in flight. The flow rate, W_1 equals to 0;

(2) Particles impact the wall of hopper. The flow rate, W_2 is given by

$$W_2 = C_1 \rho_B \sqrt{\frac{\Delta v}{\Delta T}} D_h^{5/2} \tag{2.25}$$

where Δv is the relative velocity of free fall particle and the wall of hopper at impact. ΔT is the duration of the impact period. C_1 is a constant;

(3) Particles remain on the wall of hopper. They are accelerated by the wall and therefore, the acceleration of particles is $g[1\text{-}Gsin(2\pi ft)]$, where G is the intensity of vibration and equals to $a(2\pi f)^2/g$ and a is the amplitude of vibration. Then, the flow rate, W_3, is given by

$$W_3 = C_2 \rho_B \sqrt{g[1 - G\, sin(2\pi ft)]} D_h^{5/2} \tag{2.26}$$

where t is the time and C_2 is a constant.

Therefore, the flow rate from vibrating hopper can be presented by

$$W = W_1 + W_2 + W_3 = C_1 \rho_B \sqrt{\frac{\Delta v}{\Delta T}} D_h^{5/2} + C_2 \rho_B \sqrt{g[1 - G\, sin(2\pi ft)]} D_h^{5/2} \tag{2.27}$$

Wassgren et al. [102] suggested equation (2.27) can be also presented by

$$W \propto \rho_B g_{\text{eff}}^{1/2} D_h^{5/2} \tag{2.28}$$

where D_h is the hydraulic diameter of either circular orifice or non-circular orifice. The flow rate was assumed to be a function of an effective gravity acceleration of particles, g_{eff}, in the vibrating hopper.

2.3. Bulk Solids Dispensing

2.3.1. Bulk Solids in Manufacturing Industry

Bulk solids are involved as raw materials, intermediates and final products in manufacturing industry. Accurate and efficient handling of bulk solids is always a hot issue and research object. So far, coarser particles (normally larger than hundreds of microns) have been proved easier to be transferred from one vessel to another, since the movement of each particle is not dominated by cohesive and adhesive forces but by the force of gravity [114]. Fine powders are mainly used in pharmaceutical industry as the particle size of drug can affect its dissolution rate [115]. A reduced particle size, often micrometre or nanometre, can improve the bioavailability of the drug substances [116] and the absorption of poorly water-soluble drugs in humans [115, 117]. Biomaterials, such as calcium phosphate, used in bone tissue regeneration are often nanosized for new bone formation and new bone attachment [118]. However, the reduced particle size often presents difficulties in the flow of fine powders.

Several studies on flowability of fine-particle cohesive pharmaceutical powder have been reported on tableting [119, 120] and powder inhalation [121]. The particles of excipients are always micronized and the size of API particles is even smaller than a few of microns. As a result, the powders show a strong cohesion and poor flowability when they are handled in the process. In the pharmaceutical research and development, the process of synthesizing new chemical entities and identifying them as potential drug candidates often involves with a limited availability of high value powder materials. The production efficiency is also highly concerned as the screening time of these candidates governs the development time of drug products [104]. Therefore, accurate and efficient handling of small amount of fine powders is a necessity for pharmaceutical manufacturing industry.

In pulmonary drug delivery system, the drug powder should have a narrow particle size distribution and micronized particles, size of which is no more than 5 μm in average, with no particle larger than 10 μm [122]. Dry powder inhaler (DPI) has been used for pulmonary delivery of drugs by humans for more than 40 years since 1967 [123]. A typical formulation of dry powder inhaler for the treatment of respiratory disease [124] is listed in Table 2-5. DPIs are subject to strict pharmaceutical and manufacturing standards by regulatory bodies, the most challenging of which is the demonstration of device reliability in terms of delivered dose uniformity [125]. Single- or multi-unit dose

devices of DPI have individual pre-metered doses sealed in the device, whereas in reservoir devices the patient dispenses the dose at each use [125]. Besides the development of the device should provide accurate dose delivery in different dose types (capsule, reservoir or blister package) over a wide range of inspiratory flow rates, the drug formulation in each dose must be uniform whether single or multiple dose devices [126]. A good dose-to-dose conformity in DPIs is especially crucial as it determines the consistent therapeutic effect to patients [126]. However, dispensing cohesive inhalation drug powders, normally below few of micrograms, in the DPI device with good dose-to-dose conformity is difficult [127].

The demand for an accurate and efficient dry powder metering and dispensing technology in pharmaceutical industry is unprecedentedly high. Besides the capability of fast and accurate dispensing very small amount of fine powders, the dispensing device is also required to keep the physical properties of pharmaceutical powders, such as particle size and shape, unchanged in the process as the physical properties of particles have influence on the drugs dissolution rate [128].

Table 2- 5 Dry powder inhalation formulation (per dose) for the treatment of respiratory decease [124]

Ingredients		**Action**	**Amount per Dose /mg**	**Particle Size /µm**
Active Pharmaceutical Ingredients (API)	Salmeterol Xinafoate	long-acting beta-2 agonist	0.0725	0.1 – 5
	Fluticasone Propionate	inhaled corticosteroid	0.25	0.1 – 5
	Tiotropium Bromide	anticholinergic agent	0.0225	0.1 – 5
Excipients	Lactose	carrier	20	30 – 120
Total			20.345	55 – 65 in average

2.3.2. Bulk Solids Dispensing Technology

The study on the transportation of bulk solids was initially started with handling a large quantity of grain in a bunker in nineteenth century [1] (p. 1). In the past half century, the improvement in the field of engineering sciences has provided abundant solutions to the issues of bulk solids flow and discharge. Meanwhile, the researchers have been paying more attention to the techniques used to dispense small amount of fine powders in pharmaceuticals and biomaterials industry [129-132].

Yang and Evans [14] have provided a comprehensive review on micro-dispensing techniques. The most common dispensing techniques for small amount of powders adopt pneumatic and volumetric methods which are simpler and still widely used in industry nowadays. In pneumatic method, conveying the powder is completed in two steps: powder is dosed by aspiration of a pre-selected volume; and then powder is conveyed and deposited by injection [22]. The disadvantage of this method is that it cannot provide continuous dispensing of powder as the powder collection and delivery were finished alternately; the dispensing mass management and metering is achieved by recesses with pre-determined volume so that the accuracy of dispensing is strongly related to the capability of the recess in holding the powder. Thus, the pneumatic method is always applied with other methods rather than solely finishing a dispensing task.

Volumetric methods involve dipping the capsule or blister package into a bed of powder, then scrapping off excess residue with a blade. Or it works with the pneumatic method to retrieve and eject powder samples via a recess with certain volume. Volumetric powder dispensing devices can usually dispense powder with higher accuracy but are very sensitive to any change of packing density [14]. The disadvantage of volumetric method is that it is not possible to dispense very small amounts of powder using this method, and if more than one ingredient is to be dispensed then the ingredients must be mixed in large quantities, which can result in inhomogeneous doses.

A simple technique combined the pneumatic and volumetric methods in powder dispensing was designed by Gupte et al. [22], shown in Figure 2-16. The brief operating principle was reviewed in Yang and Evans work [14]. It is able to draw off powder in discrete metered quantities of 0.5 to 10 mg. It comprises a tubular aspirator having a dosing chamber at one end. The other end of the aspirator is connected to the vacuum and/or compressed air sources. In powder collection, the recess end is dipped a few millimetres into powder bed from which a quantity is drawn off. The volume of dosing chamber is adjusted according to the dose requirement. When the dosing chamber is retrieved, extra powder is scraped off and the dosing chamber is moved to the dosing site. The pressure within the tube is then increased to a pressure exceeding atmospheric pressure so that the quantity of powder in the dosing chamber is ejected.

There are a wide range of powder dispensing techniques and devices on the market combined with various principles and methods. It often has more than one techniques applied in one micro-dispensing device. Therefore, it is hard to classify the devices with

the techniques they've used. Podczeck and Jones [23] reviewed powder micro-dispensing devices for producing capsules in pharmaceutical industry. These techniques can be classified into indirect dispensing techniques and direct dispensing techniques according to their operating principles.

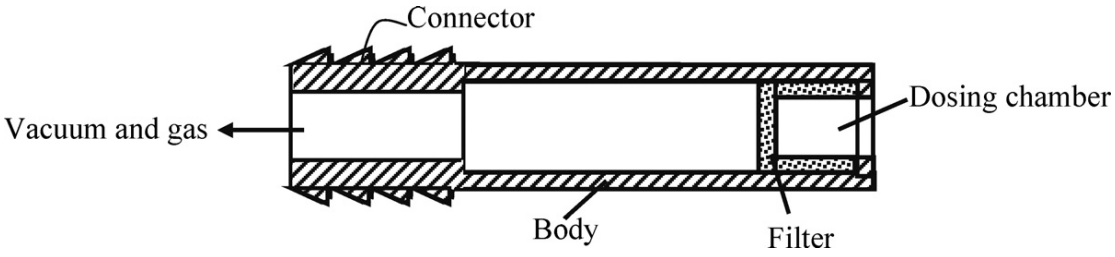

Figure 2- 16 Aspirating–dispensing head for volumetric dosing, originally invented by Gupte et al., re-printed from Yang and Evans [14]

2.3.2.1. Indirect dispensing techniques

Indirect dispensing techniques are very common in pharmaceutical industry for the filling tasks of solid form drugs, such as capsules, blisters etc., on the production line. It still has been used for many large-scale productions in pharmaceutical manufacturing company these years. Pneumatic, volumetric and the techniques combined both are all ascribed to the indirect dispensing techniques. In these techniques, the powder is firstly filled into a pre-selected volume of cavity by aspiration, and then moved to the target sites with the assistant of the likes of robot, to the end the powder is ejected by high atmospheric pressure into capsules or blisters. Another way is dipping a slotted tube with piston into the bed of powder, retrieving the recess of tube with the powder in a selected volume. The powder has been compacted in the process. The compact stress should be sufficient to lock the powder in the recess. After scrapping off excess residue on the edge of tube with a blade, the powder is then ejected into the target by pushing down the piston. This technique is also called dosator in some place. A principle scheme of dosator is shown in Figure 2-17. The dosator consists of a body and a pin in the centre. The pin is set a height to form a certain volume of recess at the end of dosator. When the dosator is inserted in the powder bed within a powder bowl, the powder is filled in the recess with a degree of compaction and hence, the powder can be held in the recess of dosator. The dosator will be then extracted from the powder bed and moved to the target receptor. The held powder is ejected by pushing the pin downwards. The dosage of powder can be adjusted with the volume of recess through setting the initial position of pin in the dosator.

Yang and Evans [14] reviewed a type of indirect dispensing device based on the powder feeding from a hopper into a rotating plate with a groove. Volumetric metering is achieved by drawing the powder from the groove in the conveyor, shown in Figure 2-18. A circular groove in a rotating disc receives powder from a hopper when the groove rotated to the position underneath the hopper. An aspirating pipe is located above the point where the groove is when the disk rotates the groove to this side. The pipe is then used to draw powder from the groove to the destination. The disk has a constant speed of rotation, so the volume of powder delivered to the groove in unit time is constant which can be adjusted by changing the rotation speed. A constant powder level is maintained in the hopper by an automatically controlled screw feeder. The hopper is agitated by a wire-frame stirrer to avoid variation of static pressure on the groove and the formation of a density gradient within the powder. The machine is able to meter powder with high instantaneous precision (less than 1% variation) and at high speed (3 to 11 g/s) [14]. The error of this device is mainly from the variation of powder packing density in the hopper despite the stirrer is used. For the powder with high Carr's index, a very large variation of dosage can be expected. The feeding of very cohesive powder from the hopper to the groove is also a problem.

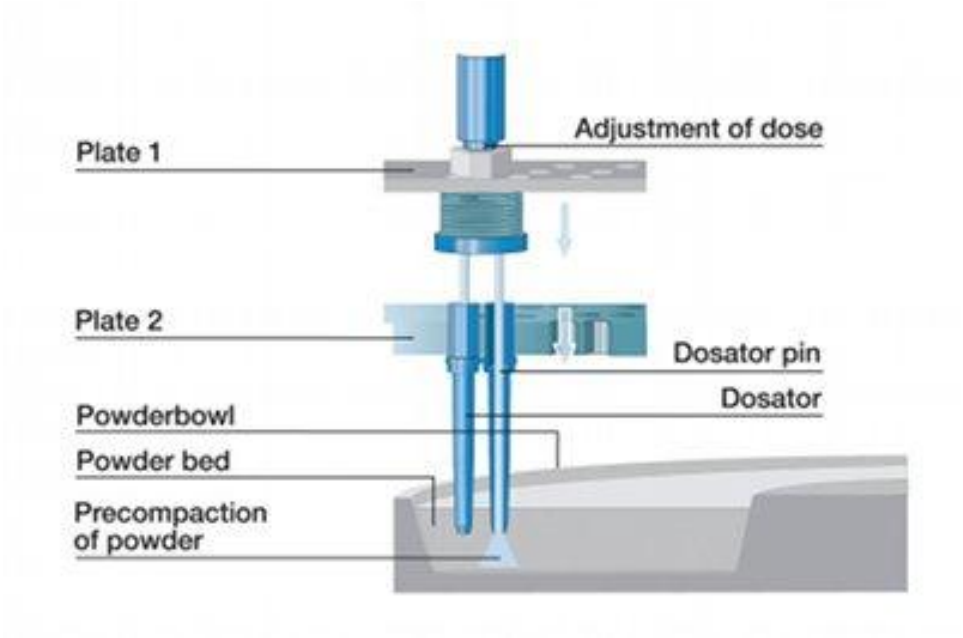

Figure 2- 17 A principle scheme of dosator. Copied from online article "Enhancing dose consistency" in manufacturing CHEMIST PHARMA, 2010

Omnidose [133] is one of Harro Höfliger's products based on pneumatic and volumetric techniques (Figure 2-19). The device consists of a wheel with several volume-defined cavities on it and a vacuum/air channel. When the cavity is rotated to the position

underneath the powder bed, the powder is drawn in the cavity by vacuum through a filter membrane. The wheel rotates 180° and powder is released in the blister under gravity. It is reported that the dosage of 1 to 50 mg can be dispensed from this system. The problem of this device still lies on the feeding of powder from powder bed to the cavity on the wheel. Although the vacuum could draw the powder in the cavity, non-free flowing fine powders are most likely to stick on the channel and block it. Moreover, even if the powder could be drawn into the cavity by the vacuum, the release of non-free flowing powder would be still a challenge due to strong cohesive and adhesive forces of fine particles. The fine particles tend to stick on the surface of cavity so that the mass loss of powders in the dispensing process has big influence on the variation of dosages.

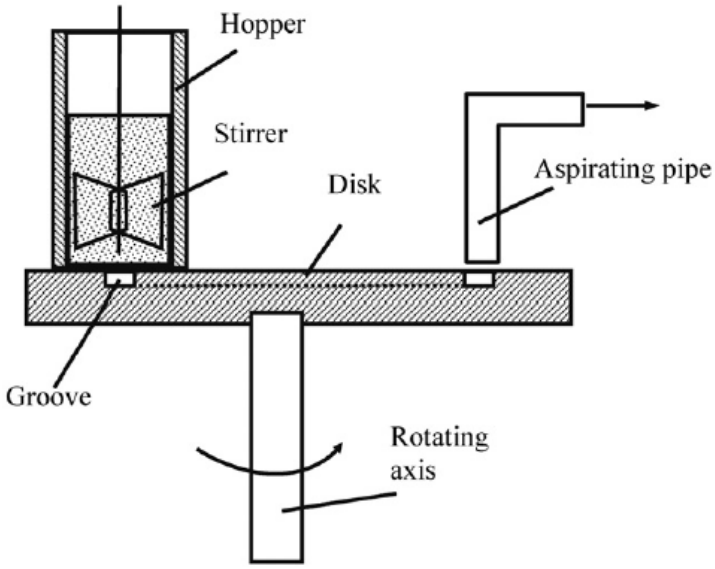

Figure 2- 18 Schematic diagram of rotating groove dispensers originally invented by Douche et al., re-printed from Yang and Evans [14]

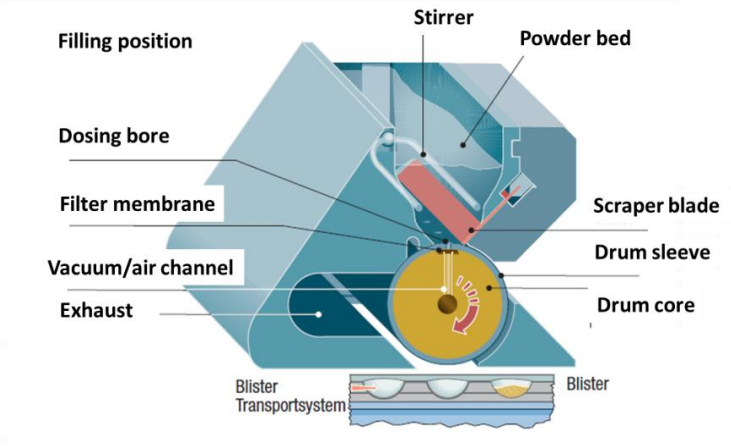

Figure 2- 19 Omnidose dosing wheel system by Harro Höfliger company [133]

2.3.2.2. Direct dispensing techniques

The powder can be also dispensed directly to the target sites without using a recess or cavity. Direct dispensing techniques have the advantages such as it is simple in device construction, fast in dispensing process and able to achieve continuous dispensing of powders. In some occasion, direct dispensing can complete smaller dosage task than volumetric techniques. Therefore, the direct dispensing techniques are more and more accepted and used in practice.

Gravimetric method

Gravimetric method is a simple direct dispensing solution. The powder is dispensed through a nozzle from the container to target sites under the influence of gravity. However, the flowability of fine powders is not good enough to develop a free flow under the gravity. The dispensing accuracy is also very susceptible to the wear of fine powders on the container which causes mass loss [134, 135]. In order to achieve accurate dosages, dispensing powder from a nozzle may require an iterative feedback loop of weighing by a balance system [136]. The system can determine the next additive amount according to the difference between dispensed dosage and the target, and send the information back to the dispensing amount control mechanism, such as valve or switch. This will improve the dispensing accuracy but is time consuming and hard to lend itself to large scale production-line processes.

Vibration-assisted method

Vibration controlled micro-dispensing through a capillary, tube or hopper has evolved as a feasible alternative in accurate dispensing of fine powders [24, 28, 114, 137-141]. The use of vibrations aids in breaking domes or the agglomerated powder clots by applying a distributed and continuous force on the powders. As a result, these vibrations when switched on, can initiate the flow of powder from a fine nozzle. When switching off the vibrations, particle-particle and wall-particle stresses lead to the formation of domes which causes powder flow arrested in the nozzle without using a mechanical stopper [28, 142]. Such kinds of dry powder micro-dispensing can be used in many fields, such as solid freeform fabrication, drug delivery and pharmaceutical screening [25, 143-145].

The mechanical vibration was studied earlier on powder flow in hoppers. Staffa et al. [21] used a classic Hall flow meter [146] (Figure 2-20) fitted with vertical and horizontal

sinusoidal vibration to test the flowability of powders. An electromagnetic vibrator was attached to provide vibrations in both directions. With and without the vibration, Cu, AlNiCo and Al_2O_3 powders passed 2.5 mm and 5 mm orifices of Hall flow meter. The sample powders were categorized into two classes, free-flowing and non-free-flowing, by their flow properties. They found that the flow time of a free-flowing powder is usually increased by vibration compared to gravity flow conditions, since an increased packing density causes a transition from core to mass flow. The mass flow is created by continuous breakdown of domes, which, with increasing intensity of vibration, become strong enough to stop flow. A critical value of vibrational intensity, at which flow begins, exists for non-free-flowing powders. When flow is imitated by a single, high-intensity impulse, lower intensities suffice to keep the powder flow.

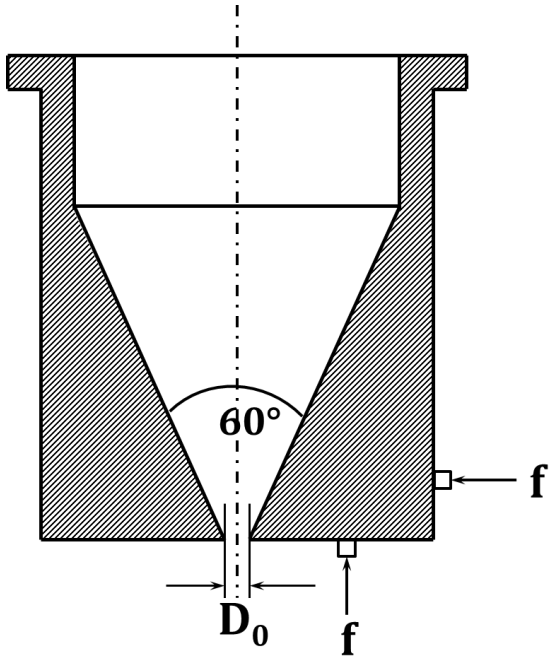

Figure 2- 20 Hall flow meter used by Staffa et al. [21] for the investigation of influence of vibrations on powders flowability

Matsusaka and co-workers have reported continuous micro-feeding of fine particles from a vibrating capillary tube under the influence of mechanical vibration [114] and ultrasonic vibrations [137]. The system of motor-driven vibrating capillary tube was under conditions of less than 760 Hz and 30 μm in amplitude (Figure 2-21). The alumina and fly-ash of about 10 μm in particle size can be discharged continuously at a constant rate as small as 0.2 mg/s. They found the flow rate increased with the frequency and however the maximum flow rate was determined by the diameter of capillary and powder flow properties. The system of ultrasonic vibrating feeder was similar, which

applies 20 kHz ultrasonic vibration through a piezoelectric transducer to the capillary. In the study, water was used as the medium of propagation of the ultrasonic vibration and thus a factor corresponding to the viscosity of fluid medium was investigated in characterizing the powder discharge.

Yang et al. [24-27] developed an acoustic controlled dry powder printer which can "print" dry powders synchronized with motion planar analogue to a desktop drop-on-demand inkjet printer (Figure 2-22). In a glass capillary attached to an electromagnetic transducer, the wave characteristics of the forced vibration control both flow rate and switching of powder flow. The vibration was reported effectively increase the flow rate of powders at or below 200Hz. The flow rate of powder was controlled on the basis of intermittent arrest and stasis of particles in the gravitational field. Since flow stops when acoustic vibration stops, the vibrating tube is like a valve that provides computer controlled powder flow metering, mixing and dispensing. The effects of acoustic frequency, amplitude, tube diameter, mechanical damping and particle size distribution have been investigated [25, 27]. The dispensing device is being used to make three-dimensional functional gradients by selective laser sintering (SLS) [25, 147].

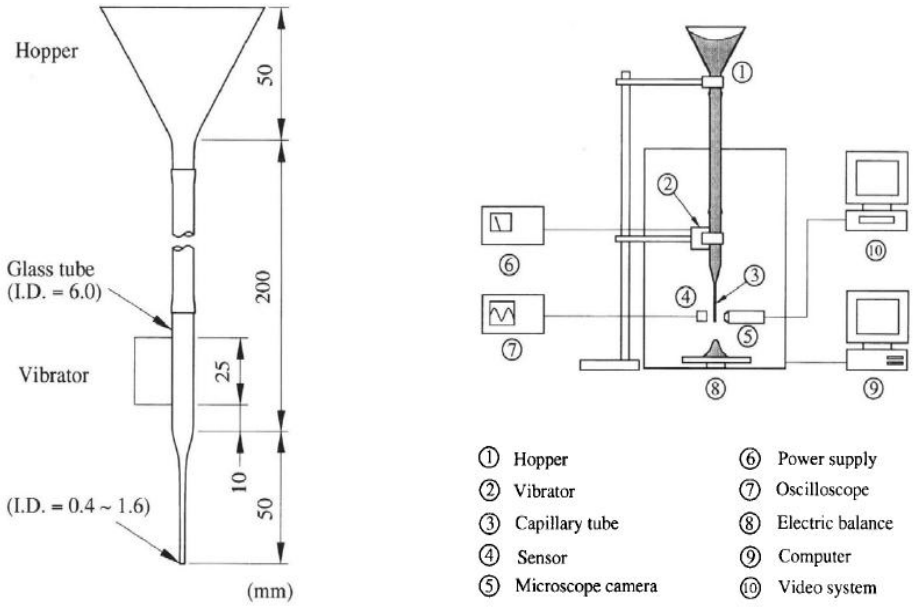

Figure 2- 21 Vibrating capillary feeding apparatus, reprinted from Matsusaka et al. [114]

One recent work published by Chen et al. [130] about vibration based system introduced a micro dosing system for fine powder of lactose using a vibrating capillary. The capillary is assembled on a piezo-electric actuator of 1 to 1.5 kHz in frequency shown in Figure 2-23. The vibration principle is based on the piezo effect, where the

application of an electrical field creates mechanical deformation in the crystal. They mainly investigated the flow rate and its variability in relation to parameters such as capillary diameter, frequency, and amplitude. It was found that both the frequency and the amplitude affect the flow rate and variability of dosing. The frequency is more predominant in the process comparing with the amplitude. The impact of powder properties such as density, particle size, size distribution and shape was also studied with five different kinds of lactose powder. The powder with larger particle size and smaller Carr's index normally obtains a higher flow rate. This technique can achieve flow rate from 1 mg to 10 mg per second and less than 3% relative standard deviation (RSD).

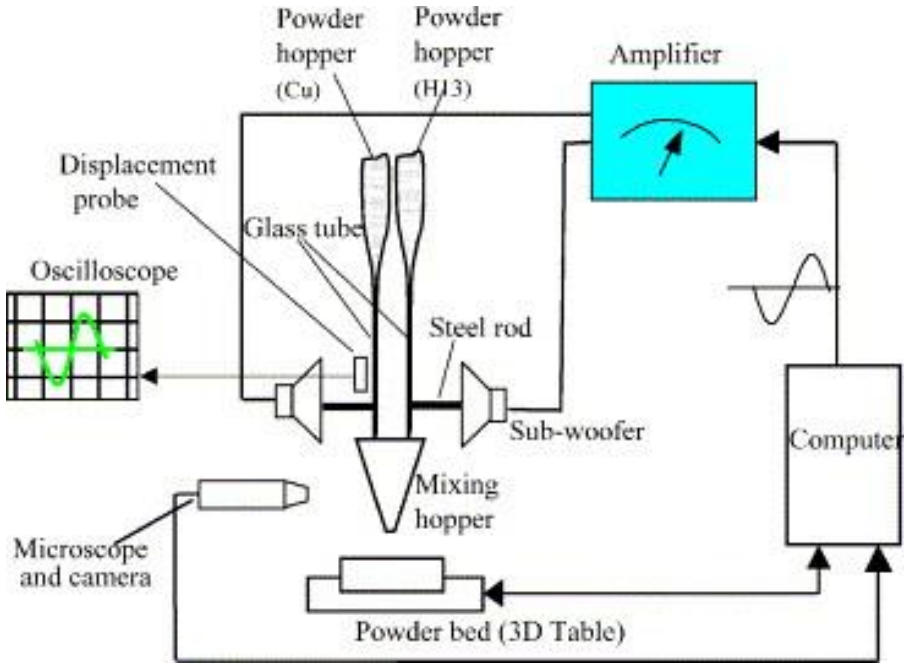

Figure 2- 22 Acoustic controlled dry powder printing system, reprinted from Yang and Evans [25]

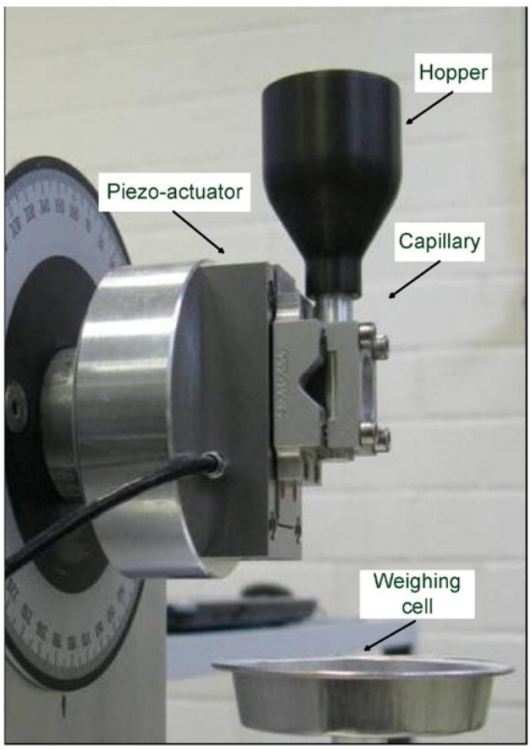

Figure 2- 23 The view of micro-dosing system, copied from Chen et al. [130]

Auger method

Besides the vibration dispensing technique, there is another semi-automatic direct dispensing technique: auger filling. It is the earliest adopted capsule filling technique in pharmaceutical industry. The Figure 2-24 shows the auger principle. The powder in a hopper is dosed by a central rotating auger, which typically operates in conjunction with a counter rotating agitator. As a powder passes through the auger a number of particles are transferred through the clearance between the auger and the straight funnel, as the auger rotates [148]. The dose weight of auger filling is a function of the auger speed, pitch and diameter [23, 148].

The disadvantage of auger filling technique is: (1) the inconsistent filling efficiency due to the variations in bulk density of agitated powder bed; (2) the poor repeatability due to powder randomly detaching from the auger when it stops; (3) the reduction of particle size by comminution; (4) the need of ranges of auger designs for different material and dosage requirements.

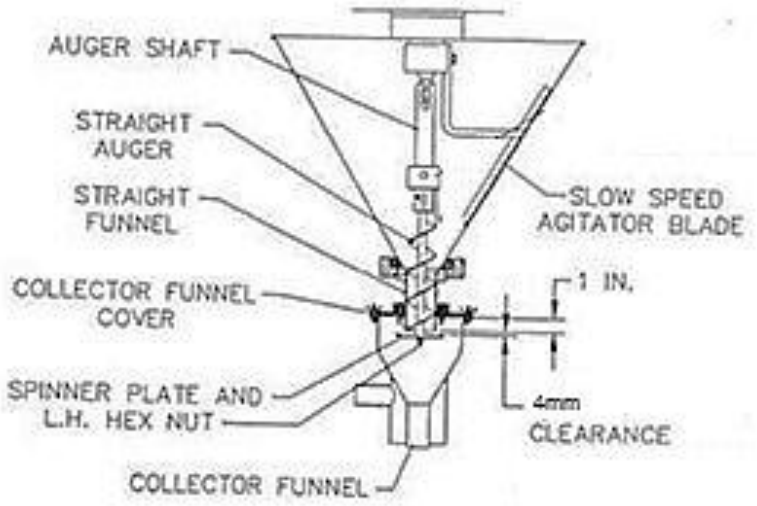

Figure 2- 24 Schematic of auger filler, re-printed from Hewitt et al. [148]

2.4. Summary

In this chapter, the fundamentals and important researches on properties of individual particle, bulk solids fluidising mechanism and flow properties were reviewed. The particle size, size distribution and shape have influence on the bulk solid flowability which can be represented by the collective behaviours of bulk solid, such as bulk density and angle of repose.

The flowability of bulk solids was studied based on the state of stresses. A flow function is able be used to characterize the flowability of materials. The theories can be applied to the investigation of bulk solids flow and the design of dispensing hoppers.

The requirement of micro-dispensing fine powders in pharmaceutical industry was introduced. The current indirect and direct techniques for powder dispensing were reviewed and compared. The vibration dispensing techniques was focused in the review as it was proved effective in dispensing fine powders and has not yet been rigorously explored.

Chapter 3

Materials and Experimental Method of Bulk Solids Dispensing

This chapter introduces materials and experimental methods in this project. All bulk solid materials are categorized in two classes according to mean particle size and bulk solids properties are probed and measured by general bulk solid characterization processes. The experimental methods of dispensing hopper and vibratory dispenser design are described. A computer controlled auto dispensing and weighing system are set up for the dispensing tests with two mechanical vibration dispensers and an ultrasonic vibration dispenser. The weighing and data evaluation method of dispensing test is described. The mass of dose and relative standard deviation (RSD) of dropwise dispensed samples will be used to evaluate dispensing test results in following chapters.

3.1. Materials

Pharmaceutical and biomaterial powders and granules listed below are widely used in industry. These bulk solids exhibit diverse flowability when they are handled in the process. Accurate and efficient dispensing of these materials is a main objective in this project. The materials involved in dispensing tests are generally categorized in two classes according to mean particle size:

Coarse granules (>1 mm): Actifuse® hydroxyapatite (HA) granule

Fine powders (≤100 μm): Inhalac®70, Inhalac®120, Inhalac®230, Sorbolac®400 (lactose); starch; Merck hydroxyapatite, CAPTAL®R, CAPTAL®S (hydroxyapatite); β-TCP (β-tricalcium phosphate)

The information of these materials is listed in Table 3-1.

3.1.1. Materials Characterization

Mean particle size and particle size distribution (PSD) of powders were measured by laser diffraction particle sizing (Mastersizer 2000 with Hydro 2000S side feeder, Malvern Instruments, Worcestershire, UK). The powders were dispersed and prepared in the suspension. It was found difficult to de-agglomerate the cohesive powders in the dispersant due to the strong cohesive forces between particles. Therefore, the D50 of particles shown in Table 3-1 may be larger than the size reported somewhere else measured by dry methods, such as air jet sieving. More details of PSD measurements from laser diffraction particle sizing are shown in Appendix I.

The morphological properties of material particles were observed by scanning electron microscopy (SEM). It describes a broad outline of particle shape in Table 3-1. The SEM images of materials are shown in Appendix III. Actifuse® hydroxyapatite granule is a particular case. Not only are the granules hard to disperse in the suspension, but also the feret diameter of granule is unlikely to be measured from microscope images due to its irregular and porous morphology. Thus, the D50 particle size for hydroxyapatite granule in Table 3-1 is actually the average size determined by mesh sieving.

The bulk density and tapped density of materials were measured in a graduated cylinder by using the method introduced in section 2.1.2. The Hauser ratio, H, was then calculated by equation, $H = \frac{\rho_T}{\rho_B}$.

Table 3- 1 Materials used for dispensing tests in this project

Sample	Material	Particle Size D50 /µm	Shape	Bulk Density /gL^{-1}	Angle of Repose /°	Hausner Ratio	Dispensing Method (Vibration)	Manufacturer
Inhalac® 70	lactose	200	angular	590	33±0.5	1.12	ultrasonic	Meggle
Inhalac® 120	lactose	130	angular	700	35±0.5	1.13	ultrasonic	Meggle
Inhalac® 230	lactose	90	angular	710	39±0.5	1.15	ultrasonic	Meggle
Sorbolac® 400	lactose	9	angular	330	>50	1.79	ultrasonic	Meggle
Starch	wheat starch	21	angular	490	46±1.5	1.57	ultrasonic	Merck
Merck HA	hydroxyapatite	1	near spherical	1030	>50	1.85	ultrasonic	Merck
CAPTAL® R	hydroxyapatite	0.5	needle shape	1120	>50	1.85	ultrasonic	Plasma Biotal
CAPTAL® S	hydroxyapatite	1.3	angular	980	>50	1.77	ultrasonic	Plasma Biotal
β-TCP	β-tricalcium phosphate	1	near spherical	960	>50	1.82	ultrasonic	Plasma Biotal
Actifuse® HA	hydroxyapatite	1500	irregular and porous	490	28±1	1.14	mechanical	ApaTech

The angle of repose (AoR) was measured from the conical pile by pouring the powders through a standing hopper with sufficient large opening onto a plate (see section 2.1.2.6). The value of AoR in Table 3-1 is the average based on 3 times of tests at 25°C and 40% relative humidity (RH). As a precise value of AoR is hard to be obtained for cohesive powders, such as Sorbolac®400, hydroxyapatite fine powder and β-tricalcium phosphate, an approximate range is given in Table 3-1.

3.1.2. Sample Preparation

Each of the materials was moved from its original package to a glove box and stored at 25°C and 40% relative humidity (RH) for 24 hours prior to the dispensing test, which was carried out in the glove box maintained at 25 ± 1°C and 40 ± 2% RH. It is supposed that the moisture content of powder sample could be equilibrium with the moisture of atmosphere in the glove box if it is well sealed for long hours [149].

Then, all the samples were sieved with different meshes in the glove box before testing. The sieving of powders has two purposes. Firstly, the fine powders tend to form agglomerates due to strong interparticle forces in storing and handling. The presence of agglomerates affects the actual flow behaviour of the powder. Thus, the inherent agglomerates need to be broken down by high shear force with the sieve before dispensing. The fine powders were sieved by 425 μm mesh which is larger than the individual particle size and thus, the particle size distribution of these fine powders is not changed in sieving. Secondly, the hydroxyapatite coarse granule has a wide particle size distribution. The sieving aims to filter each batch of samples by removing the excess large and small particles from the majority with 2.8 mm and 0.7 mm mesh, respectively. After sieving, the dispensing test was carried out promptly to avoid the time consolidation and re-agglomeration in sample storage.

3.2. Dispenser Design and Dispensing test

3.2.1. Design of Dispensing Hopper

A micro-dispensing hopper analogue to the traditional large scale silo has been designed in a much smaller dimension, shown in Figure 3-1. The specification of all the dispensing hoppers used in this project is listed in Table 3-2. The hopper is made from 1.5 mm thick raw borosilicate glass straight open tube. The diameter of vertical section, D, is determined by the internal diameter of straight tube. A conical hopper section was drawn from the vertical section with a half conical angle, α. A few example images of

hopper with different angle are shown in Figure 3-2. Yellow sand was filled in the hopper in order to improve the recognisability of internal slope for angle measurement in the images. A series of hopper angle from 6° to 39° were planned to be processed and duplicated for testing. However, as making the exactly same angles for dispensing hopper is unable to be assured technically, there was an average error of ±1.5° for processed hoppers and duplicated hoppers from batch to batch. The conical hopper was drawn with a closed end and then ground to a circular orifice with size D_o. A few example images of hopper orifice are shown in Figure 3-3. The orifice was carefully ground with observing under the microscope. The size error due to the rough edge of orifice was controlled in 0.02 mm which is smaller than general particle size of sample material. Besides the diameter D, the capacity of dispensing hopper is also determined by the total height of hopper which is in the range of 100 mm to 150 mm in this project.

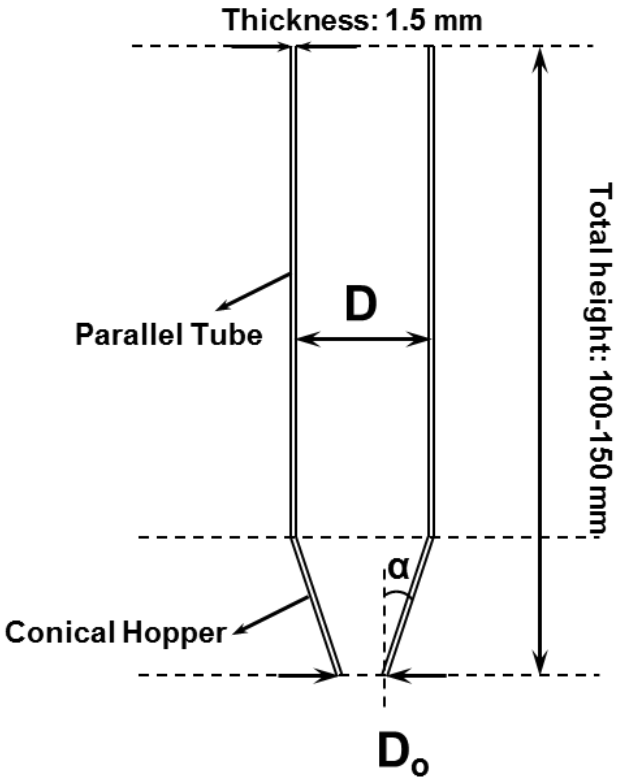

Figure 3- 1 Sketch of micro-dispensing hopper with three variable design parameters: orifice size, D_o; half conical angle, α; and diameter, D.

Table 3- 2 Specification of dispensing hoppers used in this project

Diameter, D /mm	Orifice Size, D_o /mm	Half Conical Angle, α /°	Applications in Dispensing	Appearances in Chapters
6	0.8, 0.9, 1.0	15±1.5	Merck HA, CAPTAL®R, CAPTAL®S, β-TCP	5
8	0.6, 0.7, 0.8, 0.9, 1.0, 1.2	6 – 39 (with an average error of ±1.5°)	Inhalac® series lactose, Sorbolac®400, starch	5, 6, 7, 8
9	0.8, 0.9, 1.0, 1.2	6 – 39 (with an average error of ±1.5°)	Inhalac® series lactose	7
10	0.8, 0.9, 1.0, 1.2	6 – 39 (with an average error of ±1.5°)	Inhalac® series lactose	7
12	0.8, 0.9, 1.0, 1.2	6 – 39 (with an average error of ±1.5°)	Inhalac® series lactose	7
	6.0, 9.0, 9.5	15±1.5	Actifuse® HA granule	4

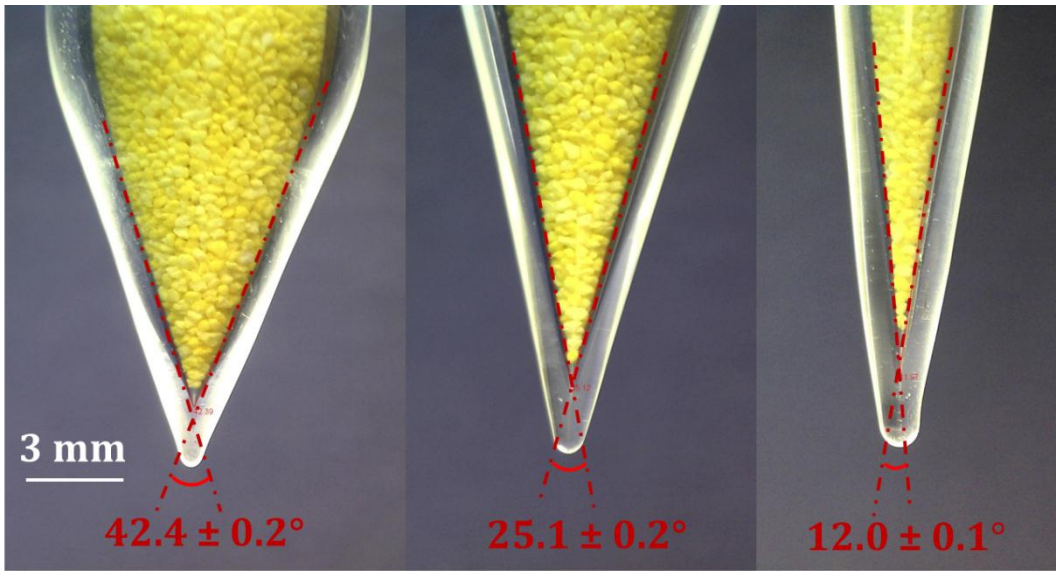

Figure 3- 2 Angle measurement of dispensing hopper. The angle is marked with error due to the blur boundary

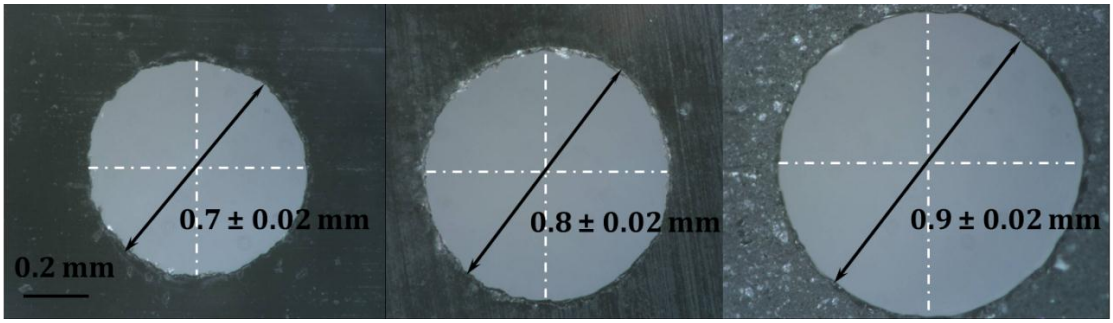

Figure 3- 3 Vertical view of cross section of hopper nozzle under the microscope. The size of orifice is marked with error due to the roughness of edge

3.2.2. Vibratory Dispenser

3.2.2.1. Electromagnetic hammering dispensing device

An electromagnetic hammering device was built and applied to dispensing Actifuse® hydroxyapatite granule. The hammering device is composed of a linear motion electromagnet solenoid and a spring plunger. The specification of electromagnet solenoid is listed in Appendix IV. The push and pull of the plunger is controlled by a 12V DC on/off pulse signal. The frequency of the pulse train is adjustable. In dispensing test, the plunger hammers the lower section of dispensing hopper at a constant frequency. The dispensing hopper is vibrated horizontally and the granules are discharged from the hopper until the hammering is shut down. The granule sample is continuously filled in the dispensing hopper during the dispensing for long hours test.

A schematic diagram of the experimental setup is shown in Figure 3-4. Besides the design parameters of dispensing hopper and the frequency of hammering, there are three variables in device setting investigated in the dispensing test: L1 is the height of plunger to the outlet of hopper in the vertical direction; L2 is the distance between the plunger at its original position (when push type solenoid recoils) and the dispensing hopper; L3 is the height of clamps fixing the dispensing hopper vertically to the outlet of dispensing hopper. The effect of dispensing hopper size, the frequency of hammering and device setting variables on HA granules dispensing will be discussed in section 4.2 of Chapter 4.

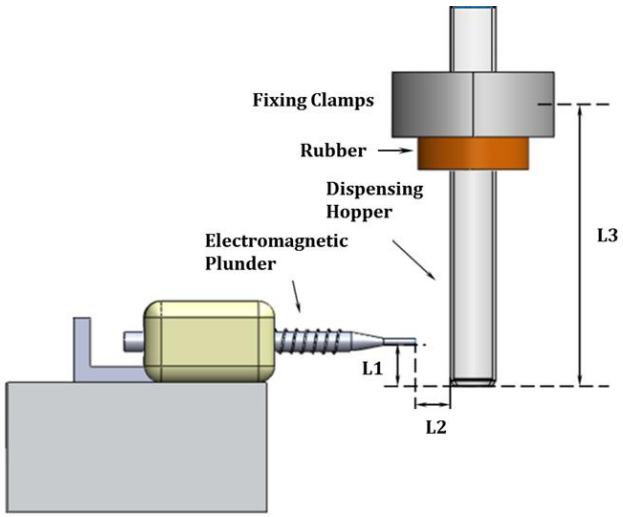

Figure 3- 4 Schematic diagram of the experimental setup of electromagnetic hammering device. L1, L2 and L3 are variables in device setting. For full explanation refer to the text

3.2.2.2. Vibration motor aided dispensing device

An eccentric rotating mass (ERM) vibration motor (Vibration motor 312-401, Precision Microdrives Ltd., UK) was used to vibrate dispensing hopper for dispensing hydroxyapatite granules. The ERM vibration motor is a DC motor with an offset (non-symmetric) mass attached to the shaft. As the mass rotates, the asymmetric centripetal force of the offset mass causes the vibration of motor and therefore, the displacement of dispensing hopper. The vibration produced by ERMs is an example of "harmonically excited vibration" [150]. This means there is an external driving force causing the system to vibrate at the frequency of the excitation. In the case of the ERM model, the excitation input is not the DC voltage applied to the motor. Instead, it is the rotation of the mass around the central motor shaft. The DC voltage controls the speed of the motor (the two are directly proportional) and therefore, the frequency. The specification and performance characteristics of vibration motor are shown in Appendix V.

The vibration motor was attached to the side of dispensing hopper as shown in Figure 3-5. A 12V DC on/off pulse signal is generated to control the motor vibration. In dispensing, the hopper is constantly being displaced by the asymmetric force at a constant frequency. The granules are discharged from the hopper until the motor is shut down. The granule sample is continuously filled in the dispensing hopper during the dispensing for long hours test. Same as the electromagnetic hammering device, the experimental setups have effect on dispensing result. As shown is Figure 3-5, L1 is

height of centre position of vibration motor to the outlet of hopper; L2 is the height of clamps fixing the dispensing hopper vertically to the outlet of dispensing hopper. A high speed camera (Phantom 7.1 colour, Vision Research) was used to investigate the vibration characteristics of motor-aided dispenser and the discharge of granules under the influence of vibration. The effect of dispensing hopper size, duration of vibration and device setting variables on HA granules dispensing will be discussed in section 4.3 of Chapter 4.

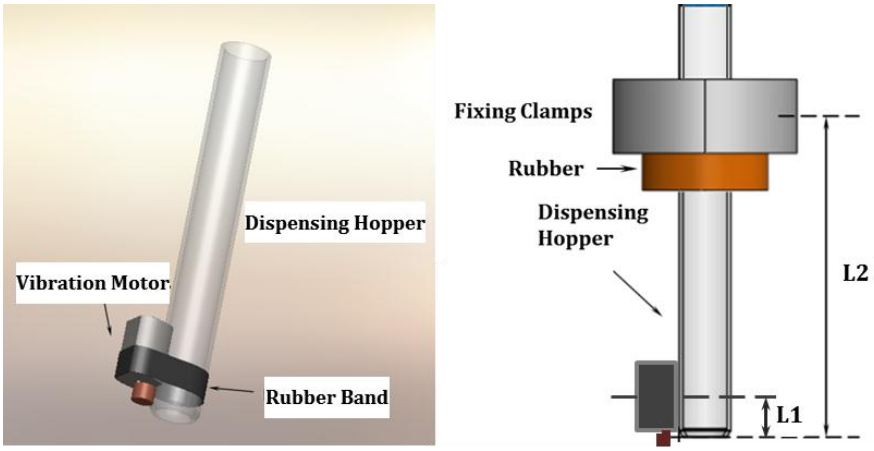

Figure 3- 5 Sketch of vibration motor dispensing device and schematic diagram of the experimental setup. L1 and L2 are variables in device setting. For full explanation refer to the text

3.2.2.3. Ultrasonic vibration dispensing device

An ultrasonic vibration dispensing device, shown in Figure 3-6, is assembled to dispense fine powders. The device is composed of a dispensing hopper, a bottle-shaped glass water tank with flat bottom and a piezoelectric ceramic ring (SPZT-4 A3544C-W, 35mm ×15mm ×5 mm, MPI Co., Le Locle, Switzerland). The piezo ring is attached to the bottom of water tank with an adhesive commonly used in ultrasonic cleaning tank construction (9340 GRAY Hysol Epoxi-Patch Structural Adhesive, DEXTER Co., Seabrook, USA). The conical section of dispensing hopper is stuck and sealed in a premade hole at the bottom of tank. The tank is filled by water which is supposed to have two functions: a medium for the vibration propagation [29] and exerting extra force on the dispensing hopper by cavitation effect [151]. The water tank is covered by a lid in which there is an o-shaped rubber ring fixing the dispensing hopper.

In dispensing, a voltage signal in square waveform is generated by computer and the signal is enhanced by a voltage signal amplifier with the “closed loop feedback” function.

The function can be described as the circuit's overall gain and response becomes determined mostly by the feedback network [152] (p. 523-527). As result, the piezo is actuated by the amplified signal at its resonance frequency of approximately 44 kHz, at which the ceramic element vibrates most readily and most efficiently converts electrical energy input into mechanical energy [29]. Due to the mechanical deformation in the crystal of piezo ring, vibration is generated and then propagated to the dispensing hopper through water inside the tank. The vibration intensity and duration can be varied with the voltage signal. When the device starts vibrating, the powder is discharged from the hopper. The flow of powder is ceased when the vibration stops. A high speed camera (FASTCAM SA5, Photron USA, Inc) was used to capture images of powder discharge during dispensing. The effect of design parameters of dispensing hopper and vibration signal parameters on the dispensing of fine powders will be discussed in Chapter 5.

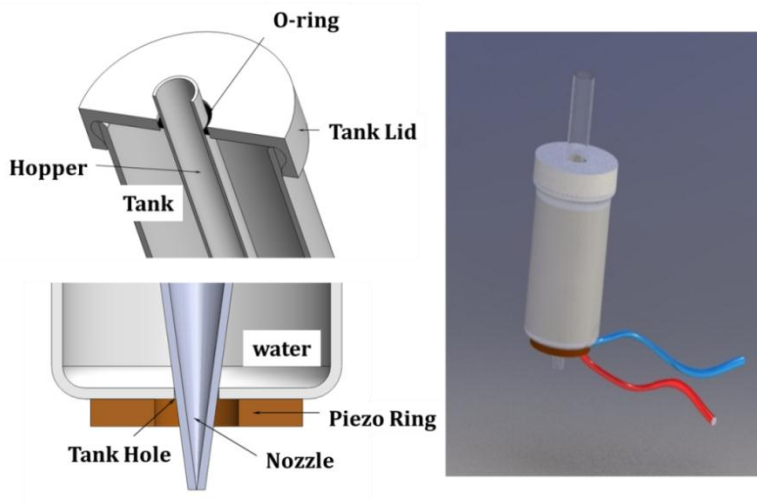

Figure 3- 6 Sketch of ultrasonic vibration dispensing device

3.2.3. Computer Controlled Micro-Dispensing and Dosage Weighing System

A computer controlled auto micro-dispensing and dosage weighing system is built for vibratory bulk solids dispensing (Figure 3-7). The system comprises a computer, a D/A Card (NI-6733, National Instruments Corporation Ltd. Berkshire, UK), a voltage signal amplifier (50w, Sonic Systems Ltd, Somerset, UK) for ultrasonic device only, a relay for mechanical vibration devices and a microbalance (2100 mg ± 0.1 µg, Sartorius AG, Germany). In dispensing test, there are two dispensing modes: continous dispensing and intermittent dispensing. In continous dispesning, the vibration device is turned on by operating voltage signal sent by the computer. The sample is continously dispensed until

the vibration is shut down by truning off the signal. In intermittent dispensing, the samples are dispensed and measured dose by dose. Therefore, a pulse wave is generated by the computer. For electromagnetic hammering device and vibration motor device, the pulse wave is used as an on/off voltage siganl for the relay to control the electromagnet solenoid and the vibration motor. There is a 12V DC power supply providing the operating voltage for mechanical vibration devices. In the ulrasonic vibration device, the pulse wave is amplified (Vrms = 370V) by the voltage signal amplifier to intermittently actuate the piezoelectric transducer. The duration of vibration, T_d, is the vibration duration induced by the wave pulse for dispensing single dose. It is normally variable between 0.1s and 10s. The dispensed dose mass is verified and recorded by the microbalance and the data is sent to the computer via RS232 serial-port. The microbalance is capable of recording instant mass data at 0.4s intervals. Thus, the time interval between each dosing, T_i, should be larger than 0.4s in order to distinguish dosages by the microbalance. One dispensing cycle per dose is composed of duration of vibration, T_d, and the time interval between each dosing, T_i.

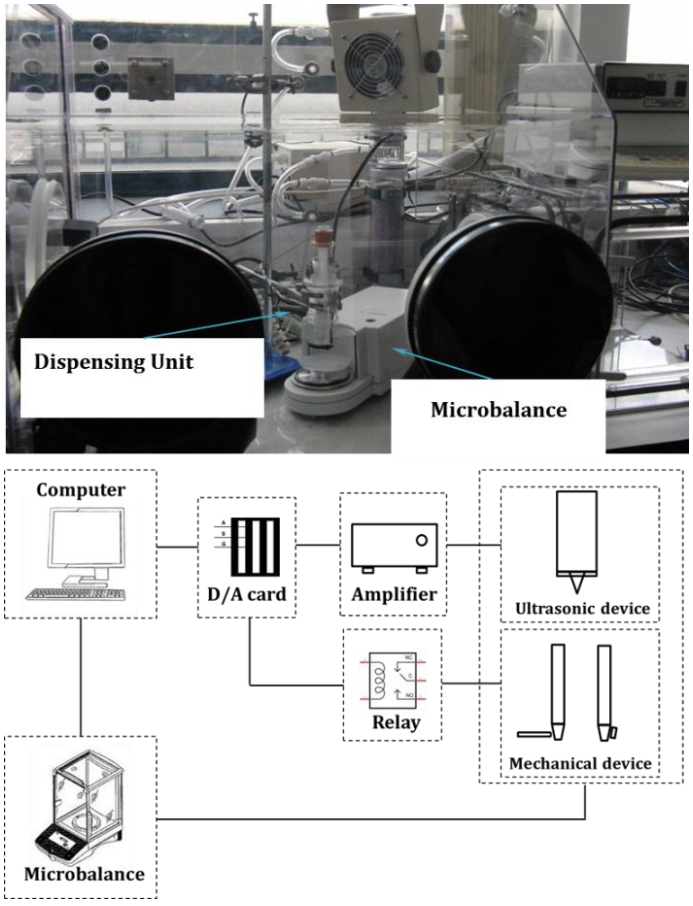

Figure 3- 7 Schematic diagram of the experimental arrangement of computer controlled micro-dispensing system. For full explanation refer to the text

The operation of data collection and signal generation are enabled by a Labview programmed interface designed by X. Lu and S. Yang in Queen Mary University of London (Figure 3-8). Three processing parameters: dispensing (wave) cycle, wave duration per dose and wave amplitude, can be tuned on the interface for different dispensing tasks.

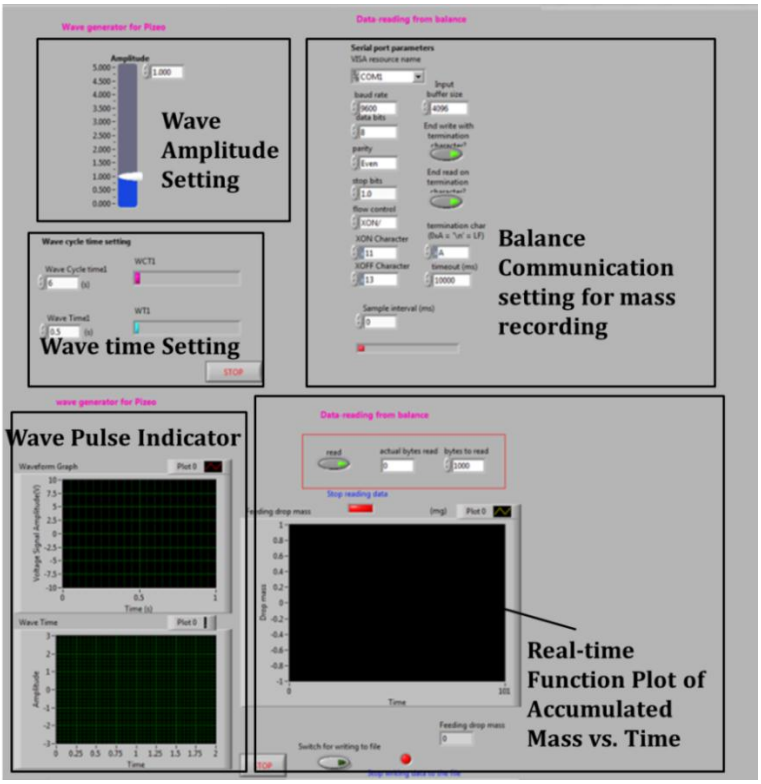

Figure 3- 8 Labview programmed micro-dispensing control interface on PC by X. Lu and S. Yang

3.2.4. Dispensing Data Evaluation

Figure 3-9 shows an example of function curve plotted by dispensed dose mass against dispensing time. In Figure 3-9(a), a "staircase" represents one cycle of dispensing which is composed of vibration duration for dispensing that dose and time interval before next dispensing. The height of "staircase" refers to the increase of dispensed mass in one cycle and also, the mass of dose. The microbalance is stabilized during the interval between each dispensing and thus a platform is plotted on the curve. Theoretically, the staircase is forwarded evenly and the gradient of the curve is constant if the doses are uniformly dispensed. An example of dispensing evaluation chart of Inhalac®120 with ultrasonic vibration is shown in Figure 3-10. The length of column represents the dose mass, and in the column chart the conformity of doses is more visualized than the

staircase curve. Mean dose mass and relative standard deviation (RSD) of dispensed doses are used to evaluate dispensing test result. It can be concluded that the larger the mean dose mass, the higher the flow rate of powder; the smaller RSD, the better the dose-to-dose conformity.

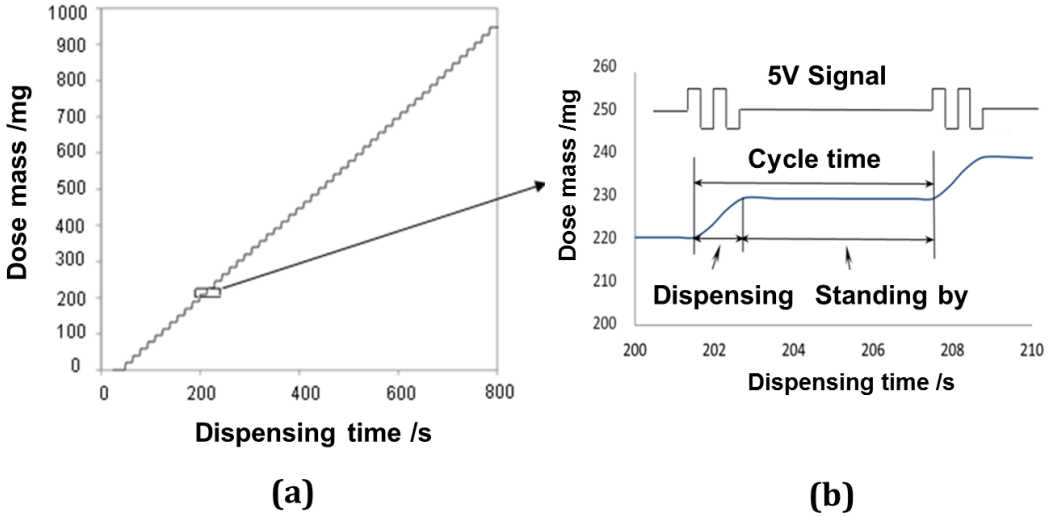

Figure 3- 9 (a) Function plot of dose mass vs. dispensing time with 1s vibration per dose. (b) Zoomed-up view of one "staircase" in plot (a). For full explanation refer to the text

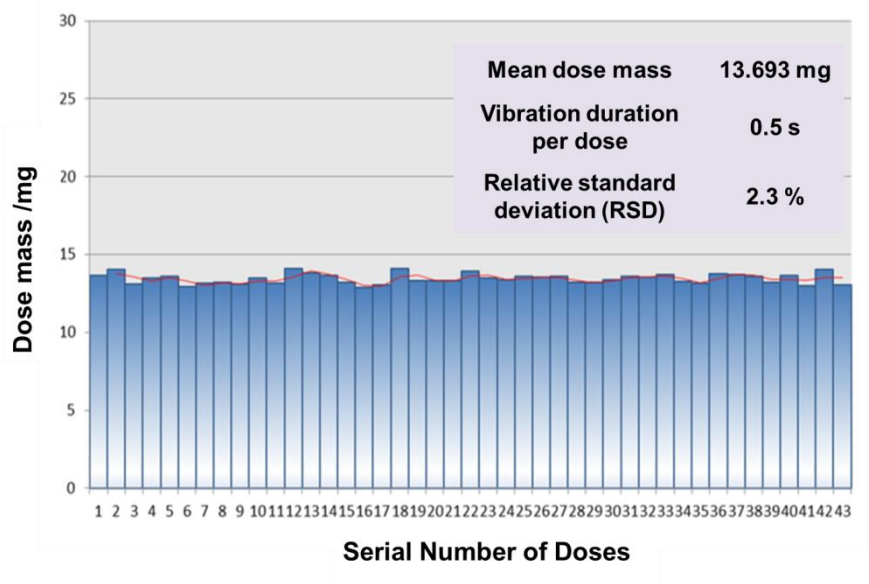

Figure 3- 10 Evaluation chart for dispensing data. For full explanation refer to the text

3.3. Summary

This chapter introduced pharmaceutical and biomaterial powders and granules used for dispensing tests in this project. The properties of these materials were given by general bulk solid characterization processes. The methodology of dispensing hopper and vibratory dispenser design were described. A micro-dispensing hopper analogue to the traditional large scale silo has been designed in a much smaller dimension. The dispensing hopper is composed of a vertical section on top and a hopper section in the bottom. Three design parameters, orifice size, hopper angle and diameter of vertical section were introduced. Two mechanical vibration dispensers were designed with using electromagnet solenoid and vibration motor as the vibration generator. The setup of the vibration source was proposed as critical design parameter. An ultrasonic vibration device was designed with using piezoelectric ceramic transducer as the vibration source. The piezo can generate a high frequency vibration to dispense materials. At last, a computer controlled auto dispensing and weighing system was setup to operate vibratory dispensing devices with voltage signal in two dispensing modes: continuous dispensing and intermittent dispensing. The dose weighing and data evaluation method of dispensing test were also established.

Chapter 4

Mechanical Vibration Induced Coarse Particles Dispensing

This chapter presents experimental study investigating the dispensing of hydroxyapatite (HA) granule with mechanical vibration devices. The basic principle of how the vibration works on fluidizing bulk solids in the hopper is presented. The experimental results show that the vibration leads to a reduction of the bridge strength of particles in the hopper. The two types of horizontal vibration provided by electromagnet solenoid and vibration motor were proved effective in dispensing irregular shaped coarse granules such as HA. The effect of dispensing hopper size, device settings and vibration characteristics on the dispensing was discussed.

4.1. Introduction

Coarser particles have been proved easier to be transferred from one vessel to another, since the movement of each particle is not dominated by cohesive and adhesive forces but by the force of gravity [114]. However, if particles are rough, sharp-edged, and large with respect to the size of hopper outlet, a granular bridge can be formed above the outlet so that discharge is stopped. The reason for bridge formation of the coarse particles is interlocking and wedging [13] (p. 294). Also, rough surface increases friction between particles and therefore, the bridge strength. The coefficients of friction normally encountered vary from about 0.3 for smooth spherical particles to about 1.5 for angular particles [1] (p. 24). Although the bridging of coarse particles can be avoided if the diameter of outlet is sufficiently large, in micro-dispensing techniques the outlet of hopper has to be small comparing with conventional large silos for such materials in order to dispense materials in small dosages. Vibration has been used as a means of promoting flow in hoppers with smaller outlet.

Actifuse® hydroxyapatite granule is a rigid, porous and irregular shaped granule. Although it exhibits a good flowability in handling, the micro-dispensing of this granule is difficult with good dosage conformity. In this chapter, the micro-dispensing of HA granule is tested with an electromagnetic hammering and a vibration motor device, respectively. The aim for this chapter is to examine the effect of dispensing hopper size, vibration characteristics of device and device setting variables on flow rate and dosage conformity of HA granules dispensing.

4.2. Hydroxyapatite Granule Dispensing with Electromagnetic Hammering Device

4.2.1. Hopper Flow and Bridging Controlled Flow Mechanism

Actifuse® hydroxyapatite granule has large particle size which is 1.5 mm in average. The cohesion between coarse particles is small. The gravity flow test of HA granules was conducted on chutes, parallel open tubes, and conical hoppers, respectively. In the test, HA granule exhibited good flowability sliding along the chute with the angle larger than 30° and freely flowing out of the parallel open tube with the diameter larger than 9 mm. Nevertheless, when the granules are filled in a hopper with 10 mm orifice size, the flow

was found obviously retarded in the convergent zone of cone. When the orifice size of hopper was reduced to 9 mm, the flow was ceased by bridging of granules above the outlet of hopper. As shown in Figure 4-1, granules are bridged by interlocking and wedging. The convergent zone in the hopper plays a key part in the formation of granular bridge. The granule occludes with one another through pronged surface so that the frictional force between granules is dominant in bridging, whereas the friction between granules and the wall of hopper is weak. The friction between granules contributes to the bearing force of bridge. The granules near the outlet were compacted when more granules filled. The strength of bridge was therefore increased and as result, the granules were found unable to be discharged under the gravity.

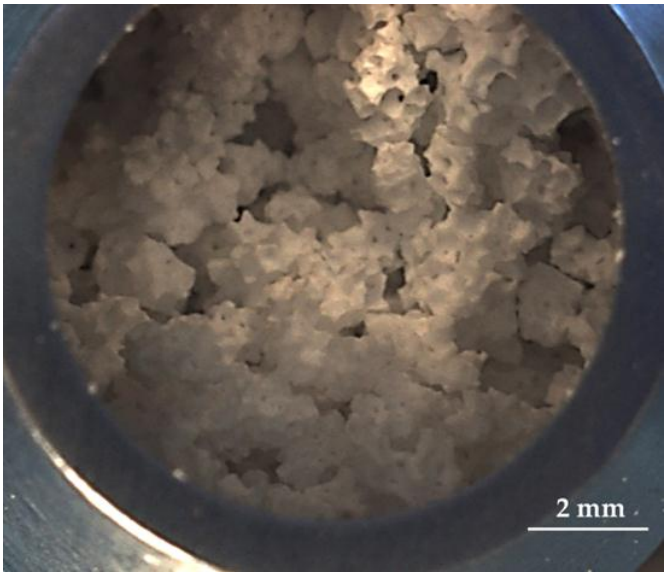

Figure 4- 1 Vertical view of hydroxyapatite granules bridge above the outlet of dispensing hopper

The electromagnetic hammering device was used to provide extra driving force to initiate the flow of granules in the hopper with 9 mm orifice size. As observed, when the hammer impacted the hopper, the granules started to discharge from the orifice; when the hammering was stopped, the flow was found ceased immediately by bridging of granules. The granular bridge acts as a valve in this process. The bridging controlled flow mechanism can be illustrated by Figure 4-2. When the hopper is vibrated by the impact of hammer, granules are dilated under the influence of vibration (Figure 4-2(b)). The voidage between granules are increased and therefore, the interlocking and wedging of granules are weakened. The bridge is failed with a reduction of unconfined yield stress (bearing stress). Then the “flow valve” is opened. When the vibration is

stopped, the granules re-bridged in the convergent flow zone of hopper and the "flow valve" is closed (Figure 4-2(c)).

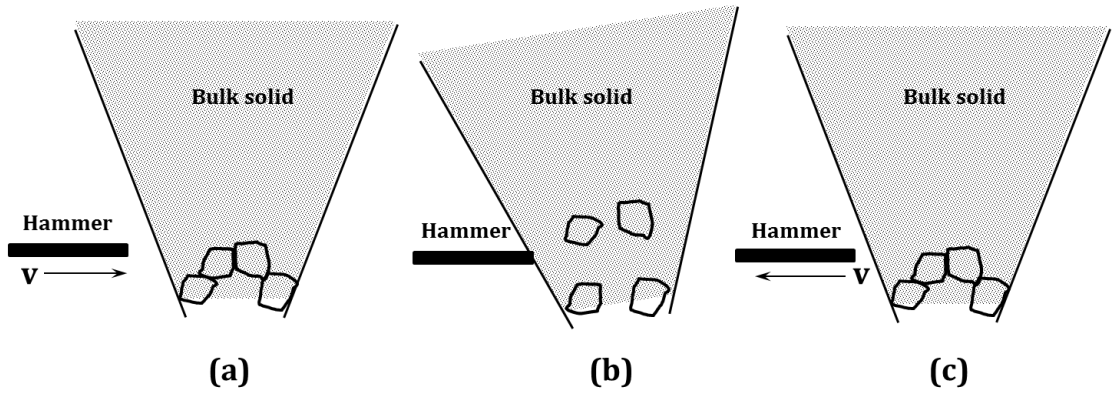

Figure 4- 2 Bridging controlled flow mechanism for HA granule. For full explanation refer to the text

The impact of hammering is very effective in promoting granules flow from hoppers with smaller outlet diameter where free flow is unavailable under the gravity. However, when the orifice size of hopper is excessively small with respect to the particle size of granule, the discharge channel is congested and the granules are easier to be bridged than dilated as the voidage between granules is hard to be increased in the convergent zone of hopper. The vibration is therefore invalid to force the flow.

Jenike proposed a critical diameter of hopper orifice in gravity flow (see section 2.2.1). In vibration promoted hopper flow, a critical orifice diameter, $D_{o,vibr}$, for a free flow under the vibration can be defined as,

$$D_{o,vibr} = \frac{H(\alpha)\sigma_{c,vibr}}{\rho_B g_{\text{eff}}} \tag{4.1}$$

where g_{eff} is the effective gravity acceleration proposed by Suzuki et al. [113]. When granules is bridged above the outlet of hopper, they are accelerated by the wall at the start of flow and therefore, equation (4.1) can be also presented by,

$$D_{o,vibr} = \frac{H(\alpha)\sigma_{c,vibr}}{\rho_B g\left[1 - \frac{a(2\pi f)^2}{g}\sin(2\pi f t)\right]} \tag{4.2}$$

where a is the amplitude of vibration. f is the frequency. $\frac{a(2\pi f)^2}{g}$ is nondimensional acceleration amplitude. Therefore, when vibration is applied to promoting flow of particles in a hopper, the vibration characteristics and location of the vibration source is critical factors for hopper orifice selection.

4.2.2. Effect of Device Settings on HA Granule Dispensing

The HA granules dispensing by electromagnetic hammering was demonstrated in the hopper with 9mm orifice size. The experimental settings are shown in Figure 3-4. Each of the three setting parameters L1, L2 and L3 had two assignments listed in Table 4-1. The flow rate of HA granule under 8.5Hz continuous hammering is shown in Table 4-2.

Table 4- 1 Electromagnetic hammering experimental setup

Parameters	Settings	Value	Note
L1	$L1_1$	5 mm	
	$L1_2$	15 mm	
L2	$L2_1$	5 mm	The stroke of spring plunger is 6mm
	$L2_2$	6 mm	
L3	$L3_1$	60 mm	The total length of dispensing hopper is 12 mm
	$L3_2$	100 mm	

Table 4- 2 Flow rate of HA granule from 9.0 mm orifice under 8.5Hz continuous hammering

L1 /mm	L2 /mm	L3 /mm	Flow Rate /gs^{-1}
5	5	60	0.533
5	5	100	1.248
5	6	100	1.176
15	5	100	0.828
15	6	60	0.350

The results in Table 4-2 shows that factor L3, the height of clamps fixing the dispensing hopper vertically to the outlet of dispensing hopper, has the most impact on the flow rate. Flow rate generated by vibration in case $L3_2$ is 130% of case $L3_1$. If the clamping position is too close to the bottom end of hopper, it will restrain the movement of dispensing hopper under the hammering. The striking force only acts on a point of hopper and the upper section is less vibrated. Thus, the factor L3 affects the distribution of energy in the whole hopper. The low amplitude of vibration is less effective to break the bridge as the extent of rearrangement of particles is less. When the clamping position moves up, the amplitude causing particles rearrangement in the hopper is increased. As shown in equation 4.2, in a hopper with orifice size $D_{o,vibr}$, increasing amplitude of vibration cause the unconfined yield stress reduced. L3 can be interpreted

as the factor of efficiency of mechanical vibration on reducing the unconfined yield stress and therefore, the bridge strength of granules.

Factor L1, the height of plunger to the outlet of hopper in the vertical direction, presents the relative position of collision point and the bridge. If the collision point is closer to the bridge, it has more influence on the movement of particles in the bridge, which makes the bridge easier to be broken by hammering. On the contrary, the hammering is invalid to break the bridge when the collision point is far from the bridge. It is because the external force is not directly acted on the bridge to provide sufficient driving force for the failure. The rearrangement of particles at higher position in the hopper has no influence on the bridge at the outlet.

Factor L2, the distance between the plunger at its original position (when push type solenoid recoils) and the dispensing hopper, also affect the flow rate shown in Table 4-2. The velocity of plunger is lower when it reaches to its more front position (6mm). In this case, less energy was transmitted when the plunger hit the dispensing hopper. The vibration is weaker.

Table 4-3 shows the influence of setting parameters on the dosage conformity of intermittent dispensing of HA granule. The results show that the effect of factor L1, L2 and L3 on the dosage conformity is similar to that on the flow rate. In dispensing, if the vibration is insufficient to provide persistent driving force causing the bridge failed, the flow rate decreases. As result, the granules get compacted in the hopper and thus, the bridge strength is increased. In this process, the dosage varies with the stress state of granules in the hopper.

It can be concluded that device settings have the same effect on the flow rate and dosage conformity of HA granule as the flow rate and dosage conformity of dispensing are subjected to the same doming mechanism and bridge failure criteria. Therefore, to achieve the highest flow rate and best dosage conformity, the optimum setting is *L1=5 mm; L2=5mm; L3=100mm*.

Table 4- 3 Dosage conformity of HA granule represented by relative standard deviation from 9.0 mm orifice under 8.5Hz, 1s intermittent hammering

L1 /mm	L2 /mm	L3 /mm	Mean dose mass /g	Relative Standard Deviation
5	5	60	0.517	6.0%
5	5	100	1.260	4.8%
5	6	100	1.159	5.1%
15	5	100	0.835	5.4%
15	6	60	0.378	7.2%

4.2.3. Effect of Frequency on HA Granule Dispensing

The hammering tests were carried out at the frequency ranging from 1 Hz to 20 Hz with the optimum device setting: L1=5 mm; L2=5mm; L3=100mm. The effect of frequency on flow rate was noticeable at or below 20 Hz. Figure 4-3 shows that hammering frequency from 1 Hz to 10 Hz caused a significant increasing of flow rate which was peaked at 10Hz. The frequency of hammering determines the number of times of particles rearrangement occurred in the hopper. Higher frequency causes more frequent rearrangement of particles, as result of which the interlocking and wedging of granules are weaken so that the strength of bridge is decreased. At lower frequency, the bridge is less effectively broken by hammering as the movement of particles is less. As result, it causes larger variation in flow rate. The dispensed mass of granules was plotted against dispensing time as shown in Figure 4-4. The slope of the curve represents the flow rate and the degree of linearity indicates the flow consistency. When the flow was proceeding, jamming was observed frequently occurred at lower frequency (Figure 4-4). The overflow is also a circumstance taken place in lower frequency hammering, in which the bulk solids fail to form a bridge in the hopper so that encounter an abrupt increasing in the flow rate. The jamming and overflow are two notorious problems causing poor flow consistency in bulk solids flow. When the frequency increased, more steady flow of granules was developed due to the decrease of bridge strength. The deviation of flow rate is the minimum at 8.5 Hz.

However, with increasing the frequency to 20 Hz, the flow rate dropped to the same level as at 5 Hz and the flow consistency was deteriorated (Figure 4-3). It can be explained that electromagnetic hammering only provides vibration in the single direction. The high frequency of hammering caused the stress prevails in horizontal direction and the vertical stress is not enough causing the failure of bridge. As result, the interlocking and wedging of granules are strengthened by high frequency horizontal vibration. Thus, 8.5 Hz can be considered as the optimal frequency at the hammer setting of L1=5 mm; L2=5mm; L3=100mm. Similar results were also reported. Hunt et al.

[101] investigated the discharge of glass spheres in a planar wedge-shaped hopper that is vibrated horizontally and indicated the discharge rate increases with vibrational acceleration. However, at the higher frequencies, the increase in discharge rate does not occur until the acceleration amplitude is greater than approximately 1. Matsusaka and co-workers [114] have reported that on increasing the frequency of vibrations, the micro-vibrating particles undergo increase activity. This further reduces the frictional stress between the particles and the wall surface leading to an increase in flow rate. The flow rate however saturates beyond a certain upper limit of frequency, as the activity of micro-vibration of particles no longer increases at higher frequencies.

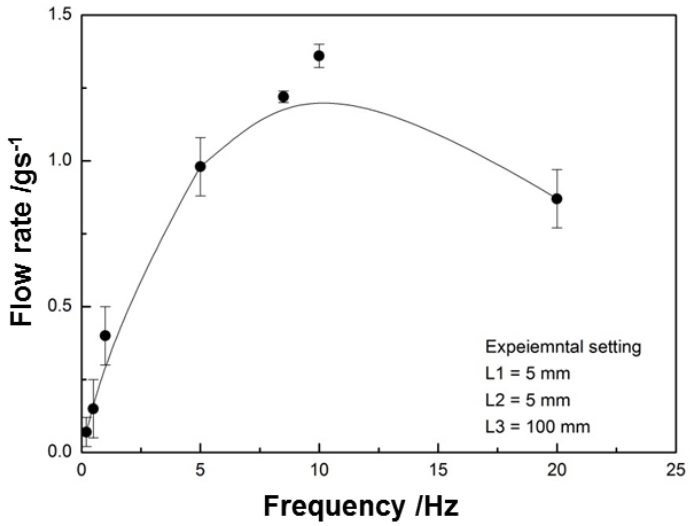

Figure 4- 3 Flow rate vs. frequency of electromagnetic hammering dispensing

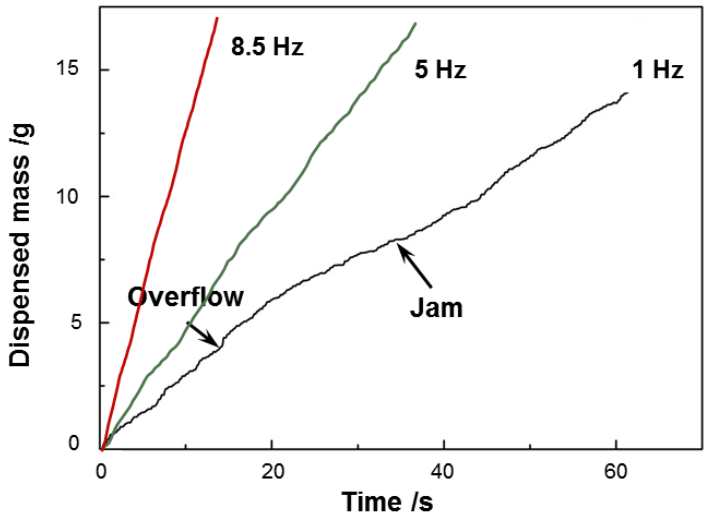

Figure 4- 4 Function plot of dispensed mass of HA granule vs. dispensing time under 1 Hz, 5Hz and 8.5Hz of electromagnetic hammering. For full explanation refer to the text

4.3. Hydroxyapatite Granule Dispensing with Vibration Motor Dispenser

4.3.1. Effect of Hopper Size on HA Granule Dispensing

As discussed in section 4.2.1, the orifice size for vibration motor dispenser must be larger than the a critical orifice diameter, $D_{o,vibr}$, under the influence of vibration to avoid intermittencies in the flow due to jamming. Brown and Richards [95] suggested the critical value as 2.5 for slots and 4.0 for circular orifices when particles are in gravity flow. Although the vibration can promote granules flow from hoppers with smaller orifice size comparing with the gravity flow, by taking account of high friction coefficient of HA granules the dispensing test with vibration motor dispenser is started with 6.0 mm nozzle at 12V. The diameter of orifice is 4 times of the average particle size of HA granule. The duration of vibration is 1s for an intermittent dispensing. As seen in the results in Figure 4-5, the dosages varied significantly. An irregularly small dosage was obtained at the 4th dose. The decreasing of dosage is supposed due to a jamming happened at the outlet. With continuous vibration, the jammed granules are dilated. Comparing with relatively large orifice, the jamming or blockage is likely happened in the hopper with small orifice. Also, low flow rate of granules from a smaller orifice may cause the rest granules in the hopper more compacted by the vibration and thus, the strength of granular bridge is increased. This is also a reason for the bad dosage conformity.

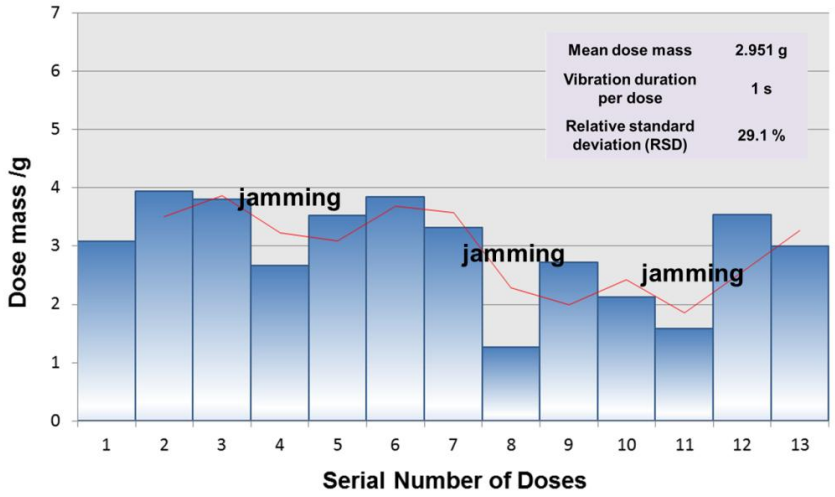

Figure 4- 5 Dispensing results of hydroxyapatite granules from 6.0 mm nozzle. Duration of vibration is 1s.

To solve this issue, the diameter of hopper orifice should be enlarged. As shown in Figure 4-6, the deviation between dosages decreases and the flow rate increases with the increasing orifice size. By increasing the orifice, granules tend to form a bridging-free flow in the hopper as the consolidation stress is increased and therefore the flowability of granules. Considering particles interaction, the increased orifice size provides more space for the movement of vibration-dilated granules in the hopper. The flowing bulk density is increased and hence the flow rate. These explanation also works on the dosage conformity which had been significantly improved when the hopper orifice diameter reached to 9.0 mm. Figure 4-7 shows the dispensing result of HA from 9.0 mm nozzle over 1s duration of vibration. In this case, the ratio of orifice diameter to the mean particle size is 6. And the best dosage conformity was obtained with 9.5 mm nozzle which RSD was less than 5% over 1s duration of vibration (Figure 4-8).

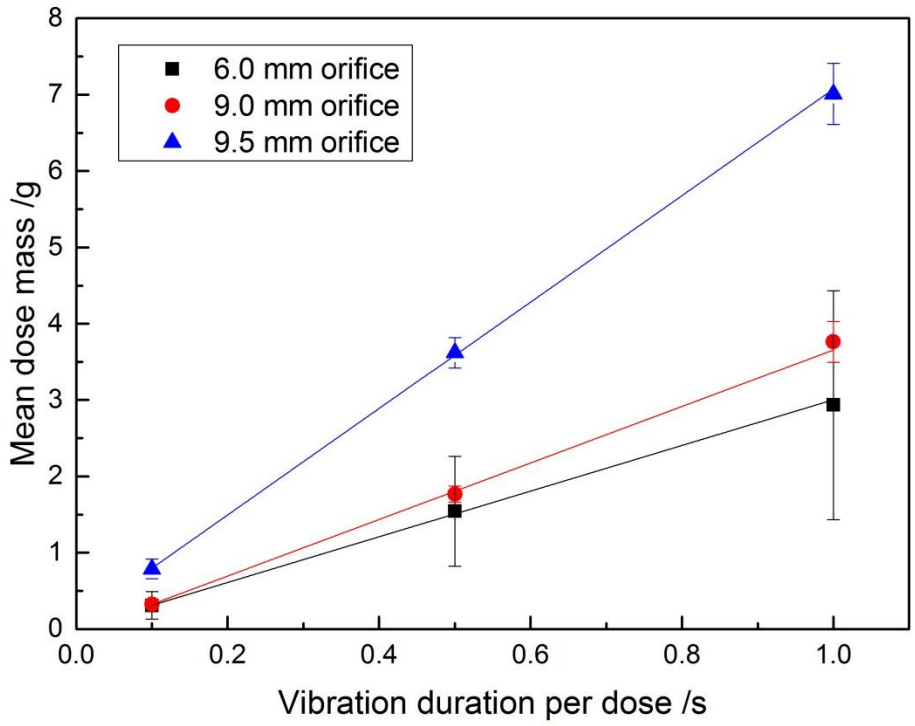

Figure 4- 6 Motor vibration dispensing results of Hydroxyapatite granules from different duration of vibration and orifice size

With increasing the orifice to 10 mm, the flow of granules could not be stopped even if the vibration was shut down. The dilated granules is failed to be bridged in the hopper in the condition of the orifice size is excessively large with respect to the particle size. The granules overflow from hopper which is in contrast to the jamming in excessively small nozzle.

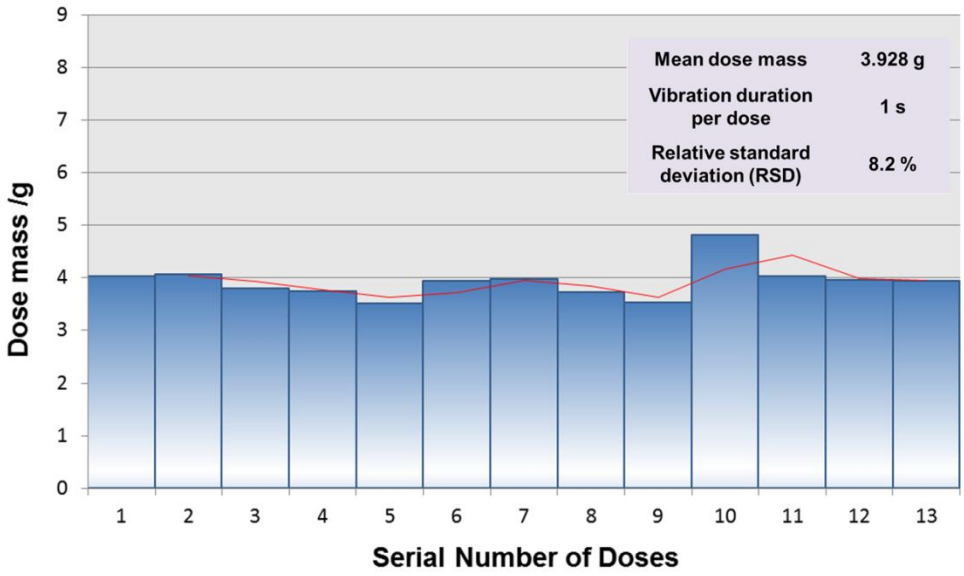

Figure 4- 7 Dispensing results of hydroxyapatite granules from 9.0 mm nozzle. Duration of vibration is 1s.

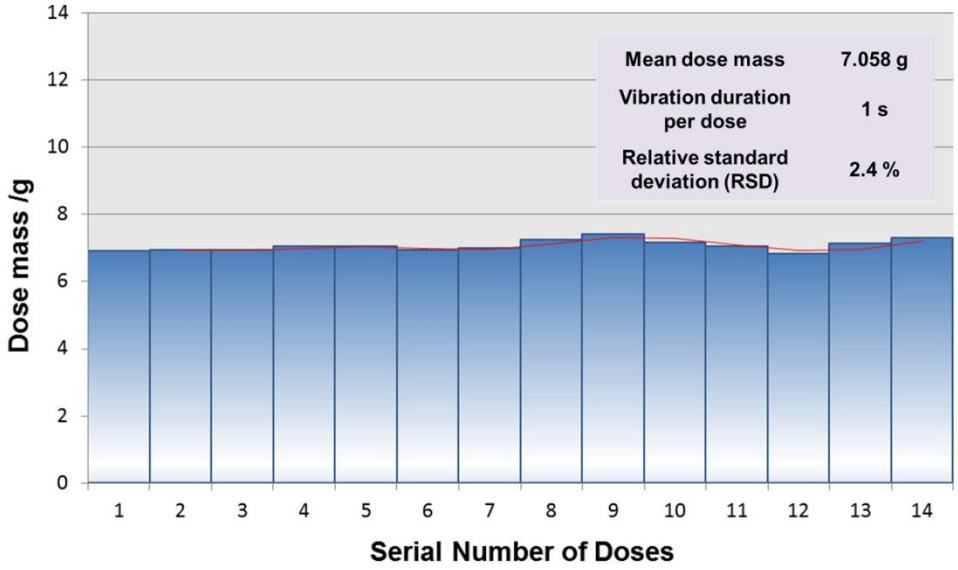

Figure 4- 8 Dispensing results of hydroxyapatite granules from 9.5 mm nozzle. Duration of vibration is 1s.

4.3.2. Effect of Vibration Output on HA Granule Dispensing

The setup of motor vibration dispensing system is illustrated in Figure 3-5. The whole dispensing device is put in motion by the rotation of eccentric mass of attached vibration motor. The location factor L1 and L2 in device setting shown in Figure 3-5

have similar effect on the flow rate and dosage conformity for HA granule as the electromagnetic hammering device. The position of motor on the side of dispensing hopper, L1 presents the relative position of vibration source to the bridge formed by granules. If the vibration source is closer to the bridge, it has more impact on the dilation of granules at the bridge, which makes the bridge easier to be broken under by reducing the bearing force of bridge. For the clamping position L2, if it is too close to the bottom end of hopper, it will restrain the movement of dispensing hopper under the vibration. The low amplitude of vibration is less effective to break the bridge.

The vibration of dispenser was captured by the high speed camera which shows that the movement of mass can be illustrated as a sinusoid (Figure 4-9) and the dispenser is vibrated sinusoidally in the horizontal plane. The frequency of this sine wave is the frequency at which the ERM vibrates. The vibration displacement of dispensing hopper was measured from the high speed camera frames in Figure 4-10, which shows that the peak-peak displacement in x direction is approximately 0.3mm in 0.5s vibration cycle.

The DC voltage controls the speed of the motor (the two are directly proportional) and therefore, the frequency. The dispensing test was conducted at different voltage. In Table 4-4, it shows that in 9.5 mm nozzle the dose mass is increased and RSD is decreased with increasing voltage.

Table 4- 4 Dispensing results of HA granule dispensed with vibration motor device from 9.5 mm nozzle at different voltage

Voltage /V	Frequency /Hz	Dose mass in 1s vibration /mg	RSD
8	200	5.90	7.5%
10	245	6.33	6.6%
12	290	7.06	2.4%
14	330	9.17	1.9%

As the vibration frequency increases, the duration of time for the force to be applied in one direction is reduced. Due to the cyclical nature of ERM, high frequency vibrations only have a short period of time to displace the motor before it is displaced in the opposite direction. This means the peak to peak displacement is greatly reduced. The dilated granules therefore have more chance to pass through the orifice in one cycle of vibration. It can be concluded the flow rate increases with the increasing frequency and decreasing vibration displacement. A harmonically excited vibration source for

promoting solid discharge in a hopper is preferred to have high frequency and low displacement.

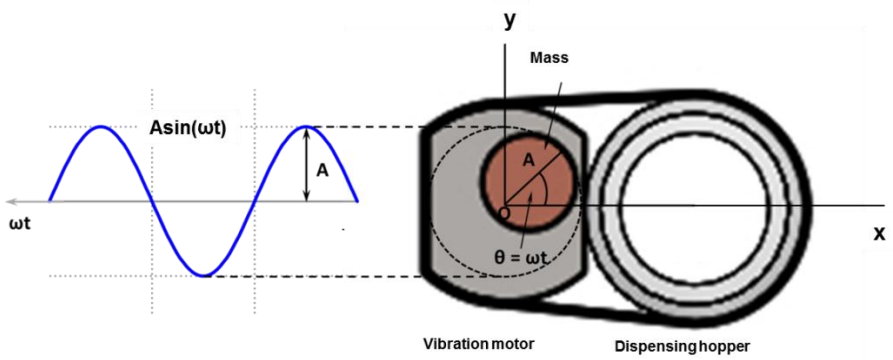

Figure 4- 9 The bottom view of vibration motor dispensing device. The eccentric rotating mass of the motor moves in a sine wave.

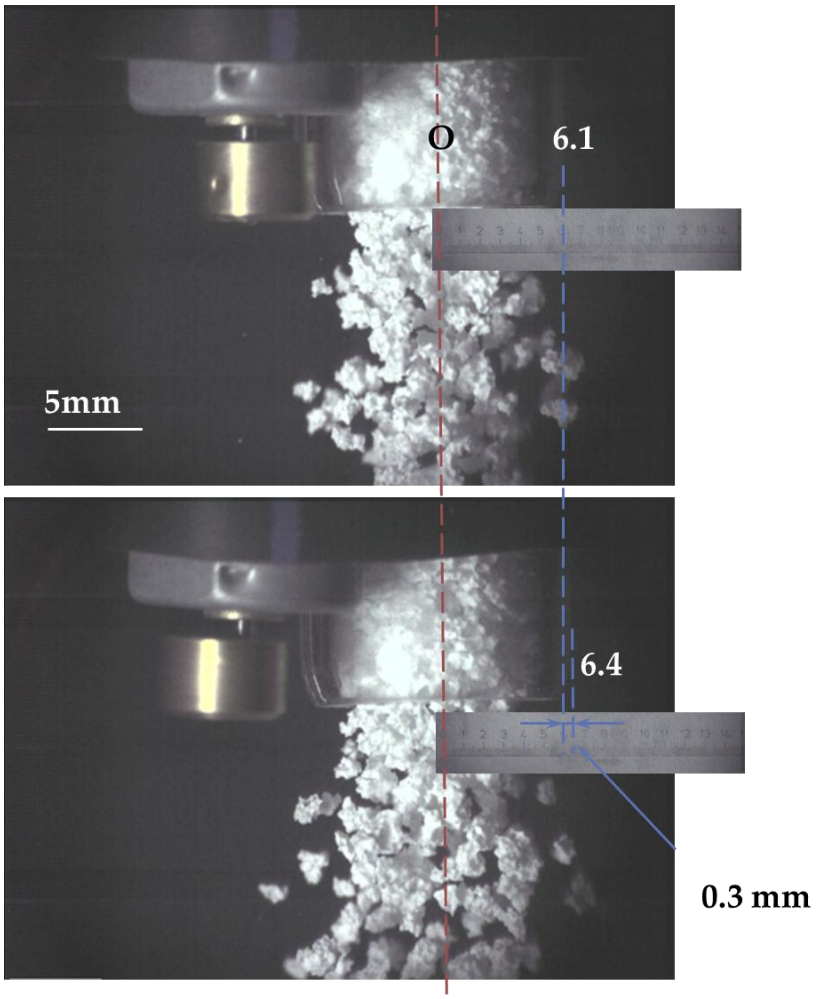

Figure 4- 10 High speed video images for displacement measurement of vibration motor dispenser

4.3.3. Effect of Vibration duration on HA Granule Dispensing

As shown in Table 4-5, HA granules can be uniformly dispensed by motor vibration device from 9.5mm nozzle over more than 0.2s duration of vibration. The dosage conformity with less dispensing durations is worse.

Table 4- 5 Dispensing results of Hydroxyapatite granules from 9.5 mm nozzle with motor vibration

Vibration Duration per Dose/s	Mean Dosage/g	RSD%	Minimum Dosage/g	Maximum Dosage/g	Flow Rate/gs^{-1}
0.02	0.220	21.6	0.116	0.317	11.0
0.05	0.407	14.2	0.272	0.538	8.14
0.1	0.788	7.93	0.656	0.949	7.88
0.2	1.55	4.99	1.333	1.686	7.75
0.5	3.62	2.57	3.410	3.845	7.24
0.7	4.87	3.39	4.596	5.095	6.96
0.8	5.52	1.84	5.329	5.694	6.90
1.0	7.01	3.06	6.602	7.413	6.98

The discharge of HA granules was captured by high speed camera. The high speed images recorded the HA granules dispensing process over a period of 0.5s vibration duration (Figure 4-11). At beginning of the period, the starting signal was sent to the vibration motor. The mass of motor started to rotate at T_0 or the first frame of the high speed footage. It can be noticed that, although the mass was rotating there was no granules discharged so far. This delay lasts 24.95 milliseconds until the granules started to move at T_1. The granules start to flow out when the bridge is failed. With the flow processing, huge amount of granules had been discharged freely without any jamming observed. With higher magnification of camera, it observed that the flow of granules was whirling in the hopper and there was void between granules and the wall of glass hopper. The emergence of the void is caused by the dilation of granules under the influence of vibration. The friction is reduced and hence the unconfined yield stress. The mass of motor stopped rotating after 480.90 milliseconds which is not same as the setup 0.5s duration of vibration. It is because of the delay of motor responding to the stopping signal. When the motor stopped at T_3, there was still a few of granules dropping off because they were below the bottom layer of formed bridge. After the last frame, there was no granule discharged from the outlet.

The vibration motor has a few milliseconds delay when the starting and stopping signal is sent. Also, the delay may vary in each vibration cycle. As result, the dosage error is increased with the decreased dispensing durations as the effect of delay accounts for a

significant proportion in a short duration of vibration. Another possible reason for the poor dosage conformity over short vibration durations is that a shorter vibration does not provide sufficient energy to break the bridge. It can be seen in Table 4-5 that over a sufficient long duration of vibration, the flow rate tends to be stable at approximately 7 g/s.

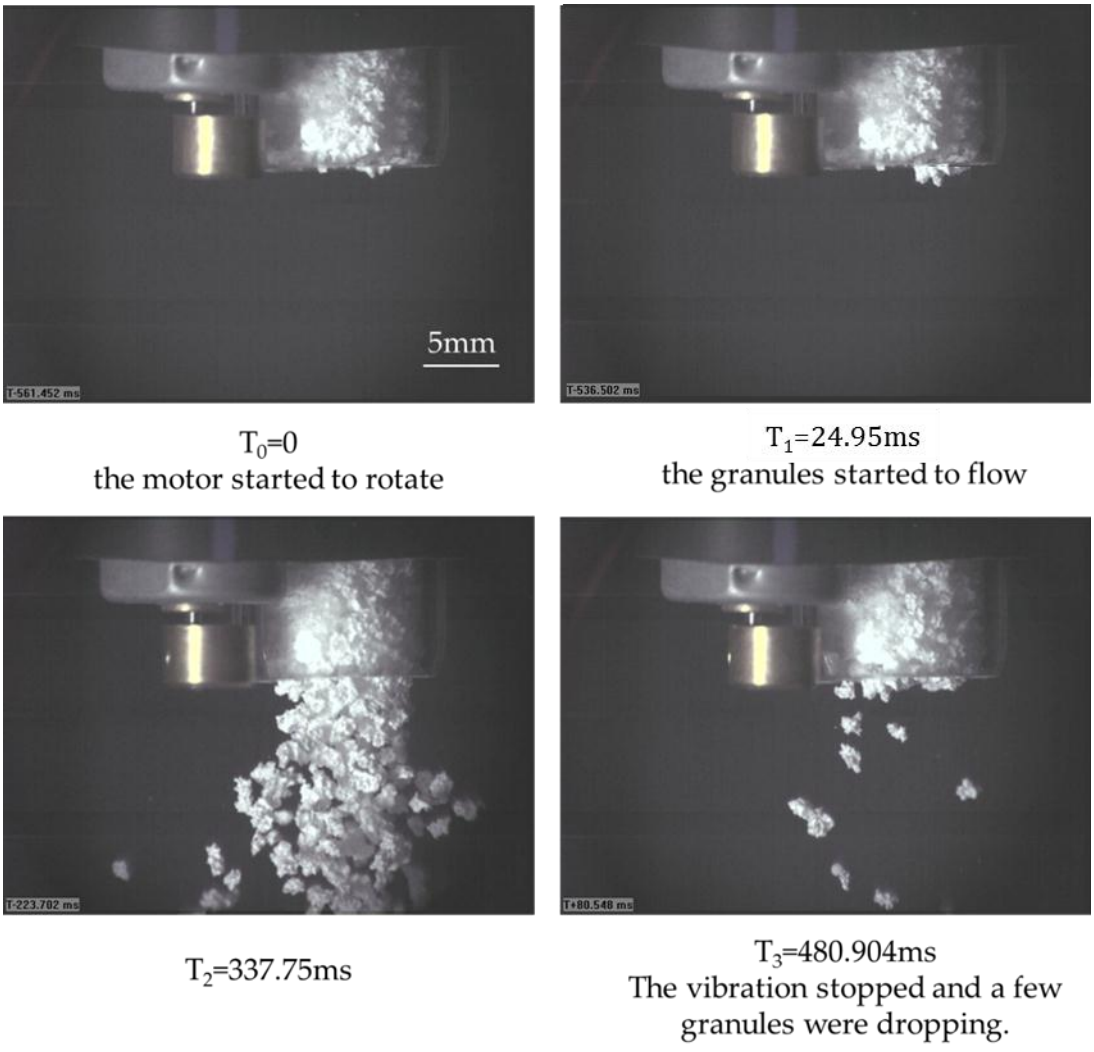

Figure 4- 11 High speed video frames of hydroxyapatite granules dispensing with motor driven vibration. T_0, T_1, T_2, and T_3 are different time points in one cycle of dispensing. For full explanation refer to the text

4.4. Summary

An electromagnetic hammering device providing a horizontal vibration to the dispensing hopper has been demonstrated to dispense an irregular shaped and porous hydroxyapatite granule. The eccentric rotating motor induced vibration has been also demonstrated as a feasible vibration mode to dispense hydroxyapatite granules. The effect of dispensing hopper size, vibration characteristics of device and device settings on flow rate and dosage conformity of HA granules dispensing was investigated.

The results suggest two vibratory dispensers follow a bridging controlled flow mechanism. The micro-dispensing of HA granule is controllable in the hopper with optimum orifice size, whereas smaller hopper size may cause jamming of granules and larger hopper size causes overflow. A critical orifice diameter, $D_{o,vibr}$, for a free flow under the vibration was defined. It is related to the vibration characteristics of vibratory dispenser. The influence of vibration source location in the device setting has been examined for the flow rate and dosage conformity. For electromagnetic hammering device, the flow rate of HA granule in dispensing increases with an increasing frequency of vibrations but no longer increases at higher frequencies. There is an upper limit of frequency at which the flow rate is highest and most consistent. For ERM, the flow rate increases with the increasing frequency and decreasing vibration displacement. A harmonically excited vibration source for promoting solid discharge in a hopper is preferred to have high frequency and low displacement.

Chapter 5

Ultrasonic Vibration Powder Micro-dispensing

This chapter presents experimental study on the ultrasonic vibration dispensing of pharmaceutical and biomaterial fine powders. The inhalation grade lactose powders exhibit a good flowability in the hopper with consistent flow rate, whereas the non-free flowing powders exhibit an “extrusion” mechanism. The experimental results show the dispensing with ultrasonic vibration device is subjected to a dome-controlled flow mechanism. The flow rate of free flowing powder is consistent so that the dosage is mainly determined by the duration of vibration. The flow rate of non-free flowing powder subjected to extrusion mechanism normally is low and less consistent under the influence of ultrasonic vibration. The dosage is found not proportional to the vibration duration due to the strong cohesions and poor flowability of non-free flowing powders. The effect of hopper geometries on the dispensing is assessed with different powder materials.

5.1. Introduction

An acoustic controlled dry powder printing technique developed by Yang et al. [24-28] has been demonstrated to accurately dispense small dosage of fine powders as low as 50 μg without weighing [28]. An ultrasonic vibration micro-feeding developed by the same group [29, 30] can precisely initiate and halt the flow of powder in a capillary. The signal amplitude voltage and oscillation period were reported as two important factors influencing dose mass of powders, such as tungsten carbide, steel tool and glass bead [30].

Inhalation grade Inhalac® α-lactose monohydrate is a series of micron-sized crystalline lactose obtained by milling with narrow particle size distribution. Products Inhalac®70, Inhalac®120 and Inhalac®230 are used as excipient in the formulation of dry powder inhalers. Micronized officinal starch is a versatile excipient used primarily in oral solid-dosage formulations where it is utilized as a binder, diluent, and disintegrant [153]. Hydroxyapatite and β-tricalcium phosphate as the biomaterials used in bone tissue regeneration are often nanosized for new bone formation and new bone attachment [118]. These powders exhibit diverse flowability when they are handled in the process (Table 3-1). Strong cohesion and poor flowability of fine powders may cause problems in the dispensing and therefore, the quality of final products [93]. Thus, accurate and effective dispensing of powders is of prime concern in the formation of pharmaceutical and biomaterial products.

In this chapter, an ultrasonic vibration dispensing device is tested with micro-dispensing pharmaceutical and biomaterials fine powders, including free flowing excipients, cohesive pharmaceutical and biomaterial powders. The dispensing results are discussed with different design parameters of dispensing hopper and vibration signal parameters.

5.2. Dispensing of Free Flowing Excipient Powders

5.2.1. Fluidization and Discharging of Free Flowing Lactose Powders

The measured angle of repose and Hausner ratio in Table 3-1 suggest that Inhalac® lactose have relatively good flowability. It can develop a free flow in a hopper with sufficient large orifice. In general, reducing the orifice size and decreasing the duration

of flow are two most direct ways to realise micro dosage dispensing. As the flow of powder is subjected to the doming mechanism in the hopper, dosage is determined by the dome failure and restore. As discussed in Chapter 2, powder can generate domes preventing particles from falling when the orifice size of hopper is smaller than the critical diameter D_c, and the flowability gets worse when the orifice size is decreased. As vibration has been proved effective in generating flows at much smaller outlet [98, 99, 101], an ultrasonic vibration is applied to initiate the flow of powder. The influence of ultrasonic vibration can be described as leading to a lower shear force between particles at the same normal stress level in the hopper and therefore, causing the dome failure. The particles in the region of the shear zone move against each other under the influence of vibration. When some of particles flow out, the distances between the particles increase. Thus, bulk density in the shear zone decreases, and the material in the shear zone dilates. When vibration was applied, a space was observed at the end of the hopper, and the position of the space was changed with the vibration. As particles flow out of the hopper, the average void fraction increases and the particles are loosely connected with each other, therefore, the particles can easily move in the horizontal and vertical directions. Consequently, particles can easily flow out. Therefore, both gravity and ultrasonic vibration can contribute to the driving force for powder flow through the orifice smaller than the critical diameter of outlet. When the vibration ceases, the shear force increases again and the dome is effectively formed, thereby particles flow stops.

The doming controlled flow mechanism of powder in the vibrating hopper has been previously introduced in Chapter 4. The dome of powder behaves like a “flow valve” so that the hopper has no need of a mechanical closure. This flow control mechanism has been reported in previous works on the acoustic vibration induced powder flow in capillaries [24-29]. Matsusaka and co-workers [114] have reported similar flow behaviour on micro-feeding of fly-ash spherical fine particles with particle size of 15 μm from a vibrating capillary tube. The adhesive fine particles adhering to the inner wall of the capillary tube act as a micro-vibrating layer of particles which avoid contact of the larger or small agglomerates with the wall of the capillary tube. This micro-vibration behaviour lowers the frictional stress between the inner powder and the wall, causing the agglomerates to fall under gravitational force and leading to an increase in flow rate.

The mean dose mass over 1s duration of vibration obtained using a pair of value (D_o, α) is presented by a 3D column chart in Figure 5-1, and the colour of column indicates the relative standard deviation (RSD) of dosages from the dispensing hopper.

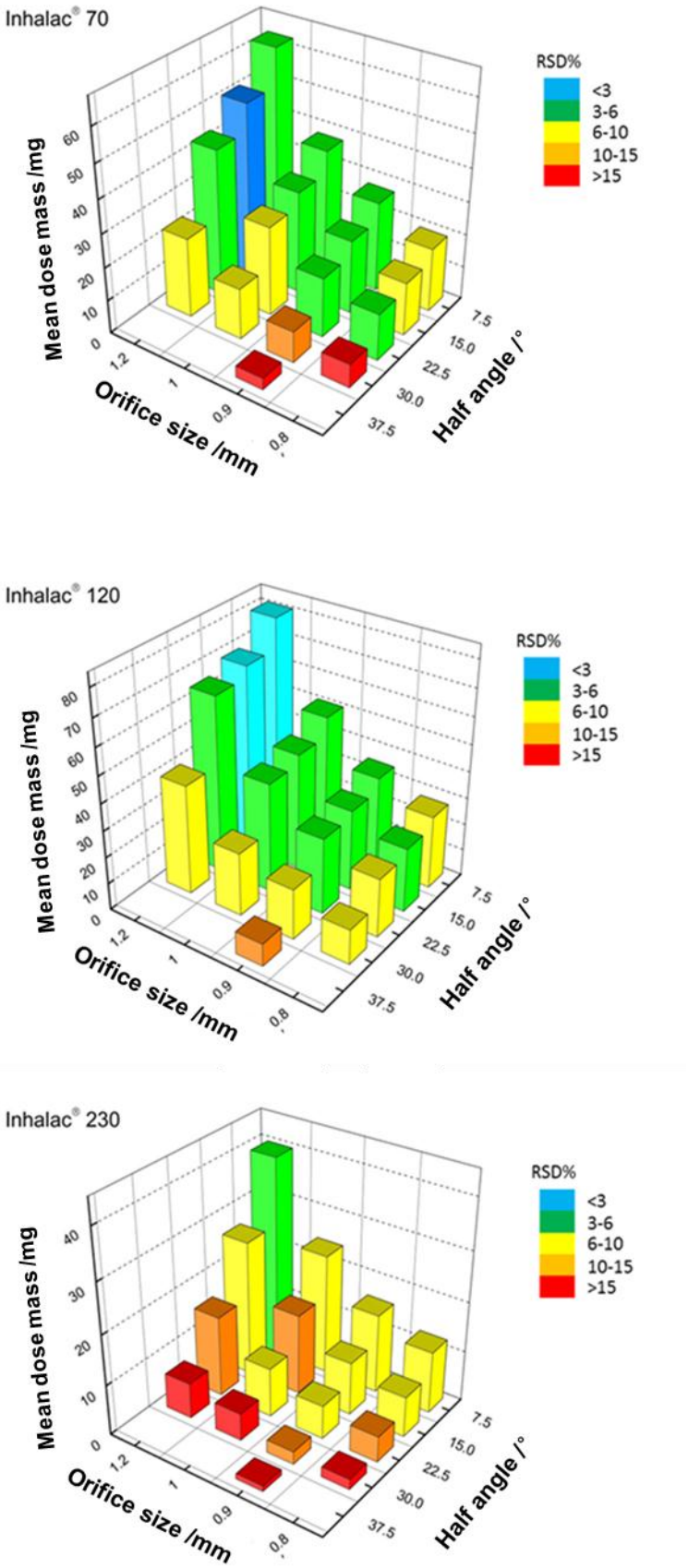

Figure 5- 1 Dispensing results of Inhalac® lactose from nozzles with different orifice size and half angle over 1s duration of vibration

5.2.2. Effect of Hopper Geometry on the Dispensing

5.2.2.1. *Orifice size*

As discussed in last section, the dosage control of micro-dispensing Inhalac® lactose is based on the powder doming mechanism. The orifice size is smaller than the critical diameter D_c as the introduction of external vibration force changed the flow criterion.

A 0.6 mm orifice was firstly used for Inhalac®70 dispensing. In the experiment, the blockage was observed during the dispensing with the function curve plotted by accumulated dose mass against dispensing time as shown in Figure 5-2. At the stage of T1, powder had been blocked for around 40 seconds as few powders were dispensed in this period shown by the hardly increased accumulated mass. As the standing time set up as 6 seconds in this test, there were at least 6 pulses of 1s vibration acted on the dispensing hopper until the blockage was fully collapsed. The orifice was estimated too small that the dilation of powder was limited and the strength of doming was increased. The continuous ultrasonic vibration may make the particles compacted densely in this circumstance.

As seen in Figure 5-2, after several vibration cycles, the blockage was broken but with several excessively large dosages dispensed at T2 due to the increased bulk density of powder at T1. The stage of T3 in Figure 5-2 represents non-uniform dispensed dosages in dome-controlled dispensing. The flow properties of powder determined by particle size (distribution), time-dependent bulk density and stress state in each dispensing of 1 second are all the possible reasons for the inconsistent dosages, which are common in a poorly designed dispensing hopper with, i.e. inappropriate orifice size and insufficiently narrow angle (see section 5.2.2.2).

The results show that 0.6 mm orifice size for Inhalac®70 is too small to maintain a steady flow under ultrasonic vibration. It can be expected that a ratio of orifice size to particle size should be larger than 3 to avoid blockage for Inhalac® lactose.

Figure 5-3 shows the staircase curve of accumulated dose mass against dispensing time for Inhalac®70 from 0.8mm, 0.9mm and 1.0 mm nozzle. The constant staircase and linear increase indicate the consistency of dosage from these orifices. The static powder is activated and starts to flow when a pulse of vibration is applied. In 0.8mm, 0.9mm and 1.0 mm nozzles, it can be observed the dose mass read by the balance is equal to the mass of powder ejected from the hopper within 1 second of vibration. In other words,

the discharge of powder has prompt response to the on/off signal and there was no obvious delay observed in 1s discharging. The rearrangement of particles with the dilation induced by the vibration caused the bulk density of powder in the shear zone less changed. As result, the dosage indicated by the height of platform on the curve in Figure 5-3 is consistent in the dispensing. When the vibration stopped, the discharge of powder ceased immediately by the formation of dome as the size of orifice is smaller than the critical diameter of orifice in the static condition. The balance was stable until next pulse come. The slope of staircase curves compares the dispensing rate of Inhalac®70 from different orifice size. The results show that with larger orifice size of hopper Inhalac®70 has higher flow rate in ultrasonic vibration dispensing. The relationship between flow rate and orifice size of hopper will be further discussed in section 7.2.2.

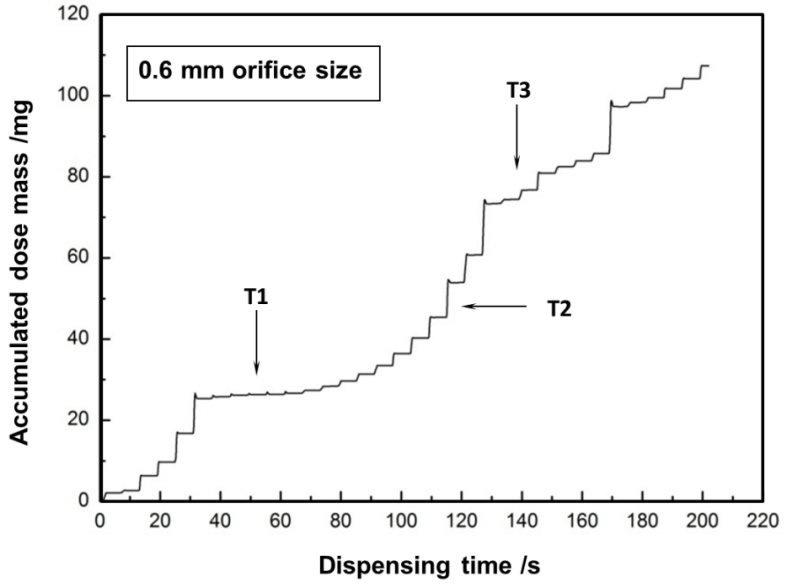

Figure 5- 2 Function plot of dose mass vs. dispensing time with 1s dispensing vibration per dose from 0.6 mm orifice size. Sample: Lactose Inhalac®70. Conical angle: 30°. Vibration mode: Ultrasonic. At the stage of T1, T2 and T3, three irregular flow patterns occurred. For full explanation refer to the text

Figure 5-4 shows the result of Inhalac®70 dispensed from 1.4 mm orifice. The powder was discharged consistently at the beginning of dispensing because of the pre-compaction of the powder at the outlet which contributes to the strength of dome to prevent failure. However, along with the descending level of powder bed and the dilation of powder during the dispensing, the consolidation stress was decreased and the dome of particles was failed to form at a high level of strength after the ultrasonic

vibration stopped. An irregularly large dosage was dispensed at T1. The orifice size was too large that the particles may take longer to form the dome after it failed and excessive powder was dispensed before the dome was formed. The unstoppable overflow occurred at T2 until the powder run out. When the orifice size is sufficiently large, the dome is hardly formed and the powder is subjected to the gravity flow.

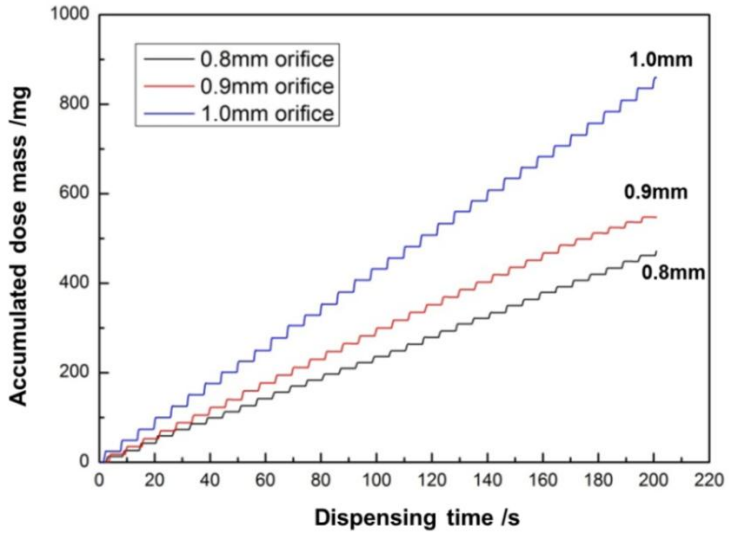

Figure 5- 3 Function plot of dose mass vs. dispensing time with 1s dispensing vibration per dose from 0.8 mm, 0.9 mm and 1.0mm orifice, respectively. Conical angle: 30°. Sample: Lactose Inhalac®70. Vibration mode: Ultrasonic

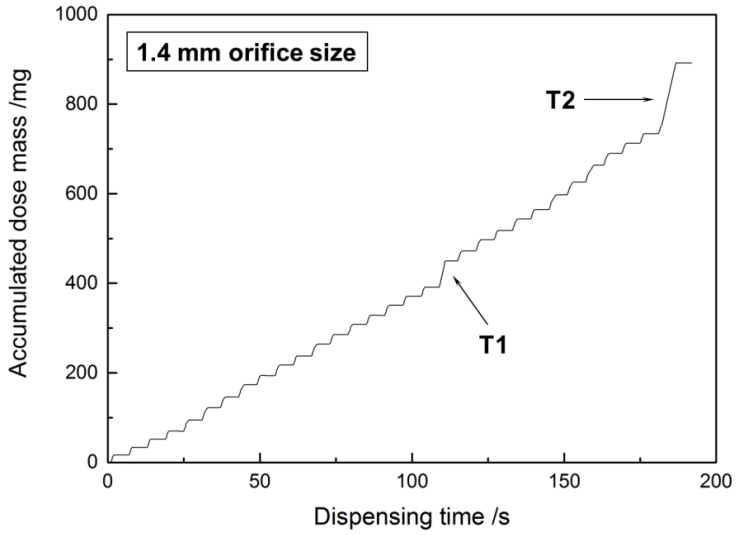

Figure 5- 4 Function plot of dose mass vs. dispensing time with 1s dispensing vibration per dose from 1.4 mm orifice size. Sample: Lactose Inhalac®70. Conical angle: 30°. Vibration mode: Ultrasonic. At the stage of T1 and T2, overflow occurred. For full explanation refer to the text

Thus, 1.4 mm orifice size for Inhalac®70 is too large to maintain a steady dosing under ultrasonic vibration. It can be speculated that the size of 1.4 mm is close to the critical value D_c and the ratio of orifice size to particle size should be smaller than 7 to avoid overflow for Inhalac® lactose.

In the tests with different orifice size of hopper, there are three main discharging situations, i.e. consistent discharge, blockage and overflow. Powder discharged in which situation is determined by the relationship of powder properties and orifice size of the dispensing hopper. Inhalac®70 is feasible to be handled with 0.8 mm to 1.2 mm orifices while 0.6 mm caused occasional blockage and 1.4 mm caused overflow. The appropriate orifice size which guaranteed a stable flow and uniform dosing is between 3 and 7 times of particle size for free-flowing Inhalac®70. The selection of orifice size for dispensing powder material is related to the properties of particles, such as particle size, shape and flowability. Yang et al. [26] have dispensed several fine metal powder and ceramic powder sized below 100 μm. They found for these free flowing powder, nozzle size, D_o, should be at least twofold but less than fivefold of the particle size, d, in order to achieve a good switching control of the flow ($2 < D_o/d < 5$). Lu and co-workers [29] in their studies with different powders have shown that ultrasonic vibration induced micro-feeding depended on the balance between compaction and dilation of the powder in the nozzle. Powders such as H13 tool steel powder (<22μm) and tungsten carbide (<12μm) showed stable micro-feeding in smaller nozzle sizes under ultrasonic controlled vibrations at a fixed voltage. The micro-feeding was more controllable and stable at 0.21 mm and 0.35 mm than at 1.35 mm. The authors speculated that arches of lower strength could form in larger nozzles leading to dispensing of excessively large dose masses.

5.2.2.2. *Hopper angle*

As described in section 2.2.2, the selection of nozzle angle is determined by the property of bulk solids (angle of internal friction, δ) and the wall of hopper (angel of wall friction, ϕ_w). To analysis the influence of hopper angle on the powder dispensing, two assumptions are proposed:

(1) The angle of repose of material can be used to represent the angle of internal friction in the experimental condition;

(2) The angle of wall friction is very small between lactose particles and glass wall when comparing with the angle of internal friction.

The angle of repose of Inhalac®70 is 33° as shown in Table 3-1. According to the critical half conical angle of hopper, α_{max}, recommended by Jenike [6] (p.220-228), the powder of Inhalac®70 can develop a steady-state flow in the hopper with angles between 0° and 38.5°. Figure 5-5 shows the dispensing results of Inhalac®70 from the hopper with half angle of 7.5° and 22.5°, respectively.

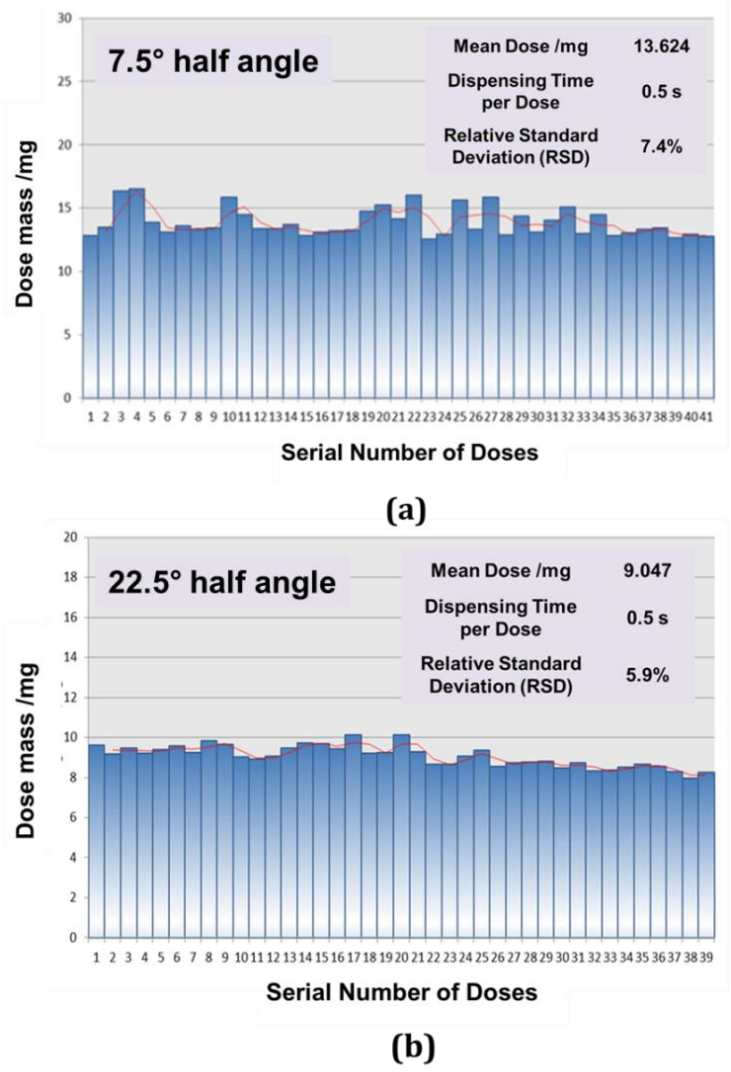

Figure 5- 5 Evaluation chart of ultrasonic dispensing of lactose Inhalac® 70 with half conical angle (a) 7.5° and (b) 22.5°. Orifice size is 0.8 mm and duration of vibration is 0.5s

As shown in Figure 5-5, the mean dose mass of Inhalac®70 dispensed from the nozzle with 7.5° half angle is larger than the mean dosage from 22.5° nozzle. The half conical angle, α, can indicate the angle between wall normal stress, σ_w, and major principal stress, σ_1 in the powder at the inclined wall. Figure 5-6 shows the analytical solution of stress level of powder at the wall of nozzle. A larger angle α causes higher wall shear stress τ_w when the powder sliding down on the wall of hopper in a mass flow. The

unconfined yield stress increases with the increasing angle of nozzle, which determines the strength of dome in the radial stress field. The vibration needs to overcome higher unconfined yield stress to break the dome in a shallower nozzle and thus in certain vibration duration the dosage is less. Therefore, a steeper nozzle is preferred to obtain a higher dosage in a mass flow. The correlation between the flow rate and half angle of nozzle will be further discussed in Chapter 7.

Figure 5-5 also shows the relative standard deviation (RSD) of dispensed dosages, which is 7.4% and 5.9% from the hopper with half angle of 7.5° and 22.5°, respectively. Figure 5-7 shows that the powder forms dome at different position in the nozzle with different angle. As discussed in section 2.2.1, if the orifice of nozzle D_o is confirmed, the position of dome is related to the angle of nozzle. When α = 7.5°, the dome formed with larger distance between the outlet and the dome position as shown by the distance h_1 between point A_1 and point B_1 in Figure 5-7(a). In the nozzle with 22.5° half angle, it was observed that the dome was formed closer to the outlet with distance of h_2 between point A_2 and point B_2 in Figure 5-7(b). As the unconfined yield stress is increased in the hopper with larger angle, the critical diameter D_c is larger. It can explain why the dome in the shallower hopper is more likely formed close to the outlet of nozzle.

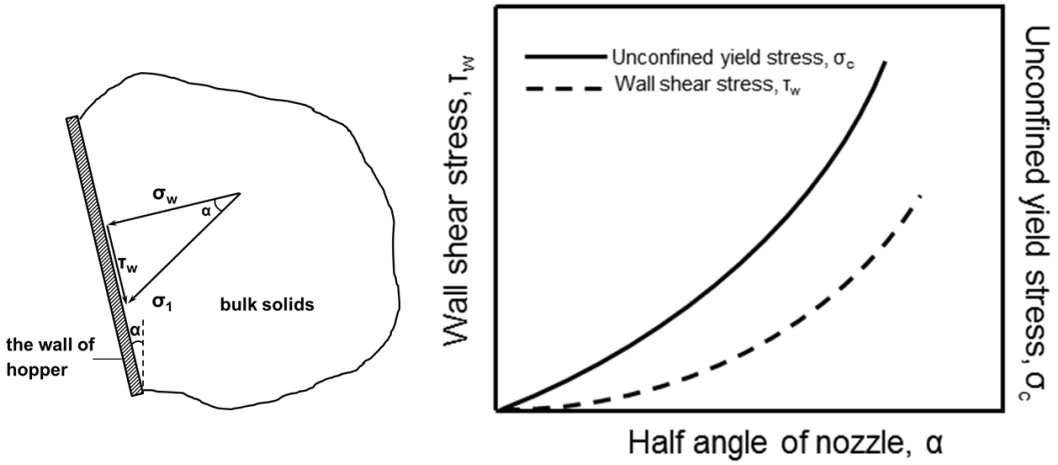

Figure 5- 6 Analytical solution of stress level of powder at the wall of nozzle inclined with angle α

The deviation of dispensing can be explained by the changing of dome position after vibration stops in each cycle of dispensing. When vibration stops, the dome may form at a random position (Figure 5-8(b)) between the actual outlet opening (Figure 5-8(c)) and the critical diameter, D_c (Figure 5-8(a)). Thus, flow promoting devices have to be installed between the actual outlet opening and the critical diameter. In a steep hopper,

the distance h is larger than a flat hopper if the actual outlet opening is same and thus, when the vibration stops, the variation of dome position in steep hopper is large which may cause bad dosage conformity. However, taking account of the friction between wall and powder, it generates larger shear stress on the wall of flat hopper and therefore, the unconfined yield stress is high. The flowability of powder is worse in the flat hopper than in steep hopper. In addition, when flow property of powder is changed as the result of time-dependent consolidation stress and bulk density, the dome position h will be changed. The changing of the void between the dome position and the nozzle outlet is assumed the main cause of the dose mass deviation and the deviation is larger in the steeper nozzle than the shallower one in case that both angle can assure a mass flow.

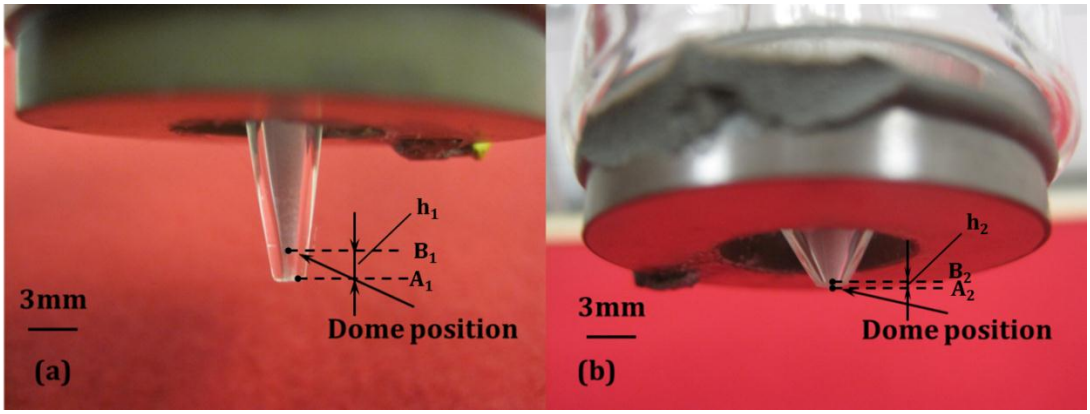

Figure 5- 7 Images of dispensing nozzle with 0.8 mm orifice and half conical angle (a) 7.5° and (b) 22.5°: The dome of lactose Inhalac® 70 is formed at different position in the nozzle, h is the distance between the possible dome position and the outlet

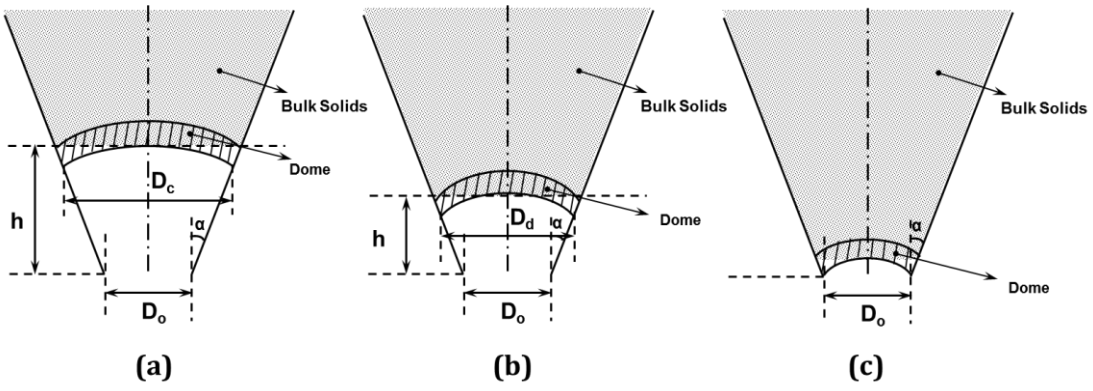

Figure 5- 8 Possible dome position in a vibrating hopper. For full explanation refer to the text

5.2.2.3. *Internal diameter of the vertical section* of hopper

Dispensing hoppers with different vertical section internal diameters have been tested with same orifice size 0.9 mm and conical angle of 30°. As shown by the results in Table 5-1, the mean dose mass shows a relatively stable amount. As in the vertical section, the diameter of vertical section is much larger than the critical diameter for powder free flowing. Powder exhibits a steady plane flow as the level of powder bed descents gradually in the dispensing. Also, there is no strong correlation between the RSD of dosages and the diameter of vertical section of hopper. However, it can be speculated that the RSD may increase with the increasing internal diameter shown in Table 5-1. When powder is dispensed in a certain flow rate, the descending level of powder bed is determined by the internal diameter D. The level change of powder bed, *dh,* in the hopper with a larger internal diameter (Figure 5-9(a)) is less with a discharged mass, M, than in a smaller internal diameter (Figure 5-9(b)). As result, the movement of particles in vertical direction is less so that it causes more compaction in the powder in the vertical section of hopper. The formed dome is getting stronger during the dispensing due to the pre-compaction in the upper section. The dose mass may decrease and thus the variation of doses increases. Therefore, the internal diameter has influence on the dispensing consistency despite it has no effect on the flow rate. In dispensing hopper design, the internal diameter also determines the capacity of dispensing hopper. As long as the flow rate and dispensing consistency are not harmed, the hopper can be given a bigger diameter to be applied in large amount sample dispensing and long hours dispensing task. Also, for some small scale application, the smaller diameter is preferred to reduce the overall dimension of dispensing device.

Table 5- 1 Dispensing results of Inhalac®70 from hoppers with different diameter of vertical section

Diameter /mm	Cone Angle /°	Orifice Size /mm	Initial Bed Level /mm	Duration of Vibration /s	Mean Dose Mass /mg	RSD%
8	30	0.9	70	0.5	11.1	2.85
11	30	0.9	70	0.5	10.4	3.37
16	30	0.9	70	0.5	11.3	3.06
23	30	0.9	70	0.5	10.6	3.88

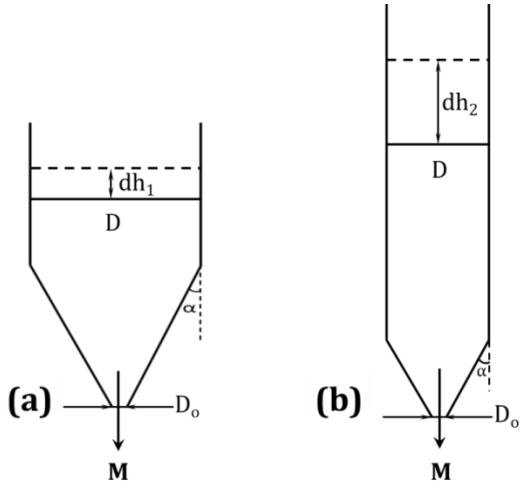

Figure 5- 9 Powder flow in dispensing hoppers with different internal diameter of vertical section; *dh* represents the descending level of powder bed

5.2.3. Effect of Vibration on the Dispensing

5.2.3.1. *Vibration duration*

The dispensing amount can be controlled by setting up the vibration duration for the single dose. With the assistant of high speed camera, it can be observed that the flow halted on stopping the vibrations as the powder formed a dome structure at the outlet of nozzle (Figure 5-10). The domes are constantly disturbed by vibrations enabling flow and recreated by jamming. In Figure 5-10, particles start to change their positions when vibration induced at T_0=0. It is hard to investigate what time it is exactly the point the first particle leaves bulks in the high speed camera, it is assured that first particle come out from nozzle at T_1 = 0.004 s. Particles maintains a steady flow after T_1 until the last particle comes out from nozzle at T_3 = 0.11s. The vibration has already stopped earlier before the point T_3. Suppose the delay between real time and observation point are exactly same at the start and the end of dispensing, the vibration time is the difference between T_3 and T_0, then the time of particles discharging T = 0.106 s which is very close to the setup duration of vibration, T_d = 0.1s. It is positively proved the dispensing is very sensitive to ultrasonic vibration signal to start and stop the powder flow.

Figure 5-11 shows the mean dose mass of InhaLac®70 dispensed from hoppers with different orifice size over the duration of vibration in the range of 0.1s to 1.0s. Compared with the results from different nozzles, the dosage is increased from 0.6 mm nozzle to 0.9 mm. The change of dosage dispensed over different duration of vibration is getting

larger with the increased orifice size. As shown in the high speed camera images, InhaLac®70 may be dispensed in form of discrete particles or large agglomerates from the nozzle. The large-size agglomerate formed in the hopper is supposed as an important cause of lower flow rate. In a larger orifice, the effect of particle agglomeration on the flow rate is less severe so that the increase of dosage with the increasing duration of vibration is more significant. Also, a longer vibration increases the dilation of powders in the nozzle and reduces the agglomerates. Therefore, longer vibration and larger orifice benefits a large flow rate with less chance of jamming and blockage.

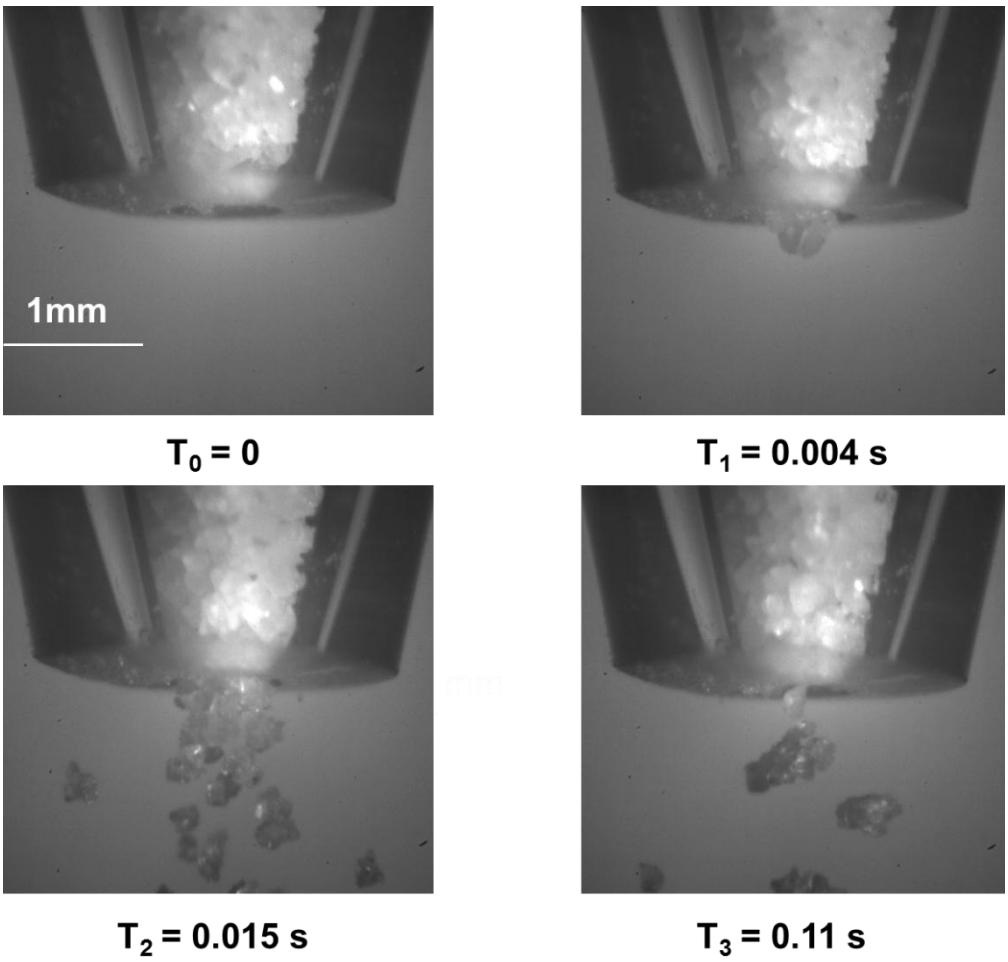

Figure 5- 10 High speed video frames of InhaLac®70 from dispensing with ultrasonic vibration. T_0, T_1, T_2, and T_3 are different time points in dispensing. They make a full cycle of dispensing starting at T_0 and ending at T_3

The linear relationship of mean dose mass and duration of vibration is presented with different orifice size in Figure 5-12. The results show that very linear function curve of

mean dose mass against duration of vibration was obtained. The flow rate of lactose powder dispensing is independent of the duration of vibration and dependent on the nozzle size. The slope of linear curve indicates the flow rate for Inhalac®70. The ultrasonic vibration causes the wall of the hopper to release stress over the powder in the nozzle so that the dome was unable to be formed during the vibration. If it is further sheared after failure, the powder in the shear zone will dilate increasingly until steady-state flow prevails, where shear stress and bulk density are constant. In steady-state flow, the excitation energy input during shear causes the plastic deformation of powder without changing particle properties. The shear stress during steady-state flow is reduced. The powder in a doming controlled hopper can develops a constant flow under ultrasonic vibration. The constant flow rate suggests the powder exhibits a steady switch from doming to free flow in the hopper which is similar to the flow of fluid with a closure valve. The longer the vibration lasts, the more powder is dispensed in one dose. The mean dose mass range from 0.15 to 21.8 mg of InhaLac®70 could be dispensed within 1 second using different nozzles.

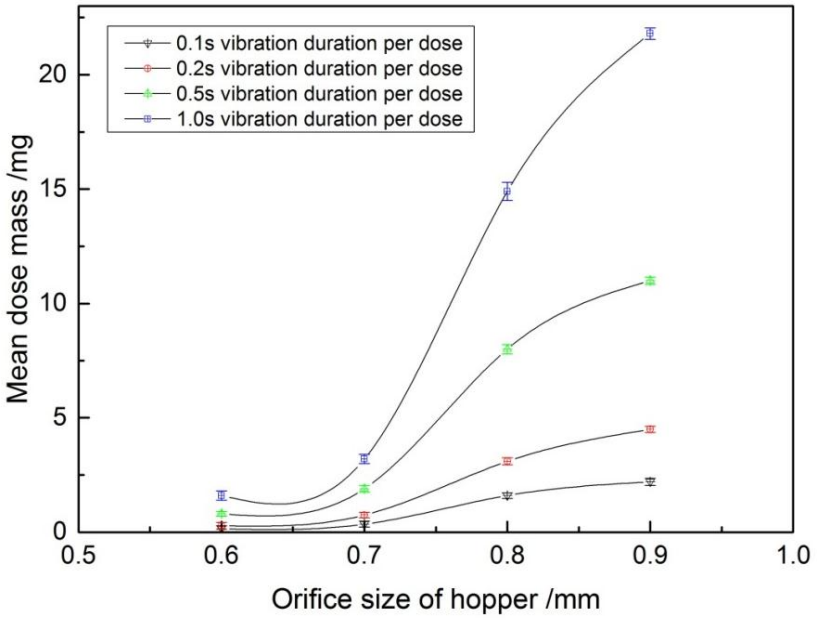

Figure 5- 11 Mean dose mass vs. orifice size of dispensing hopper over different duration of vibration. Sample: Inhalac®70 lactose. Conical angle of hopper: 30°

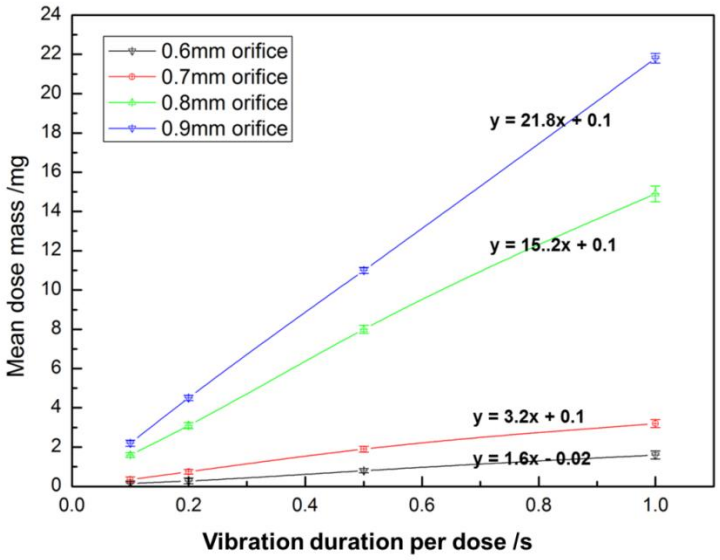

Figure 5- 12 Mean dose mass vs. duration of vibration with different orifice size. Sample: Inhalac®70 lactose. Conical angle of hopper: 30°

5.2.3.2. *Amplitude of vibration signal*

Figure 5-13 shows the effect of increases in signal amplitude on the dispensed mean dose mass of InhaLac®70. At a pulse vibration of 0.1s and signal amplitude of 2V, an initial mean dose mass of 0.96mg was dispensed. No change in dispensed mean dose mass was evident by increasing the signal amplitude to 4V. However, a significant increase in mean dose mass takes place at signal amplitude of 5V. The stability of the dome in vibrated conical hopper has been explained using a model derived by Matchett [103, 154]. Under the influence of vibrations, two limiting conditions i.e. push mode and pull mode has been considered which governs the flow behaviour of contained materials through small outlet diameters. The push mode leads to compression of the material by vibrated wall section, while pull mode releases the stress upon the contained material and causes a switch in stress orientation from passive to active stress state. The active stress state causes the dome to collapse and material to flow. The switch to active stress should be quick and the flow should be established before it reverts back to the push mode. The achievement of active stress state also requires the vibrations to cover large portion of the hopper and should last for larger part of the vibration cycle for the flow to be reliable. In order to achieve this, larger amplitude or longer duration is preferred. The significant increase in flow rate and mean dose mass at 5V is supposed due to the switch to an active stress state. However, the switch could not be correlated to changes

in amplitude as the real amplitude remained constant above 2V (Figure 5-13) suggesting the saturation of the output from the ultrasonic power amplifier.

The maximum force produced by a piezoelectric block in a vibrated system is influenced by the signal amplitude as explained by Loverich [155]. This was exemplified by Lu and co-workers while studying the effect of different parameters on the ultrasonic micro-dispensing behaviour of fine powders [29]. The authors found that H13 tool steel fine powder showed linear increases in mean dose mass dispensed, while titanium dioxide showed a similar change in mean dose mass as InhaLac®70 on increasing the signal amplitude from 3-6 V under square wave form actuation. In addition, an upper limit of voltage amplitude was defined beyond which an irregular dose mass was dispensed indicated from the width of the error bars. The inconsistent dispensing is also observed in dispensing of InhaLac®70 with unstable amplified signal from current equipment shown in Figure 5-13. The big error are found when the amplitude is lower (≤ 3V), while a more consistent dispensing with less deviation is noted beyond 4V. One explanation may be that irregular low vibration amplitudes are less effective to force the flow which bring the system into blockage as explained by Janda et al. [105].

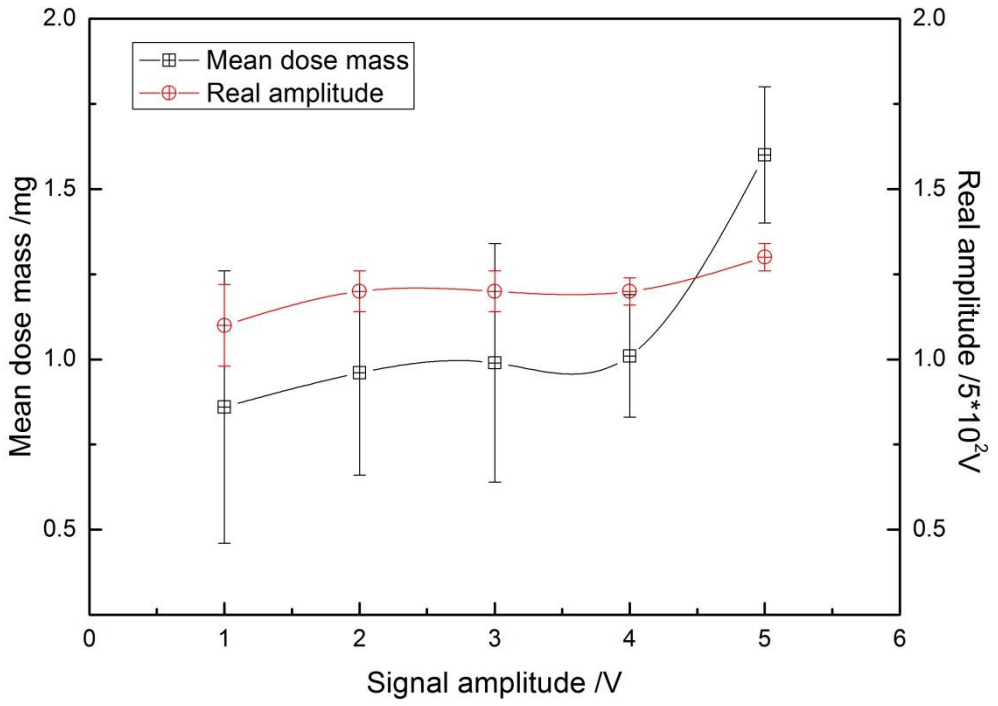

Figure 5- 13 Mean dose mass vs. signal amplitudes and real amplitude after amplification vs. original signal amplitude. Sample: Inhalac®70; duration of vibration: 0.1s; orifice size: 8mm; conical angle: 30°.

5.3. Dispensing of Non-Free Flowing Powders

5.3.1. Fluidization of Non-Free Flowing Powders

The very fine particles tend to stick to the wall of hoppers and form agglomerates due to the strong adhesive and cohesive forces. They exhibit very limited flowability in the hopper. Under the influence of ultrasonic vibration, the plastic deformation of fine powder is induced when the vibration acts on the dispensing hopper. The kinematic friction between a powder and the wall of hopper can be reduced by applying ultrasonic vibration equivalent to the reduction of the internal friction [100]. It was reported by Kollmann et al. [109] that while the angle of internal friction δ is nearly independent of the vibration application, the unconfined yield strength σ_c decreases with increasing vibration velocity. The wall shear stress τ_w decreases with increasing vibration velocity to approach a minimum value.

The vibration also leads to a compression of the material by vibrated wall section and powder is "extruded out" of nozzle following Jenike's flow criteria (Figure 5-14). The powder is extruded in a rod shape and each dose is dispensed as a fracture of the stretched out powder rod. In the extrusion, the powder agglomerates may not be broken by the vibration force, but it does not affect the deformation of bulks. In High-speed camera images (Figure 5-15), the nanosized biomaterials were extruded in the rod shape. The doses were obtained by the fracture of stretched rod in each vibration cycle.

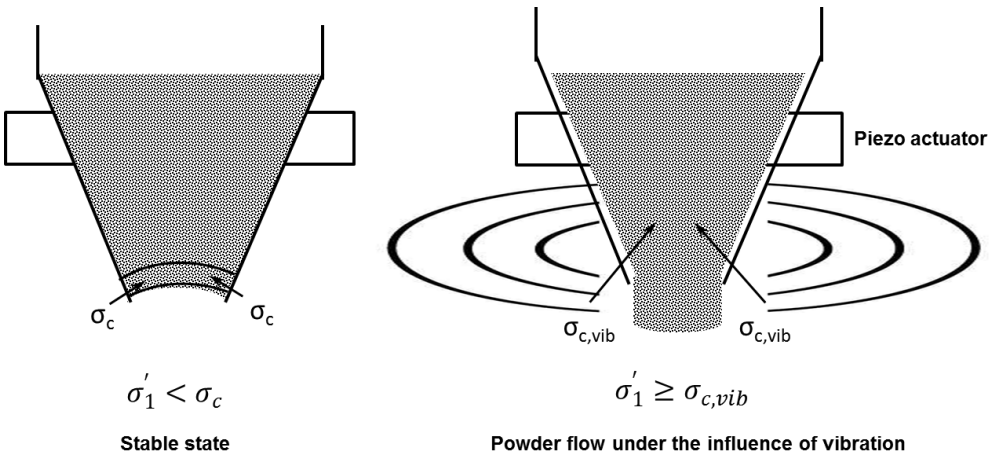

Figure 5- 14 Extrusion mechanism for cohesive powder fluidizing under ultrasonic vibration

In the high speed camera images (Figure 5-15), some cracks or bubbles in the powder was observed. It was estimated the cracks or bubbles were caused by the uneven density from particles rearrangement due to the poor flowability of fine powders.

Matsusaka et al. [156] reported the vigorous bubbling in a bed of fine particles is caused by the vibration-induced air inflow. When convective flow occurs in a powder bed as a result of vibrations, the upper powder layer with a high void ratio moves downward and is compressed. This process forces the air in the powder layer out, which leads to the formation of bubbles that rise and eventually burst at the top surface of the powder bed. A negative pressure is created below the rising bubbles. A narrow opening at the bottom allows the outside air to flow into the powder bed, which produces a vigorously bubbling fluidized bed. However, the unpredictable bubbles in the powder bed would distinctly bring deviations to the amount of dispensed powders for each dose.

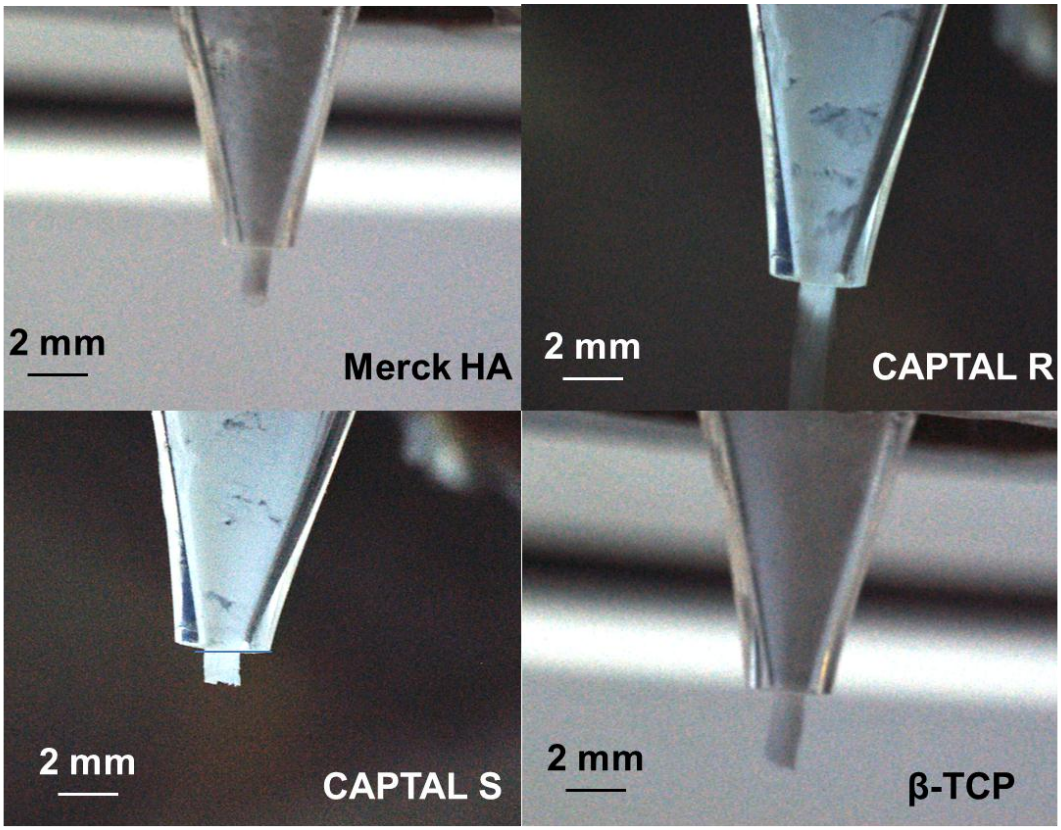

Figure 5- 15 High-speed camera images of powder flow during the dispensing. All nanosized cohesive biomaterials are "extruded" out as agglomerate rods. The rod diameter closely equal to the orifice size of hopper

5.3.2. Effect of Orifice Size on the Dispensing

The particle size of cohesive powders is small but they always form larger agglomerates in handling. Because of strong cohesive and adhesive forces, the unconfined yield stress is large in the dome formed by cohesive fine powder. Thus, cohesive powders have large

critical diameter D_c. Subjected to the extrusion mechanism, cohesive powders can be dispensed in hoppers with a wide range of orifice size. Xie [157] and Feng [158] also reported for non-free flowing powder, the range of nozzle size can be much wider because the fine particles tend to form agglomerates caused by strong interparticle forces and poor flowability.

A set of parallel dispensing tests for officinal starch were performed in hoppers with orifice size from 0.6 mm to 1.5 mm. The ratio of orifice size to particle size is in the range of 30 to 70. In Figure 5-16, the dispensed dosage increases with enlarged orifice size. For the smaller orifice, the dose mass has relatively large deviation which is caused by the presence of strong dome structures.

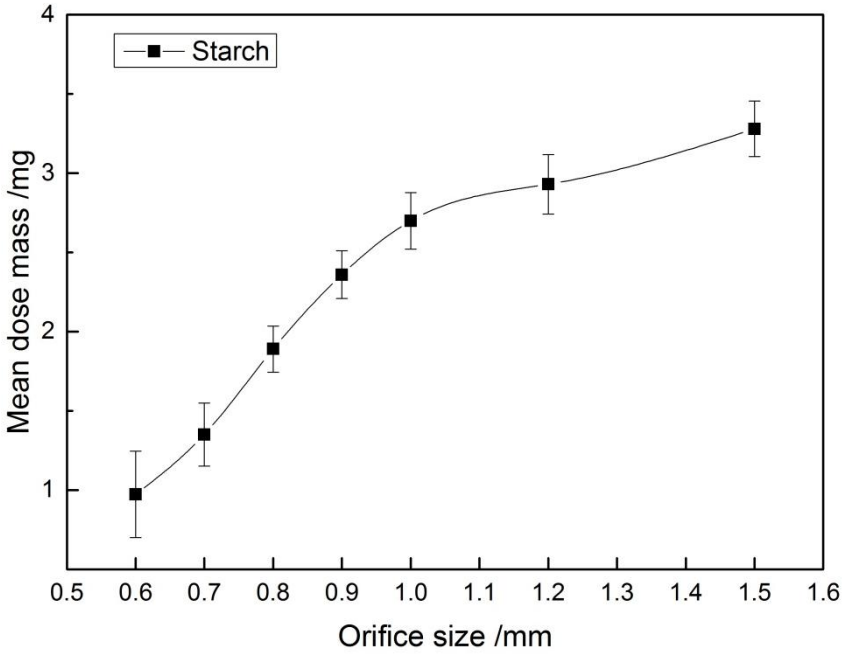

Figure 5- 16 Mean dose mass vs. orifice size of dispensing hopper, half angle: 15°; duration of vibration: 0.5s; sample: starch

5.3.3. Effect of Hopper Angle

The cohesive and adhesive force in non-free flowing powder is large. To initiate the flow of non-free flowing powder in the hopper, the deduction of friction is prior to force a flow. The friction between particles and the wall of hopper can be reduced by applying vibration. The wall friction is influenced by the hopper angle. Figure 5-17 compares the mean dosage and consistency of starch dispensed in the hopper with 7.5° (Figure 5-17(a)) and 15° (Figure 5-17(b)) half conical angle. The steeper angle has much better

consistency and larger dosage. A 22.5° was tested as well but the starch powder was even unable to be dispensed. In a hopper with larger angle, the wall friction is larger so that the unconfined yield stress is increased. With increased dome strength, the powder flowability gets poorer and thus, the flow rate decreases and the deviation between dosages is increased. Moreover, when the hopper angle exceeds a critical value, the angle of wall friction, ϕ_w is large so that the powder flow occurs when the Mohr's circle reaches to the internal yield limit. As result, a core flow of powder may develop in the hopper. Due to the uncertainty of the stagnant zone in the core flow pattern, the flow rate of powders may be inconsistent.

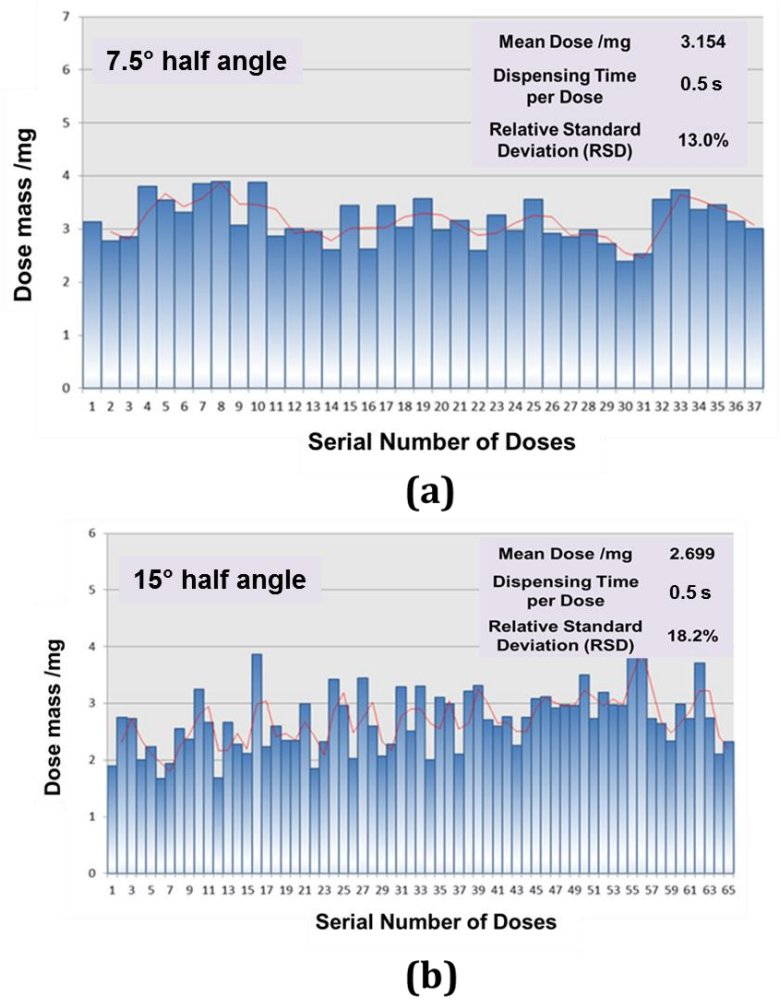

Figure 5- 17 Evaluation chart of ultrasonic dispensing of starch with conical angle (a) 7.5° and (b) 15°. Orifice size: 1.0 mm; duration of vibration: 0.5s

Therefore, for dispensing non-free flowing powder, the dispensing hopper needs to be sufficiently steep and smooth surface in order to minimise the friction between particles and wall.

5.3.4. Effect of Vibration Duration on Dispensing

Table 5-2 shows the dispensing results of starch from the hopper with 0.6 mm orifice size over different duration of vibration. The dose mass from 0.05 mg to 1 mg can be obtained from different duration. Larger dosage is also available by increasing the vibration time and it can be noticed that the dosage conformity represented by relative standard deviation (RSD) gets better when the duration of vibration increases. It is because the powder compressed by the vibration for a longer time will attain a constant flowing bulk density. Consequently, the extruded rod fracture will be uniform. Also, the longer vibration provides more energy to overcome the friction and break the dome. However, with increasing the duration of vibration, the void between particles and glass wall will not expand further. The separation of boundary only occurs at the beginning of vibration acting. Therefore, with the increasing of vibration duration, the dosage is increased but not in a linear trend shown in Figure 5-18. The flow rate of non-free flowing starch is dependent on the duration of vibration, T_d, which is a dominant factor in the mass control of dispensing non-free flowing powder.

Table 5- 2 Dosing results of Starch dispensed with a 0.6 mm nozzle at different time of vibration, 5V signal amplitude

Duration of Vibration /s	Mean Dose Mass /mg	Relative Standard Deviation /100	Total Dispensing Time /min
0.01	0.054	19.4	5
0.02	0.127	9.2	5
0.05	0.685	9.2	5
0.5	0.973	6.1	5

5.3.5. Dispensing of Nanosized Biomaterials

The nanosized calcium phosphate biomateral powders show a very poor flowability with angle of repose larger than 50°. The needle shape of particles makes CAPTAL® R powder even more difficult to flow. The particles of these biomaterial powders are often found sticking on the surface of glass capillary or to each other due to interactions between a particle and surface of another material or between particles of the same material which act as strong adhesive and cohesive forces. Because the fundamental mechanisms for the occurrence of van der Waals forces are of electrostatic nature, the

primary source of particle adhesion and cohesion is electrostatic forces [158]. Powder particles can acquire charge in many different ways such as by triboelectric charging with other contacting materials, corona ions, or by induction in an externally applied electric field, etc.[159] In the dry powder dispensing system, the electrostatic force has negative effect on the uniformity of the dispensing by immobilizing particles to the wall of glass capillary.

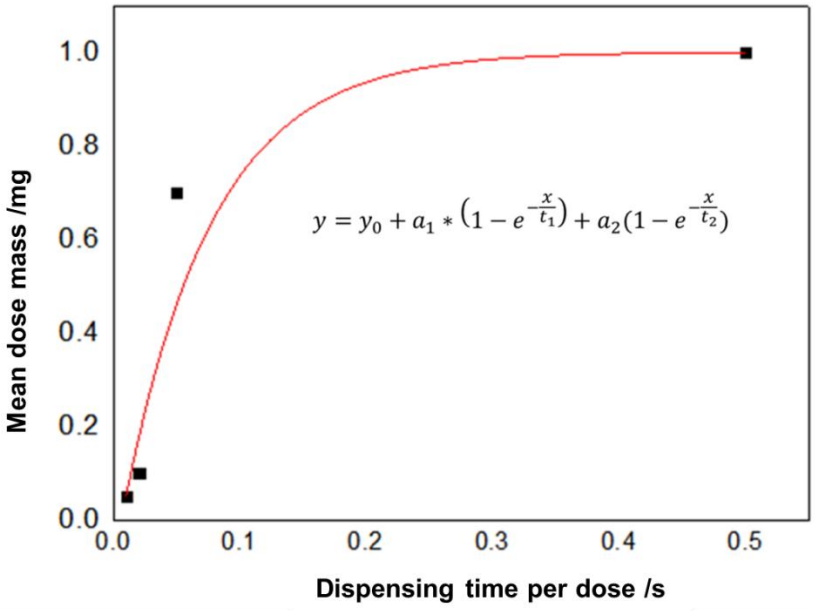

Figure 5- 18 Mean dose mass vs. duration of vibration. Sample: Starch. Orifice size: 0.6mm. Conical angle of hopper: 30°

For nanosized biomaterial powders, the nozzle size can be selected from about 0.2mm to about 6.5mm, which gave great flexibility on the nozzle selection and dosage control. Figure 5-19 shows the dosing results of dispensing of those four nano biomaterials from 1.0 mm nozzle at different time of vibration. The peaks in the curves are assumed due to the impact of trapped air in the powder bed on the balance when powder being extruded under the ultrasonic vibration. Also, this phenomenon is often observed in dispensing very cohesive powders as they are easy to trap air and the dispensed weight read by the balance for each dose is small.

As dicussed in last section, for non-free flowing powder the most convenient way to control the dosage is by adjusting the duration of vibration, T_d. T_d normally varied from 0.1s to a few seconds, which is the most significant approach to change the dose mass, from a few micrograms to several grams. In other word, by adjusting T_d, arbitrary mass of dispensing is available once the dispensing device is calibrated.

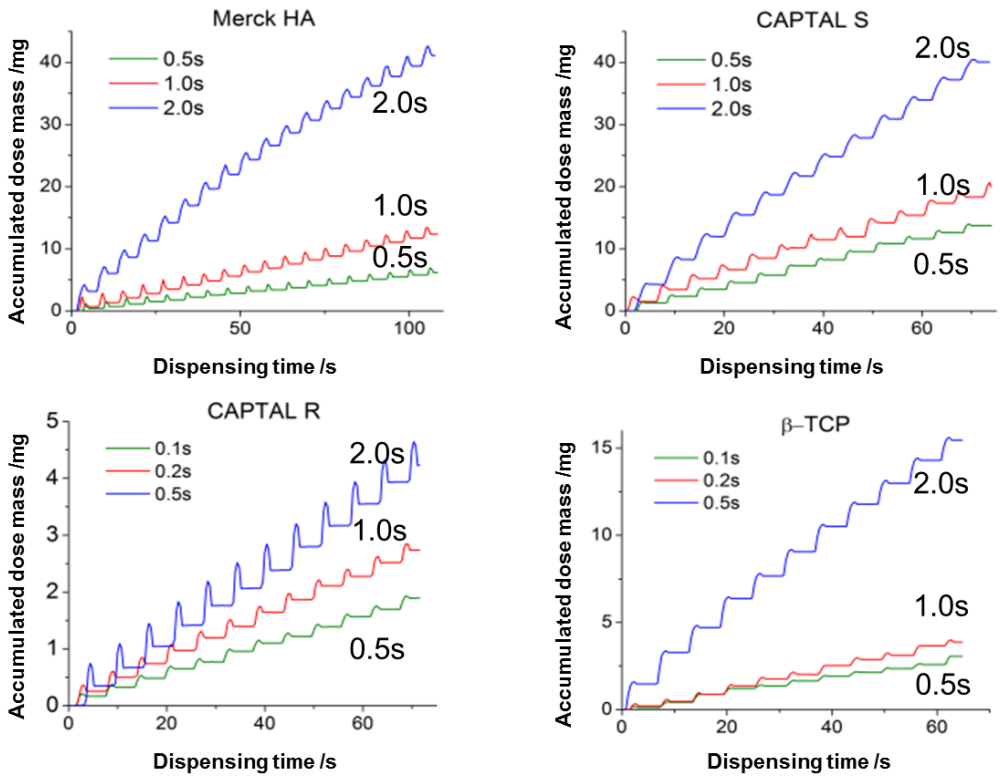

Figure 5- 19 Dispensed mass vs. dispensing time for biomaterials dispensed over 0.5s, 1.0s and 2.0s duration of vibration. Orifice size: 1.0mm. conical angle: 15°. The uniformity of "staircase" curve represents the consistency of dipensed dosage.

Table 5- 3 Dosing results of different samples with a 1.0 mm nozzle at different time of vibration, 5V signal amplitude

Sample	T /s	Mean dose mass /mg
Merck HA	0.5	0.1602
	1.0	0.6313
	2.0	2.3175
CAPTAL S	0.5	1.0318
	1.0	1.349
	2.0	3.3762
CAPTAL R	0.1	0.1594
	0.2	0.2509
	0.5	0.374
β-TCP	0.1	0.3096
	0.2	0.3842
	0.5	1.4533

The dispensing results of nanosized biomaterial powders show a non-linear correlation between dosage and vibration duration of dispensing similar as the starch (Table 5-3

and Figure 5-20). CAPTAL®S exhibits a better consistency in flow rate under different signal of vibration. This can be explained by the different leve of cohesion between particles with different particle size and shape shown in the SEM picture (Appendix III), and the manufacturing process of the materials [60]. CAPTAL® S was sintered and re-ground which has bigger particle size, rounded particle shape and it's assuemed with a smaller internal friction and less agglomeration comparing with others, which gave better flowablity. The Merck® HA has very fine particles which formed very strong agglomeration and lowest flowability.

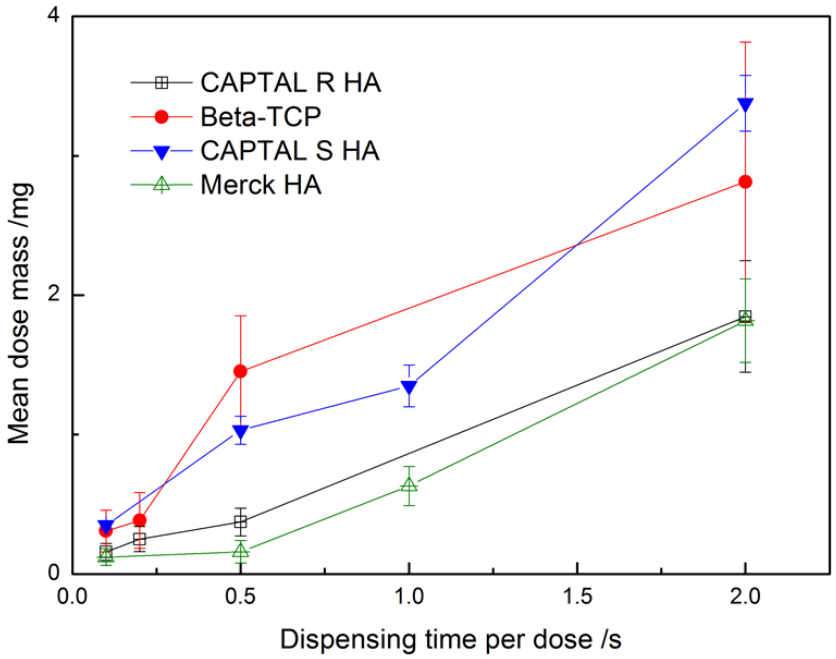

Figure 5- 20 Mean dose mass of Merck® Hydroxyapatite, CAPTAL® S Hydroxyapatite, CAPTAL® R Hydroxyapatite and β-TCP vs. duration of vibration at 5V amplitude in 1.0 mm nozzle. CAPTAL R with the best flowability has a linear fuction of dose mass against duration of vibration

5.4. Summary

The study of dispensing free flowing powder shows that use of different dispensing hoppers of an ultrasonic vibration micro-dispensing system with from 0.1 s to 1s pulse of vibration at 5V could aid in obtaining a mean dose mass range of 0.15 – 21.8 mg in InhaLac®70 micro-dispensing. The consistency of InhaLac®70 particles flow suggested

the dome structures formed easier at smaller nozzle sizes which the flow rate is dependent on the orifice size. The dose mass has a linear correlation to time of vibration per dose suggesting that an accurate amount of dosage of InhaLac®70 could be modulated depending on different time of vibration. The present work further shows that modulating the signal voltage of an ultrasonic vibration could also be used to control the flow rate and dosing of InhaLac®70. These results provide a strong basis for exploring the application of an ultrasonic controlled micro-dispensing system as a feasible method in dispensing of inhalation grade micron-sized pharmaceutical materials.

The micro-dispensing system was also used to dispense non-free flowing pharmaceutical powders. The powders with fine particle size are “extruded” from the hopper. The system was proved suitable for low doses (as low as a few milligrams) dispensing and accurate and fast in dispensing of powders with wide particle size distribution and cohesiveness. The hopper design parameters such as orifice size and hopper angle, and the duration of vibration have influence on the mean dose mass. The dosage exhibits a nonlinear trend regarding to the duration of vibration. It is assumed to be due to the strong interparticle force and poor flowability of powders.

Chapter 6

Triboelectric Charging in Ultrasonic Vibration Dispenser

This chapter describes a triboelectric charging phenomenon investigated in ultrasonic vibration dispensing of pharmaceutical powders. The charge of powder influences the accuracy and consistency of powder dispensing. A solution to the charging issue is proposed by modifying the contact surfaces in the hopper with platinum coating. Glass dispensing hopper and platinum coated hopper was tested respectively to investigate the flow and discharge behaviour of pharmaceutical excipient powders. With comparing the dispensing results from both hoppers, the Pt-coated surface favourably changed the powder charging and flow in the dispensing hopper. The hopper surface modification provides a possible solution to the charging issue in ultrasonic vibration powder dispensing in order to improve dispensing results of pharmaceutical powders.

6.1. Introduction

In powder processing and handling, operations such as milling, sieving, mixing and conveying cause particles to make frequent contact amongst each other and with the walls of the vessel. During these operations, the electrification of particles takes place. This refers to a process where two dissimilar materials contact each other through impact, friction or sliding and are then separated [160]. When fine powders get charged, the resulting electric forces can change their flow behaviour, and as a result, they may adhere to contact surfaces and attract/repel each other. This can lead to a loss of powder in process.

Most pharmaceutical powders are dielectric materials. They are very prone to electrostatic charging by colliding and sliding contacts with walls and other particles because they normally have a high resistivity, which prevents the transferred charge from leaking back [161]. As a result, electrostatic charging may cause the agglomeration or segregation of particles during powder transportation. The electrostatic forces acting on charged pharmaceutical particles may dominate in adhesion and deposition of the particles to walls, especially in the case of fine particle systems, such as dry powder inhalers (DPI) [162, 163]. In the pharmaceutical industry, particle charging is often a nuisance and can cause problems in manufacturing, such as affecting powder flow, and reducing fill and dose uniformity. However, there are also cases where the electrostatic forces are used advantageously for control of drug particles such as for a DPI [164, 165] or mixing of ordered powders [166, 167].

The charge was found to depend on both the nature of the powders and the vessel surface [134]. Although the factors affecting the tribo-electric charging is not fully understood, it is necessary to control the charging propensity of pharmaceutical powders in process. Bennett et al. [168] studied to reduce static charge on the mixes of inhaled carrier lactose particles with adding fine particles. Coating the vessels with drug or excipient can reduce the influence of the vessel material on charge generation [134]. Previous study by Eilbeck et al. [169] reports that static charge of lactose powder in contact with stainless steel reduces with increasing surface contamination. Cassidy et al. [170] studied the surface contamination and in their work the charge was found to increase with increasing adhesion.

As the static charging of pharmaceutical powders has been observed in the ultrasonic vibration dispensing, the influence of charged powders on the dispensing result will be

primarily investigated in this chapter. One traditional method to measure the electrostatic charge is using Faraday cage [171-173]. The charged powders can be dispensed into Faraday cage and the mass and the charge is measured with balance and electrometer, respectively. Alternatively, an approach of measuring static charge with a non-contact vibrating capacitive probe has been developed by Kwek et al. [174].

The work presented in this chapter also aims to find a solution to the charging problem for ultrasonic vibration micro-dispensing technique to improve the dispensing accuracy with pharmaceutical powders.

6.2. Experimental

6.2.1. Static Charge Measurement in Faraday's Cup

The static charge of intermittently dispensed doses from ultrasonic vibration dispenser was measured in a shielded Faraday's cup (Figure 6-1). Faraday's cup consists of two stainless steel cups which are electrically insulated from each other. The charge inserted inside the inner cup generates a potential difference V between the cups. An electrometer (Keithley 6514, Keithley Instruments Inc. USA) was used to measure the charge of dispensed doses in the Faraday cup. The specific charge, Q, of powder dose was calculated by dividing the charge, q, by the mass of dose, m, $Q = \frac{q}{m}$. The powder sample was dispensed with one dose at a time into the inner cup through a small hole on the top of the Faraday's cup. The dose was dispensed in every 6s and every one of the five doses was collected and the charge of dose was measured in the Faraday's cup. The interval between every charge measurement is therefore 30s. During this interval, the Faraday's cup was cleaned and grounded and the reading of electrometer was reset with auto discharge function of the electrometer. Measurements were repeated at least five times for each sample. The dispensing hopper was carefully cleaned after the measurement of each sample.

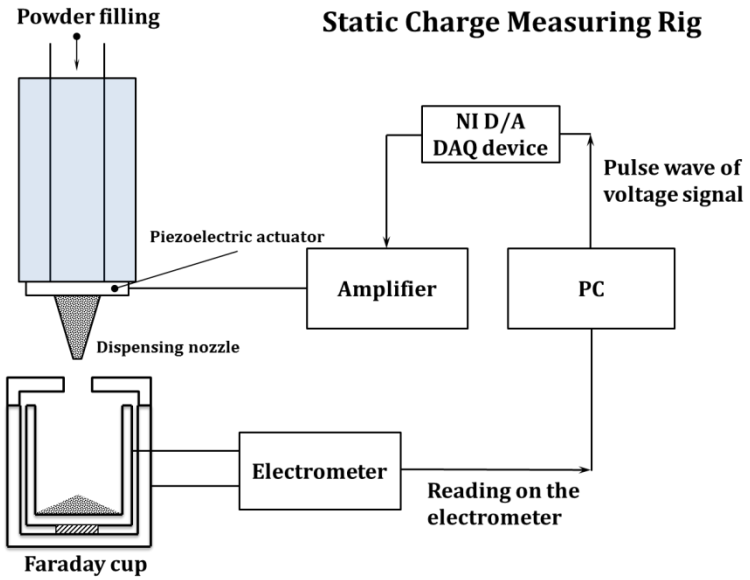

Figure 6- 1 Schematic diagram of static charge measurement for dispensed doses

6.2.2. Electroless Plating of Platinum on Borosilicate Glass Hopper

The borosilicate glass dispensing hopper was coated with platinum by using electroless plating method to modify the contact surface of excipient powders against the wall. The aim of modifying the contact surface was to reduce the tribo-electric charging of powders in the process of dispensing. The borosilicate glass hopper was firstly heated to 600°C and cooled down in air, then immersed in 5% (w/w%) hydrofluoric acid for 10 minutes to clean the contamination on the surface. After rinsing with deionised water, the hopper was immersed in 20g/L $SnCl_2$ acidic solution for 30 minutes and then moved into 0.5g/L $PdCl_2$ acidic solution for 1 minute. After dried in an oven, it was rinsed with $NaBH_4$ solution. Dinitrodiammine platinum was dissolved in ammonia solution (pH ≈ 10.6.) to form an alkaline bath. Pre-treated glass hopper with palladium catalyst active sites on the surface was placed in the solution. 3g/L hydrazine was added gradually in 50µl per drop. The equations of proceeded reaction can be illustrated by:

(a). $2(NH_3)_2Pt(NO_2)_2 + N_2H_4 \cdot H_2O \xrightarrow{Pd} 2Pt + 5N_2 + 9H_2O$

(b). $N_2H_4 + 4OH^- \rightarrow N_2 + 4H_2O + 4e^-$

The electroless plating was proceeding at 58°C in a water bath. After being evenly coated, the glass hopper was taken out, air-dried and annealed at 600°C for 10 minutes. The process flow diagram was shown in Figure 6-2. The Pt-coated dispensing hopper was grounded when being applied in the dispensing device.

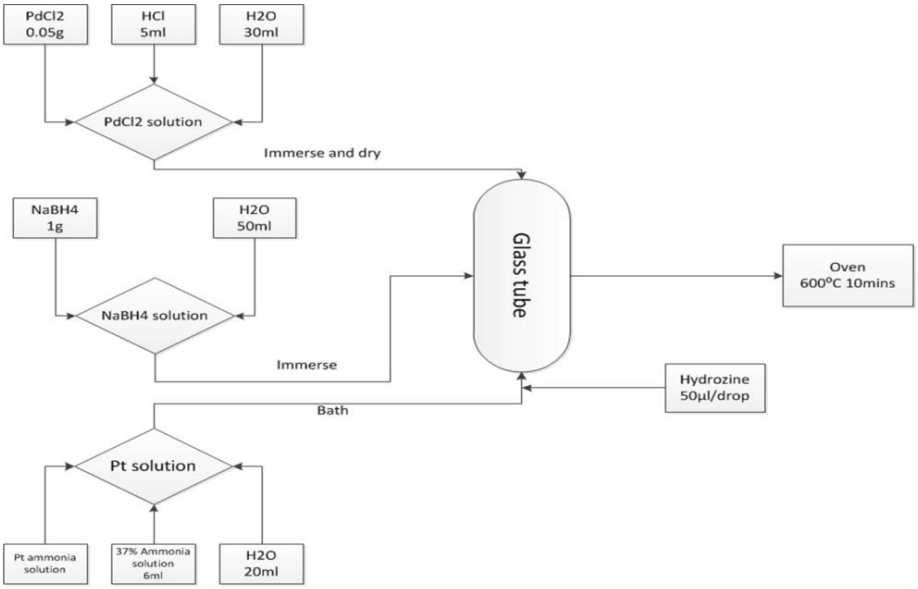

Figure 6- 2 Process flow diagram of platinum plating on glass hopper

6.3. Results and Discussion

6.3.1. Powder dispensing from borosilicate glass hopper

In Figure 6-3 the dispensed mass of dose from ultrasonic dispensing device was plotted for Sorbolac®400 (S400), Starch and Inhalac®70 (I70) in a run chart. The doses were dispensed in every 6s. All three samples were stored and grounded at 25 ± 1°C and 40 ± 2% RH before the start of dispensing. The initial status of samples may be different as they has different moisture sorption propensity [149]. But for one material, the status is invariable when the sample is stored in a constant temperature and relative humidity. The trend of dose mass shown in Figure 6-1 indicates the quite different flow behaviour for materials. The dose mass of S400 and starch decreases gradually from the beginning to the end of dispensing. The variation of dose was significant in the end of dispensing with a deviation of approximately 2mg to the dosage dispensed at the start. It was almost 200% and 70% as much of the average dose mass of S400 and starch, respectively. The difference between maximum and minimum value in the whole run was even larger comparing with the average. The poor consistency of dispensing was represented by relative standard deviation (RSD) in Table 6-1. As for I70, the dose decreased as well but less significant than the other two. After a period of time, the dose mass tend to be stable at approximately 13mg after 60 doses. To investigate the difference of dispensing results between materials, it focused on the flow and discharge status of powders in the dispensing hopper. The high speed image of dispensing nozzle in Figure 6-4(a) shows that near the end of dispensing S400 powder was often stuck at

the nozzle tip with a strong agglomerated powder cluster formed and unable to fall off from the hopper under the influence of vibration. When the rest powder was unloaded run out in the nozzle, it could be observed that on the inner surface of glass hopper there was a thin film of fine particles (Figure 6-4(c)), although it could be easily blown off to get a relatively clean hopper. It is supposed that the static charge was generated during the dispensing which plays the most important role in changing the flow behaviour of powders. It has been already studied in other powder delivery systems for plastics [171] and pharmaceuticals [135, 162, 163, 173]. Charge generated by frequent inter-particle and particle–wall collisions in the vibrating hopper often differs from dose to dose. At the beginning, the tribo-electrification took place between glass surface and particles with initial charge. The initial charge of samples in this work is assumed neglectable as all the samples were stored and grounded in a same condition before dispensing. The powder got charged in the vibrating hopper and charge accumulated when it approaching to the outlet. The dosage got less and less as the charge increased in the powder bed. Some of the material may eventually reaches the saturation value of charge [175] such as I70 in this work. The dosage stayed at approximately 13mg at the end. However, when the powder bed descended along the hopper, fine particles are easier to stick on the surface due to a large adhesive force. The powder film formed by fine particles could get thicker in dispensing such as S400 and starch. It's hard to evaluate the charge variation along with the changing of thickness of this powder film. Also, the static charge is not the only factor as other inter-particle force may influence on the flow behaviour in this case. However, the static charge was dominant in fine particles which inevitably hindered the flow and get the dosage less and less.

Tribo-electrification of the powder inside the hopper was caused by particles impacting and sliding against the glass surfaces under the influence of high frequency vibration. When insulating pharmaceutical powders, such as lactose and starch, are transported in the glass hopper, a large amount of frictional charge will build up.

Table 6- 1 Dispensing results for dose of excipient samples from 1.0 mm glass dispensing nozzle

Sample	Doses	Max(dose mass) /mg	Min(dose mass) /mg	Mean (dose mass) /mg	RSD
Lactose Sorbolac®400	106	2.319	0.022	1.188	45.7%
Starch from wheat	106	5.709	0.833	3.138	35.1%
Lactose Inhalac®70	104	14.518	12.641	13.471	3.0%

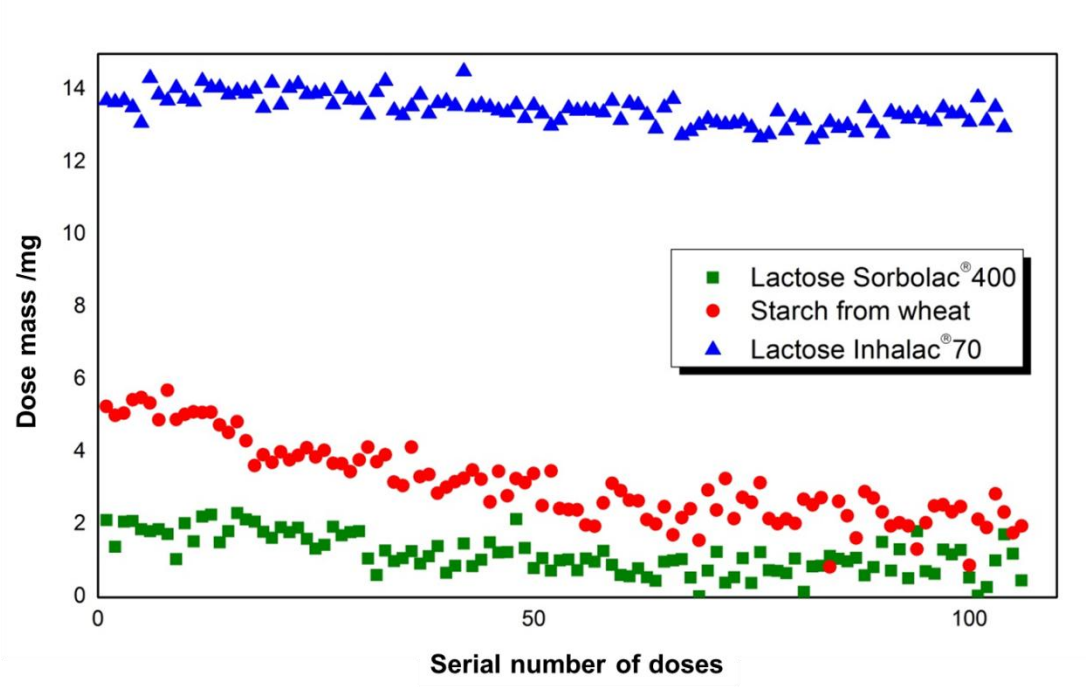

Figure 6- 3 Run chart of mass of dispensed doses for excipient samples from 1.0 mm glass dispensing hopper

6.3.2. Electroless plating of Platinum on borosilicate glass hopper

Several reports on basic electroless platinum plating can be seen in previous technical papers and patents. There are two types of electroless platinum plating bath, essentially alkaline [176] and acidic baths [177]. In this work, an modified alkaline bath was utilized with dinitrodiammine platinate, $Pt(NH_3)_2(NO_2)_2$, as the source of metal.

The borosilicate glass needs special pretreatments to serve as the substrate of electroless platinum plating. First of all, the cleaning of hoppers with detergent is not enough to remove the contamination on the surface so that the glass hopper was heated to 600°C in the fire. And then the use of hydrofluoric acid was to further clean and coarsen the glass surface. The concentration of HF acid and immersing time needs to be controlled as an excessive coarsened surface may influence the powder flow with the higher friction between powder and glass wall.

The hopper is different from plane substrate when placing in the bath. To make sure the inner surface was fully coated, the hopper was firstly designed with one end closed. All the sensitizer and catalyst solution and alkaline bath was filled in the vertical hopper to react in the water bath. $NaBH_4$ was used as reductant to restore elemental palladium on the glass surface. However, later filled alkaline bath might affect the uniform

distribution of palladium on the surface. As a result, the platinum couldn't grow on the spot lack of palladium catalyst where the platinum coating fell off during the reaction (Figure 6-5(a)). Therefore, to obtain a decent platinum coating on the inner surface on glass hopper (Figure 6-5(b)), the $NaBH_4$ was added after alkaline bath filled in the hopper reached to 55°C. Improper pre-treatment may also cause the bad coating quality.

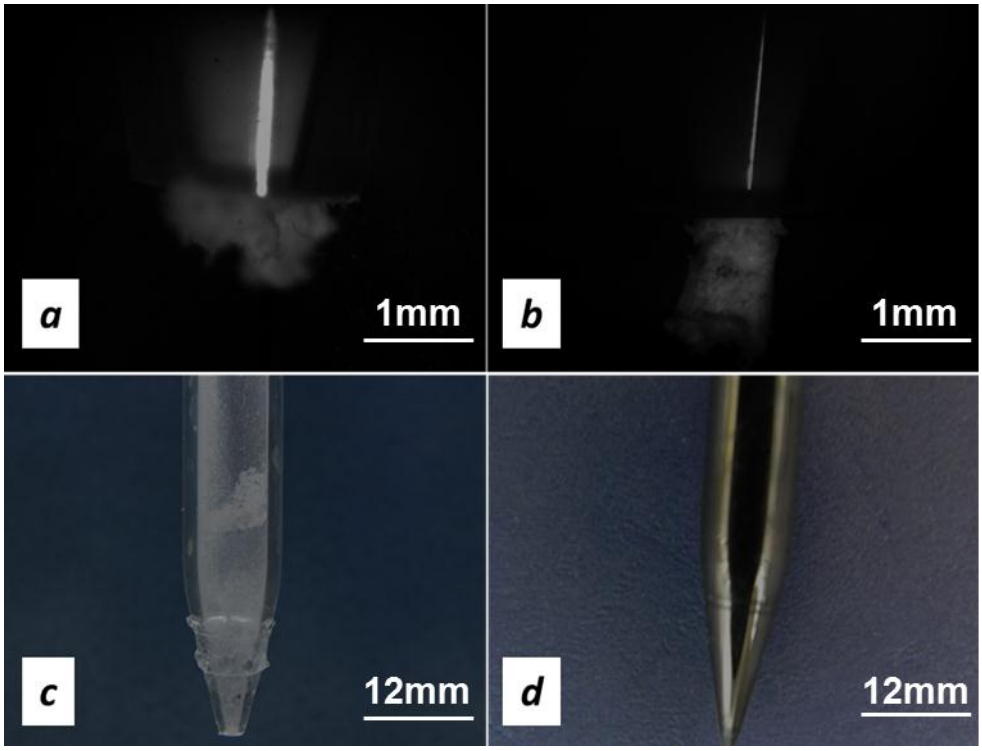

Figure 6- 4 High speed images of dispensing nozzle with extruded powder (a) from glass hopper; (b) from Pt-coated hopper; (c) empty glass nozzle and (d) empty Pt-coated nozzle after powder run out

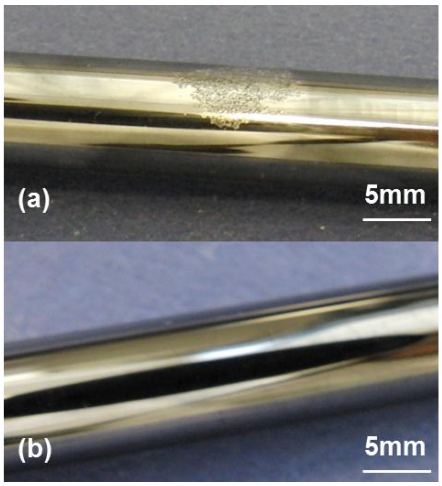

Figure 6- 5 Platinum plating on the surface of borosilicate glass hopper, (a) coating defect and (b) decent coating

6.3.3. Powder dispensing from Platinum coated glass hopper

The results of dispensing tests from Pt-coated dispensing nozzle were plotted in Figure 6-6. When comparing with the results from the glass hopper, the doses of all three excipient samples did not show an obvious decreasing trend in dispensing process, especially for S400 and starch. The dose mass tend to be stable after a few doses despite the variation of dose still existed in cohesive powder samples such as S400 and starch. Notably, the average dose mass had increased significantly for all three materials. That increase for starch was more than 30% and the dose mass was doubled for S400. The high speed image shows that S400 powder was extruded in form of a rod (Figure 6-4(b)) without huddling at tip of nozzle. Moreover, the diameter of powder rod was measured as same as the orifice size which means there was no bulk deformation caused by attraction/repellent of highly charged particles. When powder was run out, residues and powder film on the surface of nozzle was hardly observed (Figure 6-4(d)).

The improved dispensing consistency and increased dose mass (shown in Figure 6-6 and Table 6-2) suggests that the modified contact surface between powder and dispensing hopper has favourably influenced the triboelectric charging behaviour for fine excipient powders. The results of static charge measurement are shown in Figure 6-7 for lactose S400 and I70 and Figure 6-8 for wheat starch. In the charge measurement, the influence of impact charge proposed by Watanabe et al. [139] on the charge of each dose is not considered in this work as the method is a rate-based process by which the charging rate and the saturation value or maximum of charge are only evaluated. Generally, the charging rate for S400 between doses is higher than I70. In glass hopper, I70 eventually reached to a saturation value of charge whereas the charge of S400 kept increasing. With Pt-coated dispensing hopper, the charging rate is lower between doses in the dispensing. All the materials in the Pt-coated hopper can attain a acceptable charge level after a few doses.

Table 6- 2 Dispensing results for dose of excipient samples from 1.0 mm Pt-coated glass dispensing nozzle

Sample	Doses	Max(dose mass) /mg	Min(dose mass) /mg	Mean (dose mass) /mg	RSD
Sorbolac®400	64	3.287	1.149	2.120	22.5%
Starch	89	5.448	2.540	4.118	14.0%
Inhalac®70	86	16.168	14.413	15.296	2.4%

The results are yet satisfactory for S400 and starch comparing with I70 even though they were all improved. We have two concerns on this issue. Firstly, although the Pt-coated contact surface shows a promising solution to the triboelectric charging issue for fine excipient powder dispensing, the charge generated in the vibrated powder bed is yet fully eliminated. The coating morphology on the hopper surface reveals fundamental differences compared to coatings on flat substrates. The latter can obtain a homogeneous and coherent coating, whereas for the hopper it is very difficult. On both sides of the hopper, defects of coating are observed, especially for the inner coating which has a low density and an almost continuous network of cracks. Secondly, the inner coating exhibits an inhomogeneous distribution in the average roughness R_a. For fine particle which has proverbially strong adhesive force, a very smooth inner surface especially in the convergent zone of hopper is vitally important to reduce the friction between particle and wall. The improvement on the plating method may provide a better surface modification for promoting the powder flow.

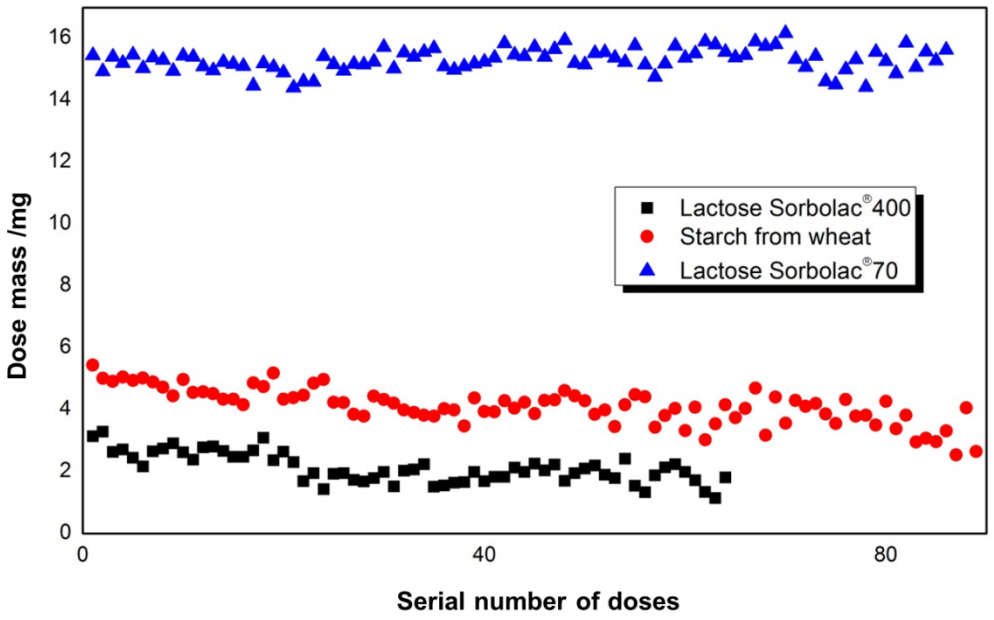

Figure 6- 6 Run chart of mass of dispensed doses for excipient samples from 1.0 mm Pt-coated glass dispensing nozzle

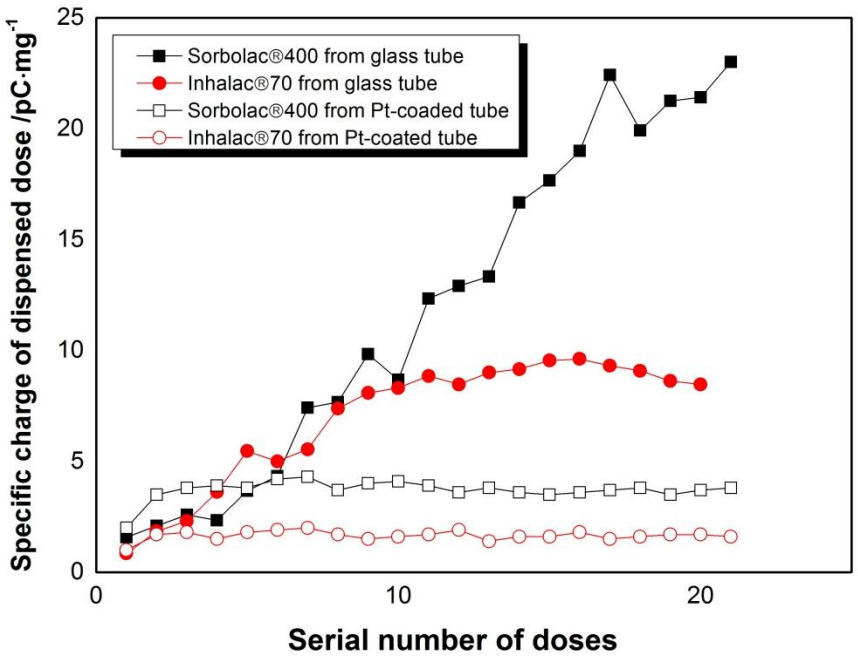

Figure 6- 7 Specific charge of dispensed dose of Lactose Sorbolac®400 and Inhalac®70 measured from ultrasonic vibrating dispenser

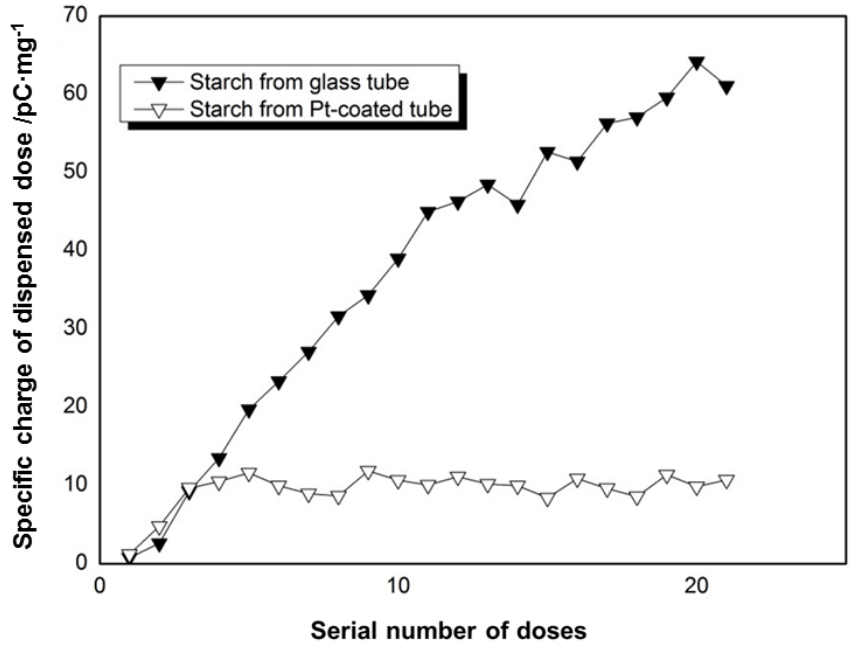

Figure 6- 8 Specific charge of dispensed dose of wheat starch from ultrasonic vibrating dispenser

6.4. Summary

The glass vibrating hopper often leads to a severe problem on powder dispensing due to triboelectric charging generated during the sliding and collision between particles and glass wall. The charging will change the flow behaviour of powders and it may cause a decreasing flow rate and irregular variations in dispensed dosages. For finer lactose powders, the charging rate is higher than the coarse one. A Pt-coated glass hopper was demonstrated in ultrasonic vibration dispensing device. The modified surface of dispensing hopper has effectively reduced the accumulated charge in the vibrating powder bed and therefore the dispensing consistency has been improved and the flow rate is increased for pharmaceutical excipient powders. The dose weighing and charge measuring tests have shown the evidence of the favourable influence of modified glass nozzle on the triboelectric charging issue and meanwhile a further improvement on fine powder dispensing can be expected.

Chapter 7

Flow Rate Prediction for Ultrasonic Vibration Powder Dispensing

This chapter presents the derivation of a correlation between ultrasonic vibration dispensing results and device design parameters taking account of different properties of material particles. The correlation aims to predict the flow rate in dispensing with the information of device specification and material properties. Compared with the experimental results, the predicted results suggest the correlation is able to predict the discharge rate for inhalation grade lactose in ultrasonic vibration dispensing when the flow of powder is steady and controllable in the vibrating hopper.

7.1. Introduction

The development of bulk solids micro-dispensing technique aims to improve accuracy and efficiency in storing and delivering bulk solids at a controlled rate. An accurate prediction of the discharge rate in the dispensing process is therefore critical. Moreover, knowledge of correlations between discharge rate and device design and processing parameters is necessary in applying micro-dispensing technique to practical applications.

A number of correlations have been proposed for the prediction of discharge rate of free-flowing bulk solids. Fowler and Glastonbury [5] and Beverloo et al. [110] proposed the most widely used correlations to predict discharge rate of granular materials from flat-bottomed hopper, which suggested the discharge rate is determined by the relationship between the orifice size of hopper and the particle size. Rose and Tanaka [15] studied the discharge of bulk solids from conical hopper and indicated the dependence of the discharge rate on the hopper angle. Verghese [112] studied the influence of fine particles on the discharge rate from hopper and expanded the application of Beverloo's and Rose and Tanaka's correlation to the prediction of discharge rate of fine particles sized below 500 μm. Suzuki et al. [113] and Wassgren et al. [102] proposed the acceleration of particles has been changed in the hopper under the influence of vibration. As result, the discharge rate in a vibrating hopper is a function of the instantaneous ''effective gravity'' acting on the particles.

The present work in this chapter aims to propose a correlation to predict discharge rate of inhalation grade lactose powders from ultrasonic vibration micro-dispenser. The factors that may influence the discharge rate of powders, i.e. orifice size, hopper angle, particle size and vibration, will be discussed with previous discharge rate models. The measured discharge rates of Inhalac® lactose from dispensing tests will be used in the derivation of new equations.

7.2. Results and Discussions

7.2.1. Discharge Rate

In the continuous dispensing mode, the discharge rate of samples can be directly measured by weighing the accumulated mass in a defined dispensing time. When samples are dispensed dose by dose in the intermittent dispensing mode, difficulties in obtaining discharge rate may be encountered. If the deviation between dosages is large,

the discharge rate varies from dose to dose and the mean dose mass may show a nonlinear relationship with the duration of vibration. In this case, a constant discharge rate is not available and thus the discharge rate cannot be simply calculated by $\frac{\overline{m}}{T_d}$, where $\overline{m}$ is the mean dose mass. This problem is especially significant in the case of very cohesive powder and inappropriate orifice size and/or angle of hopper being used (see Chapter 5). For intermittent dispensing, the mean discharge rate is obtained by linear regression between the mean dose mass and the duration of vibration. The discharge rate equals to the slope of fitted line. Therefore, a good dosage conformity and linearity of mean dose mass to the duration of vibration is the premise of obtaining a constant discharge rate.

Table 7-1 shows the discharge rates for three Inhalac® lactose: Inhalac®70, Inhalac®120 and Inhalac®230, measured from hoppers with different orifice size, D_o and half conical angle, α.

Table 7- 1 Discharge rate of Inhalac® lactose, in **mg/s**, measured from hoppers with different orifice size and half angle

	Half Angle, α /°	**Orifice Size, D_o /mm** 0.8	0.9	1.0	1.2
Inhalac®70	7.5	19.3	27.2	37.5	63.0
	15	16.0	22.2	30.9	52.1
	22.5	14.1	18.0	27.1	43.9
	30	7.0	9.4	15.3	23.8
	37.5	-	3.5	4.8	7.7
Inhalac®120	7.5	27.4	34.7	50.7	81.0
	15	24.1	30.3	44.0	69.9
	22.5	21.9	28.4	40.9	66.2
	30	12.7	18.8	23.7	40.8
	37.5	-	8.5	11.1	18.6
Inhalac®230	7.5	12.3	15.8	24.0	39.9
	15	8.0	10.5	16.1	27.0
	22.5	5.1	6.6	9.7	16.1
	30	2.2	2.5	5.4	6.7
	37.5	-	1.1	1.6	2.8

Based on the conclusions in previous chapters, the discharge rate of powder from ultrasonic vibration micro-dispenser is considered to be influenced by the factors listed in Table 7-2.

There are other factors affecting the discharge rate not listed in Table 7-2 as they are coupled to some of the listed factor. For example, the angle of repose and the flowability of powder are reported to be influenced by particle size, size distribution and shape [60].

Table 7- 2 Proposed factors influencing the discharge rate of powder from ultrasonic vibration micro-dispenser

Factor	Symbol	Dimension in terms of M, L, T
Bulk density of powder	ρ_B	$M \cdot L^{-3}$
Particle size	d	L
Particle shape	λ_s	1
Orifice size of hopper	D_o	L
Half conical angle of hopper	α	
Effective gravity acceleration under the influence of vibration	g_{eff}	$L \cdot T^{-2}$

Therefore, the discharge rate, W, can be expressed as a function of these factors

$$W = f\{\rho_B, d, \lambda_s, D_o, \alpha, g_{\text{eff}}\} \tag{7.1}$$

Based on mass flow equation for bulk solid (eq. 2.17), the discharge rate, W, can be given by dimensional analysis. Then,

$$W = \rho_B \sqrt{g_{\text{eff}}} D_h^{2.5} f\left\{\frac{D_o}{d}, \lambda_s, \alpha\right\} \tag{7.2}$$

where D_h is the hydraulic diameter of outlet opening. $\frac{D_o}{d}, \lambda_s, \alpha$ are dimensionless and independent of each other.

7.2.2. Discharge Rate and Orifice Size

Beverloo et al. [110] and Brown and Richards [74] (p. 193-195) suggested the hydraulic diameter of orifice D_h can be replaced by an effective flow diameter $D_o - kd$ for circular orifice. The correlation between discharge rate and orifice size of hopper were analysed by plotting $W^{2/5}$ vs. D_o with dispensing results of Inhalac® lactose listed in Table 7-1. As shown in Figure 7-1, straight lines were obtained for three Inhalac® lactose. Lines obtained from hoppers with different half conical angle were approximately crossed at one point on D_o axis but with exceptions, i.e. 30° for Inhalac®70, 22.5° and 30° for Inhalac®230. The linearity of $W^{2/5}$ vs. D_o for Inhalac®70 in the hopper with half angle greater than 30° is poor as the flow was not steady and the deviation of dosages was relatively large. Inhalac®230 shows worse flowability than Inhalac®70 and thus it only has a steady flow in hoppers with half angle smaller than 22.5°. It is supposed that for a steady flow lines obtained from hoppers with different half conical angle are crossed at

one point on D_o axis and therefore, orifice size and half angle of hopper are independent of each other.

The value of *kd* was obtained from the intercept on the D_o axis. The mean particle size *d* for Inhalac®70, Inhalac®120 and Inhalac®230 is 200 μm, 130 μm and 90 μm, respectively. Thus, it was found that k = 0.7 for Inhalac®70 and Inhalac®120, k = 2 for Inhalac®230. Brown and Richards [74] (p. 193-195) assumed there is an annulus with width d/2 adjacent to the orifice edge where no flow takes place and thus, all particles pass through an orifice of reduced diameter. According to their assumption, $D_o - kd$ represents the effective orifice size for powder discharge, and the value of k can be considered as a hypothetical number of particles in radial direction forming a reduced orifice where the majority of particles flow through. Beverloo et al. [110] indicated the variations in k are probably related to the surface properties of particle. The discharge of powders can be observed with the high speed camera. As shown in Figure 7-2, Inhalac®70 and Inhalac®120 were discharged as discrete particles, whereas less free-flowing Inhalac®230 was large agglomerate. k increases with decreasing flowability. For less free-flowing powder, the parameter k is believed larger and the effective orifice gets smaller.

Despite the value of k for Inhalac® lactose is different from k in Beverloo's model, the discharge rate in ultrasonic dispensing conforms to Beverloo's equation (eq. 2.21) with the discharge rate, W, being proportional to $(D_o - kd)^{2.5}$. Thus, equation (7.2) can be represented by

$$W = \rho_B \sqrt{g_{\text{eff}}} (D_o - kd)^{2.5} f\left\{\frac{D_o}{d}, \lambda_s, \alpha\right\} \tag{7.3}$$

7.2.3. Discharge Rate and Hopper Angle

Rose and Tanaka [15] reported the discharge rate from a hopper is a function of the half conical angle of hopper, α, and the angle between the stagnant zone boundary and the horizontal, ϕ_d (shown in Figure 2-10(b)). In Rose and Tanaka's model, the discharge rate is proportional to $(\tan\alpha \tan\phi_d)^{-0.35}$ for $\alpha < 90 - \phi_d$. As the value of ϕ_d is hard to be predicted, British Draft Design Code [111] recommends that ϕ_d equals to 45° when a mass flow is developed in a hopper with angle α less than 45°. Then, the discharge rate is proportional to $(\tan\alpha)^{-0.35}$ for $\alpha < 45°$.

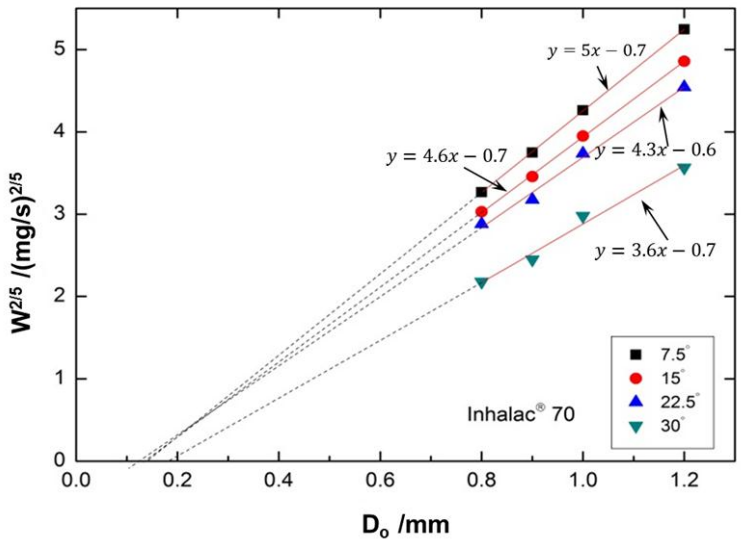

(a)

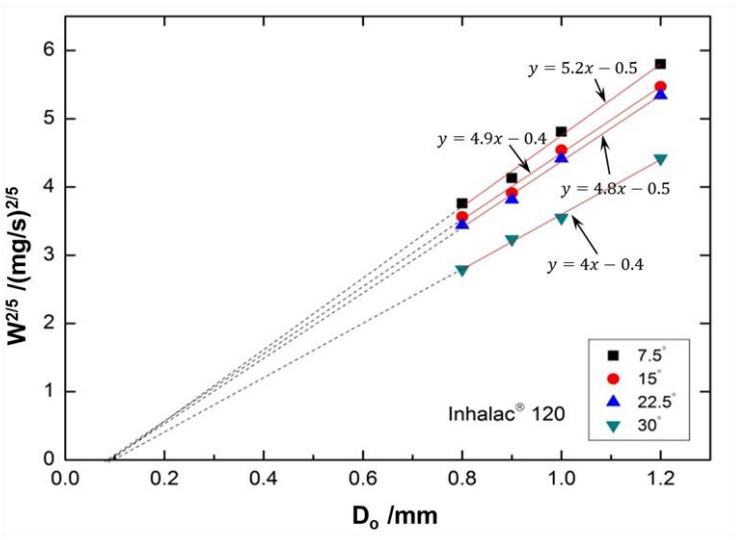

(b)

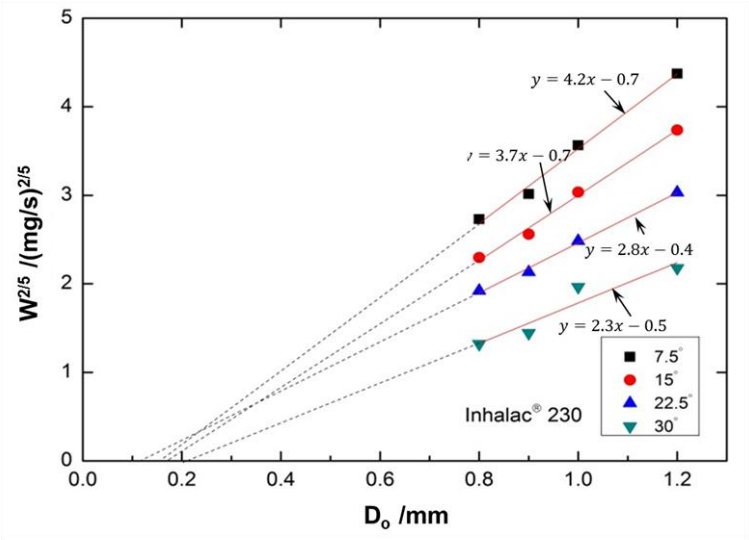

(c)

Figure 7- 1 $W^{2/5}$ vs. D_o from hoppers with different half conical angle for (a) Inhalac®70; (b) Inhalac®120; (c) Inhalac®230. For full explanation refer to the text

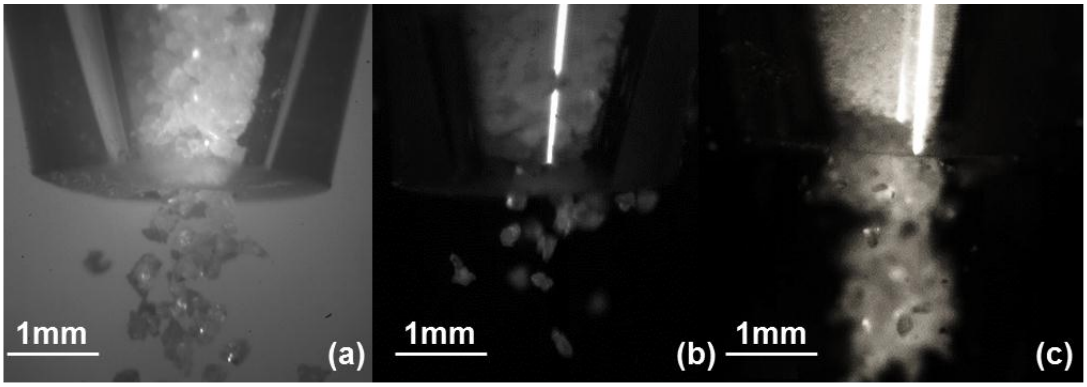

Figure 7- 2 High speed camera images of powder discharging: (a) Inhalac®70; (b) Inhalac®120; (c) Inhalac®230

To investigate the validation of Rose and Tanaka's model on ultrasonic vibration dispensing, the dispensing test results obtained by using hoppers with 0.9 mm orifice for Inhalac® lactose were analysed by plotting lnW vs. ln(tanα). As shown in Figure 7-3, piecewise linear functions were obtained for three inhalation lactose. The intersection point shown on the piecewise function plots represents α = 26°, 23° and 27° for Inhalac®70, Inhalac®120 and Inhalac®230, respectively. An average value of 25° is assumed for α, at which the function of lnW against ln(tanα) is divided into two parts with distinct slope. As discussed in Chapter 5, powders may form a core flow in the hopper with a large angle. Despite the core flow pattern is hard to be observed, the significant decreasing in discharge rate when the half angle of hopper larger than 22.5° shown in Table 7-1 is considered as a sign of core flow. The angle of 25° is supposed as the critical angle of hopper, by exceeding which the flow of inhalation lactose powder may transform from mass flow to core flow. This critical angle of flow pattern depends on various factors such as internal friction coefficient of the particles, wall friction coefficient, vibration characteristics and so on.

According to the function plot of lnW vs. ln(tanα), the discharge rate, W, can be given by

$$\ln W = \mu \ln \tan \alpha + \beta \qquad \alpha < 25° \tag{7.4}$$

$$W = e^{\beta} (\tan \alpha)^{\mu} \qquad \alpha < 25°$$

Then,

$$W \propto (\tan \alpha)^{\mu} \qquad \alpha < 25° \tag{7.5}$$

where the parameter μ and β was obtained from the slope of piecewise linear function and the intercept on the ln(tanα) axis in Figure 7-3. The parameter μ for Inhalac®70, Inhalac®120 and Inhalac®230 equals to -0.35, -0.17, -0.74, respectively.

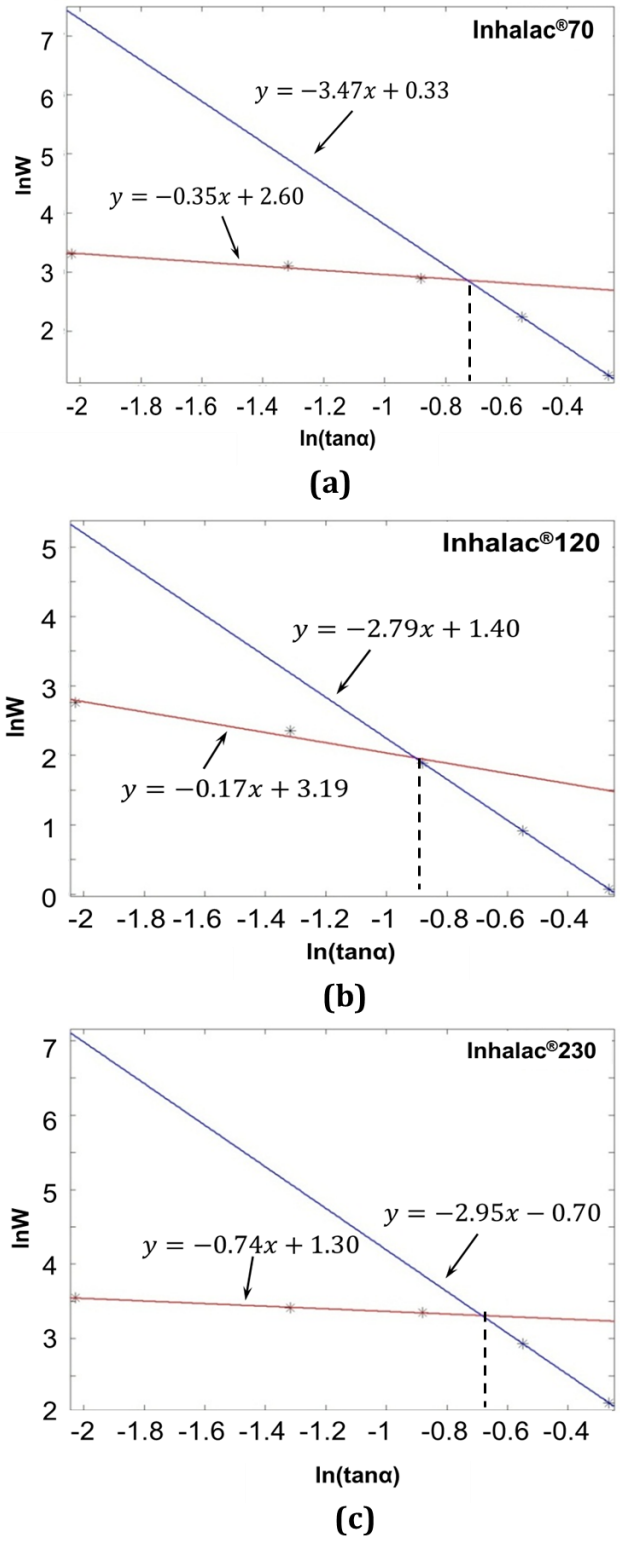

Figure 7- 3 lnW vs. ln(tanα) from hoppers with 0.9mm orifice for: (a) Inhalac®70; (b) Inhalac®120; (c) Inhalac®230. For full explanation refer to the text

In Rose and Tanaka's model, μ is a constant at -0.35. The value of μ for free-flowing Inhalac®70 equals the value in Rose and Tanaka's model as the particle size and flowability of Inhalac®70 is more like the materials involved in Rose and Tanaka's model. Inhalac®120 has smaller particle size and shows better flowability than Inhalac®70 from same orifice size. The value of μ is increased. As shown in Figure 7-3, the finer Inhalac®230 powder is cohesive and the flowability is poor. The value of μ is decreased. Rose and Tanaka [15] suggested an inclusion of a multiplicative factor of $e^{-7.7\times10^{-6}\frac{F_C}{\rho g^{1/2}d^3}}$ in discharge rate equation for cohesive materials. F_C is the cohesive force between the particles. Thus, the parameter μ is supposed as an indication of powder flowability in a hopper. It can be concluded that the larger μ is, the better flowability the powder shows in the hopper and the less influence of the convergent flow zone has on the discharge rate.

Combine equation (7.3) and (7.5),

$$W = \rho_B\sqrt{g_{\text{eff}}}(D_o - kd)^{2.5}(\tan\alpha)^{\mu} f\left\{\frac{D_o}{d}, \lambda_s\right\} \qquad \alpha < 25° \tag{7.6}$$

When the hopper angle is larger than 25°, it is assumed that the inhalation lactose powders are discharged in the core flow pattern. The flow rate is significantly decreased and inconsistent due to the presence of unstable stagnant zone. The effect of angle of stagnant zone, ϕ_d, on the discharge rate cannot be ignored. A function of angle ϕ_d is supposed as a multiplicative factor in the discharge rate equation (7.6). Thus, the discharge rate from the hopper with half conical angle larger than 25° can be given by

$$W = W_0(\tan\alpha)^{\mu} f(\phi_d) \qquad \alpha \geq 25° \tag{7.7}$$

where W_0 is the discharge rate predicted by equation 7.3. As previously discussed, the size and shape of stagnant zone are varied in dispensing cycles and therefore, the angle ϕ_d *is* not a constant and hard to be predicted. As shown in Figure 7-3, the slope for three Inhalac® lactose is close to a constant value -3 when angle α is larger than the critical angle. Thus, it is assumed that the discharge rate for α ≥ 25° can be given by replacing $(\tan\alpha)^{\mu} f(\phi_d)$ with $(\tan\alpha)^{-3}$ in the absence of information of angle ϕ_d. Then,

$$W = \rho_B\sqrt{g_{\text{eff}}}(D_o - kd)^{2.5}(\tan\alpha)^{-3} f\left\{\frac{D_o}{d}, \lambda_s\right\} \qquad \alpha \geq 25° \tag{7.8}$$

However, the dosage conformity for three lactose powders is poor with RSD larger than 10% from hoppers with angle larger than 25° (see section 5.2.2). Therefore, the hopper with angle larger than 25° is often avoided for dispensing inhalation lactose in practical application.

7.2.4. Ratio of Orifice Size to Particle Size

In equation (7.3), the influence of orifice size and particle size on the discharge rate is expressed by the term $D_o - kd$, which represents an effective zone where particles pass through of the orifice. The orifice size determines the discharge rate with particle size giving the useless annular zone along the margin of the orifice. As previously discussed, the orifice size must be in a range compared to the particle size to avoid flow obstructions and assure a controllable discharge rate in vibratory dispensing. As shown by equation (4.1), the orifice size assuring controllable discharge is dependent on the hopper angle and the flowability of powder in vibrating hopper. Thus, it is assumed that the dimensionless group $\frac{D_o}{d}$ coupled with tanα affects the discharge rate, subjected to the flow factor μ. The discharge rate therefore reads:

$$W \propto \left(\frac{D_o}{d}\tan\alpha\right)^{\mu} \qquad \alpha < 25° \tag{7.9}$$

The dispensing test results for Inhalac® lactose were analysed by plotting W vs. $\left(\frac{D_o}{d}\tan\alpha\right)^{\mu}$. With regression analysis, discharge rate, W, is proportional to $\left(\frac{D_o}{d}\tan\alpha\right)^{\mu}$ expressed by the linear relationship shown in Figure 7-4. Therefore, $\frac{D_o}{d}\tan\alpha$ is an inclusion of a multiplicative factor in the discharge rate equation. It can be concluded that the larger μ is, the better flowability the powder shows in the hopper.

The particles of three inhalation grade lactose are all angular-shaped and have same morphology observed by SEM (see Appendix III). The particle shape has same influence on the discharge rate of three lactose powders, and the effect of particle shape can be presented by the parameter k and μ in the discharge rate equation. Therefore, the discharge rate is given by

$$W = \rho_B\sqrt{g_{\text{eff}}}(D_o - kd)^{2.5}\left(\frac{D_o}{d}\tan\alpha\right)^{\mu} \qquad \alpha < 25° \tag{7.10}$$

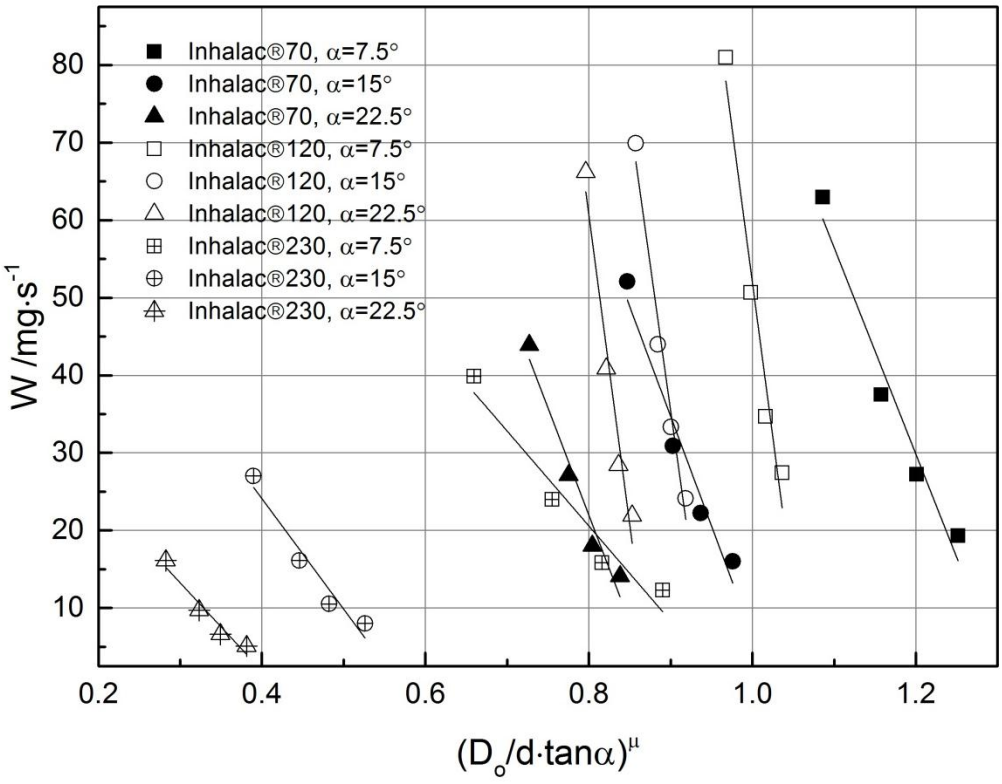

Figure 7- 4 W vs. $(D_o/d\cdot\tan\alpha)^{\mu}$ from hoppers with half conical angle less than 25° for Inhalac®70, Inhalac®120 and Inhalac®230. For full explanation refer to the text

As presented by equation (7.8), the parameter μ is a constant when the half conical angle of hopper is larger than 25°. The influence of the ratio of orifice size to particle size on the discharge rate has not been well known due to the lack of information of stagnant zone when powder is discharged in a core flow pattern. For inhalation grade lactose powders, the discharge rate is assumed to be expressed by

$$W = C^*\rho_B\sqrt{g_{\text{eff}}}(D_o - kd)^{2.5}(\tan\alpha)^{-3} \qquad \alpha \geq 25° \tag{7.11}$$

where

$$C^* = \alpha\left(\frac{D_o}{d}\right)^{\beta} \tag{7.12}$$

One can calculate the discharge rate of powder from a vibrating hopper with half conical angle larger than critical angle of flow pattern if the constant C^* are determined. An average value of 0.09 is obtained for the constant C^* by using dispensing test data of free-flowing powders Inhalac®70 and Inhalac®120 from hoppers with 30° half conical angle. The following equation is therefore proposed:

$$W = 0.09\rho_B\sqrt{g_{\text{eff}}}(D_o - kd)^{2.5}(\tan\alpha)^{-3} \qquad \alpha \geq 25° \tag{7.13}$$

7.2.5. Effect of Vibration on the Discharge Rate

In ultrasonic vibration micro-dispensing, vibration plays as an extra driving force to promote powders discharged from the hopper. As previously discussed in section 5.2.3, the movement of a single particle of Inhalac®70 was tracked by the high speed camera frame by frame. The particle is accelerated by the vibration prior to flowing out of the hopper. Therefore, the effective gravity acceleration in equation (7.10) can be presented by

$$g_{\text{eff}} = \gamma^2 g \tag{7.14}$$

where coefficient γ depends on various factors such as cohesion of particles, powder flowability, vibration characteristics and so on. It can be evaluated by selecting two discharge rates at two values of g_{eff} under the condition that the other variables are constant. For α < 25°, an average value of 0.85 is obtained for the coefficient γ by using dispensing test data of three lactose powders listed in Table 7-1.

7.2.6. Discharge Rate Prediction

In conclusion, the discharge rate of inhalation grade lactose from ultrasonic vibration micro-dispensing device can be predicted by general equation

$$W = 0.85\rho_B\sqrt{g}(D_o - kd)^{2.5}\left(\frac{D_o}{d}\tan\alpha\right)^{\mu} \qquad \alpha < 25° \tag{7.15}$$

$$W = 0.076\rho_B\sqrt{g}(D_o - kd)^{2.5}(\tan\alpha)^{-3} \qquad \alpha \geq 25° \tag{7.16}$$

The value of constants and variables for predicting the discharge rate of inhalation grade lactose from ultrasonic vibration micro-dispensing device are listed in Table 7-3.

Table 7- 3 Constants and variables for predicting the discharge rate of inhalation grade lactose from ultrasonic vibration micro-dispensing device

	ρ_B /mg·mm^{-3}	g /mm·s^{-2}	d /mm	k	μ	γ	D_0 /mm	α /°
Inhalac®70	0.59	9800	0.2	0.7	-0.35	0.85	0.8 – 1.2	7.5 - 30
Inhalac®120	0.70	9800	0.13	0.7	-0.17	0.85	0.8 – 1.2	7.5 - 30
Inhalac®230	0.71	9800	0.09	2.0	-0.74	0.85	0.8 – 1.2	7.5 - 30

Figure 7-5 compares the measured and the predicted discharge rates by equation (7.15) and (7.16) for three inhalation lactose. The difference between the predicted and the measured discharge rates for Inhalac®70 and Inhalac®120 is within 20%. It also shows that the predicted discharge rate for Inhalac®230 is larger than the measured, especially from the hopper with half conical angle larger than 25°. The deviation is supposed from the regression analysis when a number of assumptions are proposed:

- Particle size, d

The particle size, d in all the correlations is represented by a statistic value D50 which is the maximum particle size below which there is 50% of the sample volume exists. Such value might not accurately represent particle size for samples. Also, for Inhalac®230 which tends to be agglomerated in discharging, the use of single particle size *d* is not able to present the actual influence of particle agglomerates on the flowability and discharge rate as the flowability of less free-flowing powder is different from free-flowing powder due to the strong cohesion.

- Bulk density, ρ_B

The bulk density used in the prediction is the filled (poured) bulk density and treated as a constant. However, under the influence of periodic vibration, powder in the hopper dilates to some voidage. The voidage in bulk solid may vary in dispensing due to the duo effect of dilation and compaction of vibration. Thus, the flowing bulk density does not depend on the initial voidage and hence the original filled bulk density. However, there is not enough clarity to date on which density should be used [178].

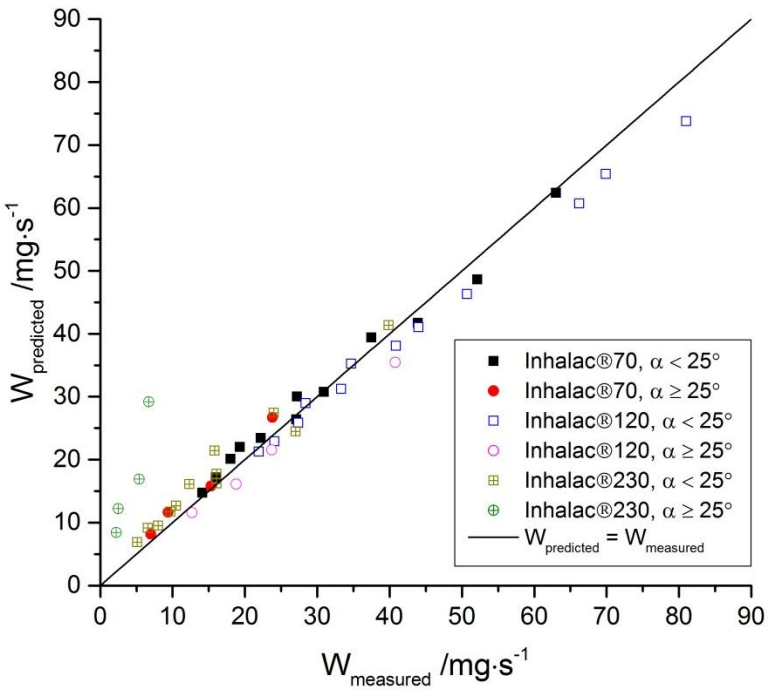

Figure 7- 5 Predicted discharge rate from equation (7.15) and (7.16) vs. measured discharge rate in dispensing tests

- Parameter *k*

It has been worked out in this project that k is 0.7 for free-flowing lactose and 2.0 for less free-flowing one. However, the value of k is obtained by using the mean particle size d in the regression analysis. Although the parameter k is reported as the surface properties of particle which contributes to an useless annulus adjacent to the orifice edge of hopper, there is not enough information on how the parameter k affects the proposed effective orifice size when cohesive agglomerates are extruded from the orifice. It is a concern on the accuracy of k for less free-flowing powder as the cohesive agglomerate shows quite different flow behaviour from the discrete particle.

- Parameter μ

For α ≥ 25°, an assumption was proposed that the parameter μ is a constant in the absence of information of stagnant zone. How the parameter μ affects the angle ϕ_d is still unknown. As the flowability of sample powders is different, the angle ϕ_d in the core flow pattern is different and the parameter μ should be a variable dependent on the flowability of powder in the hopper.

- Parameter γ

The Parameter γ is supposed as a constant for three lactose powders in discharge rate prediction. However, it can be observed for high speed camera that the flow behaviour of cohesive powder and free-flowing powder is different and thus, the extra driving force provided by the vibration on the agglomerates is unlikely equivalent to the discrete particles. The acceleration coefficient γ should be a variable for materials with different flowability.

- Measured discharge rate

The discharge rate is obtained from intermittent dispensing test. In the hopper with half conical angle larger than 25°, the deviation between dosages is large and hence the discharge rate, which directly affects the accuracy of prediction.

Although the deviation of predicted discharge rate is larger in the case of less free-flowing powder discharging from hopper with larger angle, it is an optimum correlation to predict discharge rate for the inhalation grade lactose powder when the flow is steady and controllable in the vibrating hopper. The parameters in Table 7-3 shows that the coefficients in these equations are sufficiently constant to use for all the inhalation grade lactose and it is also able to be applied to other pharmaceutical powders with similar properties. Moreover, the correlation provides a possibility for the ultrasonic vibration micro-dispensing device to be applied to evaluating the flowability of powder material with factors k, μ and γ in dispensing test. It can be concluded that k increases with decreasing flowability; μ decreases with decreasing flowability; γ decreases with decreasing flowability. These flowability indicators are different from the flow factor obtained by conventional static shear cell test. They provide the information of flowability in a vibrating hopper.

7.3. Summary

The derivation of a correlation between discharge rate of powder from ultrasonic vibration dispenser and device design parameters taking account of different properties of material particles was presented.

Based on mass flow equations of bulk solid extended from Torricelli's law, the discharge rate of powder from ultrasonic vibration dispenser is proposed proportional to

$\rho_B\sqrt{g}D_h^{2.5}$ and influenced by particle size, hopper orifice size, hopper angle and ultrasonic vibration. The discharge rate is proposed proportional to $(D_o - kd)^{2.5}$, where k is a constant related to the surface properties of particle and powder flowability. The value of k increases with decreasing flowability. The discharge rate is proposed proportional to $\left(\frac{D_o}{d}\tan\alpha\right)^{\mu}$ when powder is discharged in mass flow pattern, whereas the discharge rate was found influenced by the size and shape of stagnant zone in core flow pattern. An approximate equation is proposed for core flow in the absence of stagnant zone information. The constant μ is related to powder flowability. The value of μ increases with increasing flowability. Ultrasonic vibration influences the discharge by accelerating particles prior to flowing out of the hopper. The effective gravity acceleration for the powder is presented by $\gamma^2 g$, where coefficient γ depends on various factors such as cohesion of particles, powder flowability, vibration characteristics.

The discharge rate of inhalation grade lactose powder can be well predicted by derived correlation. The coefficients in these equations are sufficiently constant to use for inhalation grade lactose and pharmaceutical powders with similar properties. The correlation also provides a possibility for the ultrasonic vibration micro-dispensing device to be applied to evaluating the flowability of powder material with factors k, μ and γ in dispensing test.

Chapter 8

Dry Powder Printing and its Application in Pharmaceuticals and Biomaterials

---

This chapter presents an application by integrating ultrasonic vibration dispensing device with 3D printing technology. The aim is to build a powder dispensing platform to demonstrate the feasibility of producing solid form oral drugs and pharmaceutical/biomaterial dry powder libraries for high-throughput screening (HTS) of new products.

8.1. Solid Form Oral Drugs of Personalized Medicine

A traditional medication is generally designed for a heterogeneous population of patients admitted with a same or similar symptom. The main disadvantages of such traditional drug products, are the single disease treatment and the fixed dose that make it not suitable to specific groups of patients, such as children, the aged and drug-susceptible patients. Personalized medicine, as a technological advancement, can promise all prediction, prevention and treatment of disease that are targeted to individual patients' need. Solid dosage forms, popular due to their advantages comparing with liquid forms, were produced by a new dosing approach using a dry powder drop-on-demand printing technology in this chapter. Capsule filling with inhalation grade lactose demonstrated the potential of this technology to be applied in the production of personalized medicine.

8.1.1. Challenges in Modern Pharmaceutical Industry

Modern pharmaceutical industry has developed rapidly. In 2011, the annual profit of the pharmaceutical market in Europe was more than €200 billion [179] and only in the UK, the pharmaceutical industry generated a trade surplus of £7 billion which was greater than any other industrial sector [180]. The healthcare policies and the development of advanced medicine manufacturing methods promote an improved medicines availability and affordability in either developed or developing countries [181, 182]. Hence, there is no doubt the pharmaceutical industry will keep developing extremely fast and being one of the major industries for human beings.

However, not only pharmaceutical companies, but also patients and the society are currently facing more challenges and having more expectations (Figure 8-1). A serious problem is the wrong dose taken by patients carelessly or reluctantly. Poisoning, which is the cause of over 70000 of hospital admissions in the UK, is usually due to the medicines taken in overdose [183]. Although about 5% of instances were self-poisoning, inaccurate prescribed drugs or non-prescribed analgesics had led to over 90% of the poisoning instances in England and Wales. Young children, usually under 5 years of age, may swallow drugs by accident because of their curiosity about medications. And the lack of access to suitable medicines for young children has led health-care providers and caregivers to estimate the dose by breaking tablet into quarters and halves, crushing tables or opening capsule [184]. Another problem is the medicine waste: for example in the UK, used, partially used or unrecyclable medication leads to as much as £300 million

waste every year [185]. It was found that most of healthcare payers only use part of medicine products, which may contains tens of pills or tablets. Besides, rising customer expectation on pharmaceutical products is other challenge for the industry. Healthcare payers expect new products that are clinically and economically better than the existing ones, such as multifunctional medicines. Older or disable patients prefer to more convenient pill or capsule which contains all essential substances.

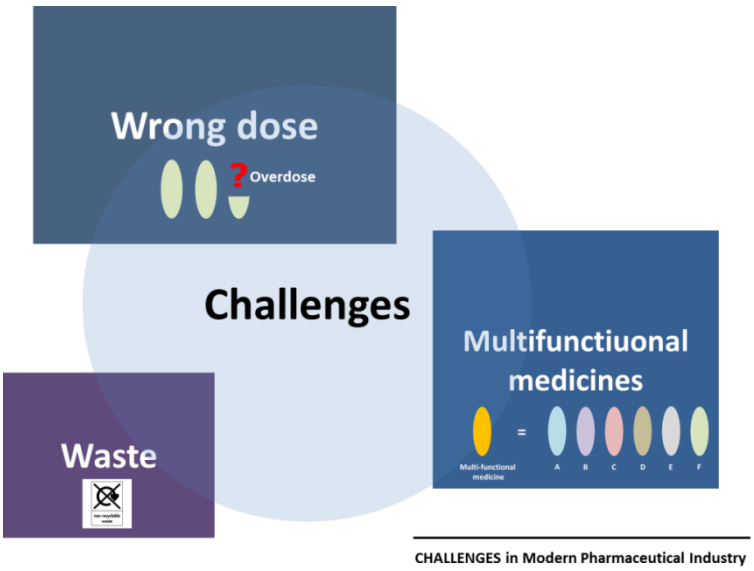

Figure 8- 1 Challenges in modern pharmaceutical industry

In the past decades, pharmaceutical companies, associations and researchers have tried their best to relieve these stresses in pharmaceutical industry: The International Committee of the Red Cross (ICRC) recommended to use four methods to minimize medicine waste: reducing the amount of waste at source, purchasing policy geared to minimizing risks, product recycling and stock management [186]. GlaxoSmithKline, the largest pharmaceutical company in the UK, did very well on medicine waste management that approximately 82% of their waste were reused or recycled in 2011. Another inspiring news was that tens of essential medicines, include Tylenol, Motrin, calcium and vitamins, have already produced in also child size, to reduce the possibility of potential accidental poisoning and overdose. However, these improvements and solutions are high cost ones, which are only possible to the largest pharmaceutical companies in the world. Besides, these improvements cannot satisfy all the expectations from both healthcare payers and pharmaceutical companies in a relatively short period, for example, 5 years. Hence, most of challenges are still blocking the development of pharmaceutical industry, as they have not yet been relieved or solved in very suitable and economical ways.

8.1.2. Personalized Medicine

Personalized medicine or PM, as a technological advancement that enables practitioners to identify and treat individual patients based on unique characteristics, is one of the most promising products in pharmaceutical industry [187-189]. Generally, it proposes the customization of healthcare with medical decision, practices and products tailored to the individual patient and mainly has three potential applications: pharmacogenomics, cancer management and customized drug products. Pharmacogenomics is the application of personal genomics to clinical medicine [189] and cancer management includes testing in cancer cells, defining prognosis and suggesting the most likely-to-succeed treatment options for individual patients [190, 191]. Customized drug products generally contain several drug substances in particular respective doses, specifically for individual patients. They are usually prescribed by physicians who have wide discretion and then the prescriptions can be custom-produced. Since customized drug product is more based on simpler characteristics such as age, weight and drug sensitivity, instead of complex genetic information, it has the higher possibility to be achieved in the next several years. With the help of an individual database, the symptom, the efficacy and bio-availability of medicines and the prescription record of a patient can always be tracked and studied and thus improve the quality and the safety of treatment.

Hence, patients, the pharmaceutical industry, and society can all be the beneficiaries from the developments of customized drug products: Because of the precisely selected drug substance, the medicine waste can be easily managed within manufacturing, sale and patient healthcare, and the risk of overdose can be significantly reduced. Besides, customized poly-pills and child size medicine, both the potential products of such customized drugs, can highly contribute to the development of medicinal products for the aged, the disable and the young patient healthcare respectively [192]. Although there are truly tens of compounding pharmacies existing in some of the Western countries, particularly in the United Kingdom and the United States [193], the extremely high costs of raw drug material, operating, labor and pharmaceutical machines are still the barriers for the development of customized drug product. Thus, both medicine specialists and engineering researchers have tried to discover the alternative methods and applications to produce personalized healthcare products, for example, the use of printing technologies (Figure 8-2). The first solid free-form fabrication printer, which can form tablets using pharmaceutical-grade materials, was designed and produced by

Massachusetts Institute of Technology (MIT) scientists in 1997 [194]. Their drug printer operates by dropping drug doses onto thin layers of fine powder. The tablet was finally formed when the doses were bound layer by layer with pharmaceutical-grade binder. They reported hundreds of pills could be produced at one time and the printing forms with higher dosage would be possible as the drug suspensions could overcome drug solubility limits and uni-axial compression could reduce tablet volume. In University of Glasgow, Lee Cronin and his team is developing a revolutionary new technique using 3D printer to print special drugs [195]. The principal of the drug printing technique is to print the last reagent first and then build other chemical layers above, finally adding a liquid at the top; this liquid flows into the layer in sequence and until at the bottom, the final drug product will be the same as prescription.

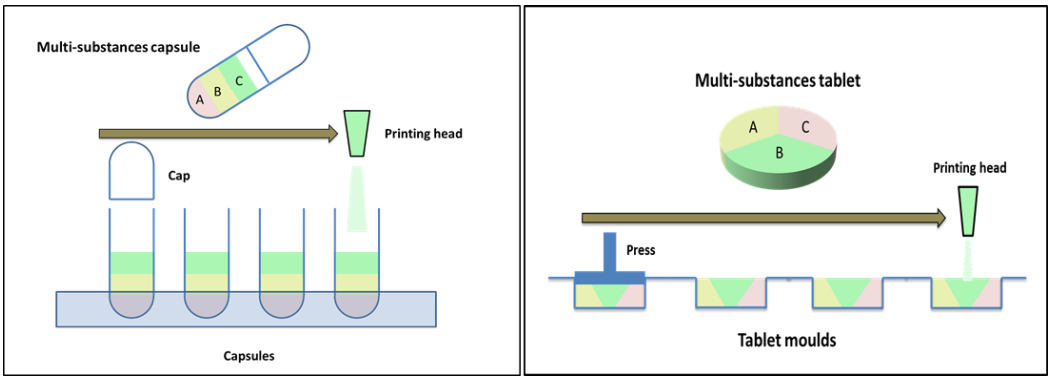

Figure 8- 2 The scheme of producing multi-substances capsules and tablets by printing technology

8.2. Dry Powder Libraries Fabrication by Printing Technology for High Throughput Screening

High-throughput screening (HTS) and combinatorial searches for the discovery, development and optimization of functional materials have been widely accepted in many new materials discovery including superconductors [196], heterogeneous catalysis [197, 198], sensors [199, 200], luminescent materials [201, 202], solid-state battery materials [203, 204], fuel-cell materials [205], coating materials [206], novel magnetic materials [207, 208], and dielectric and ferroelectric materials [209-211]. However, HT biomaterials discovery and screening is still in infancy. Recently, Hook et al. [212] reviewed high-throughput discovery of biomaterials using polymer microarrays

for many cell-based applications including the isolation of specific cells from heterogeneous populations, the attachment and differentiation of stem cells and the controlled transfection of cells. Simon and Lin-Gibson [213] has reviewed advances in utilizing combinatorial and high-throughput methods to better understand cellmaterial interactions and fabrication techniques to generate controlled surfaces (two-dimensional) and three-dimensional cell environments as well as methods to characterize and analyze material properties and cellmaterial interactions.

Although the first combinatorial approach to materials research is often attributed to Edison and Ciamician around 100 years ago [214], it was first conceptualized by Joseph Hanak in 1970 [215] but awaited the advent of computational data storage and handling. The first report of the rapid, automated synthesis of diverse organic molecules appeared in the late 1960s [216]. At that time, pioneers like Merrifield used polypeptide-synthesis machines to automate the rapid production of diverse amino acid sequences [216].

High-throughput (HT) methodology is a scientific approach to realize the rapid discovery, study, and optimization of new materials often accompanied with other relevant techniques including precise sample dispensing and metering, rapid synthesis, high throughput characterization, and massive data processing to manage and analyze large numbers of diverse material compositions [217]. They were initially widely adopted in the pharmaceutics industry for the discovery of drugs, involving a large amount of chemicals simultaneously [218, 219]. With its promise to speed up the discovery and development processes, high throughput technologies have been explored and developed for fast increasing requirements in a number of materials such as biomaterials, polymer-based materials, functional materials, and catalysts [217].

Libraries can be discrete, continuous, or random and can be constructed by thin film methods [220, 221], solution-based [222] inkjet printing methods [223-226] and/or by dry powder mixing [28, 147, 227, 228]. Though thin film technologies have been widely adopted for HT library synthesis, unsurprisingly, it is found that there is sometimes a lack of correlation between the properties of materials in thin film form and bulk. It has difficulties in achieving homogeneous mixing of solid-multi-layer thin films, and there exists a huge deviation in physical and chemical properties of solid-state materials using this thin film format.

Solution methods are complex and labor-intensive processes that are sensitive to handling procedures, for example experimental conditions, pH value, and nature of

solvents etc. [217]. The majority of small-molecule libraries generated to date have followed a solid-phase format for ease of isolation and purification of products, coupled with the ability to drive a reaction quickly to completion and then by-products and excess reagents simply removed by a washing procedure. The solution phase allows mixing at the molecular level, which reduces the need for high-temperature interdiffusion and also facilitates the isolation of metastable phases. It has several advantages: few reactions have been adapted to solid phase, and some reactions are incompatible with the heterogeneous nature of insoluble polymer supports. Although solid-phase synthesis can produce large sample libraries, utilizing the split/pool technique to afford small amounts of compound, solution-phase synthesis is often applied to lead development capable of affording larger quantities of material.

However, for many insoluble materials or materials with low solubility, such as most of bioceramics, for example, bioglass, hydroxyapatite and β-Tricalcium Phosphate, it is difficult or impossible to make solutions of these materials other than suspensions or slurry. To make stable suspensions, large amount of experiments are needed to find the best combination of additives such as dispersants, or to change pH value, or to use various solvents [229]. Though good suspensions can be optimized and achieved for individual materials, they may not able to be mixed into a uniform mixture due to different dispersants, pH or solvents used [230]. The removal of the dispersants and solvents have also negative impact into the following steps of screening, for example, the residual of the additives could be toxic to the cells. During the drying of the libraries, non-uniform pattern could be formed due to “coffee stain effect” [231, 232]. Therefore, a library started from dry powder mixing would have advantages.

The libraries based on dry powder mixing provide starting materials which can not only be used to synthesize thin film with different deposition methods (laser sintering, sputtering, and evaporation) and masking techniques (physical masks and photolithography) but also to prepare solutions an slurries consisting of nano-particles suspended in either water or an organic solvent. Such solutions or slurries are very useful for measuring and mixing the starting materials for combinatorial processing. Solid-phase peptide synthesis methods has been adopted for the combinatorial production of large numbers of different compounds [219]. Solid-phase beads were recombined, mixed and again split to repeat this process [219]. This method has also been used for producing short oligonucleotides [218], and more recently, with the advent of microwave induced solid-phase synthesis, has been used to produce nonlinear organic molecules [233].

8.3. Dry Powder Libraries Synthesis and Capsule Filling with Dry Powder Printing Technique

8.3.1. Design of Powder Printing Technique

The experimental works on powder printing application were completed by using a dry powder printing platform which was based on a modified RepRap® 3D printer (Figure 8-3). The platform employs a clear and simple interface to control the printing process with G-code. The printing target is composed of a 96-wells microplate which can be used for dry powder libraries synthesis and 0# and 1# capsules for capsule filling test.

Three ultrasonic dispensing devices (printing head) were assembled on the platform in a triangular arrangement for multi-component printing tasks. Thus, the printing area on the X-Y motion table needs to be defined and calibrated in coding (Figure 8-4). The specification of both the printer platform and the printing target is listed in Table 8-1.

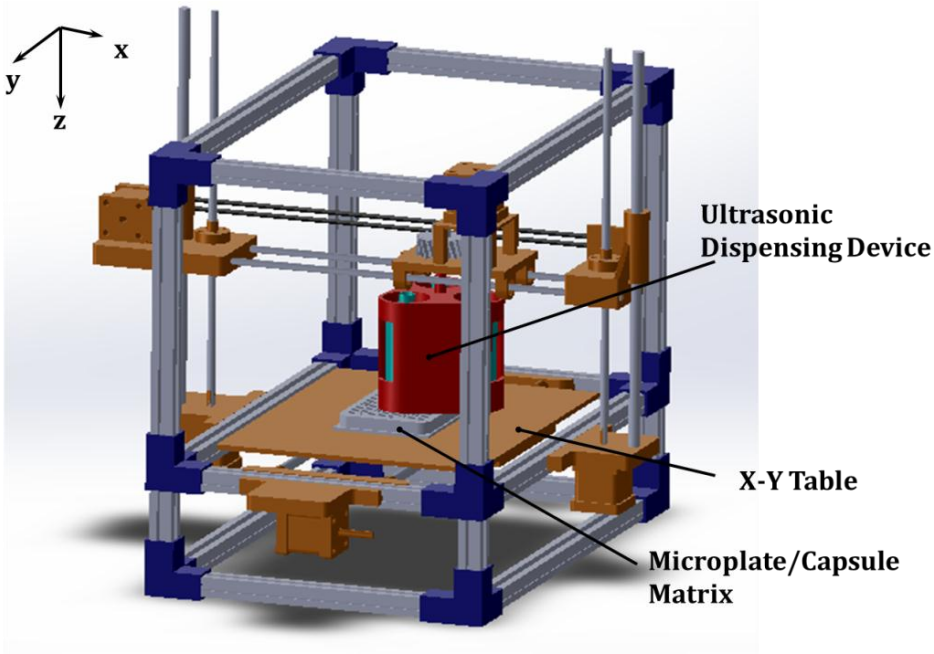

Figure 8- 3 Sketch of dry powder printing platform

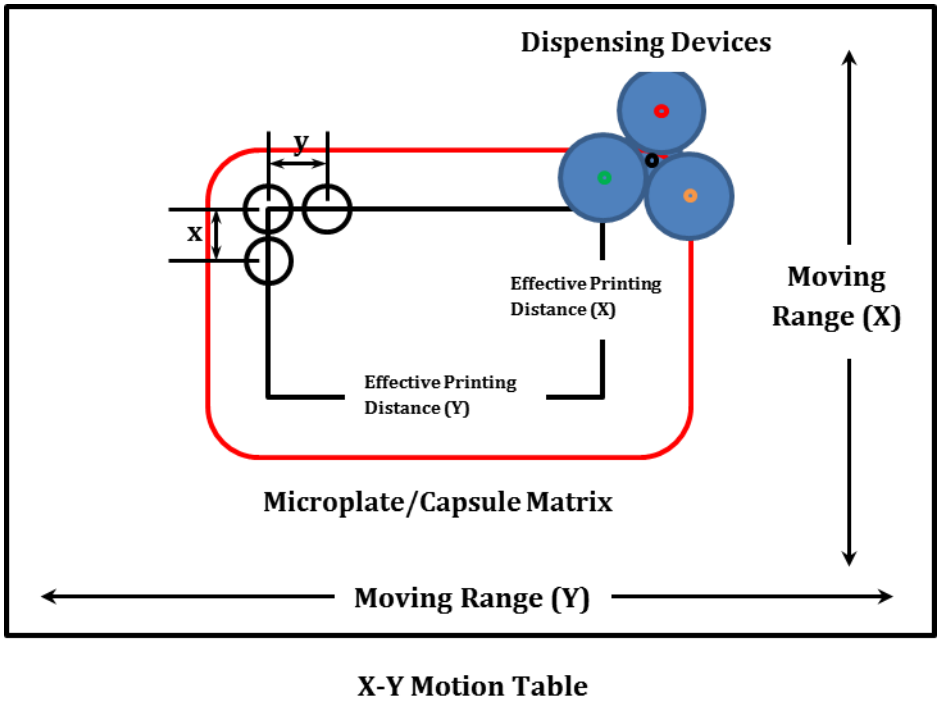

Figure 8- 4 Schematic diagram of printing area definition and calibration on powder dispensing platform

Table 8- 1 Specification of X-Y motion table and dispensing target

Specification	
Maximum moving range on X-Y table in x-axis	135.0 mm
Maximum moving range on X-Y table in y-axis	150.0 mm
Number of wells per row (y-axis)	12
Number of wells per column (x-axis)	8
Distance between well centres (y-axis)	8.75 mm
Distance between well centres (x-axis)	8.75 mm
Effective printing distance in x-axis	61.25 mm
Effective printing distance in y-axis	96.25 mm
Depth of well	16.45 mm
Diameter of well	6.85 mm
Depth of 0# capsule body	18.44 mm
Internal diameter of 0# capsule body	7.13 mm
Depth of 1# capsule body	16.61 mm
Internal diameter of 1# capsule body	6.43 mm

8.3.2. G-Code and Dispensing Test

Before testing the overall powder dispensing performance of the printer, the G-codes generated for the moving path and the dispensing were tested separately. The path test helped to improve the accuracy of printing head movement and the dispensing benefited by the precise timing control. Meeting the requirement of powder printing in all 96 wells, the created code file represented two forward paths and one reversed path, which were the moving paths for dispensing all three substances, shown in Figure 8-5.

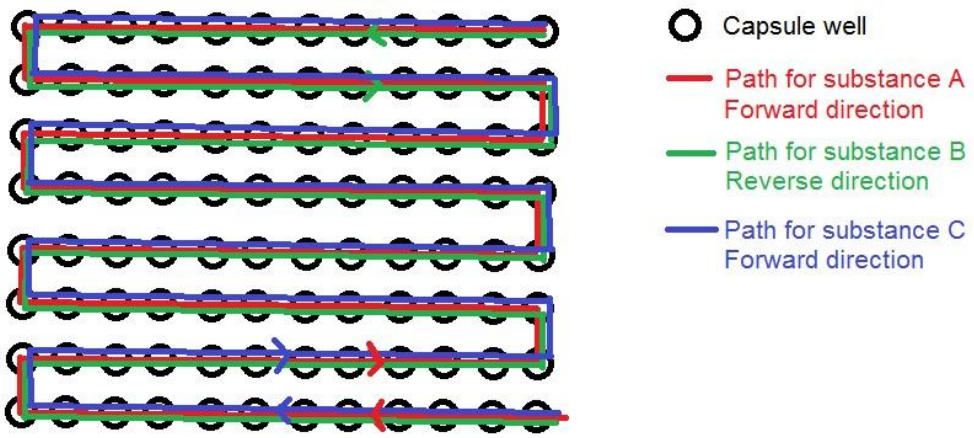

Figure 8- 5 The demonstration of the moving path for powder dispensing

The dispensing test for 3D dry powder printing was to investigate the flow pattern of dispensed powders in volume which determines the optimal vertical distance between the nozzles and the capsules.

After calibration, a nano-biomaterials proportion gradient library was synthesised with hydroxyapatite and β-tricalcium phosphate. The capsule filling has been demonstrated with Inhalac®230 in 0# capsules and three components capsules were fabricated with successively filling different colour dyed inhalation grade lactose powders in 1# capsules.

8.4. Results and Discussion

Solid dosage forms are prior consideration in personalized drugs. First of all, chemicals and drugs are most stable as dry powders. They are packaged, transported,

administered, and stored more easily than are drugs formulated in solutions or suspensions. Secondly, solid dosage forms, such as tablets and capsules, possess more chemical and physical stability and less undesirable taste when substances are in solid form than when in solution. Moreover, when it was packaged in blister packs can also enhance the stability of tablets. Besides, more accurate dosing is facilitated with dosage forms furnished as individual units, such as tablets, capsules, and divided powders. At last, controlled release is much easier to achieve with solid dosage forms than with liquids. Although the solid dosage forms have these advantages comparing with liquids, the challenge always exists in industry to dose powder material accurately and reproducibly into the capsules, blisters or reservoir containers of drugs especially when each capsule or blister is required to be filled with micro mass ingredients. Currently available powder dispensers have a few limitations in dispensing such small amounts of micron-sized powders, e.g. expensive, time consuming and require high levels of operational complexity. Most importantly, it is the drug content uniformity in each dosage which assures consistent therapeutic benefits in patient [234].

8.4.1. Positioning Path Test

Base on the data, a map of the actual and the theoretical positioning results was created as Figure 8-6 shown.

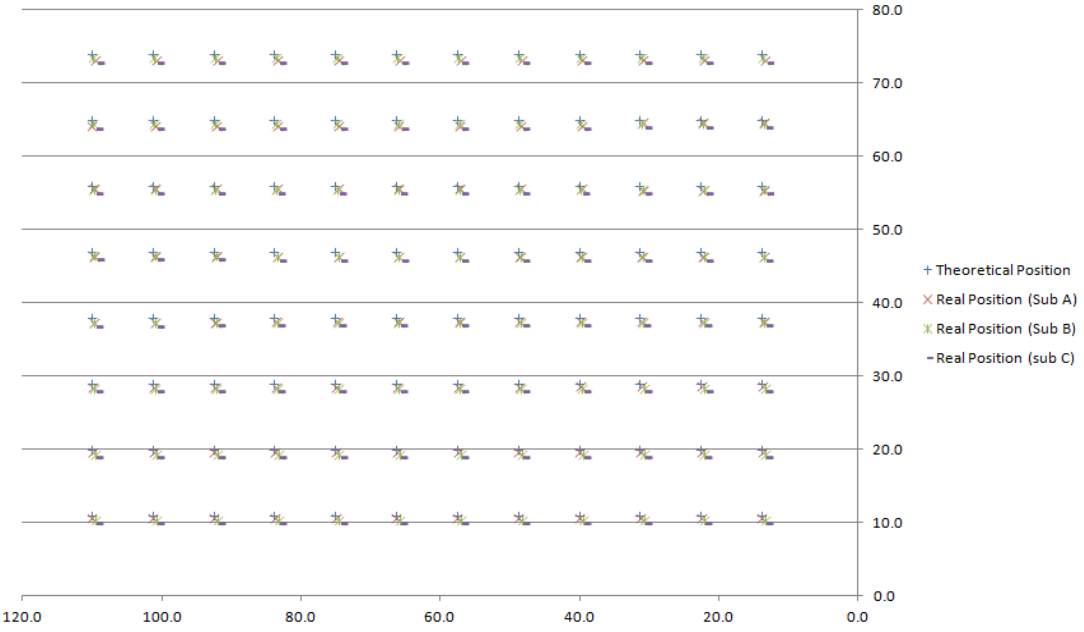

Figure 8- 6 Map of both theoretical and real resultant positions of printing process (unit: mm).

In Figure 8-6, it was easy to find that the values of error increased from the positioning process of substance A, to the positioning process of substance B, and finally to the positioning process of substance C. Notice that the positioning path of substance was a reversed one and thus the largest errors were reflected in the positioning of dispensing device B to the last capsule wells, which were at the right-bottom corner of the well plate. Statistic Table 8-2 provides more details of the results.

Table 8- 2 The relationship of error and capsule sequence

	Error range (unit: mm)					
Capsule Sequence	**Dispensing device A**		**Dispensing device B**		**Dispensing device C**	
	Y axis	X axis	Y axis	X axis	Y axis	X axis
1-23	-0.2 to -0.2	-0.4 to -0.4	-0.3 to -0.4	-0.4 to -0.5	-0.9 to -0.9	-0.5 to -0.6
24-47	-0.2 to -0.4	-0.4 to -0.7	-0.4 to -0.5	-0.4 to -0.5	-0.9 to -1.0	-0.6 to -0.7
48-71	-0.4 to -0.5	-0.7 to -0.9	-0.5 to -0.6	-0.4 to -0.5	-1.0 to -1.0	-0.6 to -0.7
71-96	-0.5 to -0.6	-0.9 to -1.0	-0.6 to -0.7	-0.4 to -0.5	-1.0 to -1.1	-0.7 to -0.8

8.4.2. Capsule filling Test

Dispensing test included two sections: dispensing volume test and mass accuracy test. The dispensing volume test was to obtain a visualization of dispensing volume to determine an optimal vertical distance between the end of hopper and the capsules and wells. The dispensing volume could be either a cone or a stream (Figure 8-7), which was affected by the properties of powders, the orifice size, hopper angle and vibration characteristics.

For free flowing powder, the flow is in form of an approximate stream and the extent of the stream is very close to the orifice size. The orifice size can be selected with the ratio to the particle size in the range of 4-6 times for free flowing powders with particle size smaller than 200μm. For free flowing powder with 200μm mean particle size, the height of the orifice to capsule/well needs to be less than 20mm, by exceeding which the drug would be sprayed out of the 1# capsule.

The discharge rate of materials can be predicted by the discharge rate equation for free flowing powder:

$$W = 0.85\rho_B\sqrt{g}(D_o - kd)^{2.5}\left(\frac{D_o}{d}\tan\alpha\right)^{\mu} \qquad \alpha < 25° \tag{7.15}$$

By using this equation, the dispensing hopper can be determined with the information of drug materials. Besides, it is programmable that different masses of powder can be dispensed into capsule/well corresponding to the specified duration. The resultant values of obtained doses are listed in Table 8-3, with the duration of vibration. As the volume of capsule and micro-well is a constant, the filling dosage can be obtained for homogeneous printing and gradient printing. The dose mass, M, can be given for homogeneous printing,

$$M = W \cdot T_d \tag{8.1}$$

and for gradient printing,

$$M = \begin{bmatrix} T_{1,1} & \cdots & T_{m,1} \\ \vdots & \ddots & \vdots \\ T_{1,n} & \cdots & T_{m,n} \end{bmatrix} \times W \tag{8.2}$$

where T_d and $T_{m,n}$ are vibration duration in second.

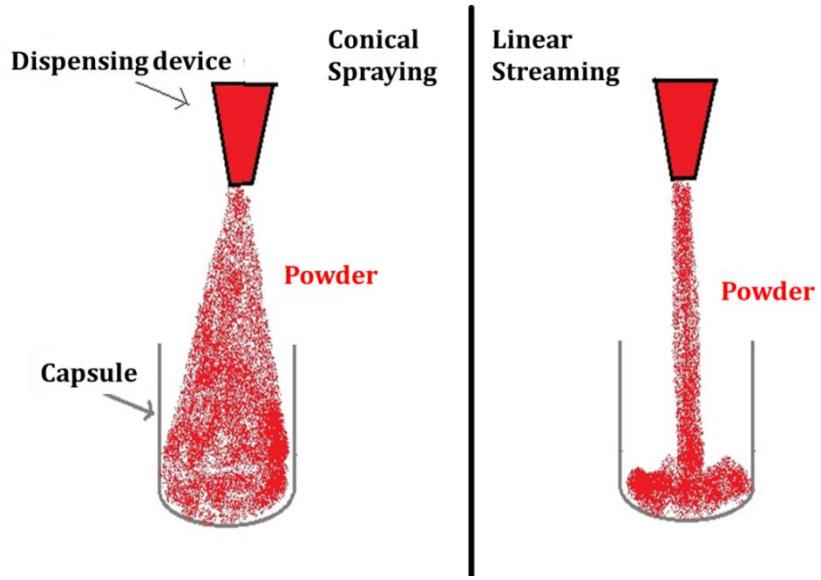

Figure 8- 7 The possible flow pattern of dispensed powders in volume: left-hand-side is conical spraying and right-hand-side is linear streaming

Table 8- 3 Results of dispensed doses

Test	Oscillation Duration /ms	Mean Value /mg
1	50	56.2
2	100	161.4
3	200	239.7
4	400	513.4
5	1000	1205.3

The results of dispensing may have variations for some material, as shown in Figure 8-8. Thus, the powder should be pre-treated to have uniform properties and fineness. Besides, the selection of hopper orifice, hopper angle and voltage amplitude has to be very careful and based on the powder properties.

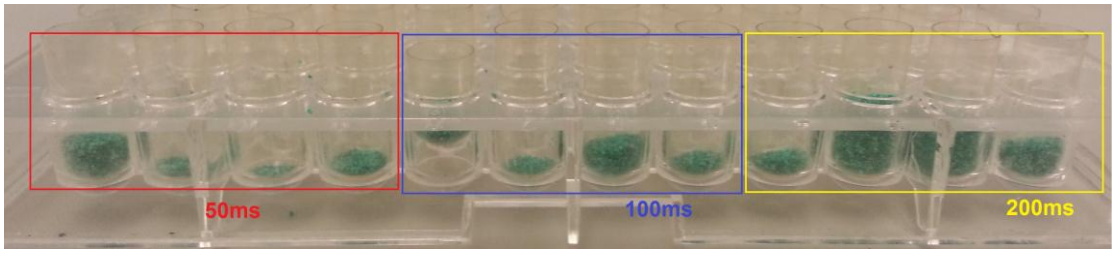

Figure 8- 8 Visualized variation of printing results in 1# capsule with different duration of vibration.

With this printing technology, the release time of drug pills can be easily controlled by defining the placement of drops in the mould, and therefore provide a better match the pharmacology of drug absorption. A three ingredients capsule filling has been demonstrated with dyed inhalation grade lactose powder shown in Figure 8-9. The ratio of three components yellow, green and red was 1:1:2 in which the amount of component yellow/green was 1± 0.1 mg.

8.4.3. Libraries Fabrication with Dry Powder Printing Technology

The desktop powder printing platform is assembled from ultrasonic powder micro-dispensing device and a numerical controlled 3D table. The platform is used for high throughput powder library fabrication and filling of pharmaceuticals capsule and blisters for dry powder inhalers (DPI).

Different biomaterial powders were loaded into different ultrasonic dispensers which were independently controlled and mounted on a computer controlled 3D table. Different amount of the powders were dispensed into each well of microplate according

to the library design. The microplate can move along x-axis and y- axis at high speed (Figure 8-10). When more than one dry powder were dispensed in each wells, a vortex mixer (SA8, Stuart®, Bibby Scientific Limited, UK) was used to mix prepared samples within the microplate after the dispensing of all of the powders. A high throughput ball milling machine can also be used for a better mixing [235].

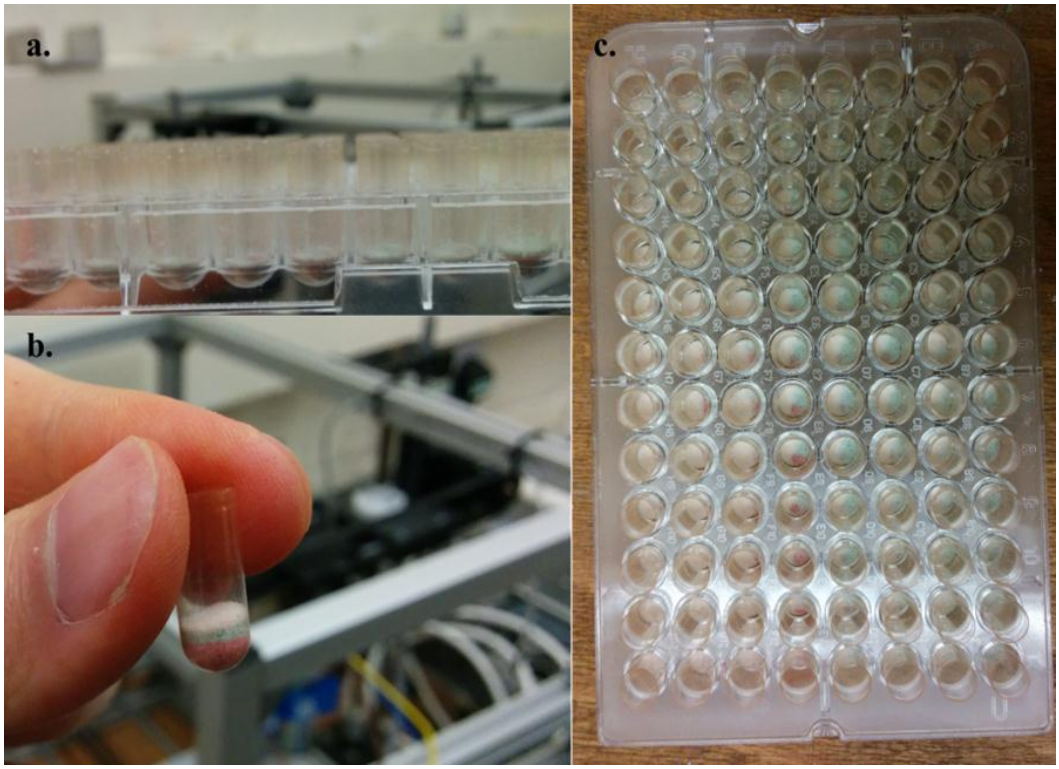

Figure 8- 9 Three ingredients capsule samples fabricated by dry powder printing platform, (a) side view of capsules in a same row; (b) single printed capsule; (c) top view of 96 capsules printed on the platform

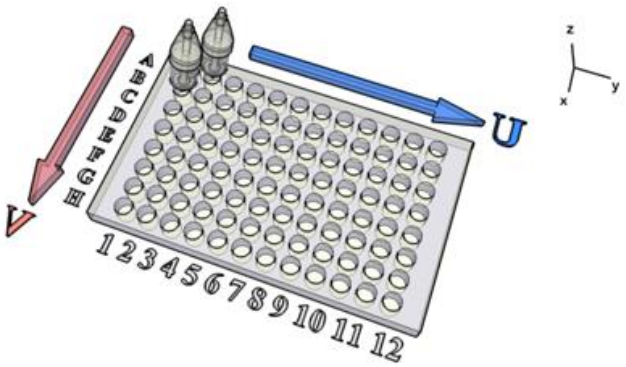

Figure 8- 10 Schematic diagram of HT library fabricated in a microplate using the dry powder printer with two independently controlled dispensing units in which different powders were loaded

By the dispensing of controllable powders dosage using the micro-dispensing system, different type of libraries can be designed and fabricated.

The HA, TCP and HA/TCP mixture libraries can be fabricated following the designs in Figure 8-12 . For library fabrication strategy represented in blue, different dosage of single material A is dispensed in different columns of the microplate (for example, 1mg in column 1, 2mg in column 2, etc). In each column, the wells are filled with same dosage. This design can be used for further dispensing of different solvents in different rows, to build a library with variable concentration of biomaterials in different solvents. This library can be used to screen solubility or effect of concentration of biomaterials in further experiments. As shown in red color, a similar library of material B can be designed with variable dosage at different rows. Those two libraries can also be mixed to form another library, by dispensing two different materials into one microplate using two nozzles, to produce a mixture of two different dry powder biomaterials with variable composition. According to different experimental requirement, more complex combinations can be achieved by changing strategy of dispensing two materials with different amount of dosage and accompanying with xy table to offer a positioning dispensing. An example of a Merck®HA library following the design of Figure 8-12(a) is shown in Figure 8-11(a), and a TCP library following the design of Figure 8-12(b) is shown in Figure 8-11(b).

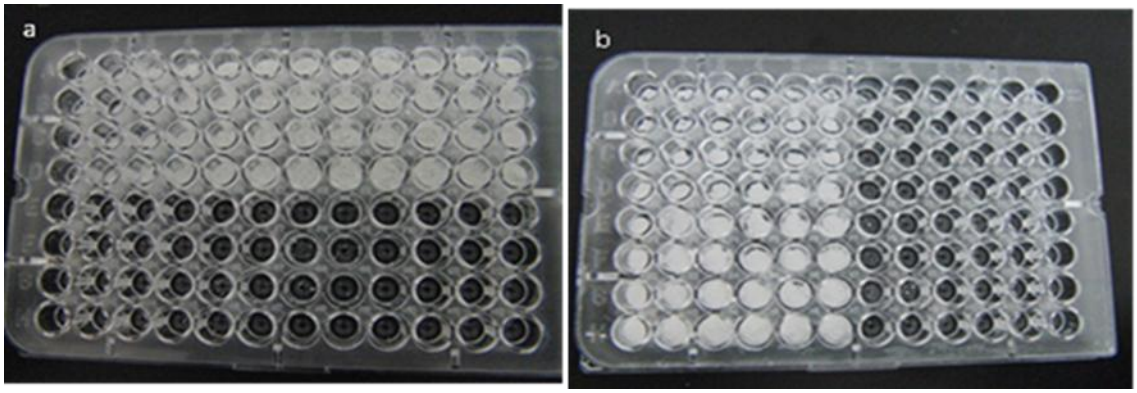

Figure 8- 11 Dry powder biomaterials libraries fabricated in the microplate (a. Hydroxyapatite; b. β-TCP)

8.5. Summary

The feasibility of dry powder printing technology has been demonstrated in the production of solid dosage forms. It provides the possibility of producing personalize

medicine in the near future, and would lead to more rapid development timeframes, from early stage clinical trials to on-line production at a reduced cost.

Ultrasonic micro-dispensing system was used to fabricate nano size hydroxyapatite and β-tricalcium phosphate dry powder libraries for high throughput screening. Different biomaterials powders with different particle size, particle shape, flowability and particle size distribution have been successfully dispensed. The dispensing speed could be as high as one dosage per second with controllable dispensing mass from micrograms to milligrams for each dose. A few different library layouts have been designed and fabricated to demonstrate the feasibility of this method which provides a platform for high-throughput experiments.

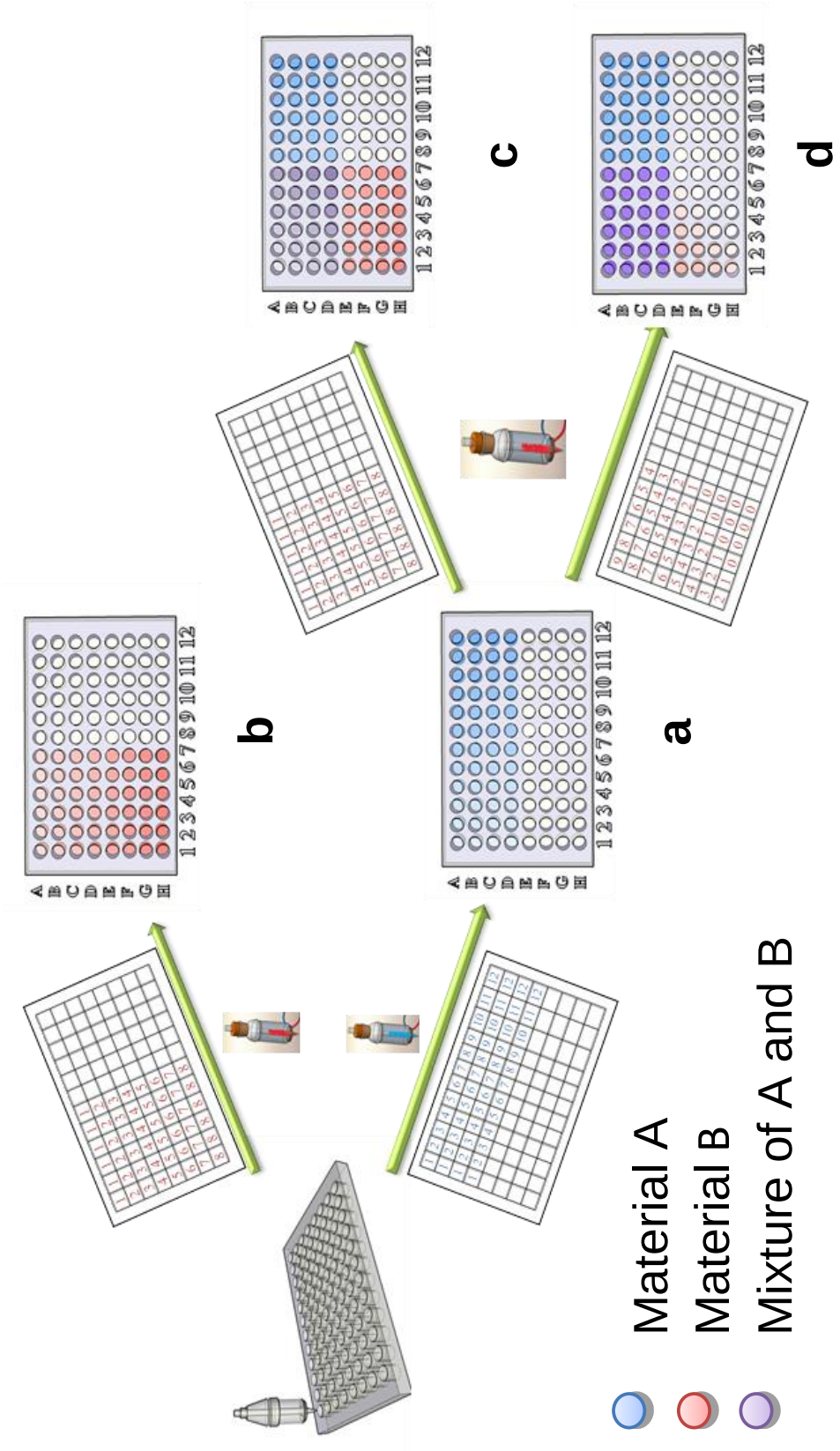

Figure 8- 12 Scheme of fabrication of HA, TCP and HA/TCP mixture libraries with micro-dispensing system

Chapter 9

Conclusions and Further Works

The aim of this Ph.D. was to investigate bulk solids fluidizing process under the influence of vibration and develop a bulk solids micro-dispensing technique taking account of material properties, device design and processing parameters. The works also included demonstrating the dispensing process with active pharmaceutical ingredients (API), excipients and biomaterials fine powders and coarse granules. The other objective of this project is to develop mathematical models to correlate dispensing results, i.e. discharge rate, dosages consistency, with device design, vibration signal parameters and materials properties. The derived equation can be used to predict dispensing results and supervise practical applications.

9.1. Conclusions

There are two main threads to the work undertaken: an experimental investigation of vibration induced bulk solids micro-dispensing, and a computational modelling for ultrasonic vibration dispensing.

9.1.1. Experimental Investigation of Vibration Induced Bulk Solids Micro-Dispensing

9.1.1.1. A micro-dispensing hopper made of borosilicate straight tube was designed with setting up three main geometry parameters: orifice size, angle of nozzle and diameter of vertical section of hopper. A computer controlled auto dispensing and weighing system were developed to verify dispensing dose mass and evaluate the dispensing results such as mean dose mass, flow rate and deviation between doses.

9.1.1.2. An electromagnetic hammering device has been demonstrated to dispense an irregular shaped and porous hydroxyapatite granule. Granules formed a bridge above the outlet of hopper to prevent the flow under the gravity. The bridge formed has a width smaller than a critical diameter determined by material properties and stress state of bulk solids. For HA granules, horizontal vibration provided by electromagnetic hammering was proved effective to

initiate the in-tube flow by agitating the rearrangement movement of granules in the hopper. The position of electromagnetic hammering to the dispensing hopper and frequency of hammering were proved to have the influence on the flow rate and dosing conformity.

9.1.1.3. An eccentric rotating motor induced vibration has been demonstrated as a feasible vibration mode to dispense hydroxyapatite granules. The ERM forces the dispensing hopper into vibrating in the horizontal plane. For a constant dispensing process, the dosage was found linear to the duration of vibration. The flow rate and dosage conformity are subjected to the output of vibration motor and the design parameters of dispensing hopper such as orifice diameter.

9.1.1.4. An ultrasonic controlled micro-dispensing system was demonstrated as a feasible method in dispensing inhalation grade micron-sized lactose powders. The dispensing with ultrasonic vibration device is subjected to a doming controlled flow mechanism. Besides the design parameters of dispensing hopper, the duration of vibration induced by pulse wave is a key factor to control the dosage. With better dosing conformity, the dosage is linear to the duration of vibration and thus the flow rate is a constant. The amplitude of ultrasonic vibration also affects the flow rate and dosage conformity.

9.1.1.5. The micro-dispensing system was also used to dispense fine pharmaceutical and biomaterial powders (particle size less than 10μm). The powders with particle size below 10 μm exhibit an “extrusion” discharge mechanism. The system was proved suitable for low doses (as low as a few milligrams) dispensing of powders with wide particle size distribution and cohesiveness. The hopper design parameters, amplitude and duration of vibration affect the mean dosage and dosage conformity. The dosage shows a nonlinear relationship with duration of vibration due to the strong cohesion and poor flowability of non-free flowing fine powders.

9.1.1.6. The glass vibrating hopper often leads to a severe problem on powder dispensing due to triboelectric charging generated during the sliding and collision between particles and glass wall. The charging will change the flow behaviour of powders and it may cause a decreasing flow rate and irregular variations in dispensed dosages. For finer lactose powders, the charging rate

is higher than the coarse one. A Pt-coated glass hopper was demonstrated in ultrasonic vibration dispensing device. The modified surface of dispensing hopper has effectively reduced the accumulated charge in the vibrating powder bed and therefore the dispensing consistency has been improved and the flow rate is increased for pharmaceutical excipient powders. The dose weighing and charge measuring tests have shown the evidence of the favourable influence of modified glass nozzle on the triboelectric charging issue and meanwhile a further improvement on fine powder dispensing can be expected.

9.1.1.7. A powder printing platform is built by integrating ultrasonic vibration dispensing device with 3D printing technology to demonstrate the feasibility of producing solid form oral drugs and pharmaceutical/biomaterial dry powder libraries for high-throughput screening (HTS) of new products. It provides the possibility of producing personalize medicine in the near future, and would lead to more rapid development timeframes, from early stage clinical trials to on-line production at a reduced cost.

9.1.2. Computational Modelling for Discharge Rate in Ultrasonic Vibration Dispensing

9.1.2.1. Based on mass flow equations of bulk solid extended from Torricelli's law, the discharge rate of powder from ultrasonic vibration dispenser is proposed proportional to $\rho_B\sqrt{g}D_h^{2.5}$ and influenced by particle size, hopper orifice size, hopper angle and ultrasonic vibration.

9.1.2.2. The discharge rate is proposed proportional to $(D_o - kd)^{2.5}$, where k is a constant related to the surface properties of particle and powder flowability. The value of k increases with decreasing flowability.

9.1.2.3. The discharge rate is proposed proportional to $\left(\frac{D_o}{d}\tan\alpha\right)^{\mu}$ when powder is discharged in mass flow pattern, whereas the discharge rate was found influenced by the size and shape of stagnant zone in core flow pattern. An approximate equation is proposed for core flow in the absence of stagnant zone information. The constant μ is related to powder flowability. The value of μ increases with increasing flowability.

9.1.2.4. Ultrasonic vibration influences the discharge by accelerating particles prior to flowing out of the hopper. The effective gravity acceleration for the powder is presented by $\gamma^2 g$, where coefficient γ depends on various factors such as cohesion of particles, powder flowability, vibration characteristics.

9.1.2.5. The discharge rate of inhalation grade lactose powder can be well predicted by derived correlation. The coefficients in these equations are sufficiently constant to use for inhalation grade lactose and pharmaceutical powders with similar properties. The correlation also provides a possibility for the ultrasonic vibration micro-dispensing device to be applied to evaluating the flowability of powder material with factors k, μ and γ in dispensing test.

9.2. Further Work

The results presented in this thesis introduce new questions about bulk solids micro-dispensing technology and a number of avenues for further research are listed in this section.

9.2.1. Stress State and Flowability Tests for Bulk Solids

Shear tester is a common tool for measuring stress state of bulk solids and flow function. However, the measurement data is inappropriate to be used for analyzing the flow of powder in the ultrasonic vibration dispenser from conventional static shear cell test, which is invalid to give the accurate information of stress state and flow function for bulk solids in a vibrating hopper.

For testing the vibration induced powder flow behaviour, a vibrating direct shear tester designed by Kollmann and Tomas [109] can be used, which was based on the test apparatus developed by Roberts et al. [99]. Two test arrangements are possible to carry out shear tests in the presence of vibrations:

(a) Vibration of the top half of the shear cell:

The shear base is fixed and the vibrations are applied to the horizontal plane, perpendicular to the shear direction. This arrangement allows the measurement of powder flow properties needed for storage and handling equipment design, including wall friction angle, as functions of the vibration parameters.

(b) Vibration of the whole shear cell:

The whole shear cell is located on a vibrating plate, which is mounted on vertical leaf springs. On the shear base and the shear ring, one piezoelectric accelerometer is located on each for measuring the base- and the response- vibration acceleration a_e and a_r respectively. The ratio a_r /a_e can be used to determine resonance and damping behaviour of powders and the influence of resonance on shear strength.

Nevertheless, the vibrating direct shear tester is still incapable of simulating the real environment in the ultrasonic vibration dispenser. Thus, we are thinking about developing the possibility of ultrasonic vibration micro-dispensing device being applied to evaluating the flowability of powder material with flow-related factors, such as k, μ and γ for fine pharmaceutical powders flowing in the vibrating vessel. It may have advantages, such as fast, small sample usage especially valuable for those high value drug materials with limited availability, and low cost.

9.2.2. Vibration Measurement

In this project, we employs different types of vibration to enhance bulk solids flow in the hopper, we've investigated the influence of wave signal frequency and amplitude on the dispensing. However, the mechanism of vibration output influencing the flow of bulk solid in the hopper is not well known yet. We are thinking about using 3-dimensional laser Doppler vibrometer to measure the vibration output of vibratory dispensing device. However, there are a number of issues needs to be considered before measuring.

- Due to the complexity of the dispenser's structure, a spatial calibration is required to establish the physical positions of the three laser heads with respect to the vibration source, dispensing hopper and the nozzle section, respectively.
- The validity of the calibration and nozzle geometry data will be inspected by scanning the nozzle surface and checking for signs of misalignment between the three laser beams. The relatively small size of the nozzle means that the surface area may be not sufficient to perform the spatial calibration with satisfactory accuracy.
- The inclined wall of conical hopper may affect the alignment of the position coordinate. In order to find the optimum spatial location on the nozzle for vibration measurements, more individual positions and times of measurement are needed to obtain statistically representative spectra.

9.2.3. Interparticle Forces Investigation

The main challenge for the ultrasonic dispensing technique is to handle ultrafine powders which consist of particles less than 1 μm exhibiting very strong cohesion and poor flowability. For some of powder materials, the current ultrasonic vibration applied is less effective to initiate the flow.

We have used high speed camera to investigate the flow and discharge behaviour of bulk solids in vibrating nozzle. We are working with Professor John Shrimpton's research group in University of Southampton using the Discrete Element Method (DEM) to simulate ultrasonic vibration dispensing described in this work in order to identify the internal mechanism that allows the flow to be controlled so precisely.

A parametric study has been conducted on the cohesion and friction properties of the particles in the simulations. It has been found that both friction and cohesion have an effect on the doming phenomena; during vibration cohesion has a clear inversely proportional effect on outflow rate and friction is required for doming to occur. The discharge rates from the dispensing tests have been compared with the DEM simulations. The range of parameters used includes cases in which the particles do not dome during the filling phase, the experimental results lie between the cases of doming and the cases that dome-free.

The doming controlled flow mechanism needs to be further studied. There is a lack of statistical data to characterise the absolute magnitude of cohesive forces for inclusion in a DEM model. Research to quantify inter-particle cohesive forces needs to be undertaken, especially for those non-free flowing powders.

9.2.4. Dispensing of Pharmaceutical Blends

Volumetric dosator is widely used in pharmaceutical industry to fill active pharmaceutical ingredient (API) in dry powder inhalers, which requires uniform mixing API with coarser carrier particles such as lactose to provide sufficient flowability. The feasibility of ultrasonic vibration micro-dispenser in directly dispensing pharmaceutical blends is therefore worth to be investigated. And the problems in dispensing blends need to be considered.

- The surface morphology and higher ratio of the carrier may affect efficient dispensing of the API [236]. What's more, the strong interparticle forces

between API and carrier could affect uniformity of mixed powders and therefore, DPI efficacy.

- Electrostatic charging has significant effect on powder blending performance. Non-uniform mixing of API and excipient may cause accumulated charges in the blend in dispensing. The accumulated charge brings strong inter-particle force to the particles and its adjacent particles in the vibrating hopper where the flow may get retarded. The influence of electrostatic charge on adhesion forces between drug and excipient particles needs to be investigated.
- The active pharmaceutical ingredient (API) concentration may be changed in blend after getting charged in vibrating dispensing hopper. The correlation between the API concentration variation and the charge-to-mass ratio of the blend samples needs to be examined.
- Although the Pt-coated glass hopper described in Chapter 6 can improve powder flowability by reducing electrostatic charging in powder dispensing, the charging behaviour of particles in powder dispensing process has not been fully studied and solved with the method mentioned in this thesis. More investigation needs to be undertaken on the charging characteristics of different materials and using antistatic material to make dispensing hoppers is in discussing.

Appendix I

Particle Size Measurement with Laser Diffraction Method

Cohesive fine powders may contain agglomerates of particles that are held together by particulate interactive forces. Since agglomerates will be measured as large particles by most particle sizing methods, complete de-agglomeration and particle detachment in the medium is necessary to ensure effective particle size measurement of all particle distributions [41].

The particle size of non-free flowing powders was measured by laser diffraction (Malvern Mastersizer 2000, Malvern Instruments Ltd., U.K.) using the 300 RF lens and the small volume sample presentation unit (capacity 150 ml). Approximately 500 mg of powder was dispersed in 5 ml of dispersant with the aid of a sonication in a water bath for 3 min. Propan-2-ol is used as the dispersant for lactose and water for starch. Ethanol is for hydroxyapatite and β-tricalcium phosphate [229].

The sonicated sample was added dropwise into sample cell containing 150 ml dispersant until an obscuration was between 10–30%. Size measurement of each sample was performed using 2000 sweeps and analysed with the reference refractive index of

- Lactose: 1.533
- Starch: 1.50
- Hydroxyapatite: 1.65
- β-tricalcium phosphate: 1.63
- Propan-2-ol: 1.378
- Ethanol: 1.36
- Water: 1.33

The measurement results of fine powders: Sorbolac®400, starch, hydroxyapatite (from Merck), CAPTAL®R, CAPTAL®S and β-tricalcium phosphate (β-TCP) are shown as follows.

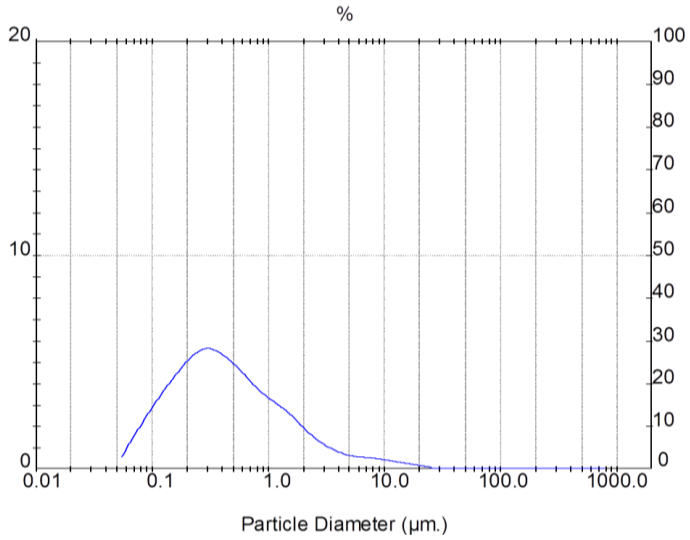

Sorbolac®400

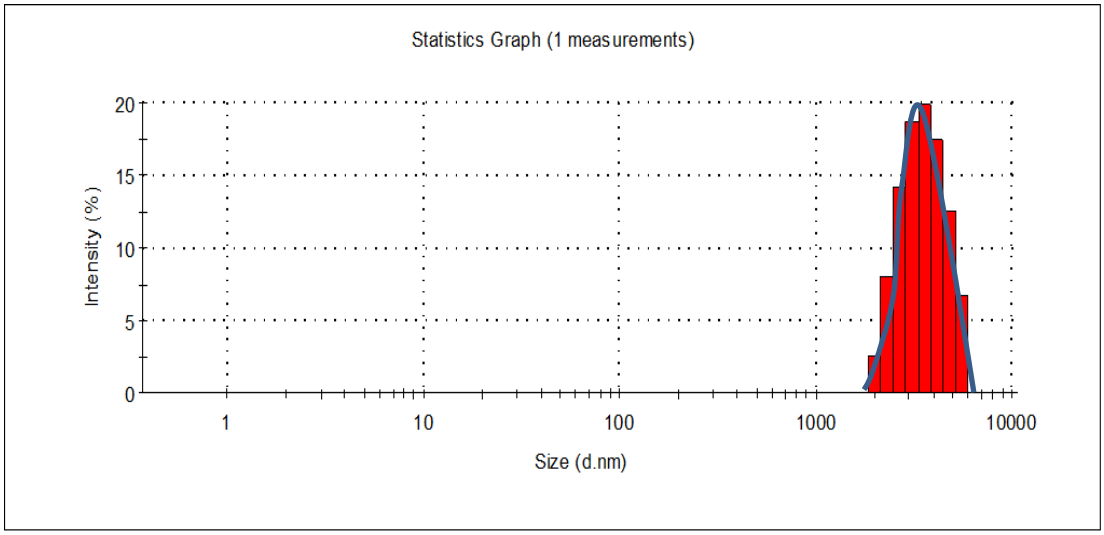

Starch, Merck®

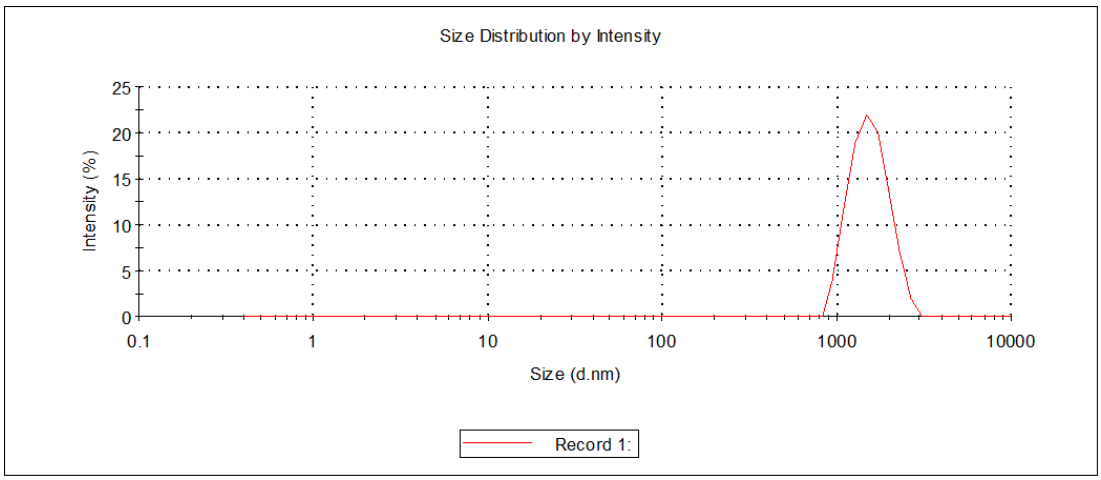

Hydroxyapatite, Merck®

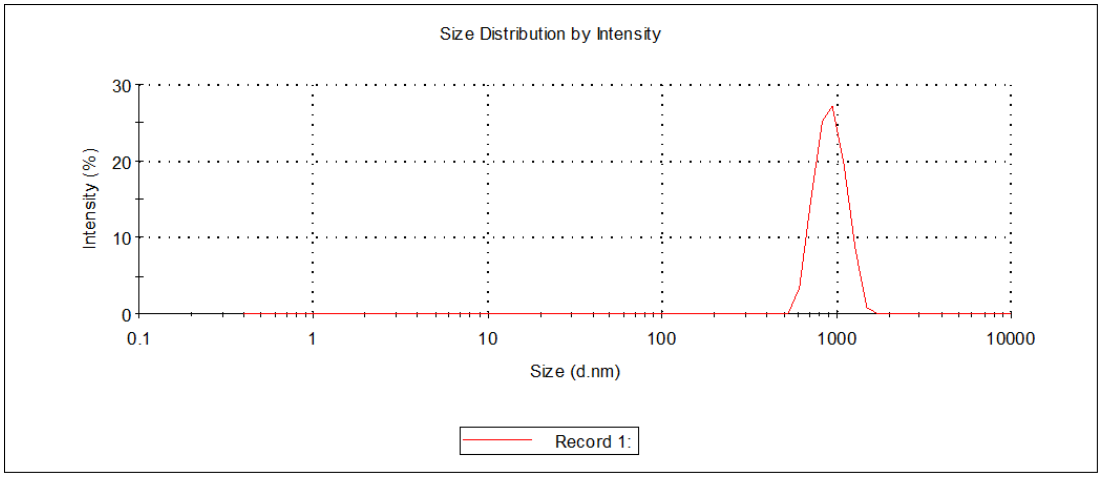

β-tricalcium phosphate, Plasma Biotal Limited

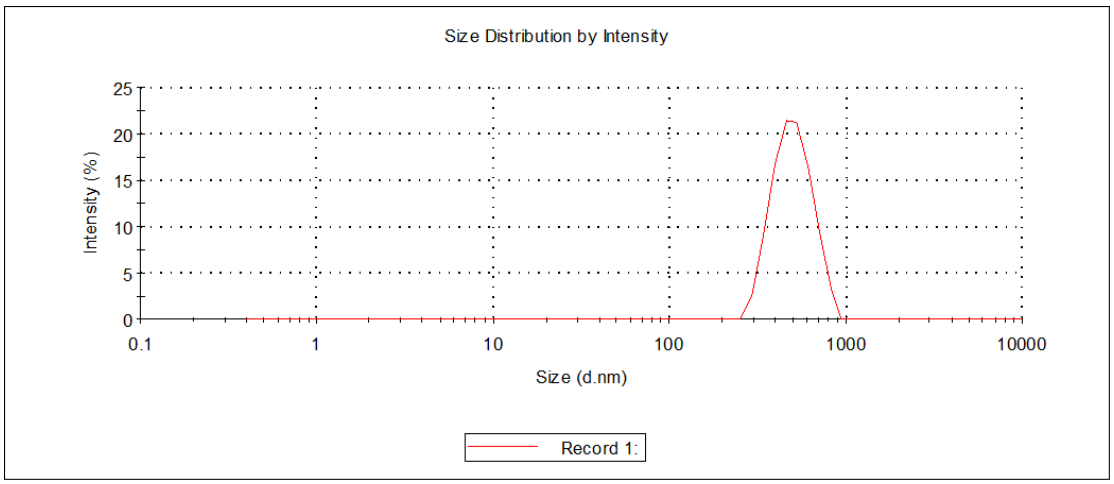

CAPTAL® R, Plasma Biotal Limited

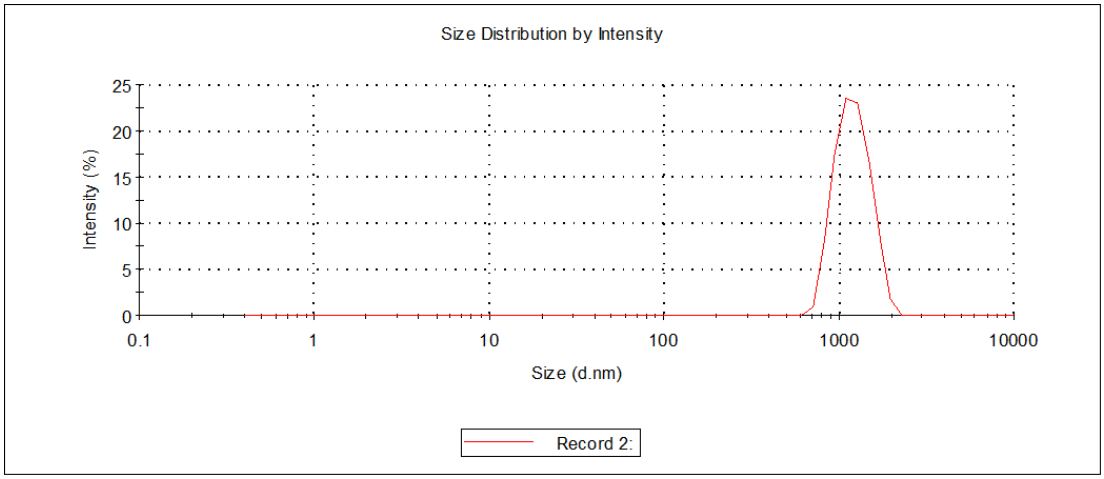

CAPTAL® S, Plasma Biotal Limited

Appendix II

Shear Test

The shear tester RST-01.pc developed by Schulze [13] is shown as follow:

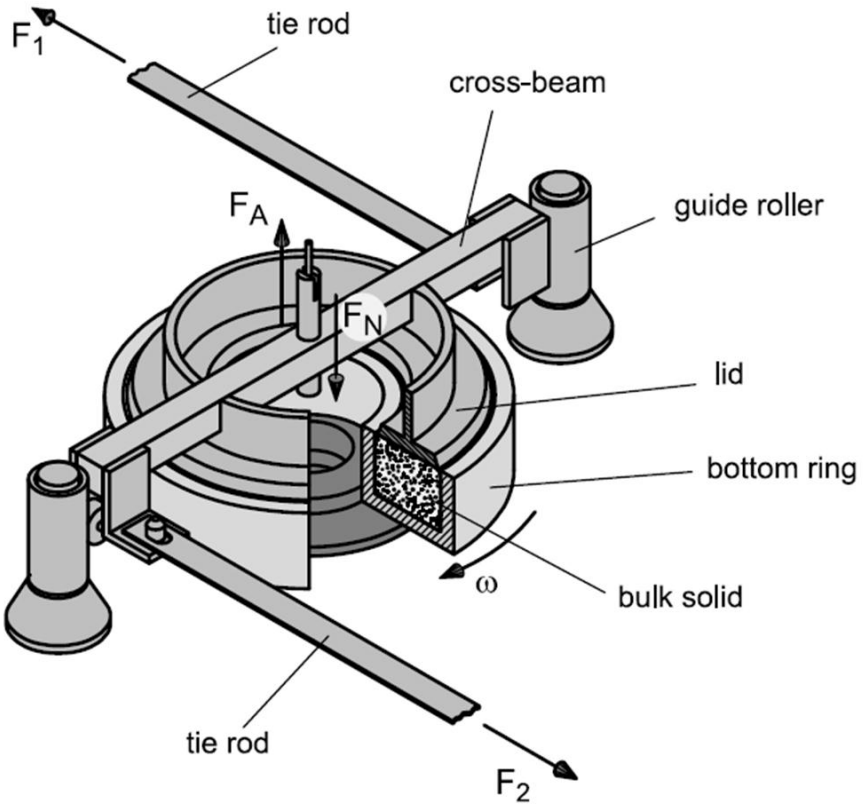

In an annular cell, the bulk solid is filled under an annular lid which is attached to a cross-beam. If the lid is connected to a displacement transducer, the vertical position of the lid can be measured so that bulk density, ρ_B, can be calculated from mass and volume. Two parallel tie rods are connected to the crossbeam. With connecting a load beam to the tie rod, the forces, F_1 and F_2, can be measured. The bulk solid is sheared by rotating the bottom ring when the lid is prevented from relative rotating by two tie rods. The sum of F_1 and F_2 acting on tie rods is therefore the shear force which is proportional to the shear stress τ.

In order to obtain a yield locus, a normal force F_N acts on the bulk solid through a hanger attached to the cross-beam to apply the vertical stress σ on the specimen. An upward force F_A is applied on the cross-beam to counterbalance the weight of the lid and all

other parts connected to it. The powder sample is sheared in two steps. In the first step, the bulk solid is sheared under a normal stress until a constant shear stress is obtained. The bulk solid is consolidated and then the shear stress is reduced to zero. In the second step, the bulk solid is sheared under a smaller normal stress until the shear stress has reached a maximum. The maximum is the point of incipient flow where the consolidated bulk solid fails. Several points of incipient flow at different levels of normal stress can be measured and drawn in σ-τ diagram. The curve through the points of incipient flow in the σ-τ diagram is the yield locus. With plotting Mohr' circles in the σ-τ diagram, major principal consolidation stress, σ_1, and unconfined yield stress σ_c can be determined and therefore the flow factor, ff_c, $ff_c = \frac{\sigma_1}{\sigma_c}$. The flow properties can be measured with a ring shear cell are:

- consolidation stress, σ_1
- unconfined yield stress, σ_c
- angle of internal friction, δ
- cohesiveness, c
- bulk density, ρ_B
- flow factor, ff_c

Appendix III

Particle Morphology Characterization with Scanning Electron Microscope

Powder samples were mounted on metal sample plates. The samples were gold coated with a sputter coater using an electrical potential of 2.0 kV and 25 mA for 3 min. The particles were examined at several magnifications under scanning electron microscope operating at 10 kV for lactose, starch and hydroxyapatite (from Merck), 15 kV for CAPTAL®R and β-tricalcium phosphate, 20 kV for CAPTAL®S. The SEM images are shown as follows.

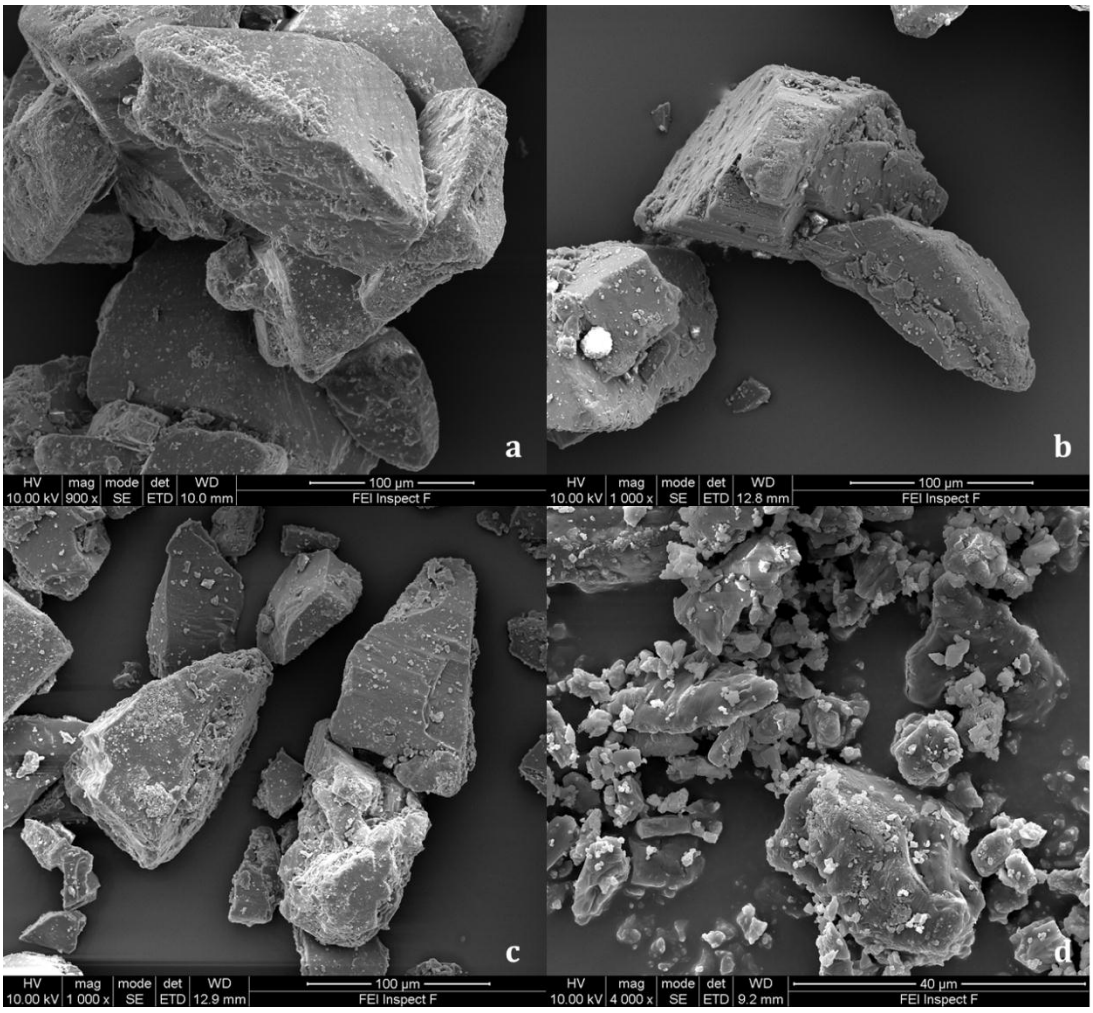

Lactose: a. Inhalac®70; b. Inhalac®120; c. Inhalac®230; d. Sorbolac®400

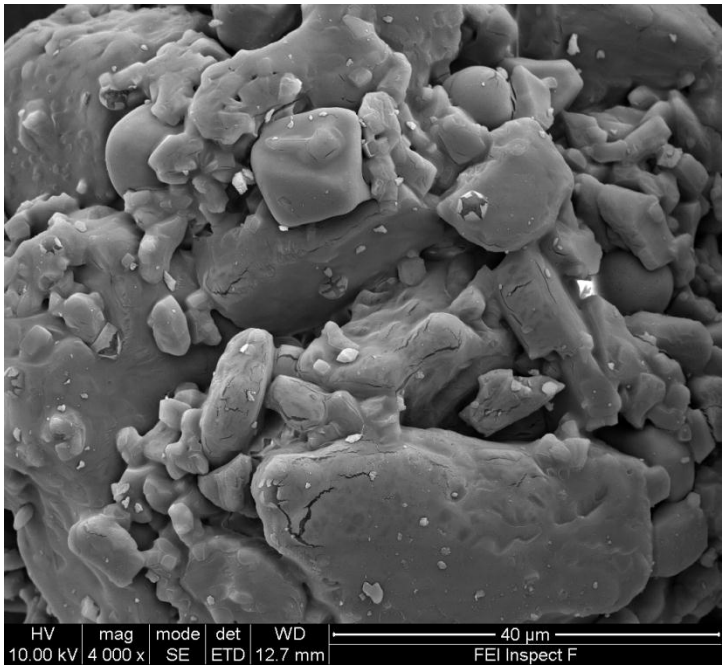

Starch

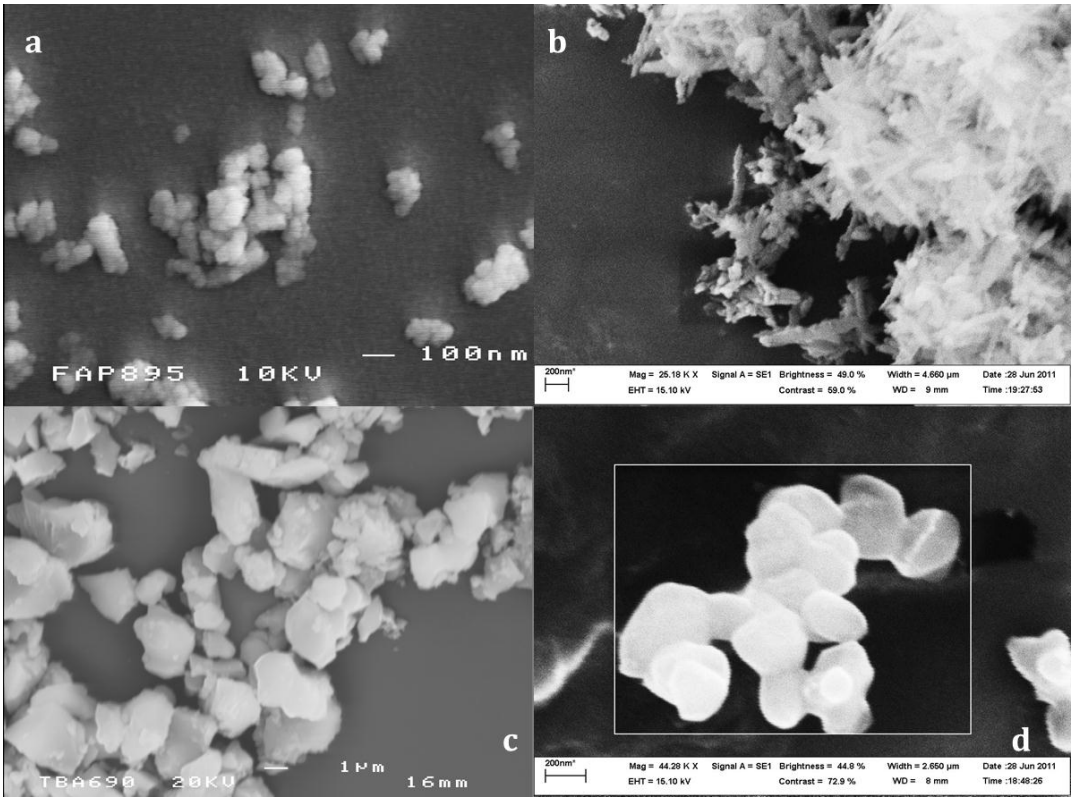

a. hydroxyapatite (from Merck); b. CAPTAL®R; c. CAPTAL®S; d. β-tricalcium phosphate (β-TCP)

Appendix IV

DC Electromagnet Solenoid for Hammering Dispensing Device

The hammering dispensing device represented in Chapter 4 was composed by a linear motion electromagnet solenoid and a spring plunger. The specification of electromagnet solenoid was listed in the table below. The push and pull of the plunger was controlled by DC 12V on/off pulse signal. The frequency of the pulse train is adjustable. During the process, the end of plunger kept hammering the lower portion of the vertical dispensing hopper with a certain frequency. A 2N hammering force exerted on the outer surface of dispensing hopper was propagated inside to overcome the inter-particle force. It provides a horizontal vibration to the dispensing hopper.

Specification of electromagnet solenoid

Product Name	DC Solenoid Electromagnet
Rated Voltage & Current	DC 24V 0.5A
Action Form	Push Type
Force	200g/0.4lb
Stroke	6mm/0.24"
Plunger Diameter	8mm/0.31"
Power On Type	Intermittent 50%
Max Power On Time	90 Second
Body Size	26 x 20 x 37mm/1" x 0.8" x 1.5"(L*W*H)
Cable Length	13cm/5.1"
Material	Metal, Electronic Parts
Weight	95g

Appendix V

Vibration Motor Used for Vibration Dispensing Device

The eccentric rotating mass vibration motor was attached with the dispensing hopper described in Chapter 4. The specification and performance characteristics of vibration motor, provided by manufacturer: Precision Microdrives™ Ltd., are shown below. The DC motor has an offset (non-symmetric) mass attached to the shaft. As it rotates, the centripetal force of the offset mass is asymmetric, resulting in a net centrifugal force, and this causes a displacement of the dispensing unit. With a high number of revolutions per minute, the unit is constantly being displaced and moved by these asymmetric forces. It is the repeated displacement that is perceived as a vibration.

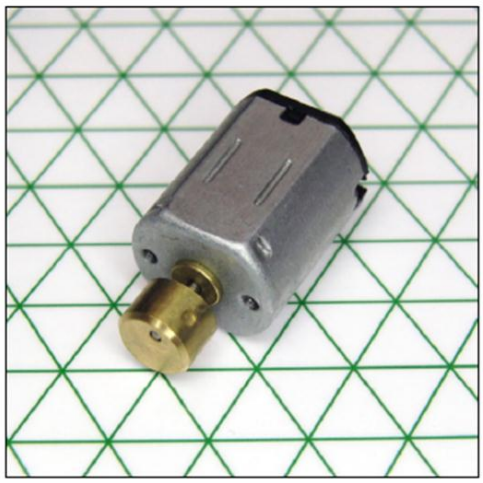

12mm Vibration Motor - 15mm Type
Shown on 6mm Isometric Grid

Key Features

Body Diameter:	12 mm [+/- 0.2]
Body Length:	15 mm [+/- 0.2]
Counterweight Radius:	3 mm [+/- 0.1]
Counterweight Length:	4 mm [+/- 0.2]
Shaft Orientation:	Inline
Rated Operating Voltage:	12 V
Rated Vibration Speed:	17,000 rpm [+/- 3,400]
Typical Rated Operating Current:	84 mA
Typical Normalised Amplitude:	8.5 G

Typical Vibration Motor Performance Characteristics

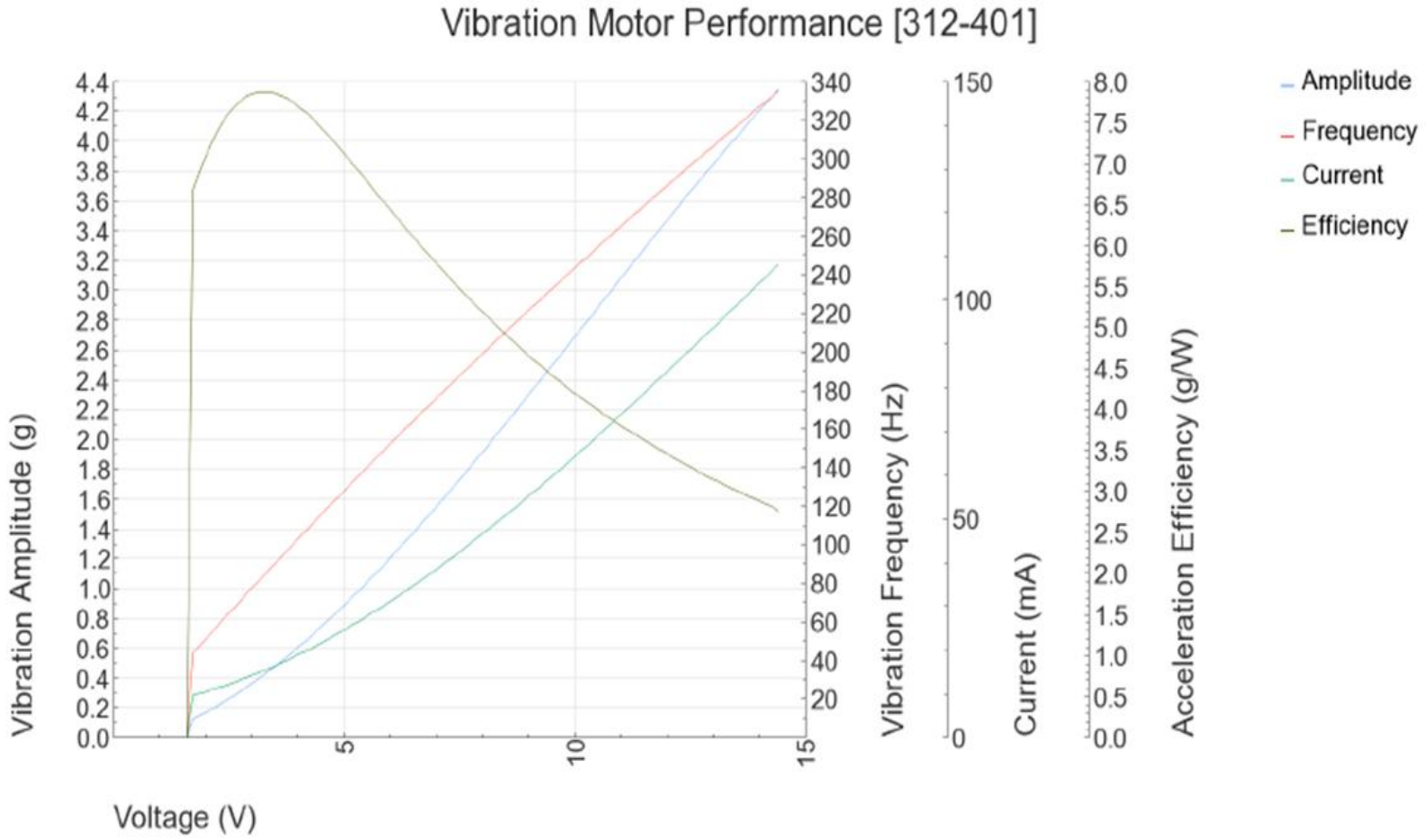

Parameter	Conditions	Specification
Typical Performance Characteristics		
Typical Rated Power Consumption	At rated voltage and load	1008 mW
Typical Rated Operating Current	At rated voltage using the inertial test load	84 mA
Typical Vibration Amplitude	Peak-to-Peak value at rated voltage using the inertial test load	3.4 G
Typical Start Current	at rated voltage	350 mA
Typical Vibration Efficiency	At rated voltage using the inertial test load	3.5 G/W
Typical Normalized Amplitude	Peak-to-Peak vibration amplitude normalized by the inertial test load at rated voltage	8.5 G
Typical Start Voltage	with the inertial test load	1.6 V
Typical Terminal Resistance		31 Ω
Typical Terminal Inductance		4700 uH
Typical Haptic Characteristics		
Typical Lag Time	At rated voltage using the inertial test load	10 ms
Typical Rise Time	At rated voltage using the inertial test load	27 ms
Typical Stop Time	At rated voltage using the inertial test load	49.5 ms
Typical Active Brake Time	Time taken from steady-state to 0.04 G under inverse polarity at max. voltage	21.3 ms

Reference

[1] Nedderman R. Statics and Kinematics of Granular Materials. Cambridge, UK 1992.

[2] McGraw-Hill Education. McGraw-Hill Dictionary of Scientific & Technical Terms, sixth edition. The McGraw-Hill Companies, Inc. 2002.

[3] Walker EE. The properties of powders. Part VI. The compressibility of powders. Transactions of the Faraday Society. 1923;19:73-82.

[4] Deming WE, Mehring AL. The gravitational flow of fertilizers and other comminuted solids. Journal of Industrial and Engineering Chemistry. 1929;21:661-665.

[5] Fowler RT, Glastonbury JR. Flow of granular solids through orifices. Chem Eng Sci. 1959;10:150-156.

[6] Jenike AW. Gravity flow of bulk solids. USA: Utah Engineering Station 1961.

[7] Carr RL, Jr. Evaluating flow properties of solids. Chem Eng. 1965;72:163-168.

[8] Hausner H. Friction conditions in a mass of metal powder. Int J Powder Metall. 1967;3:7-13.

[9] Newton RH, Dunham GS, Simpson TP. The TCC catalytic cracking process for motor gasoline production. Transactions of American Institute of Chemical Engineers. 1945;41:215-232.

[10] Richards JC, Editor. The Storage and Recovery of Particulate Solids: Inst. Chem. Engineers 1966.

[11] Sperl M. Experiments on corn pressure in silo cells - translation and comment of Janssen's paper from 1895. Granul Matter. 2006;8(2):59-65.

[12] Brown RL, Hawksley PGW. The internal flow of granular masses. Fuel. 1947;26:159-173.

[13] Schulze D. Powders and Bulk Solids: Behavior, Characterization, Storage and Flow. Germany: Springer-Verlag Berlin Heidelberg 2008.

[14] Yang S, Evans JRG. Metering and dispensing of powder; the quest for new solid freeforming techniques. Powder Technol. 2007;178(1):56-72.

[15] Rose HF, Takada T. Rate of discharge of granular materials from bins and hoppers. The Engineer (London). 1959;208.

[16] Davidson JF, Nedderma.Rm. Hour-glass theory of hopper flow. Transactions of the Institution of Chemical Engineers. 1973;51(1):29-35.

[17] Arnold P, McLean A, Roberts A. Bulk solids; Storage, Flow and Handling. New South Wales: TUNRA Ltd., University of Newcastle 1980.

[18] Visser J. Van der Waals and other cohesive forces affecting powder fluidization. Powder Technol. 1989;58:1-10.

[19] Takahashi H, Suzuki A, Tanaka T. Behaviour of a particle bed in the field of vibration I. Analysis of particle motion in a vibrating vessel. Powder Technol. 1968;2(2):65-71.

[20] Crewdson BJ, Ormond AL, Nedderman RM. Air-impeded discharge of fine particles from a hopper. Powder Technol. 1977;16(2):197-207.

[21] Staffa KH, Jahn J, Claussen N. Flowability of powders under the influence of vibrations. Powder Metall Int. 1977;9:20-23.

[22] Gupte AR, Kladders H, Struth H, inventors; Boehringer Ingelheim Ger., assignee. Device and process for drawing off very small quantities of powder patent US Pat. 4350049. 1982.

[23] Podczeck F, Jones BE. Pharmaceutical Capsules, 2nd Edition: Pharmaceutical Press 2004.

[24] Yang S, Evans JRG. Computer control of powder flow for solid freeforming by acoustic modulation. Powder Technol. 2003;133(1-3):251-254.

[25] Yang S, Evans JRG. A multi-component powder dispensing system for three dimensional functional gradients. Materials Science and Engineering: A. 2004;379(1-2):351-359.

[26] Yang SF, Evans JRG. Acoustic initiation of powder flow in capillaries. Chemical Engineering Science. 2005;60(2):413-421.

[27] Yang SF, Evans JRG. Acoustic control of powder dispensing in open tubes. Powder Technol. 2004;139(1):55-60.

[28] Yang SF, Evans JRG. A dry powder jet printer for dispensing and combinatorial research. Powder Technol. 2004;142(2-3):219-222.

[29] Lu XS, Yang SF, Evans JRG. Studies on ultrasonic microfeeding of fine powders. Journal of Physics D-Applied Physics. 2006;39(11):2444-2453.

[30] Lu X, Yang S, Evans JRG. Dose uniformity of fine powders in ultrasonic microfeeding. Powder Technol. 2007;175(2):63-72.

[31] Yang S, inventor Queen Mary and Westfield College, UK . assignee. Powder dispenser with permanently-open linear-taper nozzle operated by vibration patent GB2472817A. 2011.

[32] Jennings BR, Parslow K. Particle size measurement: The equivalent spherical diameter. Proceedings of the Royal Society of London Series A. 1988;419:137-149.

[33] Merkus HG. Particle Size Measurements: Fundamentals, Practice, Quality. *Particle Size Measurements: Fundamentals, Practice, Quality*. Dordrecht: Springer 2009:1-533.

[34] Ruf A, Worlitschek J, Mazzotti M. Modeling and experimental analysis of PSD measurements through FBRM. Particle & Particle Systems Characterization. 2000;17(4):167-179.

[35] Wang XZ, Roberts KJ, Ma C. Crystal growth measurement using 2D and 3D imaging and the perspectives for shape control. Chemical Engineering Science. 2008;63(5):1173-1184.

[36] Yu W, Erickson K. Chord length characterization using focused beam reflectance measurement probe-methodologies and pitfalls. Powder Technol. 2008;185(1):24-30.

[37] Kail N, Marquardt W, Briesen H. Process analysis by means of focused beam reflectance measurements. Industrial & Engineering Chemistry Research. 2009;48(6):2936-2946.

[38] Khanam T, Rahman MN, Rajendran A, Kariwala V, Asundi AK. Accurate size measurement of needle-shaped particles using digital holography. Chemcal Engineering Science. 2011;66:2699-2706.

[39] Jillavenkatesa A, Dapkunas SJ, Lum L. Particle Size Characterization. NIST Special Publication. 2001;960-1.

[40] Malvern Instruments Limited. A Basic Guide to Particle Characterization. Malvern Instruments Inform White Paper. 2012.

[41] Adi H, Larson I, Stewart P. Laser diffraction particle sizing of cohesive lactose powders. Powder Technol. 2007;179(1-2):90-94.

[42] HORIBA Scientific. A guidebook to particle size analysis. HORIBA INSTRUMENTS, INC. 2014.

[43] Sarabakos GD, Kosaropoulos AE. Handbook of Food Processing Equipment. New York: Kluwer Academic / Plenum Publishing 2002.

[44] Fukunaka T, Sawaguchi K, Golman B, Shinohara K. Effect of particle shape of active pharmaceutical ingredients prepared by fluidized-red jet-milling on cohesiveness. Journal of pharmaceutical sciences. 2005;94(5):1004-1012.

[45] Harter A, Schenck L, Lee I, Cote A. High-Shear Rotor-Stator Wet Milling for Drug Substances: Expanding Capability with Improved Scalability. Org Process Res Dev. 2013;17(10):1335-1344.

[46] Yasuji T, Takeuchi H, Kawashima Y. Particle design of poorly water-soluble drug substances using supercritical fluid technologies. Adv Drug Deliv Rev. 2008;60(3):388-398.

[47] Kamahara T, Takasuga M, Tung HH, Hanaki K, Fukunaka T, Izzo B, et al. Generation of fine pharmaceutical particles via controlled secondary nucleation under high shear environment during crystallization - Process development and scale-up. Org Process Res Dev. 2007 Jul-Aug;11(4):699-703.

[48] Begat P, Morton DAV, Staniforth JN, Price R. The cohesive-adhesive balances in dry powder inhaler formulations I: Direct quantification by atomic force microscopy. Pharmaceutical Research. 2004;21(9):1591-1597.

[49] Rumpf H. Particle Technology: Chapman and Hall 1990.

[50] Wadell H. Volume, shape and roundness of quartz particles. Journal of Geology. 1935;43(3):250-280.

[51] Horio T, Yasuda M, Matsusaka S. Effect of particle shape on powder flowability of microcrystalline cellulose as determined using the vibration shear tube method. International Journal of Pharmaceutics. 2014;473(1-2):572-578.

[52] Sandler N, Wilson D. Prediction of Granule Packing and Flow Behavior Based on Particle Size and Shape Analysis. Journal of Pharmaceutical Sciences. 2010;99(2):958-968.

[53] Yu WL, Muteki K, Zhang L, Kim G. Prediction of Bulk Powder Flow Performance Using Comprehensive Particle Size and Particle Shape Distributions. Journal of Pharmaceutical Sciences. 2011;100(1):284-293.

[54] Burnett DJ, Heng JYY, Thielmann F, Garcia AR, Naderi M, Acharya M. Measuring Surface Roughness of Pharmaceutical Powders Using Vapor Sorption Methods. AAPS PharmSciTech. 2011;12(1):56-61.

[55] Kwek JW, Heng D, Lee SH, Ng WK, Chan HK, Adi S, et al. High speed imaging with electrostatic charge monitoring to track powder deagglomeration upon impact. Journal of Aerosol Science. 2013;65(0):77-87.

[56] Ohta KM, Fuji M, Chikazawa M. Effect of geometric structure of flow promoting agents on the flow properties of pharmaceutical powder mixture. Pharmaceutical Research. 2003;20(5):804-809.

[57] Hussain MSH, York P, Timmins P. A study of the formation of magnesium stearate film on sodium chloride using energy-dispersive x-ray analysis. Int J Pharm. 1988;42:89-95.

[58] Roblot-Treupel L, Puisieux F. Distribution of magnesium stearate on the surface of lubricated particles. Int J Pharm. 1986;31:131-136.

[59] Irwin GM, Dodson GJ, Ravin LJ. Encapsulation of clomacran phosphate {2-chloro-9-[3-(dimethylamino)propyl]acridan phosphate}. I. Effect of flowability of powder blend, lot-to-lot variability, and concentration of active ingredient on weight variation of capsules filled on an automatic capsule-filling machine. Journal of Pharmaceutical Sciences. 1970;59:547-550.

[60] Podczeck F, Miah Y. The influence of particle size and shape on the angle of internal friction and the flow factor of unlubricated and lubricated powders. International Journal of Pharmaceutics. 1996;144:187-194.

[61] Liu LX, Marziano I, Bentham AC, Litster JD, White ET, Howes T. Effect of particle properties on the flowability of ibuprofen powders. International Journal of Pharmaceutics. 2008;362(1-2):109-117.

[62] Hughes SW. Archimedes revisited: a faster, better, cheaper method of accurately measuring the volume of small objects. Physics Education. 2005;40(5):468-474.

[63] Buckman HO, Brady NC. The Nature and Property of Soils - A College Text of Edaphology (6th edtion). New York: MacMillan Publishers, New York 1960.

[64] Heckel RW. Density-pressure relations in powder compaction. Trans Am Inst Min, Metall Pet Eng. 1961;221:671-675.

[65] Gold G, Duvall RN, Palermo BT, Slater JG. Powder flow studies. 3. Factors affecting the flow of lactose granules. Journal of pharmaceutical sciences. 1968 1968;57(4):667-671.

[66] ter Borg L. Erfahrungen aus Scherversuchen mit Schüttgütern der Chemie. Chem Ing Tech. 1981;53:662-663.

[67] Runge J. The time consolidation of bulk solids on the example of viscoelastic granules. Chem Eng Commun. 1998;170:169-183.

[68] European Pharmacopoeia 8.0. 2.9.34. Bulk density and tapped density of powders. 2014.

[69] Silva J, Splendor D, Goncalves IMB, Costa P, Lobo JMS. Note on the Measurement of Bulk Density and Tapped Density of Powders According to the European Pharmacopeia. AAPS PharmSciTech. 2013;14(3):1098-1100.

[70] Denny PJ. Compaction equations: a comparison of the Heckel and Kawakita equations. Powder Technol. 2002;127(2):162-172.

[71] Mendez R, Romanski FS, Tomassone MS. Density behavior of cohesive granular materials. Powder Technol. 2011;211(2–3):189-198.

[72] Traina K, Cloots R, Bontempi S, Lumay G, Vandewalle N, Boschini F. Flow abilities of powders and granular materials evidenced from dynamical tap density measurement. Powder Technol. 2013;235(0):842-852.

[73] Wouters IMF, Geldart D. Characterizing semi-cohesive powders using angle of repose. Part Part Syst Charact. 1996;13:254-259.

[74] Brown RL, Richard JC. Principles of Powder Mechanics. UK: Oxford Pergamon 1970.

[75] Landín M, Martínez-Pacheco R, Gómez-Amoza JL, Souto C, Concheiro A, Rowe RC. Effect of country of origin on the properties of microcrystalline cellulose. International Journal of Pharmaceutics. 1993;91(2-3):123-131.

[76] Gamble JF, Chiu WS, Tobyn M. Investigation into the impact of sub-populations of agglomerates on the particle size distribution and flow properties of conventional microcrystalline cellulose grades. Pharmaceutical Development and Technology. 2011;16(5):542-548.

[77] Patel R, Podczeck F. Investigation of the effect of type and source of microcrystalline cellulose on capsule filling. International Journal of Pharmaceutics. 1996;128(1-2):123-127.

[78] Mohammadi MS, Harnby N. Bulk density modelling as a means of typifying the microstructure and flow characteristics of cohesive powders. Powder Technol. 1997;92(1):1-8.

[79] Wouters IMF, Geldart D. Characterising semi-cohesive powders using angle of repose. Particle and Particle Systems Characterization. 1996;13(4):254-259.

[80] Krantz M, Zhang H, Zhu J. Characterization of powder flow: Static and dynamic testing. Powder Technol. 2009;194(3):239-245.

[81] Kalson PA, Resnick W. Angles of repose and drainage for granular-materials in a wedge-shaped hopper. Powder Technol. 1985;43(2):113-116.

[82] Gold G, Duvall RN, Palermo BT, Slater JG. Powder flow studies. II. Effect of glidants on flow rate and angle of repose. Journal of Pharmaceutical Sciences. 1966;55:1291-1295.

[83] Zhou D, Qiu Y. Understanding material properties in pharmaceutical product development and manufacturing: Powder flow and mechanical properties. Journal of Validation technology. 2010;Spring:65-77.

[84] Schwedes J, Schulze D. Measurement of flow properties of bulk solids. Powder Technol. 1990;61(1):59-68.

[85] Handin J. On the Coulomb-Mohr failure criterion. J Geophys Res. 1969;74(22):5343-5348.

[86] Walters JK. Theoretical analysis of stresses in silos with vertical walls. Chemical Engineering Science. 1973;28(1):13-21.

[87] Martens P. Silohandbuch: Wilhelm Ernst & Sohn Verlag, Berlin 1988.

[88] Jenike AW. A theory of flow of particulate solids in converging and diverging channels based on a conical yield function. Powder Technol. 1987;50(3):229-236.

[89] Kruyt NP. Results of jenikes (1987) radial stress-field theory for the flow of granular-materials in conical hoppers - flow regimes and flow factors. Powder Technol. 1993;76(1):109-112.

[90] Arnold P. Design of silos for flow and strength - the various contributors must communicate. Boca Raton: Crc Press-Taylor & Francis Group 2008.

[91] Fitzpatrick JJ, Barringer SA, Iqbal T. Flow property measurement of food powders and sensitivity of Jenike's hopper design methodology to the measured values. J Food Eng. 2004;61(3):399-405.

[92] Sternberger-Rützel E, Runft W, Beck M, Weber E, Kleiner M, Gimpinger B, et al. Quality by design: Concept for the proof-of-principle testing regarding automated microdosing. Pharmazeutische Industrie. 2012;74(1):145-154.

[93] Baxter J, Abou-Chakra H, Tuzun U, Lamptey BM. A DEM simulation and experimental strategy for solving fine powder flow problems. Chemical Engineering Research & Design. 2000;78(A7):1019-1025.

[94] Jasion GT, Shrimpton JS, Li Z, Yang S. On the bridging mechanism in vibration controlled dispensing of pharmaceutical powders from a micro hopper. Powder Technol. 2013;249:24-37.

[95] Brown RL, Richards JC. Exploratory study of the flow of granules through apertures. Trans Inst Chem Eng. 1959;37:108-119.

[96] McLean AG. Empirical critical flow factor equations. Bulk Solids Handling. 1986;6:779-782.

[97] Stainfor PT, Ashley RC. Analytical hopper design method for cohesive powders. Powder Technol. 1973;7(4):215-243.

[98] Eckhoff RK, Leversen PG. Further contribution to evaluation of jenike method for design of mass flow hoppers. Powder Technol. 1974;10(1-2):51-58.

[99] Roberts AW, Scott OJ. An investigation into the effects of sinusoidal and random vibrations on the strength and flow properties of bulk solids. Powder Technol. 1978;21:45-53.

[100] Roberts AW. Vibration of Powders and its Application. In: Fayed ME, Otten L, eds. *Handbook on Powder Science and Technology*: Van Nostrand 1984:181-229.

[101] Hunt ML, Weathers RC, Lee AT, Brennen CE, Wassgren CR. Effects of horizontal vibration on hopper flows of granular materials. Physics of Fluids. 1999;11(1):68-75.

[102] Wassgren CR, Hunt ML, Freese PJ, Palamara J, Brennen CE. Effects of vertical vibration on hopper flows of granular material. Physics of Fluids. 2002;14(10):3439-3448.

[103] Matchett AJ. A theoretical model of vibrationally induced flow in conical hopper systems. Chemical Engineering Research & Design. 2004;82(A1):85-98.

[104] Jiang YB, Matsusaka S, Masuda H, Qian Y. Development of measurement system for powder flowability based on vibrating capillary method. Powder Technol. 2009;188(3):242-247.

[105] Janda A, Maza D, Garcimartin A, Kolb E, Lanuza J, Clement E. Unjamming a granular hopper by vibration. Epl. 2009;87(2).

[106] Rasmussen KR, Iversen JD, Rautahemio P. Saltation and wind-flow interaction in a variable slope wind tunnel. Geomorphology. 1996;17(1–3):19-28.

[107] Faqih A, Chaudhuri B, Muzzio FJ, Tomassone MS, Alexander A, Hammond S. Flow-induced dilation of cohesive granular materials. Aiche Journal. 2006;52(12):4124-4132.

[108] Dumbaugh GD. The induced vertical flow of bulk solids from storage. Bulk Solids Handling. 1984;4:153-171.

[109] Kollmann T, Tomas J. Effect of applied vibration on silo hopper design. Part Sci Technol. 2002;20(1):15-31.

[110] Beverloo WA, Leniger HA, van de Velde J. The flow of granular solids through orifices. Chemical Engineering Science. 1961;15(3-4):260-269.

[111] British Standards Institution, ed. Draft design code for silos, bins, bunkers and hoppers. UK: BSI in association with the British Materials Handling Board 1987.

[112] Verghese TM, Nedderman RM. The discharge of fine sands from conical hoppers. Chemical Engineering Science. 1995;50:3143-3153.

[113] Suzuki A, Takahashi H, Tanaka T. Behavior of a particle bed in the field of vibration II. Flow of particles through slits in the bottom of a vibrating vessel. Powder Technol. 1968:72-77.

[114] Matsusaka S, Yamamoto K, Masuda H. Micro-feeding of a fine powder using a vibrating capillary tube. Advanced Powder Technology. 1996;7(2):141-151.

[115] Johnson KC, Swindell AC. Guidance in the setting of drug particle size specifications to minimize variability in absorption. Pharm Res. 1996;13:1795-1798.

[116] Kawashima Y. Nanoparticulate systems for improved drug delivery. Adv Drug Delivery Rev. 2001;47:1-2.

[117] Oh D, Curl RL, Yong C, Amidon GL. Effect of micronization on the extent of drug absorption from suspensions in humans. Arch Pharmacal Res. 1995;18:427-433.

[118] Webster TJ, Ergun C, Doremus RH, Siegel RW, Bizios R. Enhanced functions of osteoblasts on nanophase ceramics. Biomaterials. 2000;21(17):1803-1810.

[119] Liu LX, Marziano I, Bentham AC, Litster JD, E.T.White, Howes T. Effect of particle properties on the flowability of ibuprofen powders. International Journal of Pharmaceutics. 2008;362(1–2):109-117.

[120] Mullarney MP, Hancock BC, Carlson GT, Ladipo DD, Langdon BA. The powder flow and compact mechanical properties of sucrose and three high-intensity sweeteners used in chewable tablets. International Journal of Pharmaceutics. 2003;257(1–2):227-236.

[121] Tuley R, Shrimpton J, Jones MD, Price R, Palmer M, Prime D. Experimental observations of dry powder inhaler dose fluidisation. International Journal of Pharmaceutics. 2008;358(1–2):238-247.

[122] Rasenack N, Mueller BW. Micron-Size Drug Particles: Common and Novel Micronization Techniques. Pharm Dev Technol. 2004;9:1-13.

[123] Altounyan REC. Inhibition of experimental asthma by a new compound disodium cromoglycate intal. Acta Allergologica. 1967;22(6):487.

[124] Kim KS, Lee D, Kim DH, Kim YI, Park JH, Woo JS, inventors; Hanmi Pharm. Co., Ltd., S. Korea . assignee. Dry powder for inhalation formulation comprising salmeterol xinafoate, fluticasone propionate and tiotropium bromide, and method for preparing same patent WO2013187626A1. 2013.

[125] Islam N, Gladki E. Dry powder inhalers (DPIs) - A review of device reliability and innovation. International Journal of Pharmaceutics. 2008;360(1-2):1-11.

[126] Newman SP. Dry powder inhalers for optimal drug delivery. Expert Opinion on Biological Therapy. 2004;4(1):23-33.

[127] Bell JH, Hartley PS, Cox JSG. Dry powder aerosols .1. New powder inhalation device. Journal of Pharmaceutical Sciences. 1971;60(10):1559-&.

[128] Bisrat M, Nystroem C. Physicochemical aspects of drug release. VIII. The relation between particle size and surface specific dissolution rate in agitated suspensions. Int J Pharm. 1988;47:223-231.

[129] Edwards D. Applications of capsule dosing techniques for use in dry powder inhalers. Therapeutic delivery. 2010;1(1):195-201.

[130] Chen XL, Seyfang K, Steckel H. Development of a micro dosing system for fine powder using a vibrating capillary. Part 1: The investigation of factors

influencing on the dosing performance. International Journal of Pharmaceutics. 2012;433(1-2):34-41.

[131] Chen XL, Seyfang K, Steckel H. Development of a micro-dosing system for fine powder using a vibrating capillary. Part 2. The implementation of a process analytical technology tool in a closed-loop dosing system. International Journal of Pharmaceutics. 2012;433(1-2):42-50.

[132] Li Z, Yang S. Nanobiomaterials library synthesis for high-throughput screening using a dry powder printing method. Nano Life. 2012;2:1250006-1250001-1250006-1250011.

[133] Harro Höfliger. Omnidose. http://www.hoefliger.com/index.php?id=139&L=1.

[134] Elajnaf A, Carter P, Rowley G. Electrostatic characterisation of inhaled powders: Effect of contact surface and relative humidity. Eur J Pharm Sci. 2006;29(5):375-384.

[135] Murtomaa M, Ojanen K, Laine E. Effect of surface coverage of a glass pipe by small particles on the triboelectrification of glucose powder. Journal of Electrostatics. 2002;54(3-4):311-320.

[136] Wong SKF, Lu Y, Heineman W, Palmer J, Courtney C. Fully automated solid weighing workstation. J Biomol Screen. 2005;10:524-531.

[137] Matsusaka S, Urakawa M, Masuda H. Micro-feeding of fine powders using a capillary tube with ultrasonic vibration. Advanced Powder Technology. 1995;6(4):283-293.

[138] Kumar P, Santosa JK, Beck E, Das S. Direct-write deposition of fine powders through miniature hopper-nozzles for multi-material solid freeform fabrication. Rapid Prototyping Journal. 2004;10(1):14-23.

[139] Li X, Choi H, Yang Y. Micro rapid prototyping system for micro components. Thin Solid Films. 2002;420-421(0):515-523.

[140] Yang Y, Li XC. Experimental and analytical study of ultrasonic micro powder feeding. Journal of Physics D-Applied Physics. 2003;36(11):1349-1354.

[141] Qi L, Zeng X, Zhou J, Luo J, Chao Y. Stable micro-feeding of fine powders using a capillary with ultrasonic vibration. Powder Technol. 2011;214(2):237-242

[142] Yang S, Evans JRG. On the rate of descent of powder in a vibrating tube. Philosophical Magazine. 2005 2005/04/01;85(10):1089-1109.

[143] Seppala K, Heinamaki J, Hatara J, Seppala L, Yliruusi J. Development of a New Method to Get a Reliable Powder Flow Characteristics Using Only 1 to 2 g of Powder. AAPS PharmSciTech. 2010;11(1):402-408.

[144] Kane NR, Broce B, Gonzalez-Zugasti J, Pryce Lewis W, LeQuesne M, Lemmo AV. A system for dispensing sub-milligram doses of active pharmaceutical powders for early stage solubility assays. Journal of the Association for Laboratory Automation. 2004;9(4):218-227.

[145] Yamada Y, Akita T, Ueda A, Shioyama H, Kobayashi T. Instruments for preparation of heterogeneous catalysts by an impregnation method. Review of Scientific Instruments. 2005;76(6).

[146] ASTM. Designation B213-83 Standard Test Method for Flow Rate of Metal Powders. American society for Testing and Materials 1983.

[147] Yang SF, Evans JRG. A multi-component powder dispensing system for three dimensional functional gradients. Materials Science and Engineering a-Structural Materials Properties Microstructure and Processing. 2004;379(1-2):351-359.

[148] Hewitt C, Smith D, Ingram A. Build-up of powders in auger fillers. *6th International Granulation Workshop,*. The University of Sheffield, Sheffield, UK 2013.

[149] Rowley G, Mackin LA. The effect of moisture sorption on electrostatic charging of selected pharmaceutical excipient powders. Powder Technol. 2003;135:50-58.

[150] Thomson WT. Theory of vibration with applications, 4th Edition. UK: Nelson Thornes Ltd 2003.

[151] Anbar M. Cavitation during Impact of Liquid Water on Water: Geochemical Implications. Science. 1968;161(3848):1343-1344.

[152] Millman J. Microelectronics: Digital and analog circuits and systems. USA: McGraw-Hill International Book Company 1979.

[153] Rowe RC, Sheskey PJ, Quinn ME. Handbook of Pharmaceutical Excipients, 6th Edition. London & Chicago: Pharmaceutical Press & American Pharmacists Association 2009.

[154] Matchett AJ. The shape of the cohesive arch in hoppers and silos - Some theoretical considerations. Powder Technol. 2007;171(3):133-145.

[155] Loverich JJ. Development of a new high specific power piezoelectric actuator: Pennsylvania State University; 2004.

[156] Matsusaka S, Kobayakawa M, Mizutani M, Imran M, Yasuda M. Bubbling behavior of a fluidized bed of fine particles caused by vibration-induced air inflow. Sci Rep. 2013;3:1190, 1195 pp.

[157] Xie HY. The role of interparticle forces in the fluidization of fine particles. Powder Technol. 1997;94(2):99-108.

[158] Feng JQ, Hays DA. Relative importance of electrostatic forces on powder particles. Powder Technol. 2003;135-136:65-75.

[159] Hendricks CD. Charging Macroscopic Particles. In: Moore AD, ed. *Electrostatics and its Applications*. New York John Wiley & Sons Inc. 1973:57-85.

[160] Matsusaka S, Maruyama H, Matsuyama T, Ghadiri M. Triboelectric charging of powders: A review. Chemical Engineering Science. 2010;65(22):5781-5807.

[161] Grosvenor MP, Staniforth JN. The influence of water on electrostatic charge retention and dissipation in pharmaceutical compacts for powder coating. Pharmaceutical Research. 1996;13(11):1725-1729.

[162] Bailey AG. The inhalation and deposition of charged particles within the human lung. Journal of Electrostatics. 1997;42(1-2):25-32.

[163] Bailey AG, Hashish AH, Williams TJ. Drug delivery by inhalation of charged particles. Journal of Electrostatics. 1998;44(1-2):3-10.

[164] Byron PR, Peart J, Staniforth JN. Aerosol electrostatics .1. Properties of fine powders before and after aerosolization by dry powder inhalers. Pharmaceutical Research. 1997;14(6):698-705.

[165] Balachandran W, Machowski W, Gaura E, Hudson C. Control of drug aerosol in human airways using electrostatic forces. Journal of Electrostatics. 1997;40-1:579-584.

[166] Staniforth JN, Rees JE. Powder mixing by triboelectrification. Powder Technol. 1981;30(2):255-256.

[167] Staniforth JN, Rees JE. Electrostatic charge interactions in ordered powder mixes. J Pharm Pharmacol. 1982;34:69-76.

[168] Bennett FS, Carter PA, Rowley G, Dandiker Y. Modification of electrostatic charge on inhaled carrier lactose particles by addition of fine particles. Drug Dev Ind Pharm. 1999;25:99-103.

[169] Eilbeck J, Rowley G, Carter PA, Fletcher EJ. Effect of materials of construction of pharmaceutical processing equipment and drug delivery devices on the triboelectrification of size-fractionated lactose. Pharmacy and Pharmacology Communications. 1999;5(7):429-433.

[170] Cassidy OE, Rowley G, Fletcher IW, Davies SF, Briggs D. Surface modification and electrostatic charge of polystyrene particles. International Journal of Pharmaceutics. 1999;182(2):199-211.

[171] Higashiyama Y, Ujiie Y, Asano K. Triboelectrification of plastic particles on a vibrating feeder laminated with a plastic film. Journal of Electrostatics. 1997;42(1-2):63-68.

[172] Murtomaa M, Laine E. Electrostatic measurements on lactose-glucose mixtures. Journal of Electrostatics. 2000;48(2):155-162.

[173] Watanabe H, Ghadiri M, Matsuyama T, Ding YL, Pitt KG, Maruyama H, et al. Triboelectrification of pharmaceutical powders by particle impact. International Journal of Pharmaceutics. 2007;334(1-2):149-155.

[174] Kwek JW, Jeyabalasingam M, Ng WK, Heng JYY, Tan RBH. Comparative study of the triboelectric charging behavior of powders using a nonintrusive approach. Industrial and Engineering Chemistry Research. 2012;51(50):16488-16494.

[175] Artana G, Touchard G, Morin MF. Contribution to the analysis of the flow electrification process of powders in pneumatic conveyers. Journal of Electrostatics. 1997;40-1:277-282.

[176] Rhoda RN, Vines RF, inventors; International Nickel Ltd. . assignee. Chemical deposition of catalytically active platinum on graphite and metallic powders and surfaces patent GB1097010. 1967.

[177] Walter CW, Leaman FH, inventors; Dentsply International Inc. . assignee. Artificial tooth comprising a porcelain body containing a noble metal or alloy pin coil electrolessly plated with a continuous layer of platinum patent US3562911A. 1971.

[178] Mamtani K. Effect of particle shape on hopper discharge rate. Thesis for the degree of master of science, University of Florida. 2011.

[179] European Federation of Pharmaceutical Industries and Associations. The pharmaceutical industry in figures. 2013.

[180] Association of the British Pharmaceutical Industry. Annual review 2011/2012. 2012.

[181] Cameron A, Ewen M, Auton M, Abedunde D. Medicines prices, availability and affordability. *The World Medicines Situation 2011, 3rd edition* 2011.

[182] World Health Organization. Measuring medicine prices, availability, affordability and price components. 2008.

[183] Bennett PN, Brown MJ. Clinical Pharmacology, 10th Edition. Spain: Churchhill livingstone 2003.

[184] Finney E. Children's medicine: A situational analysis. 2011 (http://www.who.int/childmedicines).

[185] National Health Service. How you care reduce medicine waste? 2012 (http://www.berkshirewest.nhs.uk/).

[186] The International Committee of the Red Cross. Annual report 2011. 2011.

[187] Pucheril D, Sharma S. The history and future of personalized medicine. Managed Care. 2011.

[188] Personalized Medicine Coalition. The Case for Personalized Medicine, 3rd Edition. 2011.

[189] Salari K, Watkins H, Ashley EA. Personalized medicine: hope or hype? European Heart Journal. 2012;33:1564-1570.

[190] Leibman MN. Translational medicine vs. personalized medicine: Research vs. practice 2012 (http://www.ponte-project.eu/uploads/Presentations/).

[191] Mansour JC, Schwarz RE. Molecular mechanism for individualized cancer care. Journal of the American College of Surgeons. 2008;207(2):250-258.

[192] van't Veer LJ, Bernards R. Review Article Enabling personalized cancer medicine through analysis of gene-expression patterns. Nature. 2008;452:564-570.

[193] PharmWeb. Community, Compounding and Retail Pharmacies (Chemists). 2013 (http://www.pharmweb.net/).

[194] Massacusetts Institute of Technology News. MIT scientists 'Print' Drugs Into Pills. 1997 (http://web.mit.edu/newsoffice/1997/).

[195] The Guardian. The 'Chemputer' that could print out any drug. 2012 (http://www.guardian.co.uk/science/2012/jul/21/).

[196] Xiang XD, Sun XD, Briceno G, Lou YL, Wang KA, Chang HY, et al. A Combinatorial Approach to Materials Discovery. Science. 1995;268(5218):1738-1740.

[197] Hendershota RJ, Rogersa WB, Snively CM, Ogunnaikea BA, Lauterbach J. Development and optimization of NO_x storage and reduction catalysts using statistically guided high-throughput experimentation Catalysis Today. 2004;98(3):375-385.

[198] Weng XL, Cockcroft JK, Hyett G, Vickers M, Boldrin P, Tang CC, et al. High-throughput continuous hydrothermal synthesis of an entire nanoceramic phase diagram. Journal of Combinatorial Chemistry. 2009;11(5):829-834.

[199] Simon U, Sanders D, Jockel J, Brinz T. Setup for high-throughput impedance screening of gas-sensing materials. Journal of Combinatorial Chemistry. 2005;7(5):682-687.

[200] Frenzer G, Frantzen A, Sanders D, Simon U, Maier WF. Wet chemical synthesis and screening of thick porous oxide films for resistive gas sensing applications. Sensors. 2006;6(11):1568-1586.

[201] Danielson E, Devenney M, Giaquinta DM, Golden JH, Haushalter RC, McFarland EW, et al. A rare-earth phosphor containing one-dimensional chains identified through combinatorial methods. Science. 1998;279(5352):837-839.

[202] Wang JS, Yoo Y, Gao C, Takenchi I, Sun XD, Chang HY, et al. Identification of a blue photoluminescent composite material from a combinatorial library Science. 1998;279:1712-1714.

[203] Fujimoto K, Takada K, Sasaki T, Watanabe M. Combinatorial approach for powder preparation of pseudo-ternary system $LiO_{0.5}$-X-TiO_2 (X: $FeO_{1.5}$, $CrO_{1.5}$ and NiO). Applied Surface Science. 2004;223(1-3):49-53.

[204] Rossiny JCH, Julis J, Fearn S, Kilner JA, Zhang Y, Chen LF, et al. Combinatorial characterisation of mixed conducting perovskites. Solid State Ionics. 2008;179(21-26):1085-1089.

[205] Reddington E, Sapienza A, Gurau B, Viswanathan R, Sarangapani S, Smotkin ES, et al. Combinatorial electrochemistry: a highly parallel, optical screening method for discovery of better electrocatalysts. Science. 1998;280:1735-1737.

[206] Cremer R, Neuschutz D. Optimization of (Ti,Al)N hard coatings by a combinatorial approach. International Journal of Inorganic Materials. 2001;3(8):1181-1184.

[207] Kionuma H, Matsumoto Y, Murakami M, Shono T, Hasegawa T, Fukumura T, et al. Room-temperature ferromagnetism in transparent transition metal-doped titanium dioxide Science. 2001;291:854-856.

[208] Briceno G, Chang HY, Sun XD, Schultz PG, Xiang XD. A class of cobalt oxide magnetoresistance materials discovered with combinatorial synthesis. Science. 1995;270(5234):273-275.

[209] Chang H, Gao C, Takeuchi I, Yoo Y, Wang J, Schultz PG, et al. Combinatorial synthesis and high throughput evaluation of ferroelectric/dielectric thin-film libraries for microwave applications. Applied Physics Letters. 1998;72(17):2185-2117.

[210] van Dover RB, Schneemeyer LD, Fleming RM. Discovery of a useful thin-film dielectric using a composition-spread approach. Nature. 1998;392(6672):162-164.

[211] Scott DJ, Manos S, Coveney PV, Rossiny JCH, Fearn S, Kilner JA, et al. Functional ceramic materials database: An online resource for materials research. Journal of Chemical Information and Modeling. 2008;48(2):449-455.

[212] Hook AL, Anderson DG, Langer R, Williams P, Davies MC, Alexander MR. High throughput methods applied in biomaterial development and discovery. Biomaterials. 2010;31(2):187-198.

[213] Simon CG, Lin-Gibson S. Combinatorial and High-Throughput Screening of Biomaterials. Advanced Materials. 2011;23(3):369-387.

[214] Hoogenboom R, Meier MAR, Schubert US. Combinatorial methods, automated synthesis and high-throughput screening in polymer research: past and present. Macromolecular Rapid Communications. 2003;24(1):15-32.

[215] Hanak JJ. The 'Multiple-Sample Concept' in materials research: synthesis, compositional analysis and testing of entire multicomponent system. Journal of Materials Science. 1970;5:964-971.

[216] Gutte B, Merrifield RB. The total synthesis of an enzyme with ribonuclease A activity. Journal of the American Chemical Society. 1969;91(2):501-502.

[217] Maier WF, Stowe K, Sieg S. Combinatorial and high-throughput materials science. Angewandte Chemie-International Edition. 2007;46(32):6016-6067.

[218] Webster DC. Combinatorial and High-Throughput Methods in Macromolecular Materials Research and Development. Macromolecular Chemistry and Physics. 2008;209(3):237-246.

[219] Lowe G. Combinatorial chemistry. Chemical Society Reviews. 1995;24(5):309-317.

[220] Vossmeyer T, Jia S, DeIonno E, Diehl MR, Kim SH, Peng X, et al. Combinatorial approaches toward patterning nanocrystals. Journal of Applied Physics. 1998;84:3664-3670.

[221] Xiang XD, Schultz PG. The combinatorial synthesis and evaluation of functional materials. Physica C. 1997;282-287:428-430.

[222] Reichenbach HM, McGinn PJ. Combinatorial synthesis of oxide powders. Journal of Materials Research. 2001;16(4):967-974.

[223] Sun XD, Wang KA, Yoo Y, Wallace-Freedman WG, Gao C, Xiang XD, et al. Solution-phase synthesis of luminescent materials libraries. Advanced Materials. 1997;9:1046-1049.

[224] Zhan Y, Chen LF, Yang SF, Evans JRG. Thick film ceramic combinatorial libraries: The substrate problem. Qsar & Combinatorial Science. 2007;26(10):1036-1045.

[225] Chen YL, Evans JRG, Yang S. A rapid doping method for high-throughput discovery applied to thick film PTCR materials. Journal of the American Ceramic Society. 2011.

[226] Li X, Huang J, Edirisinghe M, Bonfield W. An electrically driven jetting technique for diverse high-resolution surface structures of nanometre hydroxyapatite crystals. Colloids and Surfaces B: Biointerfaces. 2011;82(2):562-570.

[227] Yang SF, Evans JRG. Device for preparing combinatorial libraries in powder metallurgy. Journal of Combinatorial Chemistry. 2004;6(4):549-555.

[228] Stegk TA, Janssen R, Schneider GA. High-throughput synthesis and characterization of bulk ceramics from dry powders. Journal of Combinatorial Chemistry. 2008;10(2):274-279.

[229] Gao F, Yang SF, Hao PW, Evans JRG. Suspension Stability and Fractal Patterns: A Comparison using Hydroxyapatite. Journal of the American Ceramic Society. 2011;94(3):704-712.

[230] Zhang Y, Chen L, Yang S, Evans JRG. Control of particle segregation during drying of ceramic suspension droplets. Journal of the European Ceramic Society. 2007;27(5):2229-2235.

[231] Tekin E, de Gans BJ, Schubert US. Ink-jet printing of polymers - from single dots to thin film libraries. Journal of Materials Chemistry. 2004;14(17):2627-2632.

[232] Zhang Y, Yang S, Chen L, Evans JRG. Shape changes during the drying of droplets of suspensions. Langmuir. 2008;24(8):3752-3758.

[233] Meredith JC, Sormana JL, Keselowsky BG, Garcia AJ, Tona A, Karim A, et al. Combinatorial characterization of cell interactions with polymer surfaces. Journal of Biomedical Materials Research Part A. 2003;66A(3):483-490.

[234] Williams RL, Adams WP, Poochikian G, Hauck WW. Content uniformity and dose uniformity: current approaches, statistical analyses, and presentation of an alternative approach with special reference to oral inhalation and nasal drug products. Pharmaceutical Research. 2002;19(4):359-366.

[235] Bysouth SR, Bis JA, Igo D. Cocrystallization via planetary milling: Enhancing throughput of solid-state screening methods. International Journal of Pharmaceutics. 2011;411(1-2):169-171.

[236] Zeng XM, Martin GP, Marriott C, Pritchard J. The effects of carrier size and morphology on the dispersion of salbutamol sulphate after aerosolization at different flow rates. Journal of Pharmacy and Pharmacology. 2000;52(10):1211-1221.